

**PETROGRAPHIC AND GEOCHEMICAL CONSTRAINTS  
ON THE ORIGIN AND POST-DEPOSITIONAL HISTORY  
OF THE HOTAZEL IRON-MANGANESE DEPOSITS,  
KALAHARI MANGANESE FIELD, SOUTH AFRICA**

A thesis submitted in fulfilment of the  
requirements for the degree of

DOCTOR OF PHILOSOPHY

of

RHODES UNIVERSITY

by

**HARILAOS TSIKOS**

March 1999

## Abstract

The giant Palaeoproterozoic manganese deposits of the Kalahari manganese field (KMF), Northern Cape Province, South Africa, have been a world renowned resource of manganese ore for many decades. In recent years, the mineralogical composition, geochemistry and genesis of these deposits have been the objects of many geological investigations, yet their origin remains contentious up to the present day. A characteristic feature of the Kalahari deposits is the intimate association of manganese ore and iron-formation of the Superior-type, in the form of three discrete sedimentary cycles constituting the Hotazel Formation. This striking lithological association is an almost unique feature on a global scale. From that point of view, the present study is effectively the first attempt to shed light on the origin and post-depositional history of the Hotazel succession, using as prime focus the petrographic and geochemical characteristics of the host iron-formation.

Petrographic and whole-rock geochemical information of iron-formation from the southern parts of the KMF, suggests that the Hotazel iron-formation is almost identical to other iron-formations of the world of similar age and petrological character. The rock exhibits essentially no high-grade metamorphic or low-temperature alteration effects. Mineralogically, it contains abundant chert, magnetite, subordinate amounts of silicate minerals (greenalite, minnesotaite, stilpnomelane) and appreciable concentrations of carbonate constituents in the form of coexisting calcite and ankerite. Such mineralogical composition is indicative of processes occurring in a diagenetic to burial (up to very low-greenschist facies) metamorphic environment. Bulk-rock geochemical data point towards a simple composition with  $\text{SiO}_2$ , total Fe-oxide and CaO being the chief major oxide components. Whole-rock rare-earth element data suggest that the iron-formation precipitated from a water column with chemical signatures comparable to modern, shallow oceanic seawater. The virtual absence of positive Eu anomalies is a feature that compares well with similar data from Neoproterozoic, glaciogenic iron-formations of the Rapitan type, and suggests but only a dilute hydrothermal signal, potentially derived from distal submarine volcanic activity.

Carbon and oxygen isotope data from iron-formation and Mn-bearing carbonates as well as overlying ferriferous limestone of the Mooidraai Formation, compare well with the literature. The

former exhibit variable depletion relative to seawater in terms of both  $^{13}\text{C}$  and  $^{18}\text{O}$ , while the latter have signatures comparable to normal marine bicarbonate. Isotopic variations appear to be related to fluctuations in the amount of co-precipitated marine carbonate, in conjunction with processes of coupled organic matter oxidation - Fe/Mn reduction in the diagenetic environment. Oxygen isotope data from quartz-magnetite-calcite triplets suggest that crystallisation took place under open-system conditions, with magnetite being the most susceptible phase in terms of fluid-rock isotopic exchange. Data also suggest that the calcite-magnetite pair may constitute a more reliable geothermometer than the quartz-magnetite one, mainly due to the interlinked diagenetic histories between calcite and magnetite.

Iron-formation from the northern parts of the KMF can be categorised into three main classes, namely pristine, altered and oxidised. Pristine iron-formation is identical to the one seen in the southernmost parts of the field. Altered iron-formation corresponds to a carbonate-free derivative of intense oxidation and leaching processes at the expense of pristine iron-formation, and contains almost exclusively binary quartz-hematite mixtures. The rock appears to have lost essentially its entire pre-existing carbonate-related components (i.e., Ca, Mg, Sr, most Mn and Ba) and displays residual enrichments in elements such as Cr, Th, V, Ni and Pb, which would have behaved as immobile constituents during low-temperature alteration. The low temperature origin of altered iron-formation is supported by oxygen isotope data from quartz-hematite pairs which indicate that isotopically light hematite would have derived from oxidation of magnetite and other ferrous-silicate compounds in the presence of a low-temperature meteoric fluid, while quartz would have remained isotopically unchanged. Occasional occurrences of acmite-hematite assemblages suggest localised metasomatic processes related to the action of NaCl-rich fluids at the expense of altered iron-formation. The conditions of acmite genesis are very poorly constrained due to the very broad stability limits of the mineral in environments ranging from magmatic to surface-related.

Oxidised iron-formation constitutes a distinct rock-type and shares common attributes with both the pristine and the altered iron-formation. The rock contains hematite as an important constituent while the amount of magnetite is substantially reduced. With regard to carbonate minerals, calcite contents are clearly very low or absent, having been replaced in most instances by a single, Mg-enriched, dolomite/ankerite-type species. Oxidised iron-formation contains somewhat higher

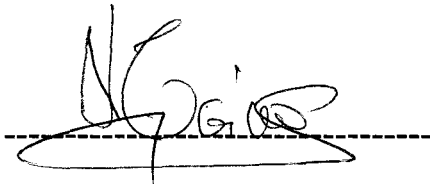
amounts of iron and reduced amounts of Sr and Ba relative to pristine iron-formation, whereas enrichments in elements such as Ni, Th, Pb, Cr, and V are seen, similar to altered iron-formation. Oxidised iron-formation appears to have originated from processes of dissolution-mobilisation-precipitation of solutes derived primarily from leaching that produced altered iron-formation.

It is proposed that the Hotazel iron-formation and associated manganese deposits were formed as a result of episodic sea-level fluctuations in a stratified depositional environment that gradually evolved into a shallow carbonate platform. A critical parameter in the development of manganese sediment may include regional climatic patterns related to a glacial event (Makganyene diamictite) prior to deposition of the Hotazel strata. This suggestion draws parallels with processes that are believed to have led to the formation of worldwide iron-formations and associated manganese deposits subsequent to Neoproterozoic episodes of glaciation. Submarine volcanism related to the underlying Ongeluk lavas appears to have had very little (if any) metallogenic significance, while evidence for a sudden rise in the oxygen contents of the atmosphere and ambient waters is lacking. With regard to later alteration processes, combination of geological and geochemical data point towards the potential influence of surface weathering prior to deposition of rocks of the unconformably overlying Olifantshoek Supergroup, possibly coupled with fault- and/or thrust-controlled fluid-flow and leaching of the Hotazel succession during post-Olifantshoek times.



## Declaration

ALL MATERIAL CONTAINED IN THIS THESIS REPRESENTS THE ORIGINAL WORK OF THE AUTHOR EXCEPT WHERE SPECIFIC ACKNOWLEDGEMENT IS MADE TO THE WORK OF OTHERS.

A handwritten signature in black ink, appearing to be 'N. G. G.', is written over a horizontal dashed line. The signature is stylized and cursive.

31st March 1999

Geology Department  
RHODES UNIVERSITY  
GRAHAMSTOWN - SOUTH AFRICA

*“There is no royal road to scholarship, and only those who do not dread the fatiguing climb of its steep paths have a chance of gaining its luminous summits”*

**KARL MARX**

(Preface to the French edition of “Das Kapital”)

## Table of Contents

### PART 1: INTRODUCTION AND REGIONAL GEOLOGY

<b>Chapter 1.1: Introduction</b> .....	1
1.1.1. Definitions .....	1
1.1.2. General .....	2
1.1.3. Previous work .....	4
1.1.4. Thesis outline and objectives .....	7
<b>Chapter 1.2: Regional geological setting</b> .....	9
1.2.1. The Transvaal Supergroup .....	9
1.2.2. The Transvaal Supergroup in the Northern Cape Province .....	11
1.2.3. The Kalahari Manganese Field (KMF) .....	14

### PART 2: PETROGRAPHY

<b>Chapter 2.1: Introduction</b> .....	19
2.1.1. Background .....	19
2.1.2. Sample selection, methods and macroscopic observations .....	19
<b>Chapter 2.2: Mineralogy and textures of the Hotazel iron-formation</b> .....	22
2.2.1. Bulk mineralogical composition .....	22
2.2.2. Diagenetic - very low-grade metamorphic paragenesis .....	23
2.2.2.1. <i>Silicates</i> .....	24
2.2.2.2. <i>Carbonates</i> .....	27
2.2.2.3. <i>Oxides and sulfides</i> .....	30
2.2.2.4. <i>Petrogenetic constraints</i> .....	31
2.2.3. Oxidised and alteration assemblages .....	33
2.2.3.1. <i>Altered iron-formation paragenesis</i> .....	35
2.2.3.2. <i>Oxidised iron-formation paragenesis</i> .....	40
2.2.3.3. <i>Petrographic constraints on alteration</i> .....	41

## PART 3: BULK-ROCK GEOCHEMISTRY

<b>Chapter 3.1: Introduction</b> .....	49
3.1.1. General .....	49
3.1.2. Material selection and methods .....	49
<b>Chapter 3.2: The Hotazel iron-formation - results and chemostratigraphy</b> .....	52
3.2.1. Southern KMF .....	52
3.2.2. Northern KMF .....	57
3.2.2.1. <i>Pristine iron-formation</i> .....	57
3.2.2.2. <i>Altered iron-formation</i> .....	61
3.2.2.3. <i>Oxidized iron-formation</i> .....	63
3.2.3. Preliminary conclusions .....	68
<b>Chapter 3.3: Geochemistry of selected sample groups</b> .....	71
3.3.1. Iron-formation .....	71
3.3.1.1. <i>Discriminant analysis</i> .....	71
3.3.1.2. <i>Principal component analysis</i> .....	73
3.3.1.3. <i>Inter-elemental relations</i> .....	80
3.3.1.4. <i>Summary of major geochemical affiliations</i> .....	86
3.3.2. Mooidraai Formation .....	87
<b>Chapter 3.4: Geochemical evidence for secondary alteration</b> .....	90
3.4.1. The isocon method .....	90
3.4.2. The Hotazel exercise .....	91
3.4.3. Mass balance constraints .....	97
<b>Chapter 3.5: Rare-earth element geochemistry</b> .....	102
3.5.1. Background .....	102
3.5.2. Results .....	103
3.5.3. Comparisons with ancient and modern equivalents .....	106

## PART 4: STABLE ISOTOPE GEOCHEMISTRY

<b>Chapter 4.1: Carbon and oxygen isotope geochemistry of Voëlwater carbonates</b> . . .	110
4.1.1. Background . . . . .	110
4.1.1.1. <i>Iron-formations</i> . . . . .	111
4.1.1.2. <i>Manganese ores</i> . . . . .	113
4.1.1.3. <i>Carbonates</i> . . . . .	114
4.1.2. Sample selection and analytical procedures . . . . .	114
4.1.3. Petrographic descriptions . . . . .	117
4.1.3.1. <i>Hotazel Formation</i> . . . . .	117
4.1.3.2. <i>Mooidraai Formation</i> . . . . .	118
4.1.4. Results . . . . .	119
4.1.4.1. <i>Isotopic compositions</i> . . . . .	119
4.1.4.2. <i>Isotopic compositions vs bulk-rock CaO - chemostratigraphy</i> . . . . .	123
4.1.5. Isotopic depletion - causes and constraints on genesis . . . . .	132
4.1.5.1. <i>Metamorphism</i> . . . . .	132
4.1.5.2. <i>Organic carbon oxidation - ferric iron reduction</i> . . . . .	133
4.1.5.3. <i>Organic matter oxidation - manganese reduction</i> . . . . .	135
<b>Chapter 4.2: Oxygen isotope systematics of silicate - Fe-oxide pairs</b> . . . . .	137
4.2.1. General . . . . .	137
4.2.1.1. <i>Quartz-magnetite</i> . . . . .	138
4.2.1.2. <i>Quartz-hematite</i> . . . . .	144
4.2.2. Oxygen isotope systematics of the Hotazel iron-formation . . . . .	145
4.2.2.1. <i>Sample selection and description</i> . . . . .	145
4.2.2.2. <i>Methods</i> . . . . .	147
4.2.2.3. <i>Limitations</i> . . . . .	149
4.2.3. Results . . . . .	151
4.2.3.1. <i>Diagenesis-metamorphism</i> . . . . .	151
4.2.3.2. <i>Alteration-metasomatism</i> . . . . .	157

## PART 5: SYNTHESIS

<b>Chapter 5.1: Origin of iron-formations</b> .....	161
5.1.1. Palaeoenvironment and source of Fe and Si .....	161
5.1.2. Genetic modelling .....	162
<b>Chapter 5.2: Genesis of the Hotazel Formation</b> .....	165
5.2.1. Previous genetic models .....	165
5.2.2. Development of the Fe-Mn cycles .....	169
5.2.3 Regional stratigraphy and implications .....	174
<b>Chapter 5.3: Alteration - metasomatism of the Hotazel Formation</b> .....	176
5.3.1. Previous models .....	176
5.3.2. Appraisal .....	179
5.3.2.1. <i>Evaluation of geological evidence</i> .....	179
5.3.2.2. <i>Constraints from the present study</i> .....	184
<b>Chapter 5.4: Conclusions - suggestions for future work</b> .....	189

## PART 6: REFERENCES

## PART 7: APPENDICES

<b>Appendix I: Borehole localities and sample selection</b> .....	A1
<b>Appendix II: Analytical techniques</b> .....	A9
<b>Appendix III: Whole-rock geochemical data</b> .....	A15
<b>Appendix IV: Additional bibliography</b> .....	A34

## Acknowledgements

I wish to extend my sincerest appreciation to the Geological staff of ASSMANG in Black Rock/Beeshoek for providing me the opportunity to carry out this project. I am especially indebted to Mr Awie Pretorius, whose continuous support at all levels from the very onset of this project, was critical towards the completion of this thesis. Also, a special thank you to Mr J.C. Steenkamp, for approving certain logistic support towards the final stages of this work. Along with Mr Awie Pretorius, many thanks must be extended to Mr Willem Grobbelaar, Andre and Lauren Deiss, I.M. van Niekerk and M. Burger, for their hospitality during my stay in Black Rock and Beeshoek in 1995, the provision of maps, access to borehole log information and assistance with the borehole sampling. Many thanks should also go to Nico Bleeker from SAMANCOR (Hotazel), for allowing the sampling of borehole material during my short visit to Hotazel in 1995.

This PhD would never have materialised without the never-ending interest, immaculate supervision and invaluable support of my supervisor, Prof J. M. Moore. Throughout this project, Prof Moore was always available for discussions, always eager to assist me in my scientific endeavours, and always prepared to help me face the hardships of this PhD with his rare ability to provide potential solutions by simply generating more queries. Working with Prof Moore has undoubtedly been the most beneficial aspect of my academic career thus far, and I am gratefully indebted to him for that. Special thanks must also be extended to my co-supervisor, Prof. R.E. Jacob, for his continuous interest and support in and out of the scientific arena. Prof. J.S. Marsh introduced me into the secrets of the x-ray fluorescence technique and I am grateful to him for his contribution. Many thanks to the remaining staff of the Geology Department at Rhodes, i.e. Prof. H. Eales, Dr R. Sheets, Dr. E. Ferré, Dr. O. Catuneanu, Dr. M. Roberts and Dr. I. Skilling, for sharing with me their scientific expertise, and to Mr J. Hepple, A. Visagie, B. Bongwana, W. Hashe for their physical and mental endurance during the preparation of my samples. Also, a very special thank you to all the good friends-geologists I made at Rhodes while working on this thesis, namely P. Kerber, A. Mason-Apps, R. Boelema, J. Wilson, P. Hoyle, L. Quinton, L. Venter, T. Strauss, D. Mooney, G. Surtees, E. Mills, S. Polteau, J-B. Aurejac, L. Ameglio and N. Hammond.

A great thank you to Dr C. Sacht from the Department of Chemistry, Rhodes University, for her assistance with the sometimes terribly unpleasant acid treatment of iron-formation samples. Many thanks also to Prof D.J. Eve from the same department for offering me free and unconstrained access to their x-ray diffraction facility. Mrs Susan Abraham (Geography Department, Rhodes University) helped with the preparation of maps and a special thank you is extended to her as well.

All isotopic and rare-earth element analyses (REE) were performed at the University of Cape Town (UCT). I am indebted to Dr C. Harris for offering me invaluable assistance by introducing me into the fascinating world of stable isotopes. Also, the contribution of Prof A. le Roex and Dr A. Spath with the rare-earth element analyses is greatly appreciated. My stay in the small but self-contained flat on the fourth floor of the Geology department at UCT, was made very pleasant by a number of people. To name a few: Dr. M. Tredoux, Dr. H. Frimmel, Prof. W.E.L. Minter, the SASSEG committee (W. Johnstone, W. Board, K. Westerlünd and P. Macey) and P. Fölling.

My appreciation is extended to Mr J.F. Bednarik (Council for Geoscience, Pretoria) for conducting whole-rock FeO analyses on selected samples of iron-formation, and also to Dr Arnot Kleyenstüber (MINTEK) for his willingness to offer me assistance with the wet chemical treatment of manganese ores, and for the immediate interest he showed in my work. A special thank you is also extended to my external supervisor Prof. N.J. Beukes, and to Dr J. Gutzmer, both from Rand Afrikaans University (RAU), for always being keen to share with me their tremendous expertise on the geology of the Kalahari manganese field. I hope that this work has complemented substantially their long-lasting efforts, and I am looking forward to working with them in the near future.

A big thank you to the Society of Economic Geologists Foundation (SEGF) for the honour of selecting me as one of the Society's recipients of a student research grant for 1998. Without these funds, part of the findings presented in this thesis would never have been accomplished. Also, Prof. St. Skounakis from the National University of Athens in Greece, deserves a great thank you for encouraging my coming to South Africa for postgraduate studies, and for his constant interest in my progress.



Over the past few years, there have been a lot of people who helped me relieve the stresses and frustrations of this truly demanding endeavour. Amongst them is Mr J. McNeill, lecturer in Information Systems at Rhodes, warden of Winchester House and very good friend, who offered me his endless support and friendship throughout my stay in South Africa. He made Winchester a warm place for me, a place where I always felt more at home than homesick. To him and to the numerous good friends I so easily made in “Winch” over the years, a great thank you for the wonderful times. I will miss you all.

To my very good friends Anastasi and Aspasia Anetos, I wish to extend my deepest appreciation and love. They have been a second family to me and I could never have imagined my stay in South Africa without them. An enormous thank-you must also be extended to Dr A. Polemitis, who so open-heartedly offered his own indispensable contribution towards the completion of my degree.

I would also like to thank Ms Julia V. Paterson and her family (Brian, Shanta and Steven) for their love, their warm hospitality and continuous support over the past three years. They always treated me as a member of their family, even in the toughest of times, and I will always be deeply grateful to them for that.

To my girlfriend and best mate, Ms Toni Balt, I wish to extend my warmest thank-you for all the support over the final stages of this thesis. During those times when my frustration peaked and my patience was stretched to the limits, she was always there for me, ready to offer me the sanity, encouragement and extra strength I needed in order to keep up with the task at hand.

My love, appreciation and an enormous thank you are extended from the depths of my heart to my parents Niko and Sotiria. Their contribution to where I am and what I have achieved today, could never be described in a few words. All I can say is that I am privileged to have such parents.

Last but not least, I wish to extend my love and gratitude to my late grandparents Harilaos Tsikos and Kaliopi Argyroiliopoulos. Sadly, their extraordinary courage and love for life did not prove enough in their fight to overcome the harsh challenges of illness and time. This thesis is dedicated to their memory.

# PART 1: INTRODUCTION AND REGIONAL GEOLOGY

## Chapter 1.1: Introduction

### 1.1.1. Definitions

The term **iron-formation** has been widely used in the geological literature as a descriptive term for any sedimentary rock containing a high content of iron (Fe). The minimum value of iron required to satisfy such a definition was arbitrarily chosen by James (1954) as 15 wt%, though most iron-formations contain between 30-40 wt% Fe on average. This iron may be contained in a variety of mineral phases such as oxides, silicates and/or carbonates, in coexistence with quartz, the main non-ferrous constituent of iron-formation. An important textural feature of iron-formation is the remarkably rhythmic banding of Fe-poor and Fe-rich bands on a variety of scales, that can sometimes be traced undisturbed on outcrop over large distances.

The very well-constrained distribution of iron-formation in space and time is a characteristic of great scientific interest. It is well-documented that the vast majority of iron-formation was deposited during the late Archaean-Palaeoproterozoic, that is, between 2.7 and 1.9Ga ago (Fig. 1.1). Iron-formation occurrences of such age have been termed “Superior-type” (Gross and McLeod, 1980), they are found in several parts of the world and exhibit remarkable petrographic and geochemical similarities. Superior-type iron-formations occur in the form of thick, monotonous and laterally extensive stratigraphic units, commonly grading into carbonate rocks or *vice versa*, but generally devoid of any intercalated clastic material.

Various comprehensive classification schemes have been proposed for the vast number of iron-formation occurrences of the Precambrian (e.g. Kimberley, 1978, 1979, 1989a,b; Gross, 1980, 1983). However, most authors agree that, besides the Superior-type occurrences, the majority of the remaining iron-formations are found in Archaean greenstone-terranes and Neoproterozoic glaciomarine sedimentary successions and belong to the Algoma- and Rapitan-type classes respectively (e.g. Gross and McLeod, 1980; Klein and Beukes, 1993). These iron-formations differ in many respects from their Palaeoproterozoic, “Superior-type” counterparts, particularly in terms of geotectonic setting and origin. Since it is beyond the scope of this study to provide a

detailed treatise on the entire spectrum of iron-formations, the term “iron-formation” will be used in the following chapters with direct reference to the “Superior-type” for the purposes of simplification. Hence, the names “Algoma” and “Rapitan” will always precede the term “iron-formation” when particular reference to these two distinct types is required.

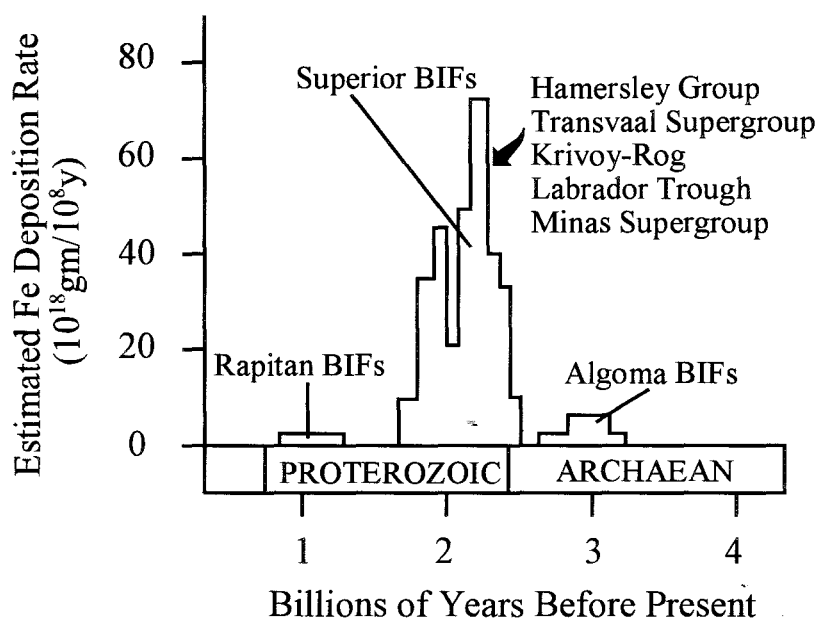


**Figure 1.1.** Estimated deposition rate of Fe in Precambrian iron-formations for those  $>10^{18} \text{ gm}/10^8 \text{ y}$ . Note the peak at 2.7-1.9 Ga corresponding to the deposition of the Superior-type class (modified after Isley, 1995).

### 1.1.2. General

The widespread development of iron-formation in Late Archaean-Palaeoproterozoic sedimentary basins of the world has been a prominent area of research in the earth sciences for many decades. In earlier years, the majority of research on iron-formations concentrated primarily on their mineralogy, petrography, metamorphism, sedimentology, whole-rock geochemistry and genetic modelling. With time, the relative increase in the number of scientific papers dealing with geochemical aspects such as the stable-isotope and rare-earth element systematics of iron-formation, provided a substantial contribution to the understanding of the deposition, diagenesis and origin of these enigmatic rocks. However, despite the current wealth of literature information,

a wide spectrum of attributes concerning the origin of iron-formations still remains unaccountable. Consequently, there is yet no widely accepted model that can satisfactorily explain all petrological, sedimentological and geochemical characteristics encountered in iron-formations worldwide. Reasons for this ought to be sought in certain fundamental geological differences amongst the various iron-formations and especially in the diversity of geological settings in which they may have formed. Such a diversity is largely attributed to the evolutionary trends that have been postulated for the Precambrian atmosphere, hydrosphere and biosphere, and their respective influences on contemporaneous sedimentary environments. Hence, any attempt to produce a single genetic model invariably carries the disadvantage of being regarded as equivocal, oversimplistic, and not directly applicable in many case studies.

From an economic point of view, areas with extensive iron-formation occurrences have been amongst the most favourable sites for large-scale exploration and mining projects for iron-ore deposits. This is despite the fact that an iron-formation does not necessarily constitute a mineable iron-ore deposit *per se*. From a mineralogical point of view, a pristine iron-formation commonly contains a variety of mineral phases that inhibit economic iron extraction, even though the bulk Fe-metal content of the rock may exceed the value of 50 wt%. Studies on world-class iron-ore deposits such as Sishen, South Africa (Van Schalkwyk and Beukes, 1986), the deposits of the Hamersley Group in Western Australia (Morris, 1980) and the iron-ore deposits in Minas Gerais, Brazil (Hoefs et al., 1982), have demonstrated that secondary processes involving primarily low-temperature oxidation and leaching of various Ca- and Si-bearing components, have been critical in transforming at least parts of an economically unviable iron-formation proper, to mineable Fe-ore.

Apart from iron, one of the few other commodities that has also been extensively mined from iron-formations is *crocidolite asbestos*. The term "crocidolite" applies to the fibrous variety of the sodic amphibole riebeckite, which may have formed in economic quantities as a result of intense and usually structurally-controlled Na-metasomatism in iron-formations. Type examples are found in Palaeoproterozoic iron-formations of the Hamersley Group, Western Australia (Trendall and Blockley, 1970), the Transvaal Supergroup, South Africa (Beukes and Dreyer, 1986), and the Chapare Group, Bolivia (Redwood, 1993).

Despite established geochemical affinities between Fe and Mn, the latter is very seldom present in economic quantities in direct association with iron-formations. Secondary manganese enrichments in iron-formations may develop as a result of supergene leaching processes at the expense of Mn-bearing phases and especially carbonates (e.g. calcite, ankerite). However, the resulting manganese ore-grades are usually very low, and the size and distribution of these deposits render them uneconomic in most instances. Examples of deposits of this kind are found in three of the world's type areas of iron-formation occurrence, namely the Hamersley Group, Western Australia (Fetherston, 1990), the Transvaal Supergroup, South Africa (Dirr and Beukes, 1990; Beukes, 1993) and the Cuyuna Range, Minnesota, U.S.A (Morey and Southwick, 1992).

The *Kalahari manganese field* (hereafter referred to as KMF) constitutes probably the most notable exception. Besides its sheer volume (it accounts for approximately 50% of the world's overall manganese resources; see Laznicka, 1992, and Fig. 1.2), the KMF has its own unique geological characteristics. The most important of these is the direct stratigraphic association between the manganese ore and a Palaeoproterozoic iron-formation, in the form of three distinct iron-formation - manganese cycles. The latter constitute what has been described in the literature as the *Hotazel Formation* (Beukes, 1983). Manganese deposits of such clear syngenetic relation with iron-formation have not been reported from elsewhere. Although some manganese ores have been found in certain iron-formation-bearing sequences of India and Brazil (Schissel and Aro, 1992), insufficient geological evidence has been provided that would permit confident stratigraphic correlations and thus potential syngenetic links (Dorr, 1973a; Banerji, 1977).

### 1.1.3. Previous work

The geology of the KMF has received considerable attention from geologists in South Africa and abroad, partly due to its economic significance and partly because of its unusual geological character. Boardman (1941) provided the first description of enriched manganese ore at the Black Rock outcrop (see Appendix I, Fig. A1), the sole surface evidence of manganese mineralisation in the entire KMF, and concluded that the ores formed as a result of metasomatic processes at the expense of iron-formation. Frankel (1958) also proposed a supergene origin for altered manganese ore from Smartt mine, along similar lines with Boardman's model (1941) for the Black Rock area.

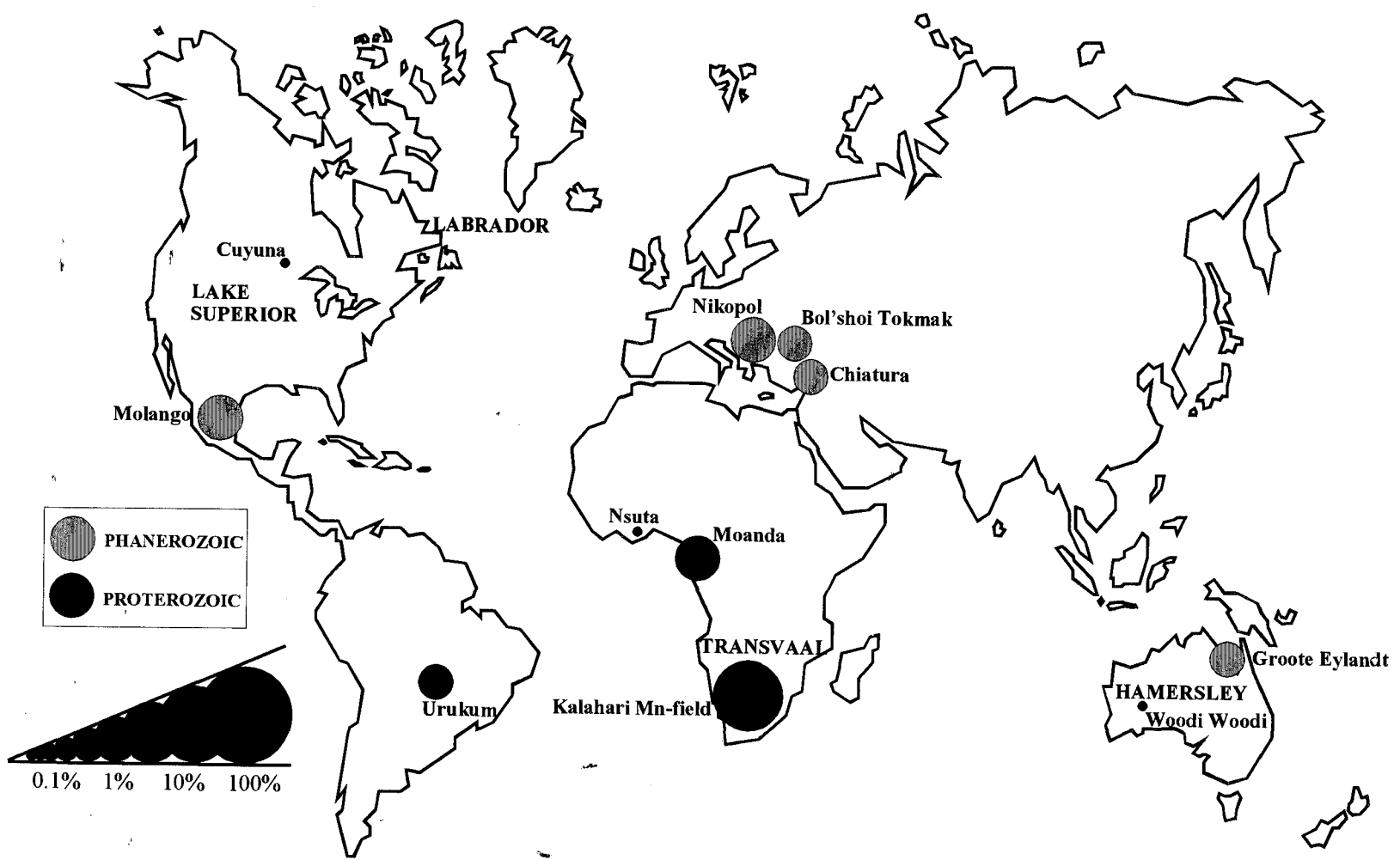


**Figure 1.2.** World map showing the distribution and relative size of world-class manganese ore districts. Manganese deposits in relation to major areas of Palaeoproterozoic iron-formation occurrences are shown in black; Phanerozoic manganese deposits are shown in shaded fill (modified after Laznicka, 1992).

More detailed accounts on the geology of the northern parts of the KMF were subsequently published by De Villiers (1960), Boardman (1964) and De Villiers (1970), the latter being the first to suggest a chemical sedimentary origin for the Kalahari manganese deposits.

In recent years, various models have been proposed for the origin of the Kalahari manganese deposits. De Villiers (1983, 1986, 1992) questioned a syngenetic origin of the deposits, favouring instead a regional metasomatic event by proposing a close genetic relation with the manganese ores of the Postmasburg area. De Villiers' model was based exclusively on detailed mineralogical studies and has been strongly challenged by Kleyenstüber (1986) and Beukes (1992). These authors envisaged a volcano-sedimentary mechanism of formation of the Kalahari manganese deposits, based on observations on the three manganese - iron-formation cycles of the Hotazel Formation (Beukes et al., 1982; Beukes, 1983). They proposed a tentative genetic model whereby this threefold cyclicity in the Hotazel Formation would have been developed as a result of transgression-regression cycles superimposed on a chemical sedimentary environment enriched in Fe and Mn from a proximal volcanic source (Ongeluk Formation). A more direct connection with a volcanic-exhalative origin was proposed by Cornell and Schütte (1995, 1996), who stressed the importance of the underlying Ongeluk Formation to their genetic scheme, in a fashion similar to metallogenic processes characterising modern mid-ocean ridge (MOR) settings. Like the epigenetic model of De Villiers (1983), the volcanic-exhalative model of Cornell and Schütte (1995, 1996) has also not escaped strong criticism (Beukes and Gutzmer, 1996).

A large database is available at present on the mineralogy, mineral chemistry and alteration geochemistry of the Kalahari deposits, a result of research studies conducted over the past two decades mainly by researchers from Rand Afrikaans University, Johannesburg, South Africa (Nel, 1984; Kleyenstüber, 1979, 1985; Burger, 1994; Gutzmer, 1996). Most of these data are found in a number of published scientific papers (e.g., Kleyenstüber, 1984; Nel et al., 1986; Gutzmer and Beukes, 1995, 1996a; Beukes et al., 1995; Gutzmer et al., 1997) and are complemented by the earlier studies of De Villiers (1943a,b; 1945a,b), as well as some additional work by Dixon (1985, 1989) and Miyano and Beukes (1987). Furthermore, a detailed PhD study on the Ongeluk Formation, a series of basaltic andesite lava flows forming the footwall of the Hotazel Formation, was carried out in the early 1990's (Schütte, 1992) and additional information on these rocks can

also be found in published form (Cornell et al., 1996).

#### **1.1.4. Thesis outline and objectives**

An important question, arising from the foregoing, concerns potential prospects for research in the KMF that would constructively complement and expand the existing knowledge. In an area where outcrop is effectively absent due to a thick sand-calcrete cover, information from borehole drilling is essential. A close inspection of existing drillhole material from the KMF has revealed a substantial amount of untouched research potential. It is in fact the nature of the Hotazel stratigraphy and particularly the striking cyclic interbedding of three manganese units with typical iron-formation, that has prompted a detailed examination of the host iron-formation and its metallogenic implications. From that point of view, the Hotazel iron-formation ought to be regarded as one of the most ignored iron-formation occurrences worldwide. The author was privileged in that he undertook the first preliminary study on the petrography and whole-rock geochemistry of parts of the Hotazel iron-formation in 1993 as an MSc project at Rhodes University (Tsikos, 1994). A representative portion of this work was subsequently published, forming effectively the only references to date on the Hotazel iron-formation and its metallogenic significance with regard to the interbedded manganese deposits (Tsikos and Moore, 1997, 1998).

This study is essentially the continuation of that early work on a much broader scale. It provides a significant amount of data derived from parts of the Hotazel stratigraphy and associated rocks, that either have received very little attention or have not been studied at all. The main emphasis has, naturally, been placed on the Hotazel iron-formation and its mineralogical and geochemical characteristics. A small amount of data from the three interbedded manganese ore units and from carbonate rock of the Moidraai Formation developed above the Hotazel succession have been included, in order to aid interpretations in a complementary fashion and allow constructive comparisons with the available literature.

The main objective of this thesis is thus to contribute to the understanding of the origin and post-depositional history of the Mn-rich Hotazel Formation. For the first time, this will be done by placing special emphasis on the mineralogy and geochemistry of the host-rock iron-formation. It



is hoped that this project will fill a major gap in the existing knowledge regarding the geology of the KMF and constitute an important starting reference towards future research and exploration programs for further manganese mineralisation, not only in the wider Kalahari area but also in other areas of similar age and geological character.

The thesis consists essentially of four main parts. The first part (PART 2) follows the introductory chapters and deals with the mineralogy and petrography of the Hotazel iron-formation as it appears in various parts of the KMF. Particular emphasis is placed on two main areas, namely the southernmost and northernmost segments. In the southernmost segment, the Hotazel iron-formation is practically devoid of any effects of metamorphism or other secondary processes, except for some localised cases where late supergene enrichment has occurred along faults and the unconformity between the Hotazel Formation and the Tertiary Kalahari Formation. In the northernmost segment, an intense alteration effect on the Hotazel rocks is readily evident. As a result, the iron-formation has been markedly enriched in secondary iron oxide, whereas the interbedded manganese ores have been significantly upgraded in terms of their manganese oxide content. The contrasting petrographic signatures observed in samples from both areas are described and provide a vital framework for the evaluation of the geochemical data that follow. Included in this section are some preliminary petrographic data from a few carbonate samples collected from the overlying Mooidraai Formation.

The second part (PART 3) focuses on the bulk-rock geochemistry of the Hotazel iron-formation. In this part, data on the major, minor, trace and REE composition of the Hotazel iron-formation are presented and evaluated. All geochemical data presented represent a large spectrum of sample material, including primarily all major types of iron-formation encountered in the field, as well as a smaller amount of Mooidraai carbonate samples. Comparisons between selected major iron-formation types are facilitated, allowing broader considerations with regard to the primary origin and subsequent alteration of the Hotazel Fe-Mn association.

The third part (PART 4) concentrates on applications of stable isotope geochemistry. Here, a detailed approach based on C and O isotope data from a number of samples of pristine, carbonate-bearing iron-formation, manganese ore and Mooidraai limestone, is provided. In addition, oxygen

isotope data from mineral pairs in both pristine and altered iron-formation are presented, providing an important means of investigating processes involving fluid-rock interaction in the diagenetic and alteration environments.

An overall account on the genesis, origin and alteration of the Hotazel Formation constitutes the final part of the thesis, which comprises a detailed discussion based on data from this study, as well as suggestions with regard to deposition, diagenesis and post-diagenetic history of the Hotazel Formation. Particular emphasis has been placed on the physicochemical conditions pertaining to the deposition of the Hotazel sedimentary precursors as well as on the processes that controlled the alteration observed in iron-formation and manganese ore from the northernmost parts of the KMF. In addition, implications regarding mineral exploration for further deposits of the Kalahari type, both on a local and on a broader scale, are briefly discussed.

## **Chapter 1.2: Regional geological setting**

### **1.2.1. The Transvaal Supergroup**

The late Archaean to Palaeoproterozoic (2.7-2.1 Ga) Transvaal Supergroup in southern Africa is developed in two major successions in the north-eastern and western segments of the Kaapvaal Craton (Fig. 1.3). These successions were formerly known as the Transvaal and Griqualand West Basins (Supergroups) respectively, in accordance with the two geographical areas in which they are typically developed (Button, 1986; Beukes, 1986). Lithostratigraphic similarities, however, particularly in the lower parts of the successions, have recently led to the abandonment of the term “Griqualand West Supergroup”, and the term “Transvaal Supergroup” as all-inclusive for both former Supergroups is now used (N.J. Beukes, pers. com.). Lithostratigraphic descriptions of, and correlations between the two successions of the Transvaal Supergroup have previously been demonstrated by Beukes (1983), and reviewed by Cheney and de la Winter (1995) in the context of the unconformity-bounded nature of the wider Transvaal stratigraphy. For the purposes of this thesis, only the stratigraphy of the Transvaal Supergroup in the Northern Cape Province will be dealt with in further detail.

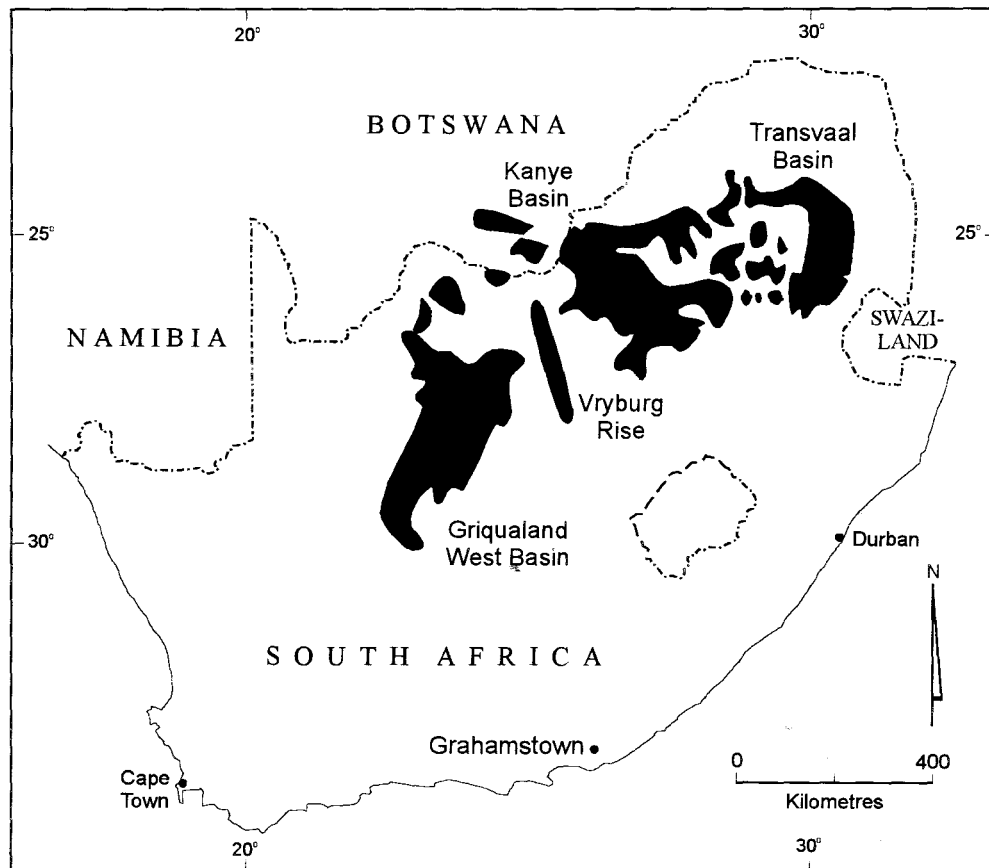


**Figure 1.3.** Simplified geological map showing the distribution of the two main segments of the Transvaal Supergroup in southern Africa, i.e. the former “Transvaal” and “Griqualand West” Supergroups (modified after Catuneanu and Eriksson, in press).

One of the most recent models regarding the tectonothermal history of the Kaapvaal Craton suggests the existence of a simple, three-stage rift system operating on a corresponding number of superimposed basins (Clendenin et al., 1988a). The model places the lower parts of the Transvaal Supergroup at the final stages of basin development on the Kaapvaal Craton as a result of thermal subsidence post-dating:

- (i) a pre-graben stage, responsible for many of the characteristics of the Dominion and Witwatersrand Supergroups, followed by:
- (ii) graben development, influencing large parts of the Ventersdorp Supergroup.

Despite the close interrelation amongst these three Proterozoic basins, their corresponding lithological, evolutionary and deformation characteristics are dissimilar (Clendenin et al., 1988b). These differences are believed to correspond to changes in intraplate deformation and transmitted intraplate stress related to subduction geometries between the Kaapvaal and Zimbabwean Cratons.

### **1.2.2. The Transvaal Supergroup in the Northern Cape Province**

The “Griqualand West Supergroup” (Fig. 1.4) is developed in the recently delineated Northern Cape and North West Provinces in South Africa to the south and west, and it extends into the southernmost parts of Botswana to the north (Beukes, 1986). The western limits of the Transvaal Supergroup in the above area coincide with the western margin of the Kaapvaal craton, which is defined by a sharp tectonic contact with the Kheis Province (Thomas et al., 1994a,b). The Kheis Province represents the easternmost tectonic block of the wider Namaqualand Metamorphic Province and has undergone a complex tectonometamorphic history involving an early (1.8-1.9 Ga) orogenic event as well as subsequent structural rejuvenation related to the 1.1 Ga Kibaran tectono-magmatic event (Thomas et al., 1994b). The rock succession of the Kheis Province has been correlated with the rocks of the mid-Proterozoic Olifantshoek Supergroup (SACS, 1980).

Large-scale thrusting is a conspicuous structural feature in the western parts of the Kaapvaal craton (Beukes and Smit, 1987; Altermann and Hälbich, 1990, 1991). In particular, Beukes and Smit (1987) recognised large-scale thrusting events related to the Kheis orogeny in the western margin of the craton and demonstrated their impact on the stratigraphic configuration of the Transvaal Supergroup in the area. As a result, rock units such as the Gamagara Formation that were previously believed to form part of the Transvaal Supergroup, are now placed in the younger Olifantshoek Supergroup. This interpretation bears important implications with respect to the overall Transvaal stratigraphy, and particularly the genesis of unconformity-related, supergene iron and manganese deposits in the Transvaal Supergroup (Beukes and Smit, 1987; Gutzmer and Beukes, 1996b).

The lower part of the stratigraphy of the Transvaal Supergroup in the Northern Cape Province is represented by the Ghaap Group (Table 1.1) which is developed either on top of tholeiitic

basalts of the Late Archaean Ventersdorp Group, or directly on crystalline basement rocks. The Ghaap Group comprises a thick succession of carbonate rocks belonging to the Campbellrand Subgroup, which is overlain by extensive iron-formations of the Asbesheuwels Subgroup (Fig. 1.4). The Asbesheuwels Subgroup is further subdivided into two formations, namely the Kuruman and Griquatown Iron Formations (Beukes, 1983). Mixed sequences of largely terrigenous clastic lithologic units with subordinate iron-formation, carbonates and lavas are locally developed at the base (Schmidtsdrift Subgroup) and top (Koegas Subgroup) of the carbonate - iron-formation succession (Beukes, 1983, 1986).

**Table 1.1.** Simplified stratigraphy of the Transvaal Supergroup in the Northern Cape Province (modified after Beukes and Smit, 1987).

SUPER-GROUP	GROUP	SUBGROUP	FORMATION	MAJOR LITHOLOGY	APPROXIMATE THICKNESS (m)
Transvaal	Postmasburg	Voëlwater	Moidraai	Carbonate, minor chert	250
			Hotazel	Fe-formation, manganese ore	
			Ongeluk	Basaltic andesite volcanics	500
			Makganyene	Glacial diamictite	50-150
	Ghaap	Koegas		Siliciclastics, iron-formation	240-600
		Asbesheuwels	Griquatown	Clastic-textured Fe-formation	200-300
			Kuruman	Microbanded Fe-formation	150-750
		Campbellrand		Carbonate, minor shale	1500-1700
		Schmidtsdrift		Siliciclastics, carbonate, lava	10-250

A diamictite unit termed the Makganyene Formation forms the basal part of the Postmasburg Group (Table 1.1) which overlies the Ghaap Group through a regional unconformity. The Makganyene diamictite is followed by a thick succession of continental flood-type basaltic andesites of the Ongeluk Formation (Sharpe et al., 1983; Schütte, 1992; Cornell et al., 1996). The Ongeluk Formation is in turn overlain by a mixed chemosedimentary succession of iron-formation interbedded with Mn ore (Hotazel Formation), locally grading into carbonates of the Moidraai Formation. The Hotazel and Moidraai Formations constitute the Voëlwater Subgroup (Table 1.1) and represent the youngest episode of chemical sedimentation in the Transvaal Supergroup.

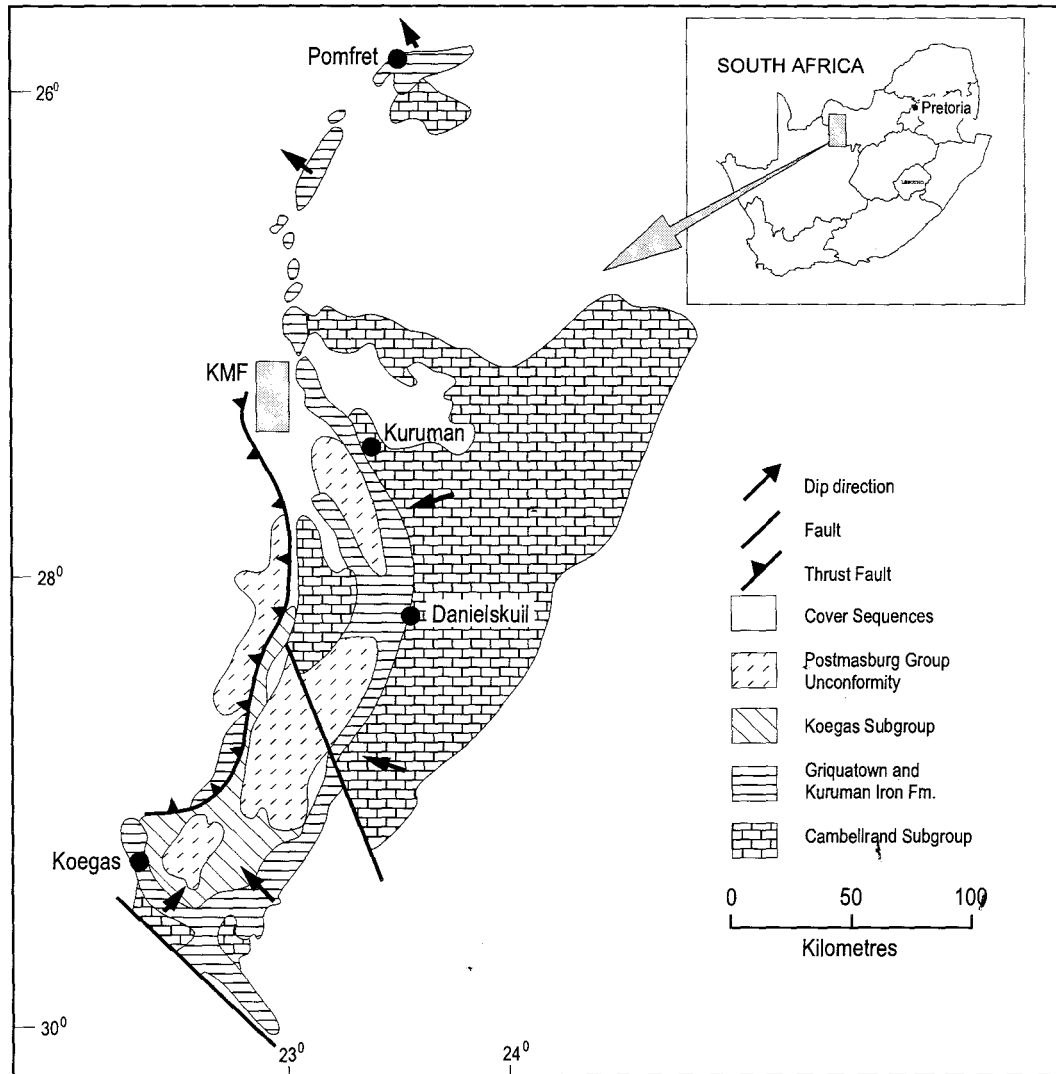


**Figure 1.4.** Simplified geological map of the Transvaal Supergroup in the Northern Cape Province, showing the distribution of major lithostratigraphic units, regional structures and the location of the Kalahari manganese field (KMF, inset) (modified after Tsikos and Moore, 1997).

An erosional unconformity separates rocks of the Transvaal Supergroup from the mid-Proterozoic Olifantshoek Supergroup. The Olifantshoek Supergroup consists of the basal Mapedi Formation, comprising intermixed cycles of predominantly red to whitish shales, organic-rich shales, siltstones and quartzites, followed by quartzites of the Lucknow Formation and volcanic-dominated rocks of the Hartley Formation (SACS, 1980). Radiometric dating of the Hartley volcanics (Cornell et al., 1998) has yielded an age of approximately 1.9 Ga, which provides the only presently available upper age constraint for the Transvaal Supergroup in the Northern Cape area.

### **1.2.3. The Kalahari manganese field (KMF)**

The KMF represents an erosional relict of a Palaeoproterozoic basin of unknown original dimensions and is the type location of the Mn-bearing Hotazel Formation. The Hotazel Formation is almost entirely covered by Cenozoic sands and calcretes of the Kalahari Formation, and the only natural outcrop is restricted to Black Rock, a small hill in the northwestern parts of the field (Fig. 1.5). To the south of the KMF, rocks which are regarded as lateral equivalents of the Hotazel succession are locally developed, belonging to the Beaumont Formation (Beukes, 1983).

In the KMF, the Hotazel Formation is underlain by hyaloclastites, pillow and massive lavas of the Ongeluk Formation, and locally grades upwards into carbonate rock of the Moidraai Formation (Fig. 1.6, 1.7). The Hotazel succession consists of iron-formation interbedded with manganese ore in three conspicuous sedimentary cycles (Fig. 1.7). The transitions between iron-formation and manganese ore are generally gradational, consisting of very fine-grained, carbonate-rich hematite rock, previously described as hematite-lutite (Kleyenstüber, 1984). The lowermost manganese unit is the most economically viable, it is generally 20-25m thick but attains a maximum thickness of 45m in the Mamatwan Mine (Fig. 1.5, 1.6; see also Appendix I, Fig. A5), where open cast mining has proved feasible due to a combination of large reserves and marginally economic manganese ore-grades (38 wt% Mn). In the northernmost parts of the KMF, the thickness of the lower manganese unit decreases markedly (4-8m), but locally, grades are sufficiently elevated to permit profitable underground exploitation. The remaining two manganese units are of no economic significance, and only the uppermost unit has been mined on a very localised scale.

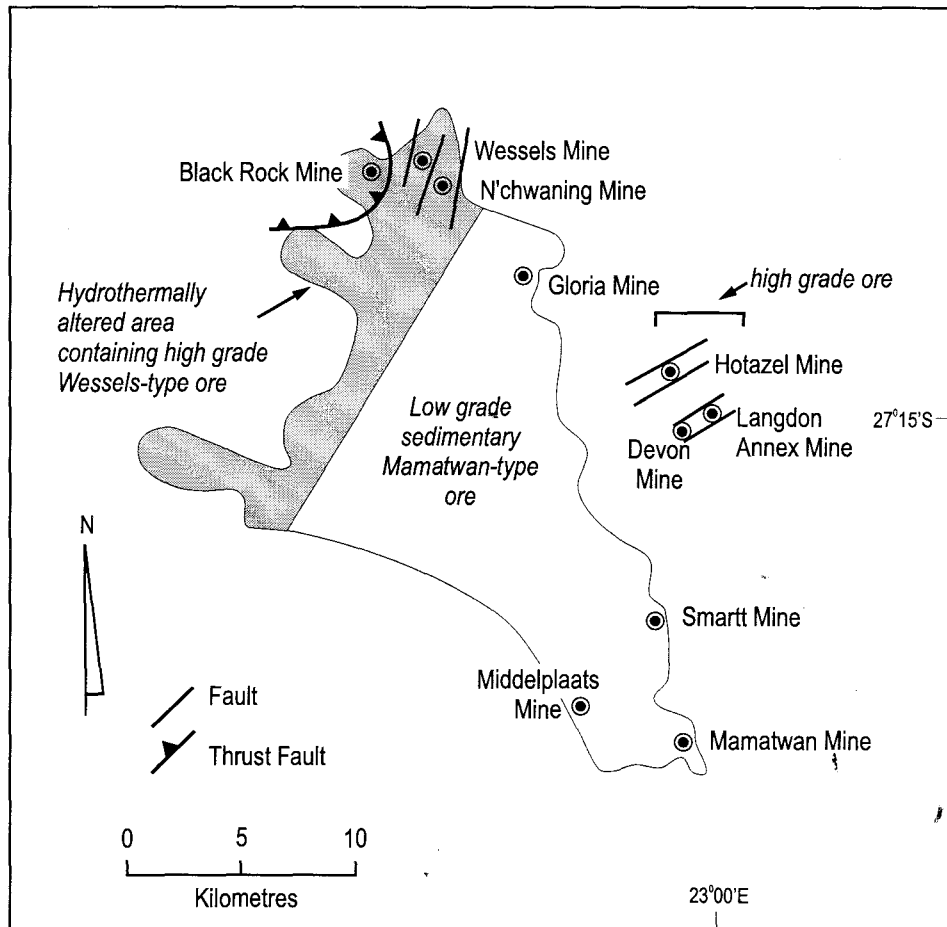
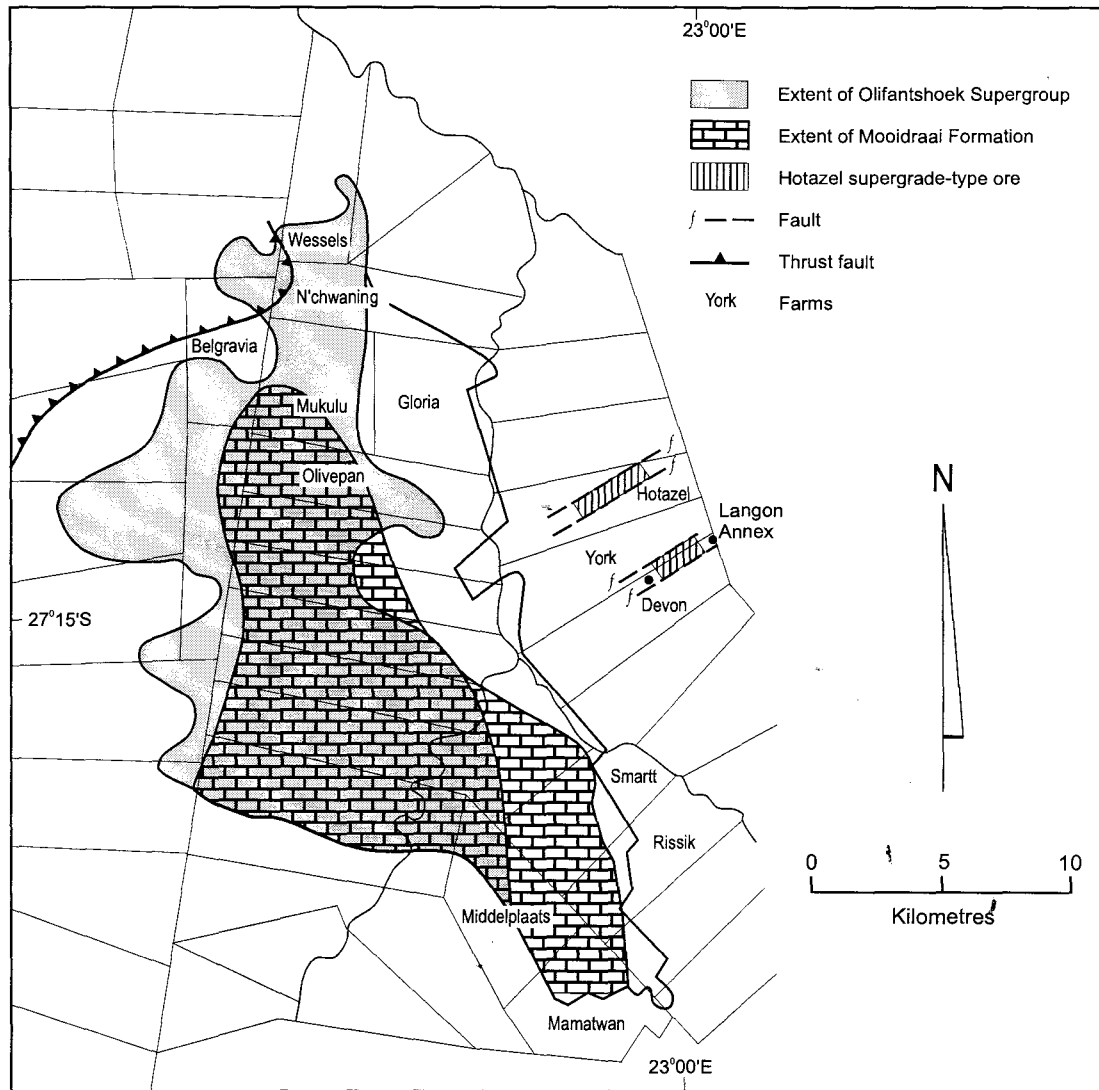


Figure 1.5. Locality map of the KMF showing major structural features, distribution of ore types and location of mines (modified after Nel et al., 1986). Note that Hotazel, Devon and Langdon Annex mines are located in graben structures developed off the KMF to the east.





**Figure 1.6.** Locality map of the KMF showing important structural features, farm localities and distribution of major lithostratigraphic units occurring stratigraphically above the Hotazel Formation (original map kindly supplied by SAMANCOR; reproduced from Astrup and Tsikos, 1998).

The Hotazel and Mooidraai Formations are unconformably overlain by interbedded red and black shales and quartzites of the Mapedi Formation of the Olifantshoek Supergroup (Fig. 1.6), while younger diamictite of the Late Carboniferous-Early Permian Karoo Supergroup is locally developed in the form of unconformable erosional relicts of glacial valleys. The strong petrographic similarities between the Mapedi Formation and the Gamagara Formation developed to the south of the KMF, in conjunction with structural data (Beukes and Smit, 1987), would support the placement of the Gamagara Formation in the lower parts of the Olifantshoek sequence.

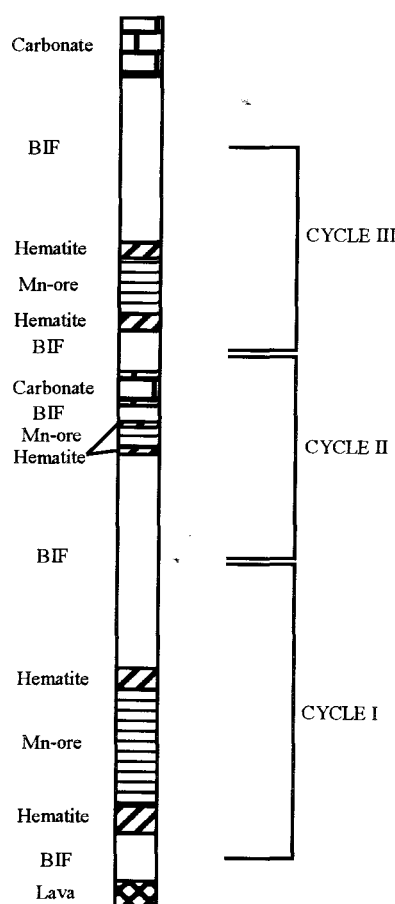


**Figure 1.7.** Simplified sketch of the stratigraphic column of the Voelwater Subgroup in the KMF (not to scale), displaying the characteristic threefold cyclicality of iron-formation and manganese ore in the Hotazel Formation (modified after Tsikos and Moore, 1997).

In earlier years, mining of manganese ore in the KMF concentrated primarily in the area around the town of Hotazel (Figs. 1.5, 1.6) where particularly high-grade manganese ore (~55 wt% Mn) occurs. Since the closure of the Hotazel mine, mining operations have been carried out in mainly two areas of the KMF, namely the southernmost and northernmost segments. The Mamatwan manganese mine is essentially the only major open-cast operation of low-grade ore from the southernmost part (Figs. 1.5, 1.6). In the northernmost portions of the KMF, underground exploitation of both low-grade and high-grade Mn ore is carried out in the farms Gloria and Wessels/N'chwaning respectively (Figs. 1.5, 1.6). Essentially all boreholes used in this study have been drilled in the above mine areas (see Appendix I, Fig. A1).

## **PART 2: PETROGRAPHY**

### **Chapter 2.1: Introduction**

#### **2.1.1. Background**

The composition and origin of mineral assemblages observed in iron-formations have been the objects of detailed investigations since the late 1930's - early 1940's, with the pioneer work of J.W. Gruner on the structure and chemical composition of various Fe-silicate minerals (Gruner, 1936, 1937, 1944a,b). Subsequently, many authors became involved in comprehensive research studies of the mineralogical composition of major world-class iron-formation occurrences from the Hamersley Group, Western Australia (Trendall, 1983), Lake Superior and Labrador Trough, USA/Canada (Morey, 1983; Gross and Zajac, 1983) and Transvaal Supergroup, South Africa (Beukes, 1983). Global research output reached a peak during the period 1970-85, and a decline was experienced thereafter, presumably as a result of a relative exhaustion of materials requiring detailed study.

The conspicuous lack of basic petrographic data from the Hotazel iron-formation represents a good example of the above-mentioned decline, particularly when one considers the emphasis that has been attributed to the mineralogical study of the manganese ores of the KMF (Nel, 1984; Kleyenstüber, 1984, 1985; Nel et al., 1986; Miyano and Beukes, 1987; Gutzmer and Beukes, 1996a). Tsikos (1994) and Tsikos and Moore (1997) have provided some preliminary information on the petrography of the Hotazel iron-formation, and this dataset is substantially expanded in the following chapters in order to include the mineralogical and textural characteristics of all major iron-formation lithotypes encountered in the KMF.

#### **2.1.2. Sample selection, methods and macroscopic observations**

Petrographic studies were conducted by means of standard microscopic investigations on thin and polished section sample material under transmitted and reflected light respectively. Sections were all cut across banding, and were selected from the majority of quartered-core samples used in

whole-rock geochemical investigations presented in PART 3 of this thesis (see also Appendix I). Powdered samples corresponding to these sections were also examined by means of qualitative x-ray diffraction (XRD) analysis, in order to determine the bulk mineralogical composition of the samples. Combination of petrographic microscope and XRD studies allowed the identification of all major mineral constituents encountered in the iron-formation samples. In very few cases, mineral chemical data are provided as obtained by means of electron microprobe techniques (ankerite) and x-ray fluorescence analyses of mineral separates (acmite).

Essentially all samples studied, including those of the Moodraai Formation, are indistinguishable in terms of two features, that is, their particularly fine-grained size and rhythmic mm- to cm-scale banding. Preliminary macroscopic identification of individual minerals was possible for those which show obvious properties such as magnetite (magnetic susceptibility), hematite (colour), chert (hardness) and carbonates (reactivity in the presence of weak HCl). Other minerals, especially Fe-silicate phases, were not visible with the naked eye, though the likely presence of the Fe-silicate mineral greenalite could be inferred by means of the strong green colouration in many of the samples.

The above observations facilitated the crude subdivision of the selected samples in essentially three iron-formation groups (Plate 1), namely:

- greenish-grey iron-formation, containing large amounts of chert, magnetite, carbonates, and lesser Fe-silicates (e.g. greenalite). This iron-formation predominates in the southernmost part of the KMF, appears to have suffered very mild regional metamorphic effects (Nel et al., 1986; Tsikos and Moore, 1997) and has been hereby assigned the term *pristine iron-formation*;

- reddish-white iron-formation, comprising abundant hematite and magnetite, chert and carbonate. This type of iron-formation is seen in certain boreholes from the northernmost parts of the KMF and shows some important macroscopic dissimilarities with pristine iron-formation. The most important of these is the conspicuous presence of secondary hematite, replacing primarily pre-existing magnetite bands/laminae. This feature indicates a certain degree of oxidation and has prompted the tentative term *oxidised iron-formation* as descriptive of this type;

- greyish-red to metallic red iron-formation, characterised by the abundance of alternating bands of microcrystalline hematite and chert and in some cases even massive hematite alone. This

is the second major lithotype observed in the northernmost KMF and exhibits lack of carbonate material and substantially reduced band-to-band thicknesses compared to the previous types. Mineralogical and petrographic data from oxide-rich, carbonate-free hydrothermally altered manganese-ore developed in the same area (Beukes et al., 1995; Gutzmer and Beukes, 1995, 1996a) suggest that this type would tentatively correspond to an *altered iron-formation*.

The petrographic signatures of the above three groups of iron-formation are discussed separately in the following sections. The main petrographic signatures of the Mooidraai carbonate formation will be discussed briefly in the section dealing with pristine iron-formation.

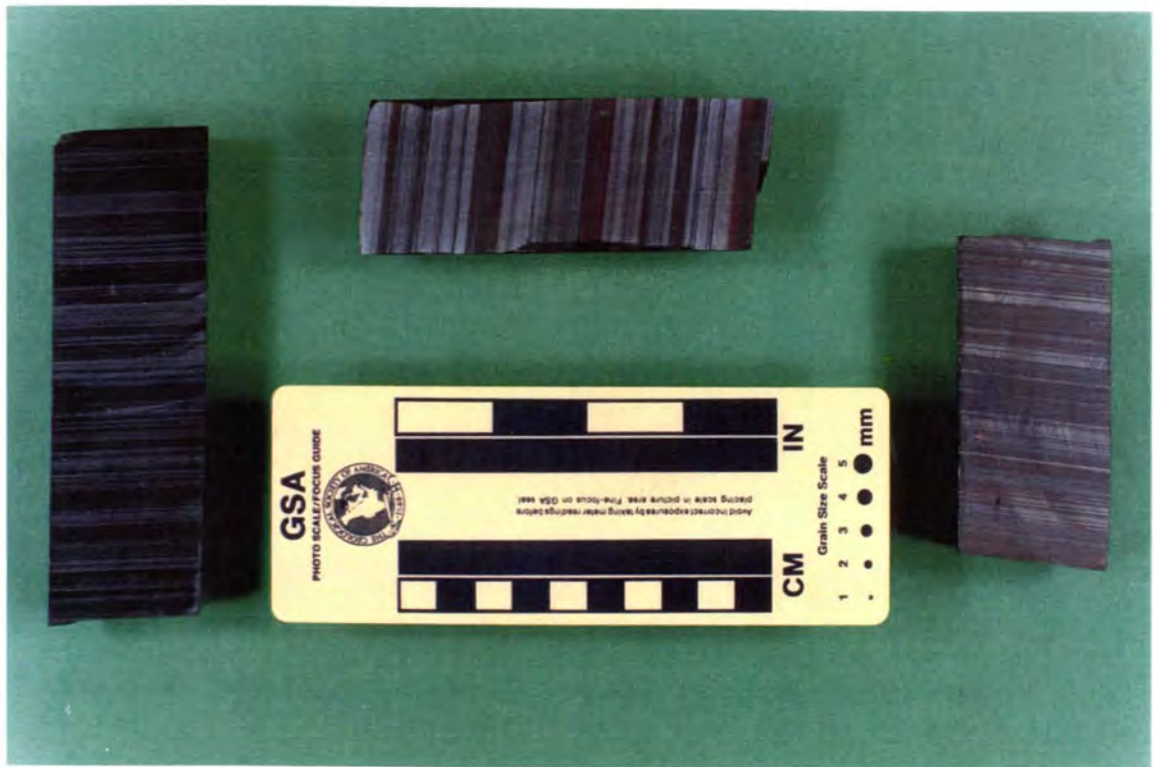


**Plate 1.** Representative half-core samples of major iron-formation types investigated in this thesis. From left to right: *pristine type* (chert-greenalite-magnetite-carbonate), *oxidised type* (chert-hematite-carbonate), *altered type* (chert-hematite).

## Chapter 2.2: Mineralogy and textures of the Hotazel iron-formation

### 2.2.1. Bulk mineralogical composition

Table 2.1 presents a summary of the mineralogical compositions of the various types of iron-formation investigated in this study. The majority of mineral phases identified are characteristic of a diagenetic/very low-grade metamorphic environment, as described in detail in many scientific papers (e.g. James, 1954; French, 1968, 1973; Klein, 1978, 1983; Klein and Bricker, 1977; Floran and Papike, 1975, 1978). Abundant hematite is known to occur primarily in iron-formations that have suffered late oxidation effects, while locally developed acmite indicates some sort of late metasomatic processes due to the presence of Na-enriched hydrothermal fluids (Grout, 1946; McSwiggen et al., 1994).

**Table 2.1:** Bulk mineralogical composition of the Hotazel iron-formation.

Mineral group	Mineral component	Pristine IF	Oxidised	Ca/Mn-rich units	Altered IF
	Chert (quartz)	XXX	XXX	X	XXX
Oxides	Magnetite	XXX	XX		
	Hematite	X	XXX	XX	XXX
	Braunite			XX	
Carbonates	Calcite	XXX	X	XXX	
	Dolomite-ankerite	XX	XXX		X
	Kutnahorite	X		XXX	X
	Rhodochrosite	X	X	XX	
	Siderite	X			
Silicates	Greenalite	XX	X		
	Minnesotaite/talc	XX	X	XX	X
	Stilpnomelane	XX		X	
	Riebeckite	X		X	
	Acmite-augite				XX
	Andradite				X
	Friedelite			X	
Sulphides	Pyrite	X	X	X	

**Key:** XXX: Abundant component (modal abundance >20% in the majority of samples)

XX: Common component (modal abundance >5% - occasionally abundant)

X: Minor-trace component (microscopically observed - usually undetectable with XRD)

In addition, minerals that are major or common constituents in the interbedded manganese ore-units are shown in Table 2.1, as they also occur in transitional, Ca-Mn-enriched lithologies of the Hotazel Formation.

### 2.2.2. Diagenetic - very low-grade metamorphic paragenesis

The pristine iron-formation is developed in the southernmost parts of the KMF (boreholes R59, R63, R65, R70 and SM31), as well as in borehole GL26 from the northern portions of the field (see Appendix I, Figs. A1,A2,A4). The iron-formation is generally well-banded, with individual bands ranging from 1mm to 1cm in thickness (Plate 1). Banding is rhythmic with sharp and/or diffuse contacts, and becomes more transgressive, ribbon- and pillow-like (Beukes, 1980a,b) as the carbonate content of the samples increases. Classic examples of soft-sediment deformation (SSD) structures (Gross, 1972) are commonly seen in samples with high amounts of carbonate material.

Petrographic variations across the stratigraphy based primarily on colour and nature of banding, permit the distinction of a number of iron-formation subfacies (Fig. 2.1). In relation to the interbedded manganese ore-units these subfacies are (stratigraphically from bottom to top):

- (i) oxide-rich iron-formation, developed below the lowermost manganese ore-unit and containing abundant cryptocrystalline (“dusty”) hematite and microcrystalline magnetite;
- (ii) green, well-banded, carbonate-poor, greenalite-bearing iron-formation, developed between the lowermost and middle manganese units; and:
- (iii) grey to greenish-grey, carbonate-rich iron-formation. This is developed in the remaining portion of the Hotazel succession and contains abundant SSD textures.

The transition between the carbonate-poor and carbonate-rich subfacies is fairly abrupt and occurs through a narrow, dark, poorly-banded cherty rock, 8-10 metres below the middle manganese unit. Also a thin, hematite-bearing calcitic unit occurs between the middle and uppermost Mn ore-units (Fig. 2.1), resembling strongly the transitional rock between iron-formation and Mn ores.

Although the above observations apply to the Hotazel intersections from the southernmost KMF,



some important differences are seen in iron-formation from borehole GL26. The Hotazel succession in the latter borehole shows substantially reduced overall stratigraphic thickness. Relative thickness relations between the iron-formation and manganese units in borehole GL26 are also strikingly dissimilar to those in the southernmost KMF, with the middle manganese unit located in close proximity to the lowermost, rather than the uppermost, manganese unit (see Appendix I, Fig. A5). Owing to these thickness changes, the thickness of carbonate-poor iron-formation in borehole GL26 is markedly reduced, relative to that observed in the southern KMF.

#### 2.2.2.1. *Silicates*

The silicate mineralogy of pristine Hotazel iron-formation comprises large amounts of microcrystalline quartz and the Fe-silicate minerals greenalite, minnesotaite, stilpnomelane and riebeckite (Fig. 2.1). All these minerals have been described from classic occurrences of essentially unmetamorphosed iron-formations of North America (French, 1973; Zajac, 1974; Klein, 1973, 1974, 1978; Floran and Papike, 1975, 1978; Klein and Fink, 1976; Lesher, 1978), Australia (Trendall and Blockley, 1970; Gole, 1980; 1981; Klein and Gole, 1981; Ewers and Morris, 1981; Miyano and Miyano, 1982; Miyano and Klein, 1983a) and South Africa (Beukes, 1973, 1978, 1983, 1984; Miyano and Beukes, 1984; Beukes and Klein, 1990). Characteristic of Fe-silicate minerals from the majority of these iron-formations is their particularly fine-grained habit which frequently hinders confident identification under the petrographic microscope.

Quartz is abundant in all iron-formation samples (up to 50% modal abundance) and is also present in small amounts in the Mooidraai Formation. It exhibits its characteristic microcrystalline or "cherty" appearance seen in most unmetamorphosed iron-formations worldwide. Quartz forms characteristic banded assemblages along with a number of mineral phases such as greenalite, minnesotaite, magnetite and ankerite (Plates 2c, 3b). Variations in the grain size of quartz across the stratigraphy are negligible, although carbonate-rich samples appear to contain somewhat coarser varieties than carbonate-poor ones do. Quartz grain-boundaries commonly exhibit sutured patterns, an indication of crystallisation under very low-grade metamorphic conditions.

Greenalite in the Hotazel iron-formation occurs in the form of very fine, green disseminated flakes

in association with microcrystalline chert, magnetite and to a lesser extent carbonates (Plate 2a). Samples rich in greenalite display a characteristic green colour to the naked eye. X-ray diffraction confirmed the presence of greenalite in most samples of the carbonate-poor iron-formation, by showing the characteristic  $d\text{\AA}$  value at 7.2 in the patterns (Blake, 1965; Zajac, 1974). Carbonate-rich iron-formation and Mooidraai limestone samples contain very little or no greenalite, while oxide-rich iron-formation may occasionally contain thin laminae of chert-greenalite-(minnesotaite) assemblages.

Minnesotaite develops in its typical textural form of needle-like masses that are arranged as sprays and "bow-tie" textures, in a matrix of microcrystalline quartz (Plates 2b, 3c). The distribution of minnesotaite is not restricted in any specific portion of the Hotazel stratigraphy. It may occur in bands in close proximity to greenalite-rich assemblages, as well as in carbonate-rich iron-formation where chert-ankerite bands may progressively "blend" with minnesotaite-bearing chert (Plate 3c). Small amounts of minnesotaite are also seen in chert admixtures in certain samples from the Mooidraai Formation. The cross-cutting textural character of minnesotaite in relation to other coexisting minerals suggests that the former is likely to have grown at a late diagenetic stage, and possibly at the expense of pre-existing phases such as greenalite. The distinctive textural signature of minnesotaite under transmitted light permits its comfortable identification, in conjunction with the characteristic reflection of minnesotaite-rich samples at  $d\text{\AA}=9.6$  in XRD patterns.

Stilpnomelane is a common constituent of carbonate-rich iron-formation samples, but occurs to a very minor extent in the Mooidraai Formation. It develops in very close association with calcite, in the form of brown needles arranged in an ascicular fashion (Plate 3a). The brown variety of the mineral suggests that all iron present in the lattice is in the ferric form, which would permit the use of the term "ferristilpnomelane" (Klein, 1983). Stilpnomelane growths are also found in the calcite-rich unit between the middle and uppermost manganese units, again in close textural association with sparitic calcite. Although the strong similarity between biotite and stilpnomelane commonly inhibits positive identification of the latter, XRD patterns of Hotazel samples containing elevated amounts of the calcite-stilpnomelane association show the characteristic reflection of stilpnomelane at  $d\text{\AA}=12$ .

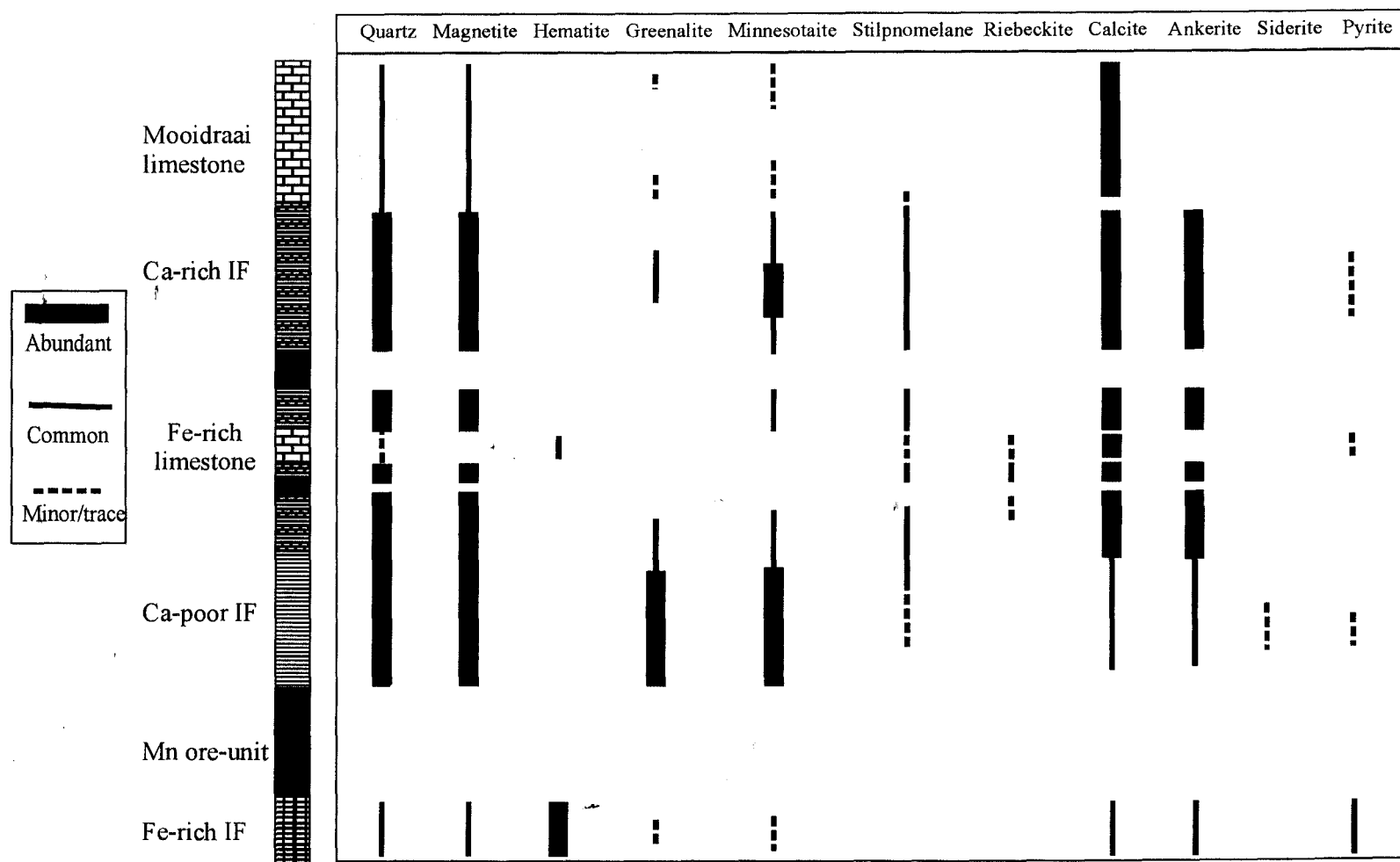


Figure 2.1. Distribution of minerals in pristine iron-formation and limestone across the Hotazel/Mooidraai stratigraphy from the southernmost and central parts of the KMF

Riebeckite is a rare constituent in the Hotazel iron-formation and is found in narrow chert-rich zones within the carbonate-rich iron-formation (Plate 2c). Riebeckite-bearing chert bands commonly contain stylolites, an indication of dissolution processes involving Na-rich diagenetic fluids. Riebeckite is also found in the narrow carbonate unit in association with calcite and stilpnomelane, and although it is easily identifiable due to the characteristic blue pleochroism and needle-like textural habit under the microscope, it was rarely detectable by means of the XRD technique due to its very low modal abundance.

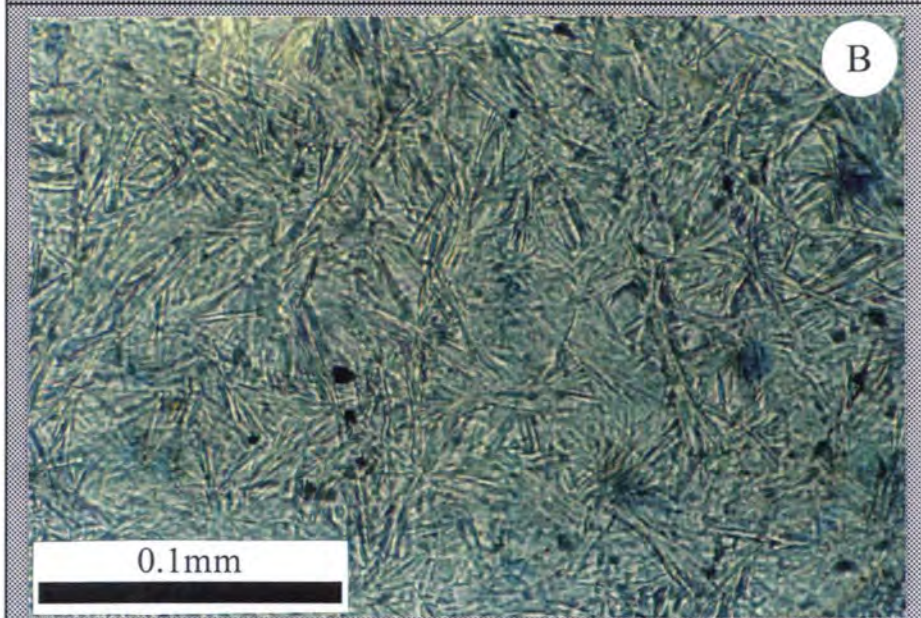
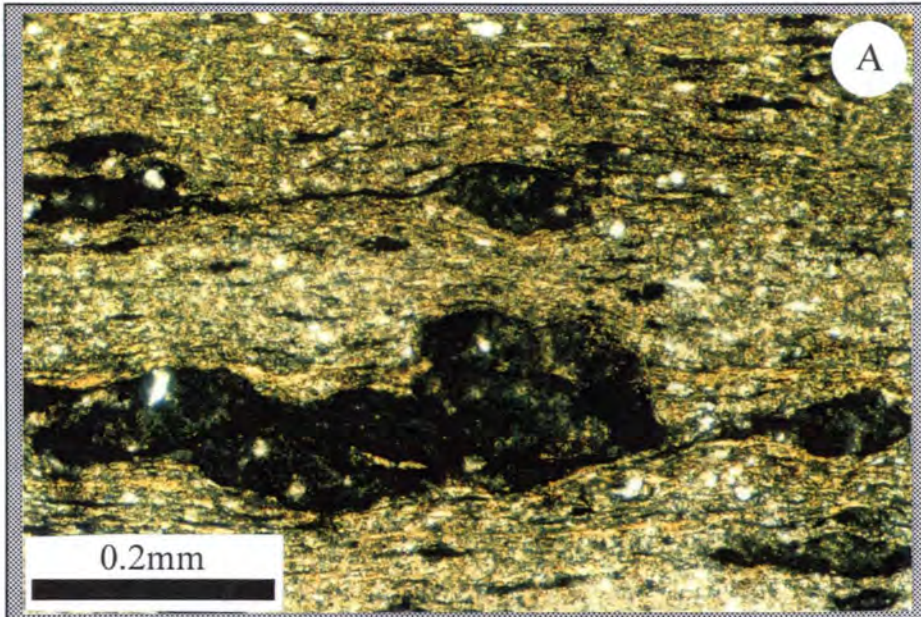
#### 2.2.2.2. Carbonates

Carbonate minerals are common constituents in unmetamorphosed iron-formations. Despite the striking resemblance between individual carbonate phases under the petrographic microscope, it appears that members of the dolomite-ankerite series are the most common carbonate species. Ankerites have been reported from several iron-formation occurrences such as the Sokoman, Biwabik and Gunflint iron-formations of USA/Canada (French, 1968; Floran and Papike, 1975, 1978; Klein, 1974; Zajac, 1974; Klein and Fink, 1976; Lesher, 1978), the Kuruman and Griquatown iron-formations of South Africa (Klein and Beukes, 1989; Beukes and Klein, 1990) and the Marra Mamba and Brockman iron-formations of Western Australia (Ewers and Morris, 1981; Klein and Gole, 1981). Siderite appears to be an equally common constituent, though one should always be aware of the difficulty in determining the exact identity of iron-bearing carbonates, particularly in the absence of mineral-chemical data. On the other hand, pure calcite is rather uncommon in iron-formations, and it has only been reported as a major constituent from the Marra Mamba iron-formation, Western Australia (Klein and Gole, 1981).

Pristine varieties of the Hotazel iron-formation contain large amounts of carbonate, to a degree which is rather unusual for a Palaeoproterozoic iron-formation of this kind. Modal abundances of total carbonate commonly exceed the value of 20%, a feature which renders the Hotazel Formation as particularly carbonate-enriched. XRD powder patterns of whole-rock samples suggest that the minerals present are variable mixtures of two carbonate minerals, namely calcite and ankerite.

**Plate 2.** Mineral occurrences and textures of carbonate-poor, pristine iron-formation (all photomicrographs are taken under transmitted light, unless otherwise stated). **A:** Very fine-grained, greenalite-rich chert band. Greenalite flakes are barely visible under this magnification, but the green colouration of the sample is conspicuous. Dispersed white blebs are minute ankerite grains, whereas dark microgranules possibly correspond to amorphous siderite. Plain-polarized light. **B:** Minnesotaite, exhibiting its characteristic sprays and “bow-tie” textures in a matrix of microcrystalline chert. Plain-polarized light. **C:** Chert band rich in disseminated riebeckite needles. Riebeckite-bearing bands of this kind are very rare in the Hotazel iron-formation and occur in association with stylolites, immediately above and below the middle Mn-unit (see also Fig. 2.1). Plain-polarized light.





Textures suggest that the two carbonates are not closely associated. Calcite forms primarily on the margins of magnetite-rich laminae, and shows a very strong paragenetic affiliation with ascicular stilpnomelane (Plate 3a). It develops very fine-grained, massive mosaics and commonly exhibits polysynthetic twinning. Ankerite, on the other hand, forms discrete bands in a matrix of microcrystalline quartz (Plates 3b, 3c). The mineral commonly exhibits perfect rhombohedral habit with clear margins and rather cloudy interiors. The ankerite rhombohedra “float” in the chert matrix, indicating effects of diagenetic recrystallisation and/or perhaps replacement of pre-existing minerals (Plate 3b). The composition of ankerite as determined by means of the electron microprobe technique (see Table 2.2) approximates that of ankerites in other iron-formations, such as the Brockman iron-formation of Western Australia (Kaufman et al., 1990), i.e:

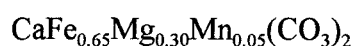


**Table 2.2.** Mean-standard deviation of 12 microprobe analyses of ankerite from pristine iron-formation.

<i>n</i> =12	Mean	St. dev.
CaO	30.07	1.51
FeO	14.94	0.83
MgO	7.33	0.80
MnO	1.09	0.32
(CO <sub>2</sub> *)	46.57	1.53

\*CO<sub>2</sub> by difference

Ankerite and calcite occur in concentrations detectable by XRD in the carbonate-rich iron-formation, and are present in much lesser amounts in the carbonate-poor and oxide-rich iron-formation. In the narrow carbonate unit, calcite is effectively the only carbonate species present, accounting for approximately 70-75% of the rock.

The Mooidraai samples are essentially calcitic in composition, a feature which is in contrast to previous descriptions of the rock as a dolomite (Beukes 1983). Neither XRD data, nor bulk-rock geochemical analyses of the ten selected Mooidraai samples (Appendix III) would suggest the presence of any dolomitic carbonate in the Mooidraai Formation. On these grounds, one could assume that dolomitisation of the Mooidraai Formation may have characterised only certain parts

of the KMF, and particularly the southernmost portion where earlier observations were made.

Siderite is conspicuously absent from the Hotazel Formation. The only evidence that would suggest the likely existence of small amounts of siderite in iron-formation samples are microgranular features observed in greenalite-rich samples of carbonate-poor iron-formation (Plate 2a). Similar microgranules have been observed by Klein and Beukes (1989) in the Kuruman iron-formation, South Africa, and are believed to be sideritic in composition. However, the particularly small size, cryptocrystalline nature and erratic presence of microgranules in the Hotazel samples did not allow the positive identification of siderite, neither in XRD diffraction patterns, nor under the petrographic microscope.

#### 2.2.2.3. Oxides and sulfides

Magnetite is, besides quartz, the most common constituent in all iron-formations of the world. It occurs as medium-grained, well crystallised, sub- to euhedral grains arranged in essentially monomineralic bands/laminae, and also as dispersed grains in chert/Fe-silicate/carbonate mineral assemblages. The similarity between the grain size and frequently well-developed habit of magnetite with those of coexisting carbonates, suggests a potential co-genetic history for both components in the diagenetic/metamorphic environment. Theories regarding the genesis of the abundant magnetite in iron-formations vary between those who propose recrystallisation of magnetite at the expense of a "hydromagnetite" precursor (e.g. Gross, 1973; Dimroth and Chauvel, 1973; Eugster and Chou, 1973; Klein, 1974, 1978; Klein and Bricker, 1978; Leshner, 1978; Klein and Gole, 1981; Mel'nik, 1982) and those who favour a replacement origin at the expense of other minerals such as greenalite, ankerite or other Fe-oxides/hydroxides (e.g. hematite). The observations of Klein and Fink (1976) on cross-cutting textural relations between magnetite and other coexisting minerals from the Sokoman iron-formation are at least one indication against the replacement origin of magnetite.

Hematite is a rather uncommon constituent in iron-formations unless the iron-formation has suffered late oxidation effects. In the cases where hematite has been described as a primary component, it occurs in the form of microbands/laminations and as granules and irregular bleb-like



masses (French, 1973; Dimroth and Chauvel, 1973; Klein and Fink, 1976; Klein 1978). The sedimentary precursors to the presently observed crystalline occurrences are probably some kind of ferric hydroxide  $[\text{Fe}(\text{OH})_3]$ , or hydrous ferric oxide ( $\text{Fe}_2\text{O}_3 \cdot n\text{H}_2\text{O}$ ) (French, 1973; Klein and Bricker, 1977; Leshner, 1978; Mel'nik, 1982).

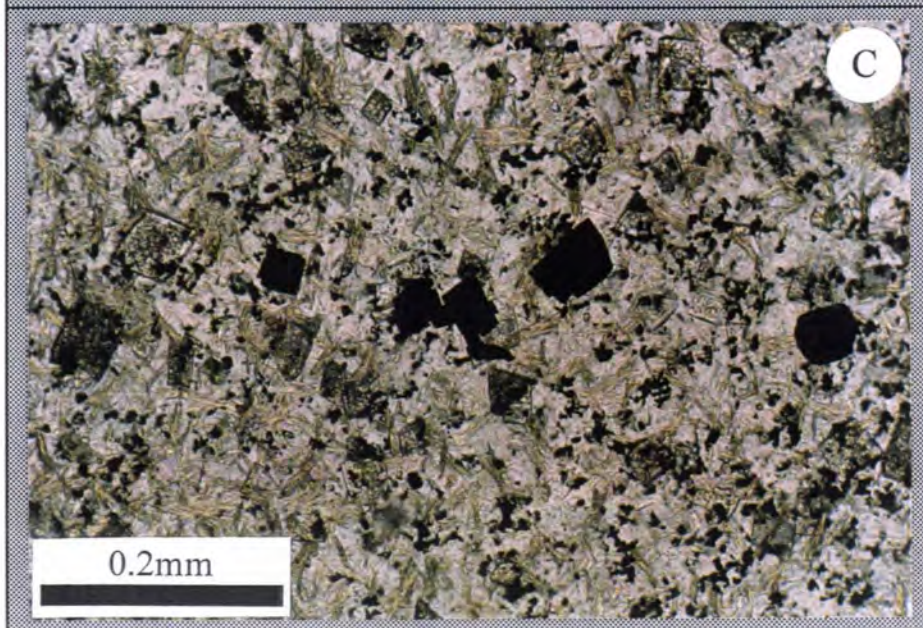
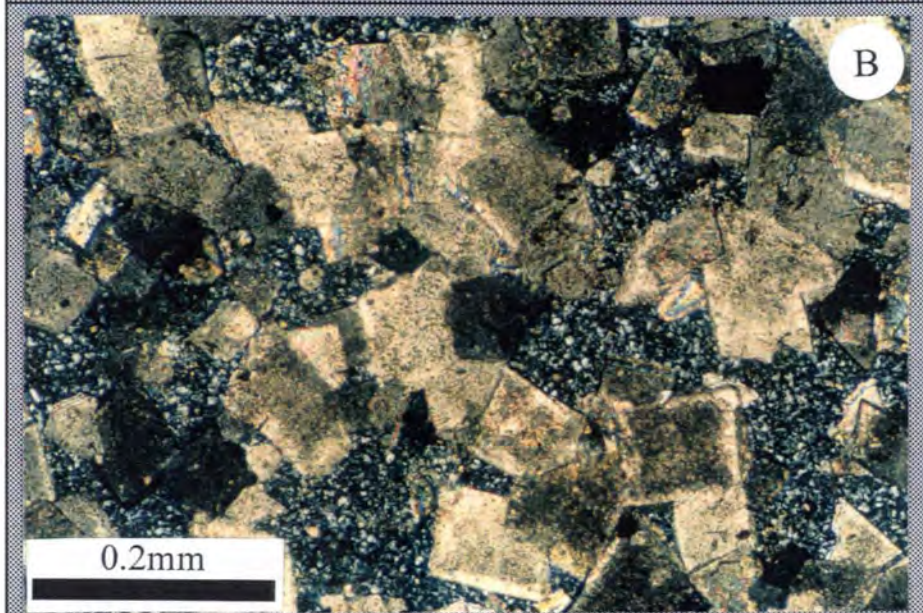
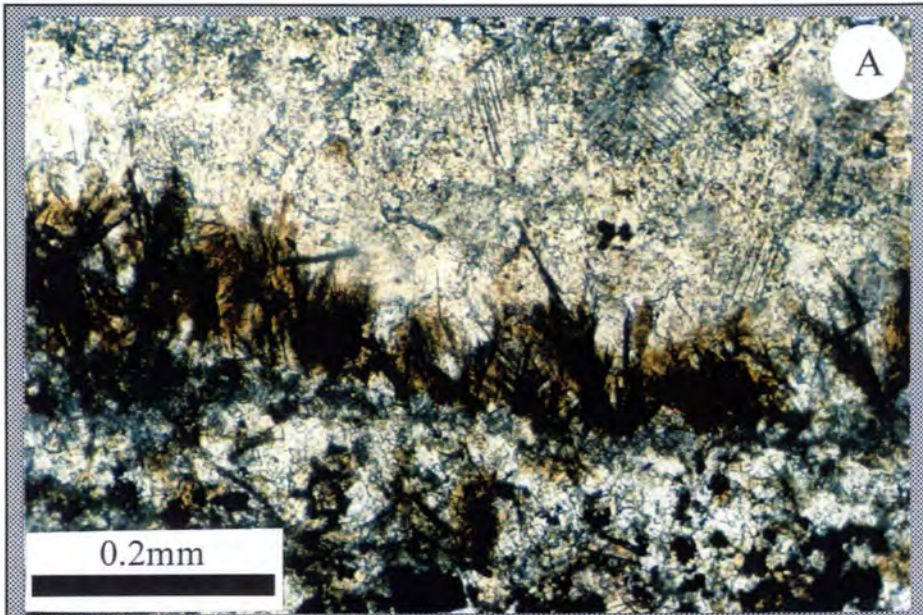
Magnetite is an abundant component throughout the Hotazel iron-formation stratigraphy in the southernmost KMF (Fig. 2.1 and Plate 3a), while hematite is practically absent. Magnetite occurs primarily as distinct bands/laminae alternating with chert-Fe-silicate and chert-ankerite bands in the iron-formation, and with massive calcite of the Mooidraai Formation. Individual magnetite grains are usually subhedral and may contain minute inclusions of a brighter mineral under reflected light, which is potentially an earlier ferric oxide (hematite?) precursor. Greenalite-rich, carbonate-poor samples occasionally contain small amounts of magnetite, while oxide-rich iron-formation contains significant amounts of disseminated magnetite grains in a groundmass consisting of chert impregnated with "dusty" hematite. Apart from the oxide-rich iron-formation, "dusty" hematite is also seen in the narrow carbonate unit, as well as in all transitional units between iron-formation and manganese ore, in close association with carbonate.

Pyrite is a very minor constituent in the Hotazel iron-formation, in concert with the majority of iron-formations of the world (e.g. French, 1968; Klein and Fink, 1976; Kleih 1978; Leshner, 1978; Gole, 1980; Klein and Gole, 1981). It shows no specific distribution and it may be seen in small, usually anhedral grains throughout the stratigraphy, with perhaps a higher frequency in the lowermost oxide-rich portion of the Hotazel Formation where it is occasionally developed in conspicuous subhedral grains, often visible with the naked eye.

#### 2.2.2.4. Petrogenetic constraints

Klein (1983) compiled mineralogical data from various iron-formations worldwide that have suffered different degrees of metamorphism, and placed them in a general paragenetic scheme corresponding to increasing grades of progressive metamorphism (Fig. 2.2). Amongst the mineral phases used in this scheme, minerals such as quartz, Fe-oxides and carbonates appear to have very little or no significance as indicators of metamorphic grade. On the other hand, Fe-silicate minerals

**Plate 3.** Mineral occurrences and textures of carbonate-rich, pristine iron-formation (all photomicrographs are taken under transmitted light, unless otherwise stated). **A:** Ascicular growths of ferristilpnomelane along the contact between a magnetite-carbonate band (bottom), and a massive calcite band (top). Note the twinning in some of the calcites. Plain-polarized light. **B:** Relatively coarse ankerite rhombohedra in a matrix of chert. Note the clear outer rim and cloudy interior of the ankerite grains. Cross-polarized light. **C:** Sprays and “bow-ties” of minnesotaite in a band consisting of chert and disseminated rhombohedral ankerite. Opaque phase is magnetite. Plain-polarized light.





are particularly useful indicators of grades of metamorphism, and have thus been widely used in constraining the conditions of the environment of formation of iron-formation mineral assemblages (e.g. Klein, 1966, 1973, 1974, 1978; Immege and Klein, 1976; Klein and Fink, 1976; Klein and Gole, 1981; Gole 1980, 1981; Gole and Klein, 1981; Miyano, 1982, 1987; Miyano and Klein, 1983b, 1989; Miyano and Beukes, 1984; Miyano et al., 1987).

On the basis of the observations of Klein (1983), the pristine iron-formation assemblages would have formed under conditions of diagenesis to very-low grade metamorphism (Fig. 2.2). In particular, the complete absence of amphibole (grunerite-cummingtonite) suggests that conditions of formation did not exceed those of a very low-greenschist facies environment. Information regarding potential chemical reactions that led to the formation of these assemblages is highly dependent upon the nature of the sedimentary precursors. For example, if the Fe-rich precursor materials were hydrous compounds of iron present primarily in the ferrous form (i.e. "hydromagnetite"), then simple dehydration reactions involving no major change in the valence state of iron would, in principle, have produced the observed mineralogy. On the other hand, should the iron-precursors had been in the ferric form, subsequent reactions in the diagenetic environment would have required the reduction of most of the iron into the ferrous state, in the form of compounds such as Fe-silicates (e.g. greenalite), carbonates (e.g. ankerite) or magnetite. Such diagenetic reactions have been described in great detail from modern sedimentary environments where organic carbon coexists in association with higher oxides of Fe and Mn deposited at the sediment-water interface (e.g. Fröelich et al., 1979). A more detailed account of such processes will be presented in PART 4 of this thesis, which deals with the stable isotope geochemistry of the Hotazel Formation.

### 2.2.3. Oxidised and alteration assemblages

Oxidised and altered iron-formation are found in the northernmost portions of the KMF. Relative thickness relations between the iron-formation and the three interbedded Mn units compare very well not only with the altered and oxidised lithologies, but also with the Hotazel succession as revealed in borehole GL26 containing pristine iron-formation (see Appendix I, Fig. A5). Altered iron-formation is developed essentially throughout the Hotazel stratigraphy in boreholes N12D,

		GRADE OF METAMORPHISM			
		LOW	MEDIUM		HIGH
DIAGENETIC	Early	BIOTITE ZONE	GARNET ZONE	STAUROLITE - KYANITE AND KYANITE ZONE	SILLIMANITE ZONE
	Late				
		Greenalite			
		Stibnomelane			
		Ferriannite			
		Talc - minnesotaite			
		Ripidolite			
			Riebeckite		
			Grunerite   cummingtonite		
				Almandine	
				Pyroxene	
					Fayalite

**Figure 2.2.** Variations in the silicate mineralogy of iron-formations as a function of metamorphic grade (modified after Klein, 1983). Hatched area defines the stability limits of mineral assemblages from pristine Hotazel iron-formation.

MK3I, MK2G and MK2H, as well as in the uppermost iron-formation unit of boreholes N91B, BEL4C and BEL7A above the uppermost Mn ore-unit (Appendix I, Fig. A3, A4). Characteristic in all these intersections is the monotonously alternating bands/laminae of microcrystalline hematite and reddish-grey chert at scales not exceeding 5mm. At the stratigraphic top of certain boreholes (i.e. N12D, MK2H) the iron-formation occurs in the form of massive, very fine-grained banded hematite, while immediately below the contact with the unconformably overlying Olifantshoek beds, dark-red hematite-rich zones of thicknesses of a few tens centimeters develop,

suggesting admixtures of manganese oxide and/or clay in the rock. Below the uppermost manganese unit and between the middle and lowermost manganese units, narrow lithologic units are seen with characteristic creamy-white bands which, as will be shown in the following section, contain acmite as a major component. Also, below the lowermost manganese unit, iron-formation similar to the oxide-rich pristine type occurs, though totally devoid of magnetite.

Oxidised iron-formation is developed in three boreholes, i.e. N91B, BEL4C and BEL7A, below the uppermost manganese ore-unit (Appendix I, Fig. A3). The rock contains thin, mm-scale magnetite and/or hematite-rich laminations, alternating with relatively thick (0.5-3cm), whitish, mixed chert-carbonate bands. The abundance of hematite varies across the stratigraphy, and it decreases drastically in the lowermost parts of the Hotazel succession below the lowermost manganese ore-unit. Oxidised iron-formation intersections exhibit some similarities to corresponding intersections containing pristine iron-formation described earlier, as rock rich in dusty hematite (equivalent to oxide-rich iron formation) is developed below the lowermost Mn-horizon, and Ca-rich transitional units occur not only between the middle and uppermost units but also above the latter as well.

#### *2.2.3.1. Altered iron-formation paragenesis*

The main characteristic of samples of altered iron-formation is the almost complete absence of magnetite, carbonate and silicate minerals (e.g. greenalite, minnesotaite, stilpnomelane) as observed in pristine iron-formation. The lack of magnetite and silicates is attributed to processes of complete oxidation of a pre-existing mineral assemblage presumably containing one or more of the above phases, whereas carbonates appear to have been leached out entirely. Hence, binary mixtures of microcrystalline quartz and microlaths of hematite are essentially the only abundant constituents in the altered iron-formation samples.

Chert-rich bands in altered iron-formation contain minute inclusions of hematite, whereas the quartz is particularly fine-grained and exhibits a cloudy appearance in transmitted light. Although the bands are essentially bimineralic, "ghost" textures indicative of pre-existing mineral phases can be clearly seen in many of the samples. The most characteristic of these are rhombohedral

outlines, blebs and irregular masses resembling strongly the habit of carbonate minerals, such as calcite and ankerite seen in pristine iron-formation (Plates 4a,b,c). Although the altered rock is totally devoid of carbonate constituents in the majority of samples, the above textural features constitute ample evidence that the pre-alteration precursor materials must have been characterised by mineralogical compositions comparable to iron-formation from the southern parts of the KMF.

Hematite-rich bands are essentially monomineralic, with only minor admixtures of interstitial chert being present. The hematite occurs in its characteristic fine-grained, lath-like habit, with randomly arranged microlaths confined within sharp, thin bands/laminae. Banded, massive hematite samples containing very little quartz are developed in the uppermost parts of the stratigraphy in certain boreholes (i.e. N12D, MK2H), indicating locally complete dissolution and remobilisation of any pre-existing silica compounds.

As mentioned earlier, altered iron-formation is almost totally devoid of silicate and carbonate minerals which characterise the pristine iron-formation. The exceptions comprise some very localised occurrences of small amounts of manganiferous carbonate (Mn-calcite, kutnahorite) and talc immediately above and below the lowermost Mn ore-unit, in co-existence with massive hematite-chert assemblages (Fig. 2.3). Also, samples in the proximity to the Olifantshoek unconformity at the top of the Hotazel succession contain appreciable amounts of very fine-grained Mn-oxide (braunite) and muscovite.

With regard to silicate minerals, notable is the occurrence of acmite in narrow banded units immediately below the uppermost Mn ore-unit as well as between the middle and lowermost Mn units (Fig. 2.3). The mineral occurs in the form of whitish-yellow bands consisting of a groundmass of very-fine grained, blade-like crystals of acmite, alternating with essentially pure hematite bands. These bands contain essentially no other mineral constituents besides admixtures of hematite and, occasionally, minor to trace amounts of quartz and andradite. The acmite appears to have replaced polymineralic assemblages, as the grain size of acmite varies slightly depending on pre-existing textures. Coarser varieties are seen in bleb-like features which potentially correspond to pre-existing carbonate-grains, whereas fine-grained acmite groundmass is developed at the expense of presumably earlier cherty material. In certain instances, veins and

irregular masses consisting of acmite and quartz are seen in samples of altered iron-formation (i.e. borehole MK2H), indicating that the acmite has probably formed subsequent to the development of the chert-hematite assemblage (Plate 4d). Chemical analyses of hand-picked chips of bands consisting almost entirely of fine-grained acmite, indicate compositions very close to the pure Na-end member of the aegirine-augite series (Table 2.3).

**Table 2.3.** X-ray fluorescence chemical analysis of acmite separate from sample MK3I-10.

	wt%
SiO <sub>2</sub>	51.35
TiO <sub>2</sub>	0.03
Al <sub>2</sub> O <sub>3</sub>	0.45
Fe <sub>2</sub> O <sub>3</sub>	33.45
MnO	0.98
MgO	0.08
CaO	0.17
Na <sub>2</sub> O	12.26
K <sub>2</sub> O	0.01
P <sub>2</sub> O <sub>5</sub>	lld
LOI	-0.32
H <sub>2</sub> O	0.57
<b>Total</b>	<b>99.03</b>

lld: lower limit of detection

LOI: loss on ignition

The occurrence of acmite in the KMF has been reported previously by Kleyenstüber (1984), Dixon (1985) and Gutzmer and Beukes (1996a) as an integral part of the complex calc-silicate skarn assemblages commonly seen in the northernmost parts of the KMF in proximity to the lowermost manganese unit. The mineral has also been reported from Fe-ores of the Cuyuna Range, Minnesota (Grout, 1946; McSwiggen et al., 1994). It has been proposed (McSwiggen et al., 1994) that acmite can form hydrothermally from hematite and chert over a wide range of temperatures and pressures, depending primarily upon the NaCl concentration of the reacting solution (Fig. 2.4). The observations of authigenic acmite in close association with surface Na-evaporite deposits of the Green River Formation, Wyoming (Milton and Eugster, 1959) also suggest that the stability of acmite is not primarily dependent on temperature and pressure, but rather on the salinity of reacting fluids. Development of acmite is also influenced by the oxygen fugacity of the system, as in more reducing environments Na-amphibole (riebeckite) would form.



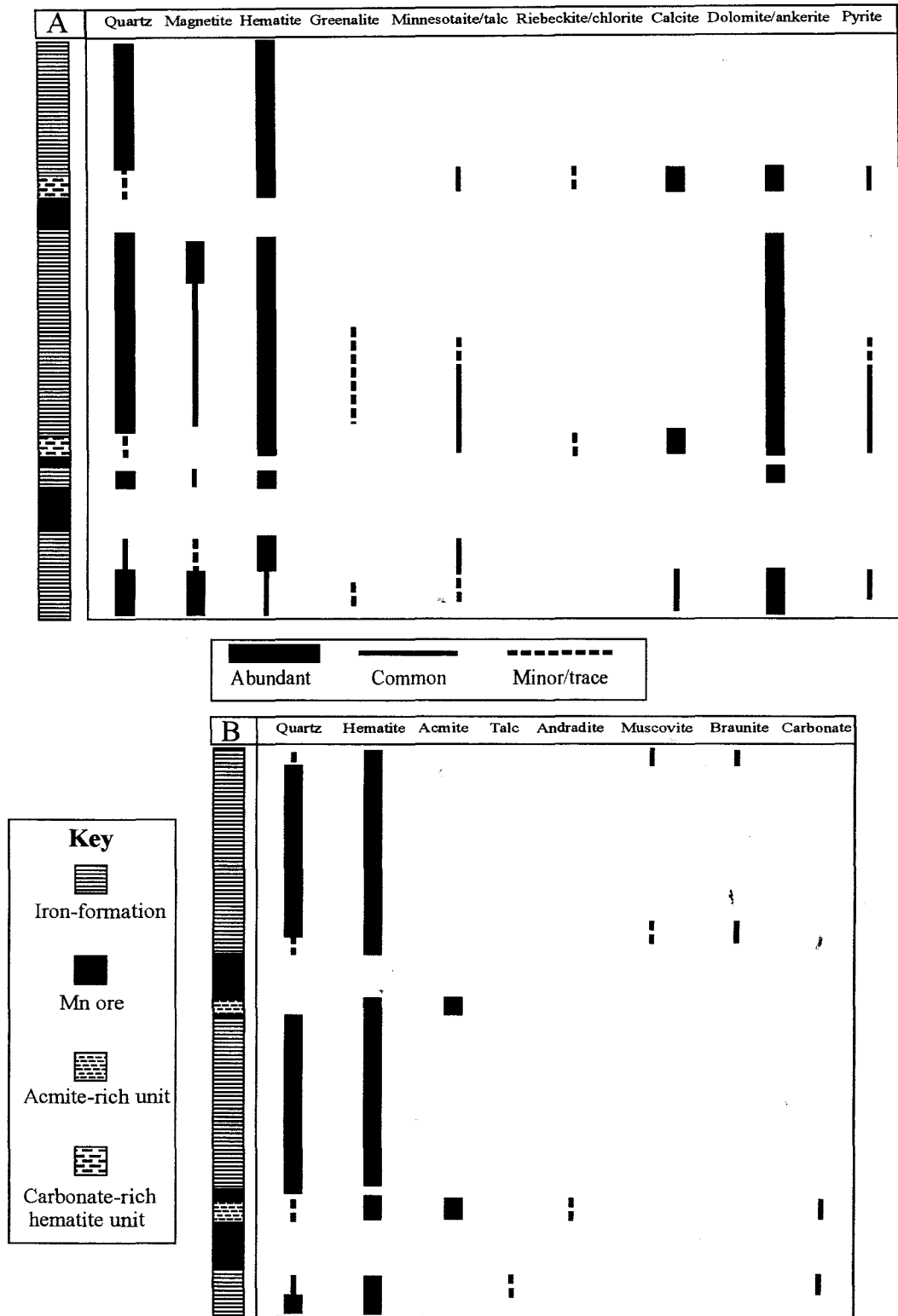
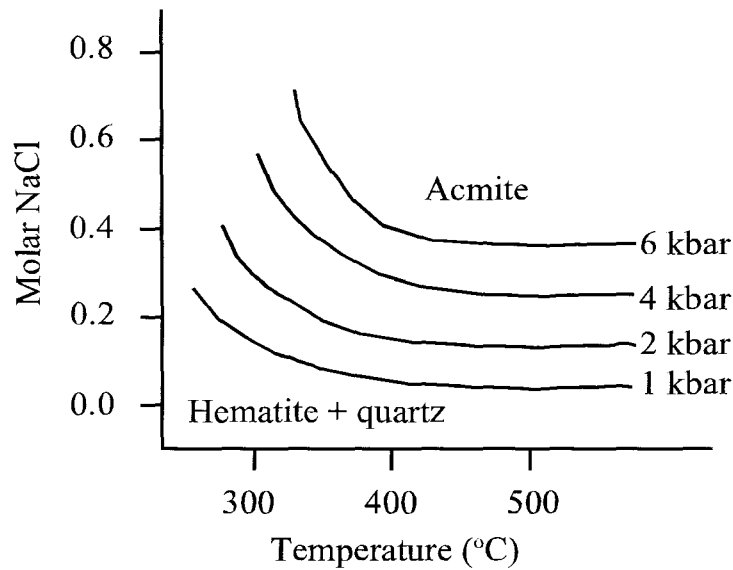


Figure 2.3. General distribution of iron-formation minerals across the Hotazel stratigraphy, as this develops in borehole intersections from the northernmost KMF containing oxidised (A) and altered (B) iron-formation.



**Figure 2.4.** Stability of aegirine relative to hematite and quartz (after McSwiggen et al., 1994).

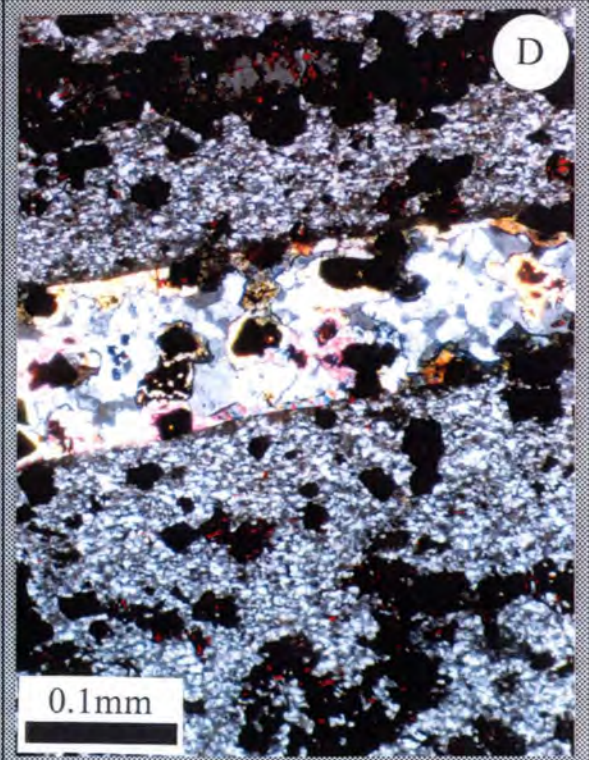
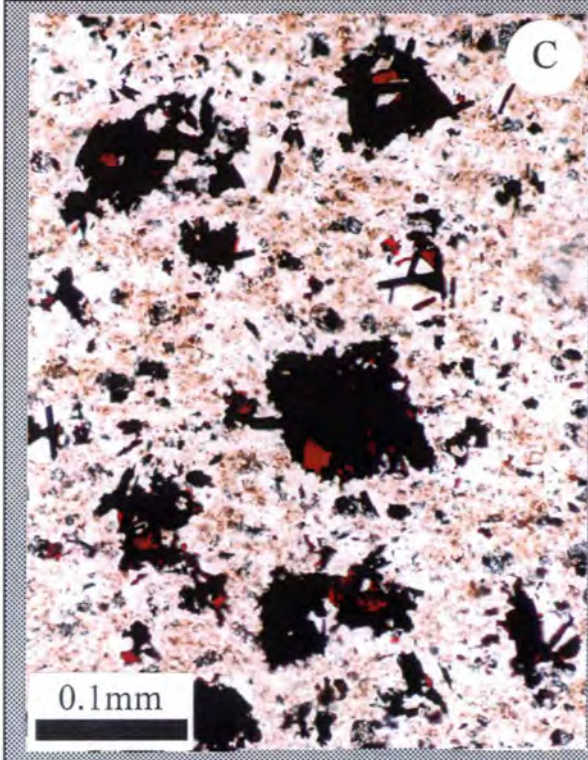
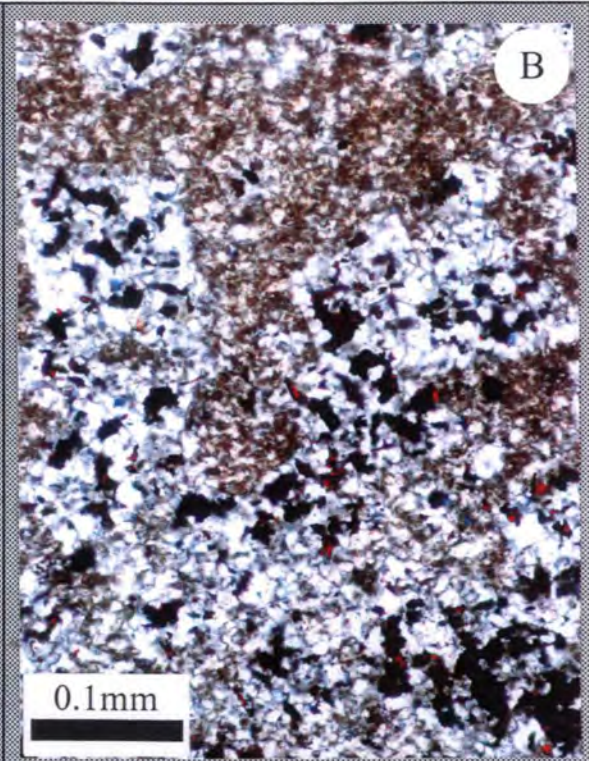
#### 2.2.3.2. Oxidised iron-formation paragenesis

The main characteristic that distinguishes the oxidised iron-formation from other rock-types described in the foregoing paragraphs, is the conspicuous occurrence of both magnetite and hematite in the rock (Fig. 2.3). Relative abundances of the two oxides may vary significantly on a band-to-band scale. In some samples (particularly ones immediately below the uppermost Mn unit in borehole N91B, and also below the lowermost Mn unit) magnetite with a habit similar to pristine iron-formation occurrences appears to be the only well-developed oxide-phase, whereas hematite occurs in chert/carbonate rich bands in the form of brownish cloudy impregnations, implying effects of incipient oxidation. In boreholes BEL4C and BEL7A however (see also Appendix I, Fig. A3), oxidation of magnetite and Fe-silicate minerals is clearly more pronounced, with hematite having replaced almost entirely any pre-existing magnetite. Hematite occurs in characteristic thin bands/clusters of lath-like and microplaty crystals (Plate 5a), and it commonly shows a striking cherry-red colour in transmitted light. Mobilisation of Fe-oxide is conspicuous in some of the samples, resulting in cross-cutting veins and limited lateral movement of Fe-enriched fluid along band-to-band boundaries.

The carbonate mineralogy of oxidised iron-formation also exhibits some contrasting features compared to the pristine rock. The most striking feature in the oxidised type is the almost

**Plate 4.** Minerals and textures of altered iron-formation (all photomicrographs are taken under transmitted light, unless otherwise stated). **A:** Preserved rhombohedral textures resembling markedly those of ankerite from pristine iron-formation. These “ghost” features now consist almost entirely of chert and subordinate hematite (opaque). Matrix is chert admixed with dusty Fe-oxide. Plain-polarized light. **B:** Same as A, but under cross-polarized light. Note the coarser variety of quartz in the rhombs, relative to the finer, “cloudy”, chert matrix. **C:** Clusters of bladed hematite replacing original grains of a rhombohedral mineral, presumably carbonate (ankerite?). Note the cherry-red colour of some hematite platelets. Plain-polarized light. **D.** Cross-cutting vein consisting of quartz, acmite (bright mineral) and hematite (opaque). Note the replacement rims of acmite developed around hematite grains. Features like these suggest that the formation of acmite may postdate an earlier alteration event of intense oxidation and leaching. Cross-polarized light.





complete absence of calcite and the abundance of a dolomitic-type carbonate as a chief mineral phase. XRD patterns of both whole-rock and Fe-oxide-free handpicked rock separates, have shown that the carbonate mineral present would fall under the general description of “ankerite” with  $d\text{\AA}=2.91$  (JCPDS, 1978). In the absence of microprobe data, it was not possible to determine the approximate mineral-chemical composition of this carbonate, but whole-rock geochemical data indicate a Ca:Mg ratio of 2:1 for most samples (see PART 3), which is clearly different from the one observed in ankerites from pristine iron-formation (Ca:Mg = 4:1; see also Table 2.2).

Ankerite occurs throughout the oxidised iron-formation stratigraphy, in the form of very fine-grained rhombohedra, in a groundmass of microcrystalline chert and minor Fe-oxide (Plate 5b). Bands consisting almost entirely of fine-grained carbonate may commonly grade into mixed microcrystalline chert/ankerite assemblages, with the ankerite being developed in lesser amounts in its characteristic, coarser rhombohedral habit (Plate 5c). Minor to trace amounts of greenalite and minnesotaite occur in some of the samples, having been detected both under the microscope and by means of the XRD technique on oxide-free, handpicked powdered rock-chips. Pyrite is conspicuous in some oxidised iron-formation samples, in the form of dispersed, subhedral grains in chert-carbonate bands.

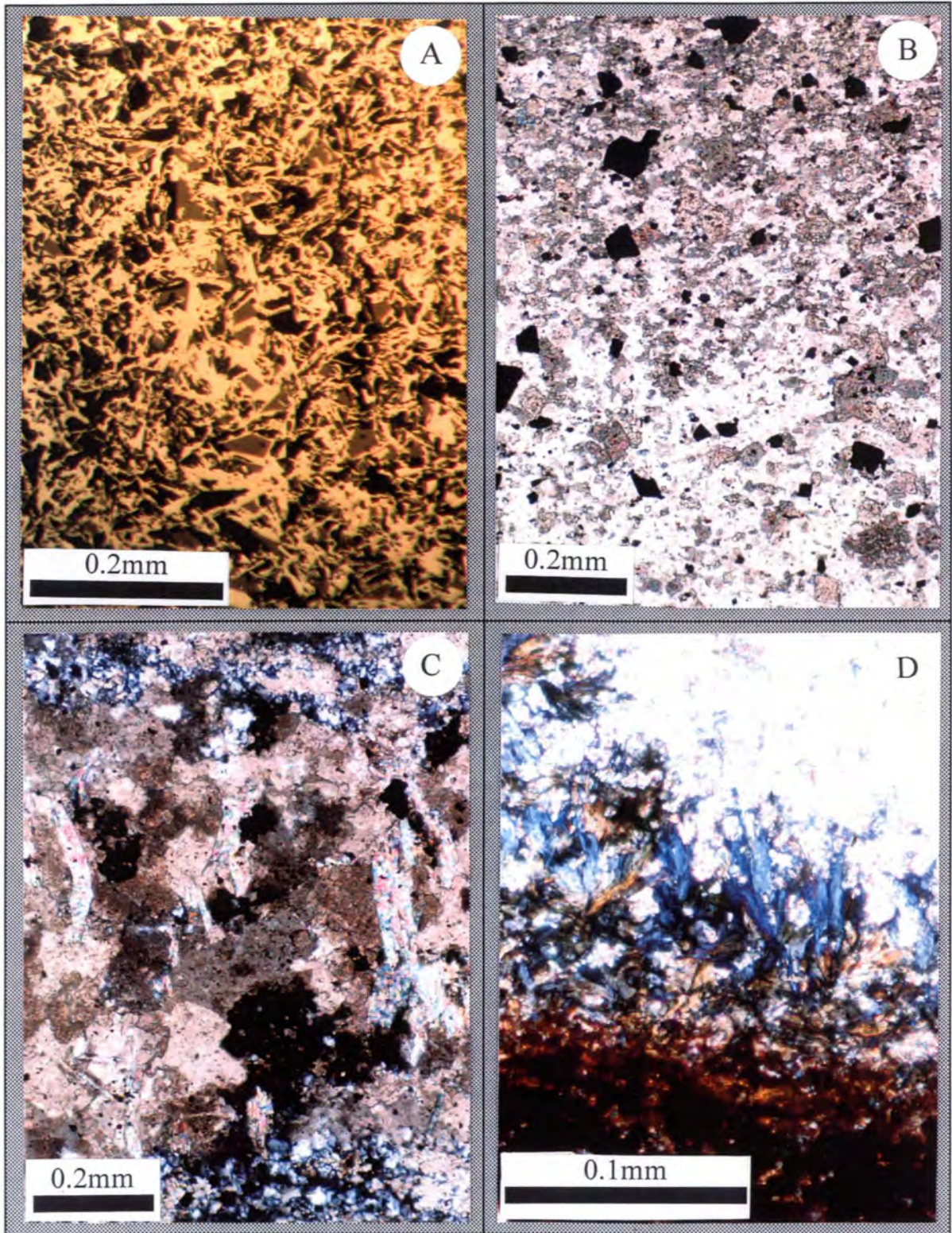
The two hematite/carbonate-rich units developed above the middle and uppermost Mn ore-units (Fig. 2.3) as well as oxide-rich rock developed immediately below the lowermost Mn unit, exhibit striking similarities with similar rock-types from pristine iron-formation, as they contain “dusty” hematite in close association with Mg/Mn-rich carbonate (kutnahorite, rhodochrosite, Mg-calcite). Quartz contents in these samples are very small, while increased amounts of silicate minerals such as minnesotaite/talc are conspicuously present, along with lesser riebeckite/chlorite and traces of the Mn-silicate friedelite (Plate 5d).

#### 2.2.3.3. Petrographic constraints on alteration

One of the most notable features of the northernmost KMF with regard to the petrographic character of altered manganese ore, is the conspicuous occurrence of a variety of unusual mineralogical associations. Dixon (1985) studied in detail perhaps the most prominent of these,



**Plate 5.** Minerals and textures of oxidised iron-formation (all photomicrographs are taken under transmitted light, unless otherwise stated). **A:** Reflected light photomicrograph of lath-like hematite (yellow) along with lesser chert (grey), developed at the expense of an earlier magnetite-rich band. Plain-polarized light. **B:** Rhombohedral grains of Mg-rich ankerite in a chert band (white). Note the gradational increase of modal carbonate relative to chert from bottom to top. Opaque is magnetite. Plain-polarized light. **C:** Coarse ankerite containing laths of talc (birefringent mineral). The assemblage is enveloped between thin bands consisting exclusively of microcrystalline chert. Cross-polarized light. **D:** Ascicular chlorite (brownish-grey to blue), developed on the contact of dusty "hematite" and Mg-rich calcite (white). Photograph taken from sample N91B-9, collected from a transitional Mg-rich carbonate-hematite unit above the uppermost Mn-unit. Cross-polarized light.



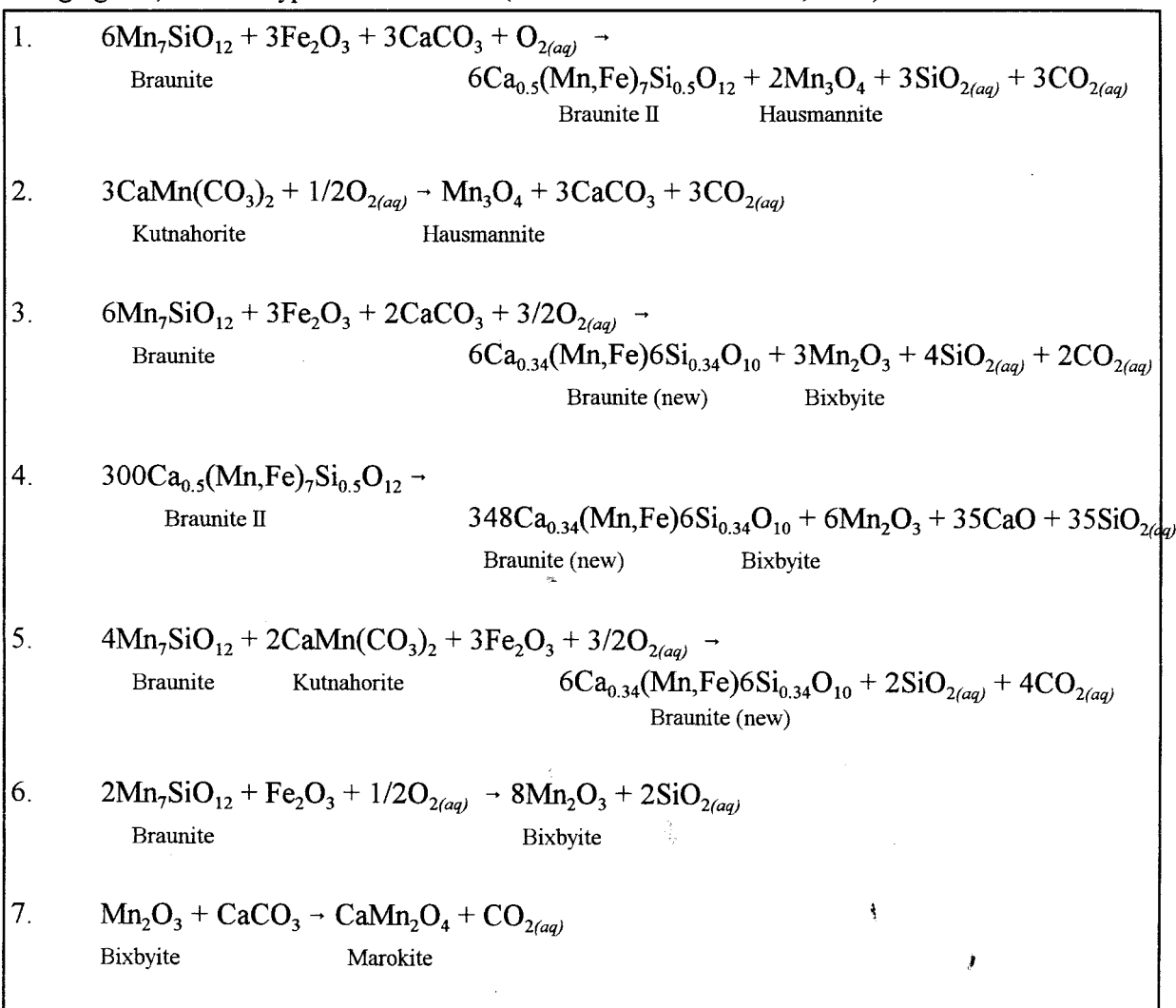
which contains the rare mineral sugilite (Dunn et al., 1980). Sugilite-bearing assemblages are observed predominantly above, below as well as within the lowermost Mn ore-unit and they develop as part of a zonal sequence comprising discrete layers which are dominated (besides sugilite) by the minerals vesuvianite, quartz, pectolite, wollastonite, andradite, glaucochroite and portlandite. Dixon (1985) proposed that the above mineral assemblages would have formed as a result of a single episode of infiltration metasomatism (skarn development), involving alkaline fluids under pressures of about 1 kb, while temperatures of formation have only been very broadly constrained (300-600°C).

Gutzmer and Beukes (1996a) provide a comprehensive synopsis of the mineralogy of the Kalahari manganese deposits and propose that the various mineral associations observed in different parts of the KMF are related to discrete geological events, operating on a variety of scales and during specific intervals in geologic time. With regard to the northernmost KMF, Gutzmer and Beukes (op. cit.) detail a number of mineral associations, namely hausmannite-rich, vein- and vug-hosted, and a sugilite calc-silicate association, the latter embracing the skarn assemblages described by Dixon (1985). They propose a single, major alteration event (Wessels event) as responsible for producing this diverse mineralogy, with different assemblages corresponding to different stages of alteration.

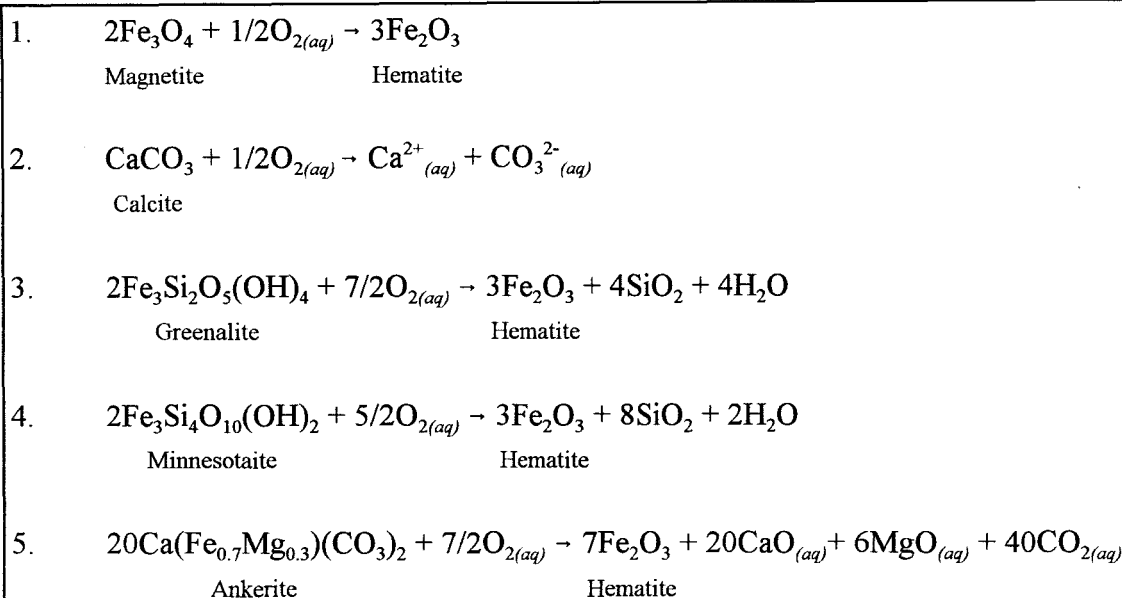
According to Gutzmer and Beukes (1995), the Wessels alteration event would have involved a number of potential chemical reactions producing mixed, Mn-oxide assemblages from the original braunite-kutnahorite-Mn-calcite-hematite assemblage that characterises unaltered, low-grade ore (Box 1). Characteristic of all these reactions is that the major chemical changes involved in the conversion of low-grade to high-grade assemblages are essentially losses of  $\text{CO}_2$ ,  $\text{SiO}_2$  and  $\text{CaO}$  from the parent rock, accompanied by oxidation of much of the initial  $\text{Mn}^{2+}$  to  $\text{Mn}^{3+}$ . No introduction of any components from an external source is assumed, nor has major redistribution of manganese been invoked. As a result, altered manganese ore exhibits substantial volume decrease compared to unaltered Mn ore, a decrease which, as also demonstrated by Gutzmer and Beukes (1997), is reflected in the substantially lower stratigraphic thicknesses observed not only in the lowermost Mn ore-unit, but also throughout the Hotazel succession (see Appendix I, Fig. A5). In a similar fashion to altered manganese ore, associated iron-formation would be expected



**Box 1.** Hypothetical chemical reactions involved in the conversion of low-grade, Mamatwan-type Mn ore to high-grade, Wessels-type ore in the KMF (from Gutzmer and Beukes, 1995).



to have undergone similar mineralogical, chemical and mass changes. Assuming a pre-alteration mineralogical composition similar to that observed on pristine iron-formation, the simple chemical reactions presented in Box 2 would have produced altered iron-formation. Combination of these reactions would correspond to mineralogical and chemical changes on a band-to-band scale, depending on the pre-alteration mineralogical composition of the iron-formation. It becomes apparent that the entire carbonate component of the rock is removed, all ferrous iron compounds are transformed into hematite, while the  $\text{SiO}_2$  component of silicate compounds may have either remained in the system as residual quartz, or may have been mobilised out of the system, depending on the physicochemical attributes (pH, Eh, temperature) of the fluid/s involved.

**Box 2.** Hypothetical chemical reactions involved in the conversion of pristine to altered Fe-formation, KMF

It appears that a combination of the above information would satisfactorily explain the generation of residual enrichments in Fe and Mn in altered Hotazel Formation, by means of effective leaching/removal of all pre-existing carbonate component and accompanying loss of volume. A direct consequence of this is that high-grade Mn-ore would be expected to be interbedded with altered iron-formation, and that the entire Hotazel Formation would have significantly reduced thicknesses in areas where such rocks are developed.

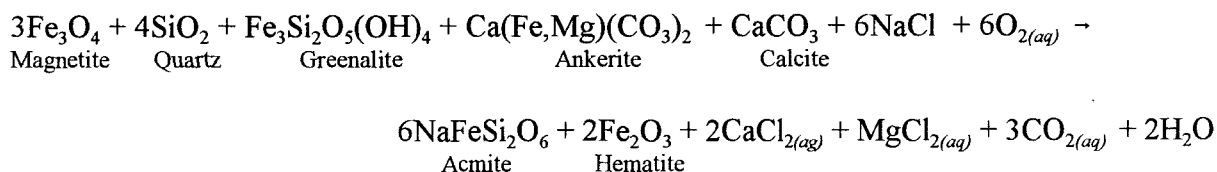
Such a process however, does not clarify the origin of the sugilite-bearing, calc-silicate assemblages of Dixon (1985). An important characteristic of this association is that it involves the introduction of a significant alkali-component to its formation. Several minerals recognised in sugilite-rich zones, such as sugilite itself, pectolite and acmite, are particularly Na-enriched, suggesting that the fluid phase involved in their formation was of an alkaline nature, possibly in the form of a NaCl-enriched brine. In the light of the very erratic occurrence of alkali-rich components in high-grade, Wessels-type Mn ore, it remains to be resolved whether these calc-silicate mineral assemblages are indeed closely related to the Wessels alteration event of Gutzmer and Beukes (1995), or whether they have possibly formed as a result of a distinct - in space and time - metasomatic event.

Important clues in this regard can be provided by the occurrence of acmite in specific stratigraphic intervals of altered Hotazel iron-formation. Acmite is an important constituent of the calc-silicate assemblage and is commonly found in association with sugilite (Dixon, 1985; Gutzmer and Beukes, 1996a). As shown earlier, acmite-rich iron-formation samples occur immediately above the lowermost Mn ore-unit and also below the uppermost Mn ore-unit as well, as represented by samples MK3I-11, 12 and MK2G-10 (see Appendix I, Fig. A4). A characteristic of the latter three samples is that they are mineralogically and chemically very simple, containing essentially acmite and hematite as the two principal components in the form of practically monomineralic alternating laminae. Microscopic and XRD analyses confirmed only trace admixtures of quartz, a fact also verified by bulk-rock analyses (see Appendix III) which indicate that these acmite-rich samples contain almost exclusively Fe-oxide, Na<sub>2</sub>O and SiO<sub>2</sub> in proportions corresponding to ideal mixtures of acmite and hematite.

Petrographic evidence (see section 2.2.3.1) supports the concept that the growth of acmite has taken place as a result of replacement of a pre-existing mineral assemblage. Information about the composition of this precursor is lacking, but textural information suggests that it may have consisted of mixtures of chert, carbonate and Fe-oxide (magnetite and/or hematite?). Despite the fact that acmite growth may have occurred at the expense of pre-existing textural features resembling carbonate material, it is somewhat unclear as to whether acmite is a direct product of replacement of a carbonate-bearing assemblage. A reason for this is that outlines of "ghost" carbonate grains are clearly visible in petrographic thin sections of altered iron-formation, suggesting that these constituents were not lost by means of dissolution, but were rather replaced by quartz and/or hematite via diffusion mechanisms during development of the altered rock. In addition, hematite commonly exhibits signs of replacement by acmite (see Plate 4d), suggesting that some Fe<sub>2</sub>O<sub>3</sub> is likely to have been consumed during acmite formation by simultaneous incorporation of the former into the lattice of newly formed acmite.

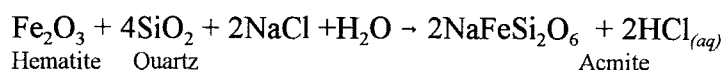
On the basis of the above, there are two possible mechanisms that may have produced the acmite-hematite assemblages, depending on the nature of the pre-acmite precursors. In the first case, it is assumed that the initial rock had a pristine composition, i.e. it contained a mixture of chert, carbonate (calcite and/or some sort of ferrous carbonate such as ankerite), magnetite, and possibly

some Fe-silicate material (e.g. greenalite). In the presence of an external, NaCl-rich oxidizing fluid, the following hypothetical reaction would have potentially caused the formation of acmite:



The reaction above requires a rather unusual set of conditions in order to precipitate essentially pure acmite-hematite assemblages like those observed in samples MK3I-11, -12 and MK2G-10. XRF analyses of these samples and of acmite separates (see Appendix III and Table 2.3), suggests that the latter approximates the ideal end-member composition, which implies that practically no Ca, Mg or Mn are accommodated in the pyroxene structure. Therefore, the assumption has to be made that the system remained open with regard to the pre-existing carbonate component/s, allowing complete mobilisation and removal of essentially all Ca, Mg (possibly as chloride complexes) and  $\text{CO}_2$  in solution. In addition, it has to be assumed that no other Na-enriched silicate phase such as the amphibole riebeckite would have formed instead of, or in equilibrium with acmite, and also that conditions were oxidising enough to convert all pre-existing ferrous iron to the ferric form.

An alternative hypothesis would suggest that acmite has formed at the expense of altered iron-formation, containing essentially pure binary mixtures of chert and hematite. In this case, and in the presence of a NaCl-rich fluid, acmite would have formed through the reaction (McSwiggen et al., 1994):



with no relative changes in the initial amounts of  $\text{Fe}_2\text{O}_3$  and  $\text{SiO}_2$  being required. It should also be noted that less pure acmite occurrences reported in this study from lower parts of the Hotazel stratigraphy between the lowermost and middle Mn-ore units, could also have formed by means of a similar mechanism. In this case however, deviations of the pyroxene compositions from those of the pure Na-member as seen in the form of Ca- Mg- and/or Mn-admixtures in these samples

(see Appendix III), may be related to either slight departures in whole-rock compositions prior to acmite formation, and/or to some metasomatic intake from the alteration fluid itself.

The feasibility of either of the above mechanisms bears important implications with regard to timing of Na-metasomatism in relation to the Wessels alteration event of Gutzmer and Beukes (1995). Specifically, evaluation of the two alternatives presented above requires that acmitisation has either occurred prior to the Wessels-type alteration, or that acmite formation postdates the main Wessels event.

In the former case, explanations need to be sought concerning the puzzling occurrence of acmite in specific stratigraphic intervals, and specifically on the margins of the lowermost and uppermost Mn ore-units. Also, it is hard to envisage such a "selective" metasomatic effect on Hotazel iron-formation producing the unusually simple assemblages of pure acmite and hematite at the expense of multi-component assemblages of pristine iron-formation. Furthermore, should altered iron-formation have formed at a later stage, it would be difficult to perceive that acmite has remained unaffected during low-temperature alteration processes which appear to have produced altered iron-formation, as suggested by isotopic evidence for hematite and chert (see PART 4).

The second case requires that acmitisation postdates (or even coincides?) with the Wessels alteration event as a distinct episode of localised Na-metasomatism. Hydrothermal processes involving Na-metasomatism on hematite-rich rocks have also been postulated by Grout (1946) and McSwiggen et al (1994) for the genesis of acmite occurrences in iron-rich rocks of the Cuyuna Range, Minnesota. In support of this hypothesis is the simple mineralogical and chemical composition of altered iron-formation comprising hematite and chert, which would constitute an ideal precursor for the formation of acmite in an alkaline environment. On these grounds it could be argued that the tentative age of ~1.3Ga provided by Dixon (1989) for metasomatism of the Kalahari Mn ore on the basis of galena (Pb) and sugilite (Rb-Sr, Pb) ages, may in fact correspond to a minimum age of the main alteration event/s involved in the economic upgrading of the Kalahari Mn ores. The above also imply that the Wessels alteration event may, in fact, have taken place at even earlier stages in the geological history of the KMF, and possibly as early as during the Palaeoproterozoic.

## **PART 3: BULK-ROCK GEOCHEMISTRY**

### **Chapter 3.1: Introduction**

#### **3.1.1. General**

Conventional whole-rock geochemical studies of major and trace element abundances in iron-formations have rarely received considerable attention in iron-formation research. Two reasons may be regarded as responsible for this:

(i) iron-formations are rocks of bimodal chemical composition, as they contain essentially two components, i.e. Fe-oxide and silica. These compounds will invariably exhibit very strong negative correlation, with an immediate result of a reduction in the statistical significance of most remaining minor and trace elements;

(ii) the widespread use of advanced geochemical data such as stable isotopes and rare-earth elements (REE) have overshadowed the potential importance of bulk-rock analyses. Consequently, bulk-rock data have been used either as a necessary attachment to mineralogical-petrographic investigations of iron-formations (e.g. Ewers and Morris, 1981; Gole, 1981) or in review articles outlining the general geochemical characteristics of iron-formation occurrences on a global scale (e.g. Gross and McLeod, 1981; Gole and Klein, 1981; Davy, 1983; Gross, 1990; Horstmann and Hälbich, 1995).

In this chapter, major and trace element analyses from the majority of iron-formation samples collected during the field component of this study are presented and evaluated. Interpretations are drawn in conjunction with corresponding mineralogical and textural information presented in Part 2 of this thesis, and focus on the two main processes that appear to have affected the Hotazel Formation, namely diagenesis/burial metamorphism and later alteration/metasomatism. The iron-formation geochemical data are also complemented by a small dataset of selected samples from the Moidraai Formation.

#### **3.1.2. Material selection and methods**

A total of 233 borehole samples were used for whole-rock geochemical investigations. The

samples were collected from 14 borehole intersections drilled in the southernmost and northern parts of the KMF. The locality map for these drillholes and details regarding the stratigraphic location of all samples selected for analyses are shown schematically in Appendix I, Figures A1, A2, A3 and A4.

Analytical data for ten major and 15 trace elements were obtained using standard x-ray fluorescence (XRF) procedures on finely powdered, quartered-core samples, according to the method of Norrish and Hutton (1969). In addition, rare-earth element analyses were performed on 12 selected iron-formation and 5 Mooidraai carbonate samples by a combination of high-performance ion chromatography (le Roex and Watkins, 1990) and ICP-MS techniques respectively. Details with regard to sample preparation, comprehensive descriptions of the analytical techniques used and analytical results for all samples are summarised in Appendices II and III respectively.

In many instances, and particularly with respect to the iron-formation in the northern parts of the KMF, detailed high-density sampling across the Hotazel iron-formation was impeded by factors such as frequent secondary veining and/or highly broken nature of core. These features were, fortunately, not particularly prominent in the boreholes selected for sampling, and all samples used for analyses were effectively devoid of any secondary features that would significantly impact on their homogeneity. However, the main drawback of this investigation concerns the poor spatial distribution of the available boreholes. Although extensive drilling has been carried out in recent years by the mining companies, only few boreholes have been stored in full and are available for detailed sampling. This immediately poses difficulties with regard to selection of borehole material situated, for example, at regular intervals in the proximity of recognised and potentially important geological structures such as faults, thrust planes etc, or across areas where major lateral changes in stratigraphic thicknesses and/or lithofacies occur. As a result, information regarding the Hotazel stratigraphy for a large part of the KMF is lacking, and respective lateral variations can only be grossly postulated. Furthermore, alteration models that would require the existence of steep-angle structures such as normal faults (e.g. Gutzmer and Beukes, 1995) and/or dyke intersections, cannot be easily evaluated in the light of randomly distributed borehole material alone. Hence, it should be noted that the selected borehole intersections of this study, although highly informative

in terms of revealing mineral/chemical variations across the Hotazel stratigraphy, cannot be regarded as ideally suitable for spatial geochemical studies in comparison to other sampling methods such as, for example, underground traverse sampling.

In the forthcoming paragraphs and as far as presentation and interpretation of the iron-formation geochemical data set is concerned, treatment of data can be subdivided into three stages/chapters:

1. The first stage (Chapter 3.2) comprises presentation of the raw data along with the use of simple variation plots for selected major and trace elements across the Hotazel stratigraphy, constructed for the majority of boreholes sampled. Combination of such graphs with existing petrographic information, allows for the recognition of major geochemical variations across the stratigraphy, thus permitting the discrimination of major groups/classes of iron-formation from the available dataset.

2. The second stage (Chapter 3.3) involves stepwise statistical analysis performed on selected data sub-sets, with the purpose of establishing the main geochemical characteristics of the various iron-formation groups present. Bivariate plots of major and trace elements are used thereafter, exhibiting the most important elemental relations and geochemical similarities and/or differences between these major rock-types.

3. The third stage (Chapter 3.4) is an attempt to seek potential evolutionary links between the individual iron-formation groups, on the assumption that one of these corresponds the closest to the original precipitate, i.e. its composition has not been affected by later metasomatic or low-temperature supergene processes. On condition that the clear recognition of such a rock-type has been facilitated by the data presented up to that stage, the geochemical characteristics of any secondary events involved in the generation of the remaining rock-types should be effectively deciphered by means of simple isocon diagrams as proposed by Grant (1986).

As will be seen in the forthcoming chapters, the three-stage treatise described above will, at times, require further separation of data based on the locality of the borehole intersections used. More specifically in the first chapter, reference will be made separately to the southernmost and northernmost parts of the KMF, owing to the distinct differences in the mineralogical and petrographic character of the Hotazel stratigraphy in the respective areas. Furthermore, additional



representative data for the 10 samples from the Mooidraai Formation will be presented in a separate sub-section of the second chapter (3.2.2), in an attempt to provide as complete an account as possible of the geochemistry of the entire Voëlwater Subgroup.

## **Chapter 3.2: The Hotazel iron-formation - results and chemostratigraphy**

### **3.2.1. Southern KMF**

The first investigation on the geochemistry of the Hotazel iron-formation in the southernmost parts of the KMF was accomplished by the author in 1993 (Tsikos, 1994; Tsikos and Moore, 1997). A comprehensive summary is presented below.

Petrographic and mineralogical evidence (PART 2), suggests that the Hotazel iron-formation from the southern parts of the KMF represents a type-example of a Superior-type iron-formation which has undergone only very mild metamorphic modifications. The simple mineralogical composition of the Hotazel iron-formation in that area points towards an essentially bimodal chemical composition, with SiO<sub>2</sub> and total Fe-oxide (as Fe<sub>2</sub>O<sub>3</sub>) being the two major components. These two components effectively reflect the relative amounts of the two chief mineral constituents in the rock, i.e. chert and magnetite. In addition to these two mineral phases, carbonates in the form of calcite coexisting with ankerite, constitute the third most important modal constituent. This is reflected by relatively high CaO contents in the iron-formation which reach levels of 20 wt% in certain samples. Fe-silicate minerals such as greenalite, minnesotaite and stilpnomelane that would contribute to the overall levels of SiO<sub>2</sub> and Fe-oxide in the iron-formation samples, are usually present in the Hotazel iron-formation in small modal amounts.

The major element spidergram of Figure 3.1 presents a visual means of comparing the average major element composition of 38 mineralogically and texturally very similar samples of the Hotazel iron-formation from the southern KMF (Tsikos, 1994; Tsikos and Moore, 1997), with a representative compositional field of iron-formations of similar age and mineralogical composition from other parts of the globe (data from Gole and Klein, 1981; and Horstmann and

Hälbich, 1995). The apparent geochemical similarities illustrated in Figure 3.1, in conjunction with petrographic evidence, would support the descriptive term “pristine” as employed in PART 2. Nevertheless, it is important to highlight here the most notable differences between the Hotazel iron-formation and the field defined by other iron-formations. Firstly, the Hotazel iron-formation is slightly more enriched in overall Fe-oxide content (approximately 48 wt%), and this invariably relates to a corresponding decrease in the amount of  $\text{SiO}_2$  present (approximately 40 wt%). Furthermore, average whole-rock CaO values are distinctly higher in the Hotazel iron-formation (mean: 8.35 wt%), whereas MgO is essentially low (~2 wt%), indicating the presence of higher calcite contents in the Hotazel iron-formation relative to Mg-bearing phases such as dolomitic carbonates and/or Fe-silicates. The absence of riebeckite is reflected by the very low values of  $\text{Na}_2\text{O}$  (generally below 0.1 wt%), while all other minor constituents fall within the expected ranges.

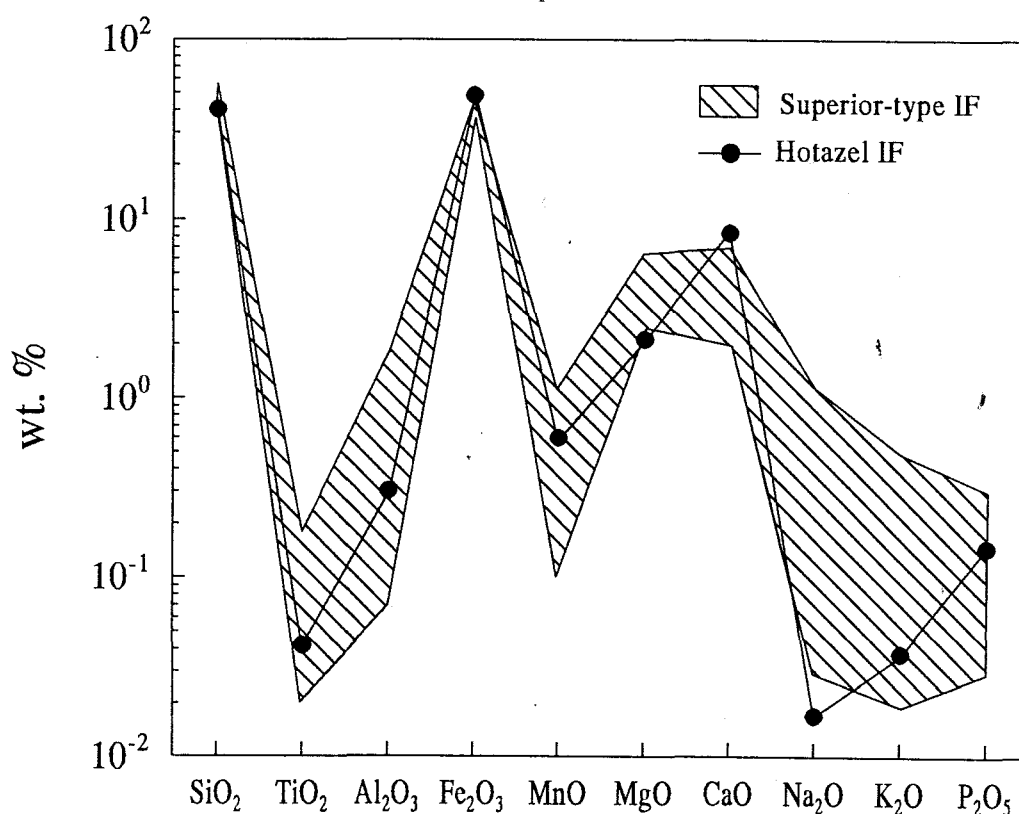


**Figure 3.1.** Average major element spidergram of pristine Hotazel iron-formation. Stippled area defines the compositional field of Superior-type iron-formation, on the basis of average data from major Superior-type iron-formations of the world (data from Gole and Klein, 1981; and Horstmann and Hälbich, 1995).

Table 3.1 contains representative whole-rock geochemical data for 12 selected samples from 4 out of the 5 boreholes drilled in the southernmost KMF (see Appendix I, Fig. A2). Geochemical variations of selected major and trace elements across the Hotazel stratigraphy are schematically illustrated on the variation plots of Figure 3.2.

It is evident that any conclusions drawn from the plots of Figure 3.2 require the combined use of petrographic data. Values for both  $\text{SiO}_2$  and total Fe-oxide show a small overall decrease upward in the stratigraphy (by 2-3 wt% on average), which corresponds to a respective increase in whole-rock CaO. This chemical change across the iron-formation stratigraphy appears to take place immediately below the middle Mn ore-unit, and is a reflection of the change in the mineralogical character of the iron-formation from a carbonate-poor member containing low amounts of total carbonate, to a carbonate-enriched member (see PART 2). The stratigraphic pattern of Fe# ( $\text{FeO}/(\text{FeO}+\text{Fe}_2\text{O}_3)$ ) suggests that this change is accompanied by a change in the valence state of total Fe, with carbonate-poor iron-formation ( $\text{Fe}\#=0.57\text{-}0.81$ ) containing primarily ferrous silicates (greenalite, minnesotaite) and magnetite, whereas carbonate-rich iron-formation ( $\text{Fe}\#=0.38\text{-}0.46$ ) is dominated by magnetite, ferrous carbonate (ankerite) and reduced amounts of Fe-silicates (mainly stilpnomelane and minnesotaite). The upward increase in whole-rock carbonate is coupled with a corresponding increase in Sr values on the order of tens, up to several hundred ppm, suggesting a likely evaporitic origin for the iron-formation carbonates.

With regard to the remaining components,  $\text{Al}_2\text{O}_3$  contents are very low (rarely above 0.3 wt%), MgO varies within fairly narrow limits (2-3 wt%), while  $\text{Na}_2\text{O}$  and  $\text{K}_2\text{O}$  are particularly low (<0.1 wt% in most samples). MnO values are almost always below 0.5 wt%, although they may be slightly higher in samples collected in close proximity to the interbedded Mn-units (e.g. sample R59-3, Table 3.1). High values for total MnO are seen only in the narrow ferro-manganiferous carbonate horizon occurring between the middle and uppermost Mn ore-units (e.g. sample R59-5), as well as in samples from the stratigraphically lowermost iron-formation unit which exhibits a petrographically "transitional" character, with significant amounts of dusty hematite and Mn-bearing carbonate (e.g. R65-30). Transition metals such as Zn, Cu, Ni and to a lesser extent Cr are present on the order of a few tens ppm and do not exhibit significant variations across the stratigraphy, with the exception of perhaps Ni and Cr which appear to show a weak similarity with

**Table 3.1.** Whole-rock chemical analysis for 12 selected samples of pristine Hotazel iron-formation from the southernmost KMF (modified after Tsikos and Moore, 1997).

	R65-2	R65-3	R59-3	R63-5	R59-9	R63-8	R70-13	R59-15	R70-17	R70-18	R65-20	R65-31
<i>wt.%</i>												
SiO <sub>2</sub>	37.66	35.97	30.38	33.50	12.96	30.30	43.15	41.87	40.15	43.86	39.60	28.63
TiO <sub>2</sub>	0.03	0.04	0.05	0.04	0.05	0.03	0.04	0.04	0.04	0.05	0.05	0.05
Al <sub>2</sub> O <sub>3</sub>	0.19	0.18	0.46	0.16	0.31	0.15	0.15	0.36	0.16	0.49	0.04	0.32
FeO	14.12	19.21	8.30	9.88	1.10	12.94	19.11	28.96	27.37	31.15	26.38	17.82
Fe <sub>2</sub> O <sub>3</sub>	19.26	22.84	23.41	28.73	9.66	21.09	24.56	13.81	20.59	7.13	20.16	28.54
MnO	0.15	0.37	2.21	1.38	7.17	0.55	0.12	0.20	0.16	0.40	0.52	5.24
MgO	2.22	2.49	2.18	3.04	1.39	2.40	1.90	2.19	2.13	2.83	2.64	2.81
CaO	12.95	7.58	15.77	10.74	35.69	15.62	4.60	2.06	2.33	2.54	2.58	4.44
Na <sub>2</sub> O	0.01	0.01	0.05	0.02	0.03	0.01	0.01	0.02	0.01	0.01	0.01	0.02
K <sub>2</sub> O	0.01	0.01	0.07	0.01	0.04	0.01	0.04	0.02	0.01	0.01	0.01	0.02
P <sub>2</sub> O <sub>5</sub>	0.05	0.11	0.05	0.08	0.04	0.07	0.10	0.13	0.22	0.09	0.18	0.07
LOI	13.81	10.84	16.75	11.44	30.93	15.78	6.76	10.24	6.98	11.54	7.66	11.38
H <sub>2</sub> O	0.23	0.30	0.37	0.38	0.36	0.35	0.20	0.40	0.32	0.53	0.29	0.37
Fe#	0.42	0.46	0.26	0.26	0.10	0.38	0.44	0.68	0.57	0.81	0.57	0.38
TOTAL	100.69	99.95	100.05	99.40	99.84	99.30	100.74	100.30	100.49	100.63	100.13	99.73
<i>ppm</i>												
Zn	11	17	17	31	9	13	12	17	15	15	16	37
Cu	19	25	20	24	17	22	23	23	21	21	27	25
Ni	39	43	42	43	35	41	45	43	44	38	54	52
Co	lld	nd	6	6	9	lld	lld	nd	nd	lld	lld	35
Cr	24	31	33	27	19	23	32	37	33	35	31	42
V	lld	lld	5	lld	nd	lld	lld	9	lld	9	lld	6
Ba	6	lld	147	38	106	40	12	8	6	7	lld	72
Sc	lld	3	lld	2	nd	nd	3	4	2	3	3	3
Th	7	12	4	9	nd	4	11	11	15	11	16	15
Pb	4	8	3	6	nd	6	9	10	9	9	9	10
Rb	lld	lld	9	nd	4	lld	4	2	4	4	5	4
Nb	3	lld	lld	4	nd	lld	lld	4	nd	nd	lld	lld
Zr	3	4	5	6	nd	lld	3	9	lld	6	5	7
Y	7	9	7	10	7	5	7	15	13	8	14	10
Sr	231	93	305	169	905	299	95	45	64	53	79	14

Totals calculated by the sum of major element concentrations only

All volatiles as LOI (loss on ignition)

nd = not determined

lld = lower limit of detection

Fe# = FeO/(FeO+Fe<sub>2</sub>O<sub>3</sub>)

total Fe-oxide in terms of their chemostratigraphic patterns. Most remaining elements display either little or very erratic variation (e.g. Zr, Y, Ba), or values very near or below the lower limit of detection (e.g. Co, Nb, Rb).

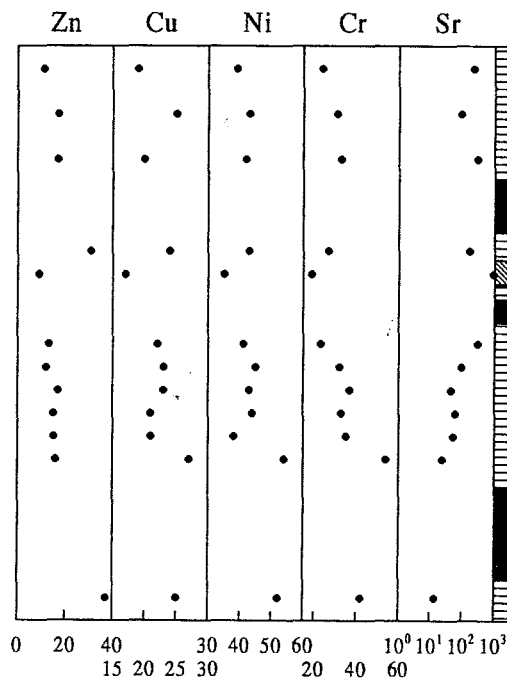
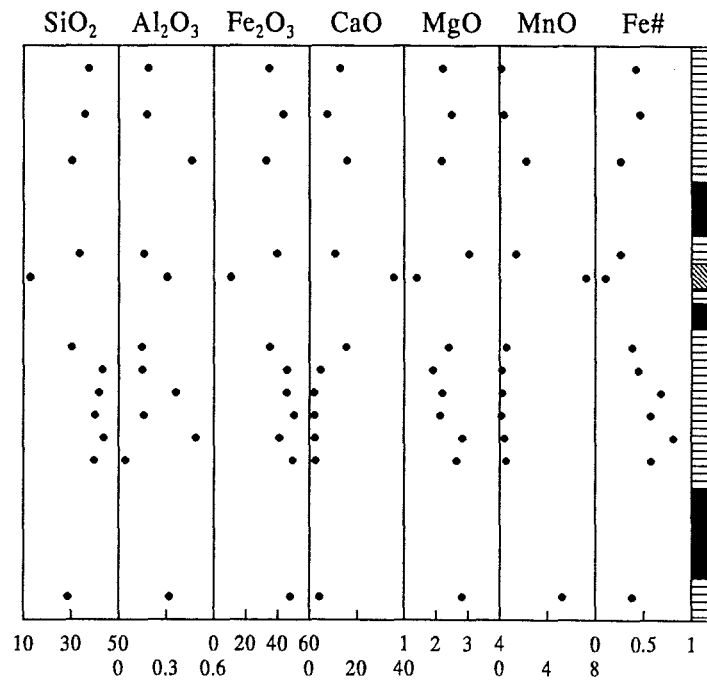


Figure 3.2. Variation plots of selected major and trace elements for a representative stratigraphic profile of iron-formation from the southernmost KMF. Stratigraphic columns are not to scale, but depict approximate stratigraphic locations of the selected samples and crude relative thickness relations between iron-formation (horizontal line fill), manganese units (black fill) and a Fe/Mn-rich carbonate horizon (inclined line fill).

### 3.2.2. Northern KMF

Mineralogical and textural investigations presented earlier, have established the existence of essentially three distinct major types of iron-formation in the KMF, tentatively assigned the terms *pristine*, *altered* and *oxidised* (see PART 2). Although *pristine* iron-formation is the exclusive rock type in the southernmost portions of the KMF, all three types persist over large portions of the Hotazel stratigraphy in the eight borehole intersections selected from the northernmost parts. Separate treatment of these iron-formation types is essential in order to establish any distinct geochemical similarities and/or differences when compared to the Hotazel iron-formation from the southernmost KMF. The first step here is to present and broadly describe the chemostratigraphic signatures of the individual intersections, before a more detailed comparative approach is undertaken between the three selected iron-formation types.

#### 3.2.2.1. *Pristine iron-formation*

Borehole intersection GL26 contains the entire Hotazel Formation except for the portion of the iron-formation above the uppermost Mn-unit which has been removed as a result of pre-Karoo erosion (see Appendix I, Fig. A3). The iron-formation here falls under the general descriptive term “*pristine*”, as the selected samples exhibit remarkable petrographic similarities with samples from borehole intersections from the southernmost portion of the KMF. In terms of thickness relations, however, there are some conspicuous differences, namely the middle Mn ore-unit in borehole GL26 is developed in close proximity to the lowermost Mn-unit, whereas the iron-formation between the middle and uppermost Mn ore-units is substantially thicker (see Appendix I, Fig. A5).

Figure 3.3 displays stratigraphic variations in selected major, minor and trace elements for samples from borehole GL26. Observations are effectively similar to those presented earlier for the composite Hotazel chemostratigraphy from the southernmost KMF. Whole-rock SiO<sub>2</sub> and total Fe-oxide stratigraphic patterns show the expected ‘mirror image’ relation with the pattern for whole-rock CaO. Al<sub>2</sub>O<sub>3</sub> contents are low (<0.5 wt% in the majority of samples) and display effectively no stratigraphic variation, while MgO behaves similarly to Al<sub>2</sub>O<sub>3</sub>, with contents approximating 1 wt%. MnO is rarely above 1 wt% and shows a relatively high value in only one

sample, that corresponding to a carbonate-rich unit developed over the transition between the middle manganese unit and the overlying iron-formation. In terms of trace element compositions, Sr concentrations are again on the order of several tens to hundred ppm and show a sympathetic relation with CaO. Ni and Cr have patterns which compare fairly well with that of total Fe-oxide, while stratigraphic variations in Zn and Cu are somewhat erratic and show no obvious correlation with any major element chemostratigraphic patterns. Most remaining trace elements exhibit very low contents and/or insignificant stratigraphic variations.

An important feature of borehole GL26 with regard to the distribution of the various subfacies of pristine iron-formation is the substantially reduced development of carbonate-poor iron-formation. It appears that this particular facies is now present as a very narrow unit between the lowermost and middle manganese horizons, and also in one sample below the lowermost Mn unit. In contrast, carbonate-rich iron formation is developed in the remaining portions of the iron-formation intersection higher in the stratigraphy. Comparisons between the two stratigraphic columns of the Hotazel Formation as crudely documented in Figures 3.2 and 3.3 (see also Appendix I, Fig. A5) suggest that the iron formation unit between the lowermost and middle Mn ore-beds has substantially decreased from its observed thickness in the southernmost KMF (20-25m), to approximately 5m in borehole GL26. This lateral thickness change appears to be in concert with a well-documented decrease in the thickness of the lowermost Mn ore-unit from 20-25m in the south, to approximately 10m to the north of the KMF, as well as with a respective overall reduction in the thickness of the entire Hotazel Formation in a north-northwesterly direction (see Appendix I, Fig. A5).

Irrespective of the above relative thickness differences, geochemical similarities between borehole GL26 and the succession from the southernmost KMF are clear and are summarised in Table 3.2. The major types of iron-formation identified are essentially two: a carbonate-rich member characterised by a mean CaO value of 11.4 wt% and a carbonate-poor member with a mean CaO value of 3.37 wt%. The average for both these two types is presented in column 6 and corresponds to the mean composition of the "pristine" iron-formation type. In addition to these two iron-formation types, a third, oxide-rich iron-formation occurs exclusively below the lowermost manganese unit and is characterised by elevated MnO, MgO, Ba and Co, and reduced

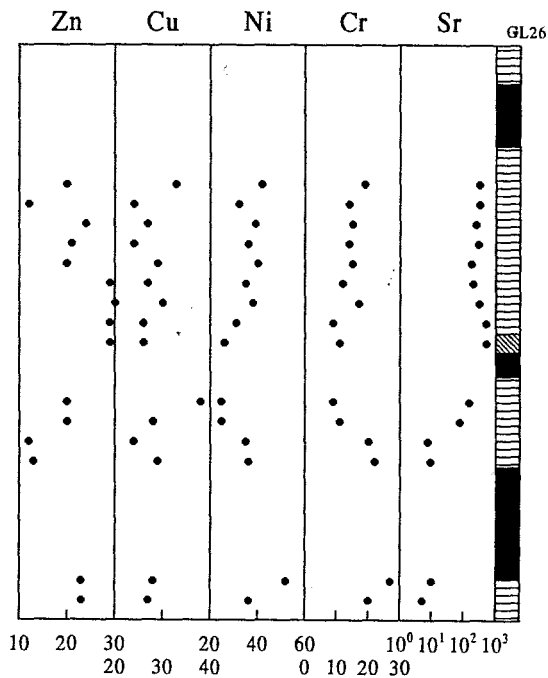
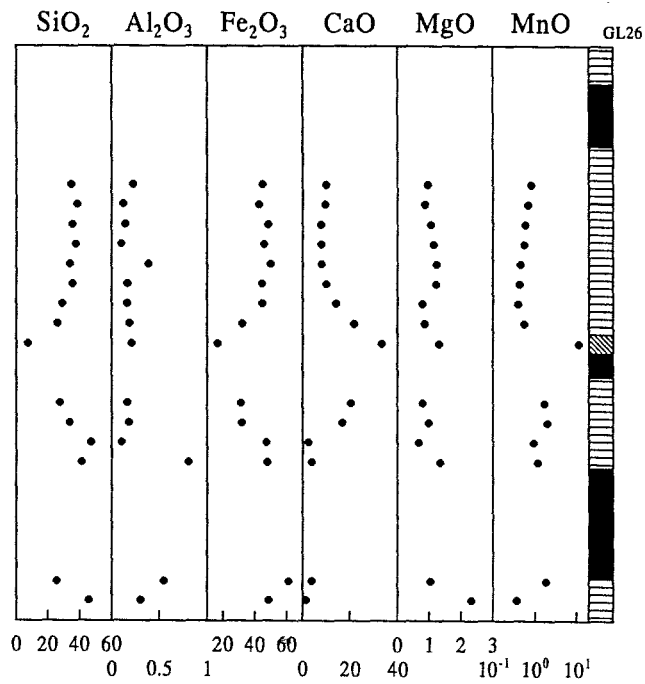


Figure 3.3. Variation plots of selected major and trace elements for borehole intersection GL26 from the northern parts of the KMF. Stratigraphic columns are not to scale, but depict approximate stratigraphic locations of the selected samples and crude relative thickness relations between iron-formation (horizontal line fill), manganese units (black fill) and a Fe/Mn-rich carbonate horizon (inclined line fill).



**Table 3.2.** Summary of whole-rock analytical data for samples from boreholes R59, R63, R65, R70, SM31 and GL26 containing pristine iron-formation.

	1	2	3	4	5	6
<i>wt%</i>	n=27	n=23	n=6	n=5	n=2	n=50
SiO <sub>2</sub>	34.01 (5.06)	41.11 (3.27)	23.43 (3.72)	8.44 (2.34)	48.97 (3.68)	37.27 (5.59)
TiO <sub>2</sub>	0.04 (0.01)	0.04 (0.01)	0.05 (0.01)	0.05 (0.01)	0.05 (0.00)	0.04 (0.01)
Al <sub>2</sub> O <sub>3</sub>	0.29 (0.25)	0.26 (0.19)	0.36 (0.10)	0.25 (0.08)	3.35 (0.50)	0.28 (0.23)
Fe <sub>2</sub> O <sub>3</sub>	41.30 (5.55)	47.78 (3.52)	48.08 (7.76)	11.96 (2.65)	36.84 (5.38)	44.28 (5.72)
MnO	0.72 (0.59)	0.35 (0.27)	10.46 (5.58)	9.53 (1.57)	0.10 (0.03)	0.55 (0.51)
MgO	1.82 (0.82)	2.13 (0.56)	4.38 (2.59)	1.84 (0.75)	4.72 (0.92)	1.97 (0.73)
CaO	11.40 (4.46)	3.37 (1.16)	3.42 (1.35)	35.78 (1.62)	0.39 (0.17)	7.71 (5.23)
Na <sub>2</sub> O	0.02 (0.02)	0.01 (0.01)	0.03 (0.04)	0.04 (0.04)	0.29 (0.02)	0.02 (0.02)
K <sub>2</sub> O	0.04 (0.09)	0.02 (0.02)	0.04 (0.04)	0.02 (0.01)	1.55 (0.21)	0.03 (0.07)
P <sub>2</sub> O <sub>5</sub>	0.11 (0.03)	0.16 (0.06)	0.07 (0.02)	0.05 (0.02)	0.08 (0.07)	0.13 (0.06)
<i>ppm</i>						
Zn	20 (6)	16 (5)	33 (11)	21 (9)	16 (1)	18 (6)
Cu	25 (4)	24 (2)	28 (3)	20 (3)	17 (2)	25 (4)
Ni	39 (7)	44 (6)	53 (4)	32 (7)	46 (20)	41 (7)
Co	1 (2)	lld	40 (22)	15 (6)	lld	lld
Cr	22 (10)	33 (9)	39 (9)	16 (6)	20 (6)	27 (11)
V	2 (4)	5 (4)	3 (3)	lld	lld	3 (4)
Ba	44 (36)	11 (8)	993 (1333)	1877 (2569)	384 (152)	29 (32)
Sc	2 (1)	3 (1)	3 (1)	lld	1 (1)	2 (1)
Pb	6 (2)	8 (2)	8 (4)	lld	10 (0)	7 (2)
Th	9 (3)	13 (3)	14 (6)	lld	17 (1)	11 (4)
Y	11 (3)	13 (4)	7 (6)	6 (5)	7 (4)	12 (4)
Nb	1 (2)	1 (2)	lld	lld	2 (2)	1 (2)
Zr	5 (2)	5 (4)	4 (3)	1 (2)	24 (2)	5 (3)
Rb	4 (9)	2 (2)	3 (5)	2 (3)	174 (16)	lld
Sr	222 (119)	65 (37)	21 (10)	740 (260)	32 (2)	150 (120)

nd = not determined

lld = lower limit of detection

n=number of samples

45.21 (2.33): Average (standard deviation)

Column 1: Carbonate-rich iron-formation

2: Carbonate-poor iron-formation

3: Oxide-rich iron-formation

4: Fe/Mn-bearing carbonate unit

5: Carbonate-free, cherty, Al-Na-K-bearing unit

6: Hotazel iron-formation, grand average

SiO<sub>2</sub> and Sr whole-rock values (column 3). The carbonate unit between the middle and uppermost Mn ore-units contains almost exclusively CaCO<sub>3</sub> and is enriched in Fe-oxide, MnO, Ba and to a

lesser extent Co (column 4). The dark, narrow, cherty horizon occurring exclusively in the southernmost KMF between the middle and lowermost Mn-units, appears Al-K-Rb-Zr-enriched (column 5) and may correspond to a carbonate-free rock with marginally higher admixtures of detrital material.

#### 3.2.2.2. Altered iron-formation

In marked contrast to borehole GL26, four of the selected boreholes from the northern parts of the KMF (MK3I, MK2G, MK2H and N12D) show diverse petrographic characteristics, at least with respect to the iron-formation intersections. The most striking of these include the highly oxidized nature of the rock which is translated into the abundance of very fine-grained hematite along with microcrystalline chert, and the complete absence of carbonate minerals (hence the term “altered”; see PART 2). Also, despite the fact that relative thickness relations between the iron-formation and Mn ore-units are similar to borehole GL26, all four of the above boreholes exhibit clearly reduced thicknesses down to a band to band scale, resulting in lower overall thicknesses for the entire Hotazel Formation (see Appendix 1, Fig. A5).

Variation plots for the four borehole intersections containing altered iron-formation are shown in Figures 3.4 and 3.5 for selected major/trace elements respectively. Major element plots show a clear antithetic correlation between  $\text{SiO}_2$  and total Fe-oxide for the majority of samples, a classic example of the “closure” effect expected from rocks of such strong bimodal composition. Most remaining major element components such as CaO, MgO and MnO are very low (generally below 0.5wt%) and/or show no significant variations (see Tables 3.3 and 3.4). Notable exceptions constitute a few samples from the iron-formation intersections between the middle and uppermost Mn ore units which contain trace admixtures of acmite and thus exhibit total  $\text{Na}_2\text{O}$  contents up to 0.5 wt%. Most trace elements (e.g. Zn, Cu, Ni, Cr, Pb) show concentrations on the order of tens of ppm and show generally very little stratigraphic variation, although the degree of variation for some elements (e.g. Cr) may differ from borehole to borehole. This is effectively the only trace element that shows a marked resemblance with total Fe-oxide in terms of their variation patterns.

Exceptions to the above trends are seen in few samples occurring at specific stratigraphic

intervals, and for that reason it is convenient to separate the 4 borehole intersections into two groups. In boreholes MK2H and N12D (see Fig. 3.4), the iron-formation intersection above the uppermost Mn-ore unit consists essentially of massive hematite (+90% total iron-oxide; see Table 3.3, columns 2, 9 and 10). In addition, the uppermost sample in borehole MK2H (Table 3.3, column 3) is characterised by geochemical signatures partly indicative of supergene weathering. These are translated into low  $\text{SiO}_2$  (12 wt%), strong enrichments in MnO (25.30 wt%) in the form of Mn-oxide (braunite), atypically high  $\text{Al}_2\text{O}_3$  (5.33 wt%) and, to a lesser extent,  $\text{K}_2\text{O}$  (1.52 wt%) (due to the presence of muscovite and minor chlorite), as well as variable degrees of enrichment in all trace elements except Th (see Fig. 3.3 and Table 3.4). Furthermore, sample MK2H-6 (Table 3.3, column 4) collected from immediately above the uppermost Mn-ore unit is also substantially enriched in MnO (32.39 wt%) and certain trace elements (Cu, Pb, Ba, Sr and Y) and contains an appreciable amount of CaO (2.48 wt%) in the form of kutnahorite.

In the remaining parts of the stratigraphy, only a few samples deviate from the monotonous geochemical character of the iron formation intersections in boreholes MK2H and N12D (Fig. 3.4). These occur immediately above and below the lowermost Mn ore-unit. In borehole MK2H, sample MK2H-17 (Table 3.3, column 5) is acmite-rich and besides  $\text{Na}_2\text{O}$  (5.35 wt%) contains appreciable amounts of CaO (4.8 wt%), mainly due to small admixtures of andradite. Also, samples MK2H-18, MK2H-19, N12D-16 and N12D-17 (Table 3.3, columns 6, 7, 11 and 12 respectively) are characterised by substantially reduced  $\text{SiO}_2$  contents (1.56-12.28 wt%) and elevated total Fe-oxide concentrations (53.24-74.21 wt%), and contain increased - yet variable - amounts of CaO, MnO, MgO, Sr and Ba associated with carbonate material (calcite-kutnahorite).

In comparison with boreholes MK2H and N12D, boreholes MK3I and MK2G exhibit some important differences (see Fig. 3.5). The uppermost iron-formation intersection in both these boreholes does not contain samples of massive hematitic signature, and this persists virtually throughout the stratigraphy. Compositions of the bulk of the samples are thus dominated by  $\text{SiO}_2$  and total Fe-oxide (see columns 1, 5, Table 3.4). Exceptions constitute: (i) one sample at the stratigraphic top of intersection MK2G (MK2G-1) which contains high amounts of total Fe-oxide (83.17 wt%), low  $\text{SiO}_2$  (9.17 wt%) and increased amounts of  $\text{Al}_2\text{O}_3$  (2.83 wt%), MnO (1.58 wt%) and trace elements such as Ni, Cr and V (Table 3.4, column 6); (ii) three samples collected

immediately below the uppermost Mn ore-unit (MK3I-10, MK3I-11, MK2G-10) which consist essentially of pure hematite-acmite binary mixtures and contain high Na<sub>2</sub>O (~7 wt%) and relatively increased Cu contents (>100ppm; see columns 2, 7, Table 3.4); (iii) four samples between the middle and lowermost Mn-units, two of which are from borehole MK3I (MK3I-15, -16), contain high Na<sub>2</sub>O contents (related to abundant acmite) and show elevated MnO and CaO concentrations (Table 3.4, columns 3 and 4), and two from borehole MK2G (MK2G-16, -17), both of which exhibit elevated CaO, MnO and MgO values due to the presence of kutnahorite (Table 3.4, columns 8 and 9).

In summarizing, the four borehole intersections containing altered iron-formation are characterised by relatively simple bulk-rock geochemical signatures for large portions of the Hotazel succession. Above the uppermost Mn-unit, massive hematite develops in some intersections, but not in others. In addition, Na<sub>2</sub>O-rich, acmite-bearing samples are seen in some boreholes, notably immediately below the uppermost Mn-ore unit as well as between the middle and lowermost Mn-units. Lower in the stratigraphy and specifically between the middle and lowermost Mn-units and below the latter, iron-formation samples may contain appreciable amounts of carbonate-related compounds (CaO, MgO, MnO) with or without Na<sub>2</sub>O, and exhibit depletion in SiO<sub>2</sub> and enrichment in Fe in samples from the proximity of the manganese ore-units.

#### 3.2.2.3. Oxidized iron-formation

A large portion of three borehole intersections (N91B, BEL4C and BEL7A) from the northern parts of the KMF exhibits iron-formation with petrographic signatures which clearly distinguish it from pristine and altered iron-formation. The main petrographic attribute of this iron-formation is the abundance of bands containing mixed microcrystalline hematite (with or without magnetite) in association with chert/carbonate-bearing assemblages. The oxidised iron-formation therefore, appears to correspond to an intermediate member, in relation to the diverse compositions observed in pristine (carbonate/magnetite-rich) and altered (carbonate/magnetite-free) iron-formation types (see also PART 2).

Selected major and trace element variation profiles for two of the three borehole intersections

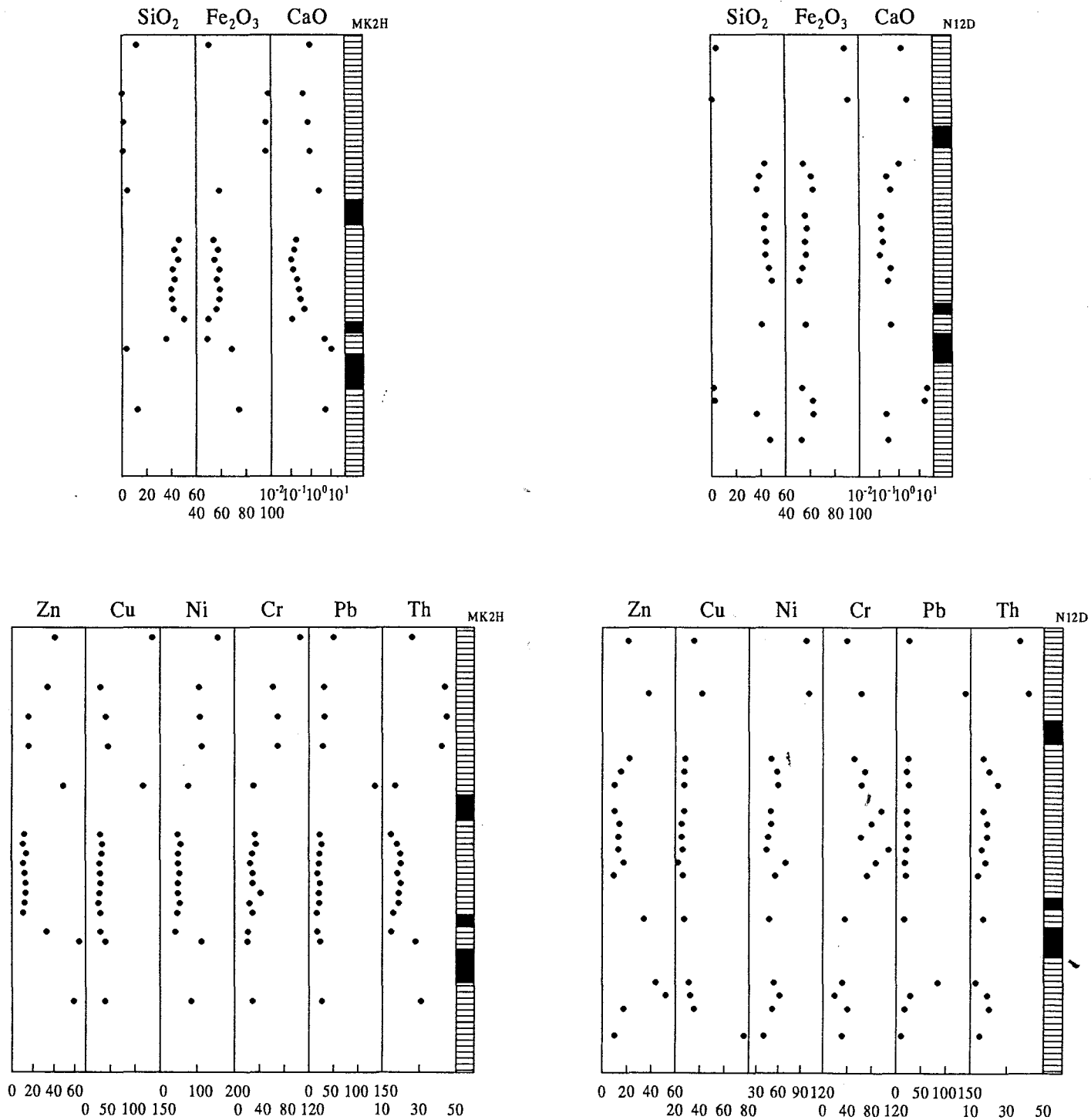


**Figure 3.4.** Variation plots of selected major and trace elements for borehole intersections MK2H and N12D from the northern parts of the KMF. Stratigraphic columns are not to scale, but depict approximate stratigraphic locations of the selected samples and crude relative thickness relations between iron-formation (horizontal line fill) and manganese units (black fill).

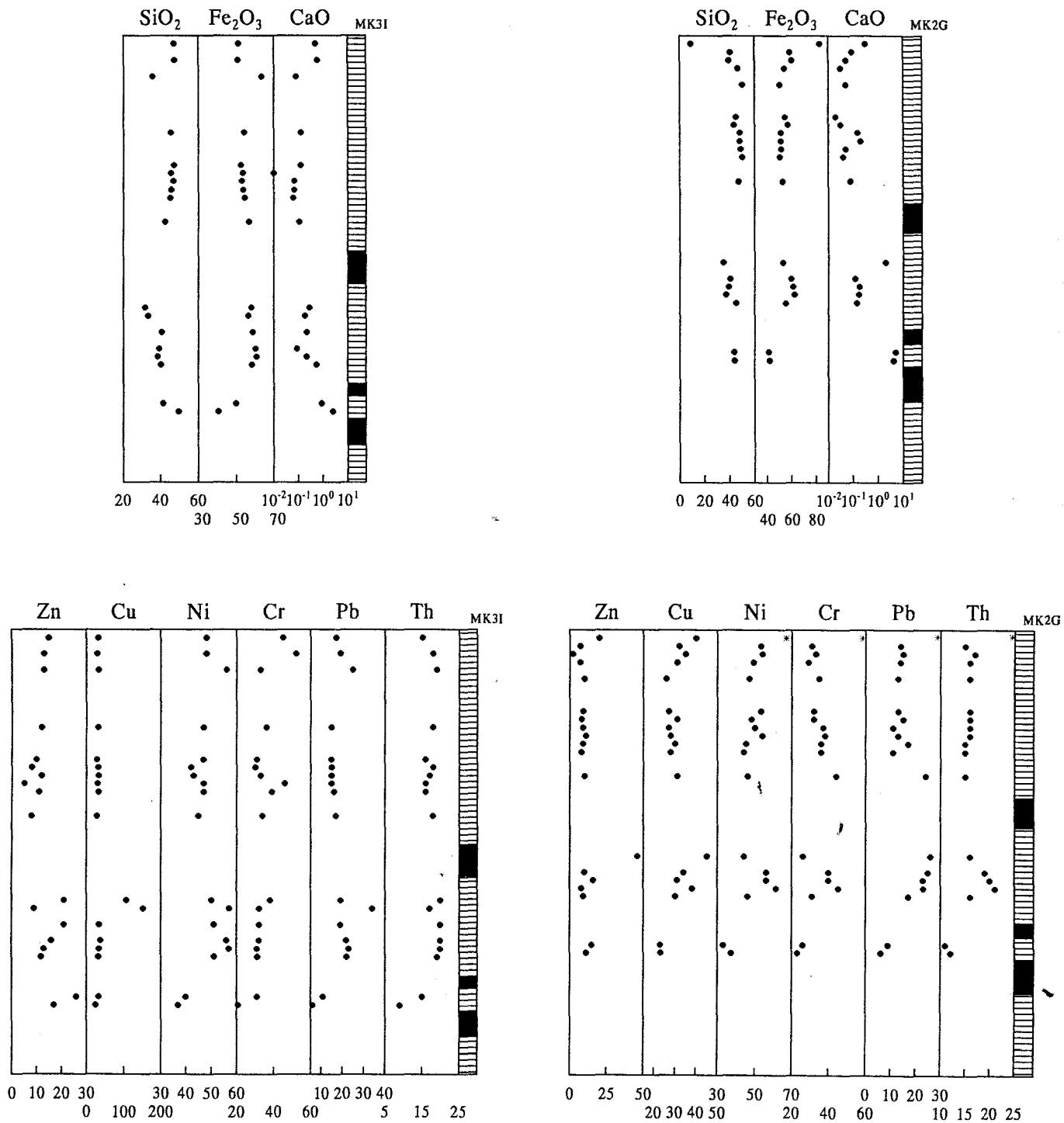


Figure 3.5. Variation plots of selected major and trace elements for borehole intersections MK3I and MK2G from the northernmost KMF. Stratigraphic columns are not to scale, but depict approximate stratigraphic locations of the selected samples and crude relative thickness relations between iron-formation (horizontal line fill) and manganese units (black fill) (asterisks represent values too high for the scale selected).

**Table 3.3.** Summary of whole-rock analytical data for samples from boreholes MK2H and N12D containing altered iron-formation.

	1	2	3	4	5	6	7	8	9	10	11	12
<i>wt%</i>	n=9	n=3						n=12				
SiO <sub>2</sub>	43.15 (3.08)	0.77 (0.31)	12.00	4.33	35.68	3.52	12.28	42.56 (3.74)	4.17	0.72	1.56	2.06
TiO <sub>2</sub>	0.03 (0.00)	0.04 (0.01)	0.25	0.07	0.03	0.05	0.04	0.02 (0.00)	0.03	0.04	0.04	0.05
Al <sub>2</sub> O <sub>3</sub>	0.18 (0.08)	0.35 (0.07)	5.33	0.24	0.34	0.42	0.33	0.18 (0.10)	0.71	0.25	0.24	0.13
Fe <sub>2</sub> O <sub>3</sub>	55.98 (2.84)	96.38 (1.18)	50.49	58.40	49.03	68.55	74.21	56.46 (3.51)	88.45	90.58	53.24	61.89
MnO	0.13 (0.08)	0.81 (0.38)	25.30	32.39	1.63	7.02	0.51	0.11 (0.09)	2.18	2.78	1.09	0.88
MgO	0.02 (0.02)	0.08 (0.02)	0.48	0.18	1.80	1.18	5.13	0.18 (0.36)	0.41	0.21	1.30	1.25
CaO	0.20 (0.11)	0.65 (0.19)	0.92	2.48	4.80	10.37	5.09	0.31 (0.23)	1.38	2.49	23.74	17.97
Na <sub>2</sub> O	0.24 (0.21)	0.08 (0.05)	0.11	lld	5.35	0.01	0.01	0.10 (0.26)	0.09	lld	lld	lld
K <sub>2</sub> O	0.01 (0.00)	0.01 (0.00)	1.52	lld	0.01	0.01	0.01	0.01 (0.01)	0.21	0.08	0.01	lld
P <sub>2</sub> O <sub>5</sub>	0.12 (0.04)	0.28 (0.07)	0.09	0.06	0.05	0.06	0.18	0.13 (0.06)	0.33	0.16	0.15	0.10
<i>ppm</i>												
Zn	12 (1)	22 (8)	41	49	33	64	59	15 (7)	21	38	44	52
Cu	30 (2)	39 (6)	134	116	30	40	39	31 (14)	35	42	31	32
Ni	50 (3)	109 (3)	155	77	42	112	84	52 (7)	97	101	54	61
Co	3 (3)	lld	31	16	lld	14	21	lld	15	9	lld	8
Cr	31 (5)	67 (4)	106	31	22	21	29	66 (23)	39	63	32	19
V	11 (3)	20 (3)	141	34	20	7	11	6 (5)	16	12	lld	lld
Ba	80 (170)	75 (34)	4317	3064	343	56	145	82 (194)	95	218	98	861
Sc	2 (0)	6 (2)	22	5	2	2	3	2 (0)	5	4	nd	nd
Pb	21 (3)	30 (2)	50	135	17	23	26	20 (4)	26	140	84	28
Th	18 (2)	44 (1)	26	17	15	28	31	18 (3)	37	42	13	19
Y	12 (2)	20 (5)	26	38	13	22	13	10 (3)	23	28	18	20
Nb	lld	lld	5	nd	lld	lld	nd	lld	nd	lld	nd	lld
Zr	5 (1)	11 (1)	97	6	5	9	10	6 (2)	11	8	8	7
Rb	lld	lld	44	lld	nd	lld	lld	lld	lld	10	lld	nd
Sr	13 (3)	20 (4)	312	447	153	124	14	9 (7)	18	279	221	85

nd = not determined

lld = lower limit of detection

n=number of samples

45.21 (2.33): mean (standard deviation)

Column 1,8: Altered iron-formation (chert-hematite)

2,9,10: Massive hematite samples

3-4: Hematite-braunite(+muscovite) rock

5: Acmite-rich iron-formation

6,7,11,12: Transitional, hematite-rich, chert/Mn-carbonate iron-formation

(Fig. 3.6) confirm the presence of two major types of iron-formation (see PART 2). The first type is developed exclusively above the uppermost Mn ore-unit and has a composition identical to altered iron-formation. This is readily evident from the well-developed mirror-image patterns for SiO<sub>2</sub> and Fe-oxide from this part of the stratigraphy (Table 3.5, column 2). Samples that do not conform with this pattern are the two uppermost samples from the boreholes BEL4C and BEL7A

**Table 3.4.** Summary of whole-rock analytical data for samples from boreholes MK3I and MK2G containing altered iron-formation

	1	2	3	4	5	6	7	8
<i>wt%</i>	n=14	n=2			n=15			n=2
SiO <sub>2</sub>	43.40 (3.78)	32.65 (0.85)	41.59	50.02	44.44 (4.10)	9.17	34.85	43.70 (0.26)
TiO <sub>2</sub>	0.02 (0.00)	0.03 (0.00)	0.03	0.03	0.02 (0.00)	0.58	0.03	0.03 (0.01)
Al <sub>2</sub> O <sub>3</sub>	0.18 (0.15)	0.21 (0.00)	0.16	0.10	0.15 (0.10)	2.83	0.41	0.19 (0.06)
Fe <sub>2</sub> O <sub>3</sub>	55.82 (3.74)	57.38 (0.78)	49.97	40.73	55.20 (4.04)	83.17	52.82	41.38 (0.44)
MnO	0.32 (0.23)	0.90 (0.23)	3.45	1.16	0.41 (0.27)	1.58	0.83	2.66 (0.06)
MgO	lld	0.06 (0.04)	0.35	0.45	lld	0.04	0.15	1.36 (0.16)
CaO	0.20 (0.19)	0.24 (0.05)	0.91	2.66	0.09 (0.06)	0.32	1.97	4.54 (0.34)
Na <sub>2</sub> O	0.04 (0.06)	6.81 (0.07)	3.13	4.59	lld	0.94	6.98	lld
K <sub>2</sub> O	0.01 (0.00)	lld	0.05	0.09	lld	0.02	nd	lld
P <sub>2</sub> O <sub>5</sub>	0.11 (0.10)	0.03 (0.01)	0.03	0.05	0.06 (0.04)	0.20	0.09	0.19 (0.01)
<i>ppm</i>								
Zn	12 (4)	15 (6)	26	17	9 (3)	20	46	13 (2)
Cu	33 (2)	130 (23)	34	25	31 (3)	40	45	23 (0)
Ni	49 (5)	54 (4)	40	37	51 (5)	125	44	35 (2)
Co	lld	3 (3)	lld	6	lld	32	7	lld
Cr	36 (7)	35 (3)	31	21	36 (5)	102	26	25 (2)
V	13 (4)	11 (2)	11	8	15 (8)	60	10	3 (3)
Ba	34 (28)	27 (1)	36	30	31 (16)	75	350	9 (1)
Sc	2 (0)	2 (0)	2	2	2 (0)	9	3	3 (0)
Pb	18 (3)	27 (8)	11	6	17 (5)	60	26	8 (2)
Th	18 (2)	19 (2)	15	9	17 (2)	35	16	12 (1)
Y	8 (5)	13 (1)	10	9	9 (7)	36	12	12 (1)
Nb	1 (1)	lld	lld	lld	lld	lld	lld	lld
Zr	7 (1)	7 (1)	5	5	6 (1)	38	6	4 (1)
Rb	lld	lld	lld	3	lld	nd	nd	lld
Sr	9 (5)	80 (11)	104	40	7 (2)	19	48	9 (1)

nd = not determined

lld = lower limit of detection

n=number of samples

42.51 (2.33): mean (standard deviation)

Column 1,5: Altered iron-formation (chert-hematite)

2,3,4,7: Acmite-rich iron-formation

6: Hematite-rich, muscovite-bearing unit

8: Chert-hematite-kutnahorite iron-formation

(BEL4C-1 and BEL7A-2 respectively; see Table 3.5, columns 4, 5), which show geochemical similarities with the uppermost samples from boreholes MK2H and MK2G (low SiO<sub>2</sub>, high MnO and Al<sub>2</sub>O<sub>3</sub> and enrichments in virtually all trace elements). A postulated "limit" in the development of altered iron-formation in these boreholes is seen above the uppermost Mn-unit, where a carbonate-enriched, "transitional" rock is developed over a fairly broad stratigraphic interval (samples BEL7A-8a, N91B-9a, BEL4C-6; see also Appendix I, Fig. A3).



The second iron-formation type develops in the remaining portions of the iron-formation stratigraphy, that is, below the uppermost manganese ore-unit, and corresponds to the oxidised iron formation (Table 3.5, column 1). Chemostratigraphic patterns (Fig. 3.6) display no clear antithetic correlations between  $\text{SiO}_2$  and total Fe-oxide; instead, there is a rather distinct positive correlation between the patterns for whole-rock CaO, MgO and to a lesser extent MnO. Furthermore, stratigraphic patterns for certain trace elements such as Th, Ni and Cr agree well with the one for total Fe-oxide, while others (e.g. Zn, Cu) do not show any clear similarities with any major element patterns.

There are very few samples with chemical compositions that strongly diverge from this general trend. These are geochemically similar to the samples from the transitional rock above the uppermost Mn-unit, and are confined either below the latter (N91B-10), or below the lowermost Mn-unit (N91B-30, BEL7A-17a). The mineralogy of these samples is dominated by hematite and Mn-carbonates (kutnahorite, rhodochrosite) with minor admixtures of quartz and silicate minerals (mainly minnesotaite/talc and minor riebeckite, chlorite and friedelite). Average major and trace element concentrations for all samples of this type are shown in Table 3.5 (column 3). In addition, two samples above the middle Mn-unit in borehole N91B (N91B-25 and N91B-26) have low  $\text{SiO}_2$  (<20 wt%) and contain increased amounts of MnO (~11 wt%) and CaO (>20 wt%; see Table 3.5 columns 7,8) in the form of mixtures of Mg-calcite and kutnahorite. One sample from below the lowermost Mn-unit in borehole BEL4C (BEL4C-24) is geochemically similar with samples from respective parts of borehole intersections containing altered and pristine iron-formation, in having low  $\text{SiO}_2$  (14 wt%) and increased contents of MnO (~10 wt%) and MgO (4.28 wt%; Table 3.5, column 6) hosted in manganiferous carbonates (kutnahorite, rhodochrosite).

### 3.2.3. Preliminary conclusions

Some important points from the above data presentation are summarised below:

(i) The Hotazel iron-formation exhibits significant geochemical variations not only amongst the various borehole intersections, but also within the same stratigraphic column as displayed in individual boreholes. These variations correspond to petrographic variations established in PART 2, and support the crude subdivision of the iron-formation into three major

**Table 3.5.** Summary of whole-rock geochemical data for samples from boreholes N91B, BEL4C and BEL7A containing oxidised iron-formation

	1	2	3	4	5	6	7	8
<i>wt%</i>	n=52	n=14	n=6					
SiO <sub>2</sub>	34.36 (4.96)	46.66 (3.49)	20.81 (2.41)	3.43	4.04	14.00	13.09	18.32
TiO <sub>2</sub>	0.03 (0.01)	0.02 (0.00)	0.03 (0.01)	0.06	0.39	0.03	0.03	0.03
Al <sub>2</sub> O <sub>3</sub>	0.22 (0.11)	0.14 (0.18)	0.21 (0.04)	1.83	3.87	0.26	0.22	0.16
Fe <sub>2</sub> O <sub>3</sub>	48.13 (6.90)	52.81 (3.58)	43.01 (4.73)	52.78	70.36	52.88	26.36	30.64
MnO	1.30 (0.66)	0.13 (0.08)	13.24 (2.78)	39.59	7.83	10.01	10.98	5.61
MgO	2.63 (1.28)	0.04 (0.05)	6.31 (2.29)	0.81	4.28	7.28	1.70	1.96
CaO	5.70 (2.84)	0.20 (0.12)	4.36 (0.87)	0.46	2.44	3.81	23.31	21.68
Na <sub>2</sub> O	lld	lld	0.24 (0.34)	nd	nd	nd	nd	nd
K <sub>2</sub> O	lld	lld	0.06 (0.09)	nd	0.01	nd	nd	lld
P <sub>2</sub> O <sub>5</sub>	0.12 (0.03)	0.12 (0.05)	0.08 (0.01)	0.10	0.21	0.08	0.09	0.09
<i>ppm</i>								
Zn	18 (6)	11 (3)	36 (11)	616	140	47	37	44
Cu	26 (4)	27 (3)	25 (3)	53	37	27	25	24
Ni	38 (7)	46 (6)	44 (3)	95	164	54	32	29
Co	4 (7)	lld	60 (18)	9	165	22	lld	23
Cr	21 (6)	35 (8)	15 (2)	58	149	15	12	11
V	3 (4)	14 (7)	2 (3)	588	62	nd	nd	nd
Ba	14 (10)	587 (1898)	249 (186)	6421	4073	51	70	26
Sc	3 (1)	2 (1)	3 (0)	14	16	3	nd	nd
Pb	8 (2)	11 (2)	8 (1)	91	41	10	3	4
Th	13 (3)	16 (2)	13 (2)	27	32	21	6	7
Y	13 (3)	8 (3)	11 (2)	8	45	11	15	16
Nb	lld	lld	lld	nd	lld	lld	lld	lld
Zr	6 (2)	6 (1)	7 (1)	13	76	4	4	3
Rb	lld	lld	4 (5)	nd	nd	lld	nd	nd
Sr	29 (54)	15 (34)	24 (14)	112	118	15	299	310

nd = not determined

lld = lower limit of detection

n=number of samples

42.51 (2.33): mean (standard deviation)

Column 1: Oxidised iron-formation

2: Altered iron-formation

3: Transitional hematite/(Mg,Mn)-rich carbonate rock

4: Hematite/braunite-rich iron-formation

5,6,7,8: Transitional, chert-poor, hematite/Mn-carbonate rock

types, namely *pristine*, *oxidised* and *altered* iron-formation.

(ii) There appears to be a lateral control in the distribution of the rock types identified. For example, massive hematite rock is found in certain boreholes above the uppermost manganese unit. The same applies to borehole intersections containing oxidised iron-formation, whereby iron-formation of the altered type develops only in the uppermost part of the stratigraphy, whereas

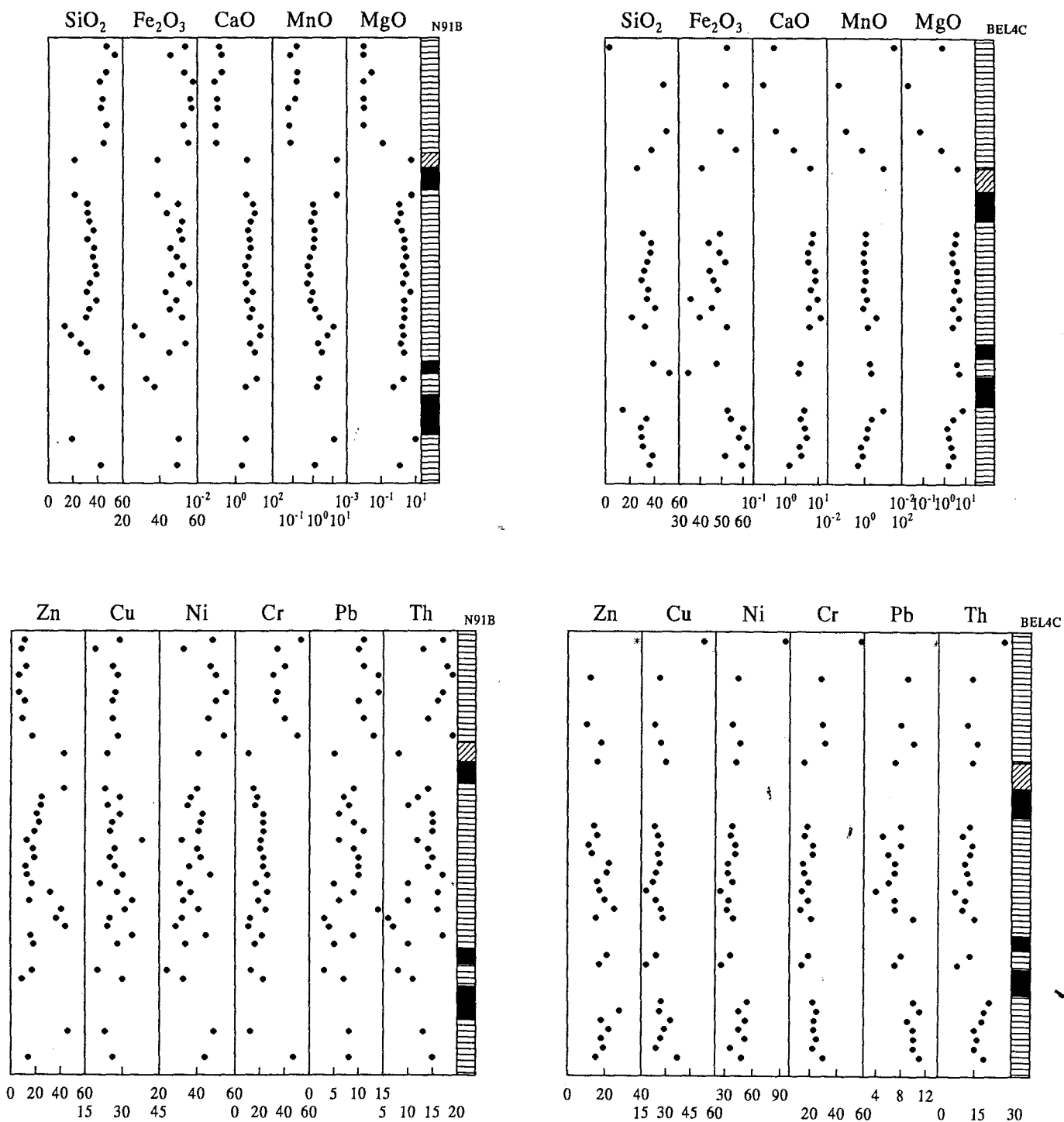


Figure 3.6. Variation plots of selected major and trace elements for borehole intersections N91B and BEL4C from the northern parts of the KMF. Stratigraphic columns are not to scale, but depict approximate stratigraphic locations of the selected samples and crude relative thickness relations between iron-formation (horizontal line fill), manganese units (black fill) and a transitional Fe/Mn/Mg-carbonate unit (inclined line fill). (asterisks represent values too high for the scale selected).

oxidised iron-formation dominates in the remaining portion.

(iii) Significant departures from the general geochemical trends seen in most boreholes are observed primarily on the transitions with the Mn ore-units, particularly in the lower parts of the Hotazel stratigraphy. Between the middle and lowermost Mn-units and below the uppermost Mn-unit, altered iron-formation samples commonly contain high Na, Ca, Mg and Mn due to the presence of acmite and/or Mn-rich carbonates. Regarding oxidised iron-formation, the main characteristics are increased amounts of Mg/Mn-rich carbonates (kutnahorite, rhodochrosite) in carbonate-rich, transitional iron-formation - manganese units, particularly those developed above the uppermost and middle, and below the lowermost manganese ore-units.

Despite the above variations the majority of the selected samples appear to fall into the three specified groups *pristine*, *oxidised* and *altered* as established on petrographic grounds. Detailed treatment of these distinct types will be presented in the following chapters.

## Chapter 3.3: Geochemistry of selected sample groups

### 3.3.1. Iron-formation

#### 3.3.1.1. Discriminant analysis

Based on the presentation of all analytical data from the previous chapter, the three major iron-formation types recognised were further treated by means of statistical analysis. Statistical analysis has been used in previous studies in conjunction with bivariate scatter plots and histograms, in order to separate metapelitic rock units from the Dalradian Supergroup of Scotland (Lambert et al., 1981, 1982), and from the Namaqualand metamorphic complex, South Africa (Moore, 1989). In such rocks, major constituents such as SiO<sub>2</sub>, FeO, MgO and K<sub>2</sub>O which correspond to the quartz/K-feldspar/mica/clay content of the pelites, appear to be relatively insensitive indicators of environmental change. On the other hand, lesser constituents such as CaO, P<sub>2</sub>O<sub>5</sub>, Rb, Sr, Nb, Ni, and Y (and to a lesser extent Al<sub>2</sub>O<sub>3</sub> and Na<sub>2</sub>O) corresponding to mineral phases such as chlorite, plagioclase, apatite, zircon and carbonates, are more sensitive indicators and constitute

the most effective geochemical discriminators.

Effective statistical separation of the selected data groups in the Hotazel iron-formation involved stepwise discriminant analysis using the computer program "STATISTICA" available on the Rhodes University Computer Services Network. The program calculated canonical discriminant functions which assisted in the classification of the three groups. The total number of cases (iron-formation samples) was 141, corresponding to the sum of 50 selected samples of the pristine type, 45 samples of the altered type and 46 samples of the oxidized type. Samples were selected on the basis of crude geochemical and petrographic signatures as presented in the previous chapters. Altered samples derive from the uppermost and middle portions of the iron-formation intersections of boreholes MK2H, N12D, MK3I and MK2G, pristine samples from respective intersections of boreholes R59, R63, R65, R70, SM31 and GL26, and oxidised samples from the middle and lowermost iron-formation intersections of boreholes N91B, BEL4C and BEL7A. The few samples showing geochemical signatures that strongly diverge from the three above-mentioned groups (e.g. acmite-rich samples, samples from carbonate-rich transitional units) were excluded for convenience. The number of variables (major element oxides and trace elements) was 25, i.e. all major and trace element components presented in Appendix III, excluding LOI and  $H_2O^-$  values. The discriminant analysis selected 9 variables, namely Pb, MgO, Sr, Y, V, Ni,  $Al_2O_3$ , MnO and  $Fe_2O_3$ , for which coefficients were calculated for two canonical variables (Table 3.6). These two canonical variables successfully segregated the three iron-formation types (pristine, altered and oxidised) into three distinct "clusters" (Fig. 3.7). The distribution of the altered type defines a distinct field, while the pristine and oxidised types show a minor degree of overlap which is nonetheless statistically insignificant.

Figure 3.8 illustrates the most important geochemical differences between the three separated sample groups in terms of their average major element compositions. Average data have been normalised against the composition of a hypothetical iron-formation which corresponds to the overall average composition of the Superior-type iron-formation used to define the compositional field of Figure 3.1 earlier. The three spidergrams of Figure 3.8 do not facilitate a clear-cut definition of a pristine iron-formation type, i.e. an iron-formation with average composition closer to the hypothetical mean in relation to the others. The pristine iron-formation approaches the ideal

composition in six out of the ten major elements, namely  $\text{TiO}_2$ ,  $\text{Al}_2\text{O}_3$ ,  $\text{Fe}_2\text{O}_3$ ,  $\text{MnO}$ ,  $\text{Na}_2\text{O}$  and  $\text{K}_2\text{O}$ , whereas the altered and oxidized iron-formations show averages closer to the selected mean for  $\text{SiO}_2$  and  $\text{P}_2\text{O}_5$ , and  $\text{CaO}$  and  $\text{MgO}$  respectively. Although reasons for the above discrepancies have been provided during the presentation of mineralogical and chemical data from the pristine iron-formation in previous chapters, further statistical treatment presented in the following section highlights the important mineral-chemical relationships between the three iron-formation types.

**Table 3.6.** Coefficients for canonical variables 1 and 2 and the U-statistics from the stepwise discriminant analysis of iron-formations from the KMF.

Variable	Coefficient for canonical variable 1	Coefficient for canonical variable 2	U-statistics (Wilks' Lambda)
Pb	-0.25010	-0.03235	0.3713
MgO	0.73299	-0.11199	0.2247
Sr	0.00369	0.00545	0.1571
Y	0.12414	0.01974	0.0971
V	-0.11387	-0.00785	0.0865
Ni	0.01972	0.10452	0.0759
$\text{Al}_2\text{O}_3$	1.81207	0.67957	0.0702
MnO	0.51193	-1.41510	0.0658
$\text{Fe}_2\text{O}_3$	0.06531	-0.16343	0.0590
Constant	-4.18021	4.29095	

### 3.3.1.2. Principal component analysis

Principal component analysis has been applied to bulk-rock compositions of metamorphic rocks with the purpose of reconstructing the pre-metamorphic distribution of the elements assuming minimal chemical modification during metamorphism (e.g. Lambert et al., 1981, 1982; Moore, 1989). Applications of this kind make use of an important property of principal component analysis, that is, no assumption about the original variables is involved (Marriott, 1974). Therefore the calculated factors are unconstrained by the metamorphic petrology of the rocks and can thus be interpreted as element associations related to the original precursor materials, assuming

isochemical metamorphism. Principal component analysis transforms the original set of variables into a new set of variables described as principal component coordinates. The principal component coordinates are not correlated with each other, and each one of them accounts for a certain amount of the variance within the data set (le Maitre, 1982). In practice, only a few sets of principal component coordinates generally account for a large proportion of the variance, thus limiting the number of relevant factors that need to be considered.

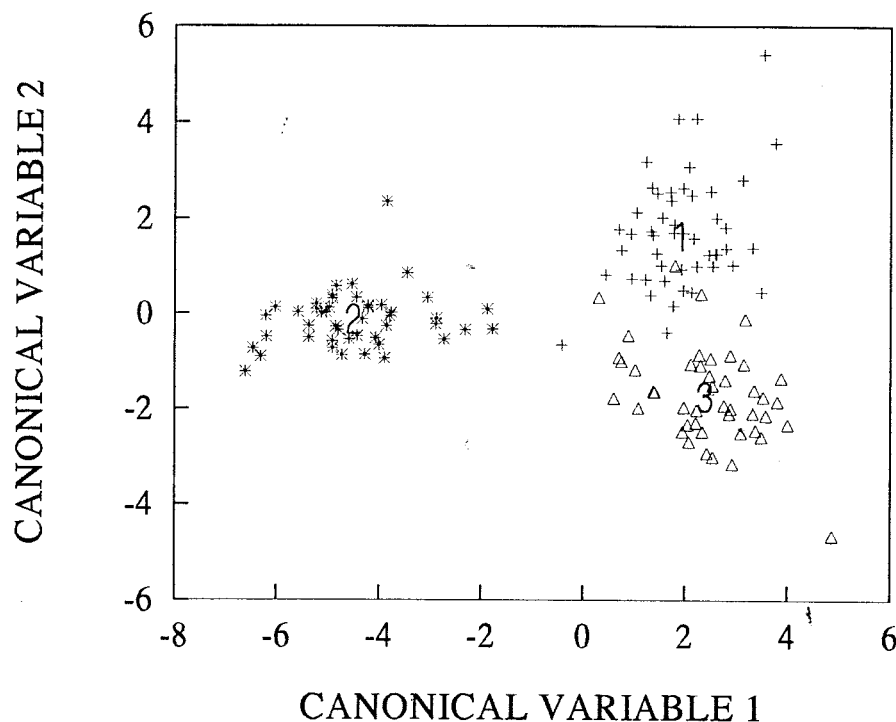


**Figure 3.7.** Plot of the two canonical variables calculated in the stepwise discriminant analysis to separate the three selected iron-formation types of this study, i.e. pristine (+ with mean value at 1), altered (\* with mean value at 2) and oxidized ( $\Delta$  with a mean value at 3).

Principal component analysis for the three iron-formation types was obtained using the computer programme "STATISTICA". The same number of samples (i.e. 141) and the same number of variables (i.e. 25) were used as in the discriminant analysis. The programme established a correlation matrix on which initial factor extraction was performed by principal component analysis. Eigen values were calculated and a varimax orthogonal transformation of the principal

factor loadings was performed using Kaiser's (1958) normalisation method. Factor loadings between 0.50 and -0.50 were omitted in order to simplify the factors to variables with significant factor loadings. Only the first 5 factors, accounting for approximately 80-90% of the cumulative variance, were used.

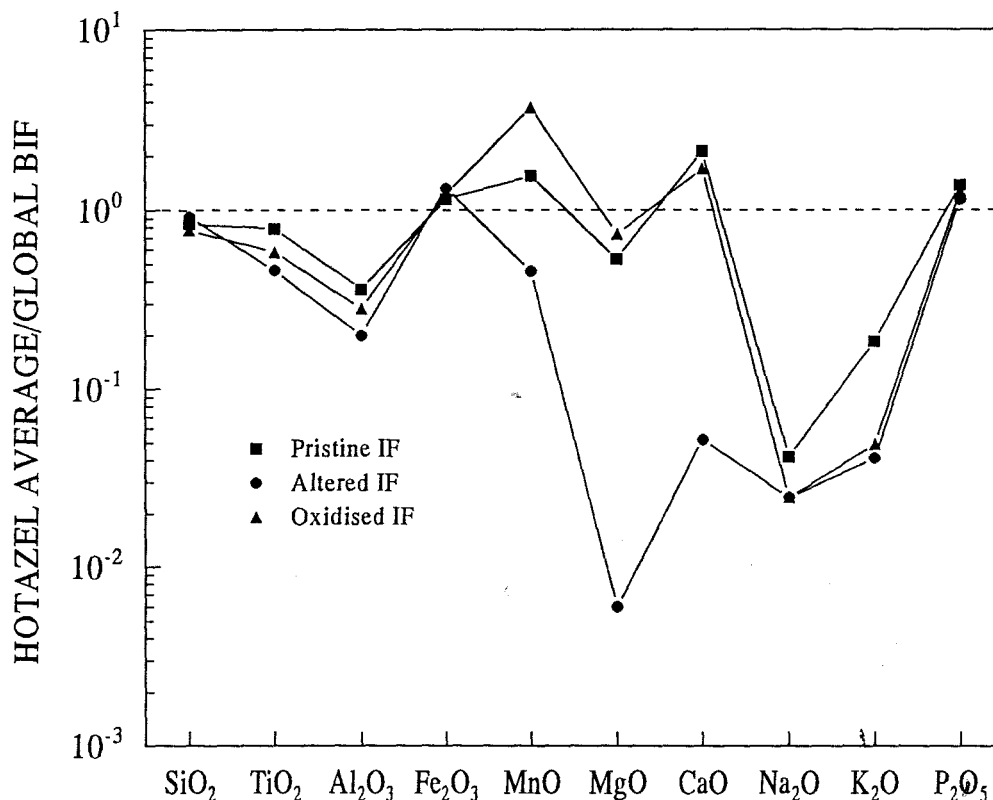


**Figure 3.8.** Spidergrams depicting major element averages for pristine, altered and oxidised iron-formation, normalised against the average composition of Superior-type iron-formation.

One important limitation of statistical techniques such as principal component analysis is that of constant-sum closure. Since major element oxides in whole-rock analyses must sum to 100%, one of these oxides cannot increase without others decreasing and *vice versa*. Closure thus invalidates the use of the null hypothesis, resulting in correlation coefficients being considerably more negative than obtained for ordinary data (le Maitre, 1982). For rocks of this study, the most marked effect of closure is related to the interrelation of the major components SiO<sub>2</sub>, Fe<sub>2</sub>O<sub>3</sub> and CaO, and this must be taken into serious account when the various factors are considered.



Fortunately, the bulk of all of these components is present in essentially three mineral constituents, i.e. quartz, iron oxide (magnetite and/or hematite) and carbonate, which dominate the mineralogy of all selected iron-formation groups and to which most remaining constituents would be expected to show negative or positive correlations.

The use of principal component analysis in the Hotazel iron-formation groups is not unconstrained by changes in bulk chemical composition during later secondary and/or metasomatic processes. Therefore, the use of this technique here does not strictly parallel previous applications on metamorphic rocks. The main objective instead is to effectively portray the most important geochemical associations of the selected sample groups. In principle, the pristine iron-formation can provide useful information concerning primary element associations, while information from the oxidised and altered types can be used to deduce pathways of open-system alteration. Evidence regarding the history of the altered and oxidised types is sought on the assumption that the material prior to the alteration process/es that produced these rocks corresponds closely to the pristine iron-formation.

In the case of the data set for the pristine iron-formation, five varimax rotated factors were calculated which cumulatively accounted for 93% of the variance (Fig. 3.9). Factor 1 (Fig. 3.9) has high positive loadings for CaO, Sr, MnO and Ba, and negative loadings for Fe<sub>total</sub> (as Fe<sub>2</sub>O<sub>3</sub>), Th, Pb and SiO<sub>2</sub>. This rather atypical "closure" factor for iron-formations accounts for 40% of the variance and highlights the strong inverse relationship between the chert-magnetite (+Th, +Pb) and the carbonate (+Sr, +MnO, +Ba) components of the rock. Factors 2 and 3 correspond to the minor detrital/diagenetic component of the iron-formation. Factor 2 shows high positive loadings for K<sub>2</sub>O, Na<sub>2</sub>O, and Al<sub>2</sub>O<sub>3</sub> (+Ba), and confirms the common presence of minor amounts of diagenetic, alkali-bearing silicate phases such as stilpnomelane (and more rarely riebeckite) in the pristine samples. Factor 3 has high positive loadings for V, Zr, Al<sub>2</sub>O<sub>3</sub> and SiO<sub>2</sub>, and points towards the otherwise very limited presence of a terrigenous component (e.g. zircon, Al-clay) in the samples. Factor 4 shows positive loadings for Ni and Cr and negative for Zn, suggesting potential geochemical affiliations to the Fe-oxide (magnetite) and carbonate components respectively. Factor 5 is a possible detrital and/or phosphate (apatite/xenotime?) factor, primarily due to the positive loadings for Y and P<sub>2</sub>O<sub>5</sub>.

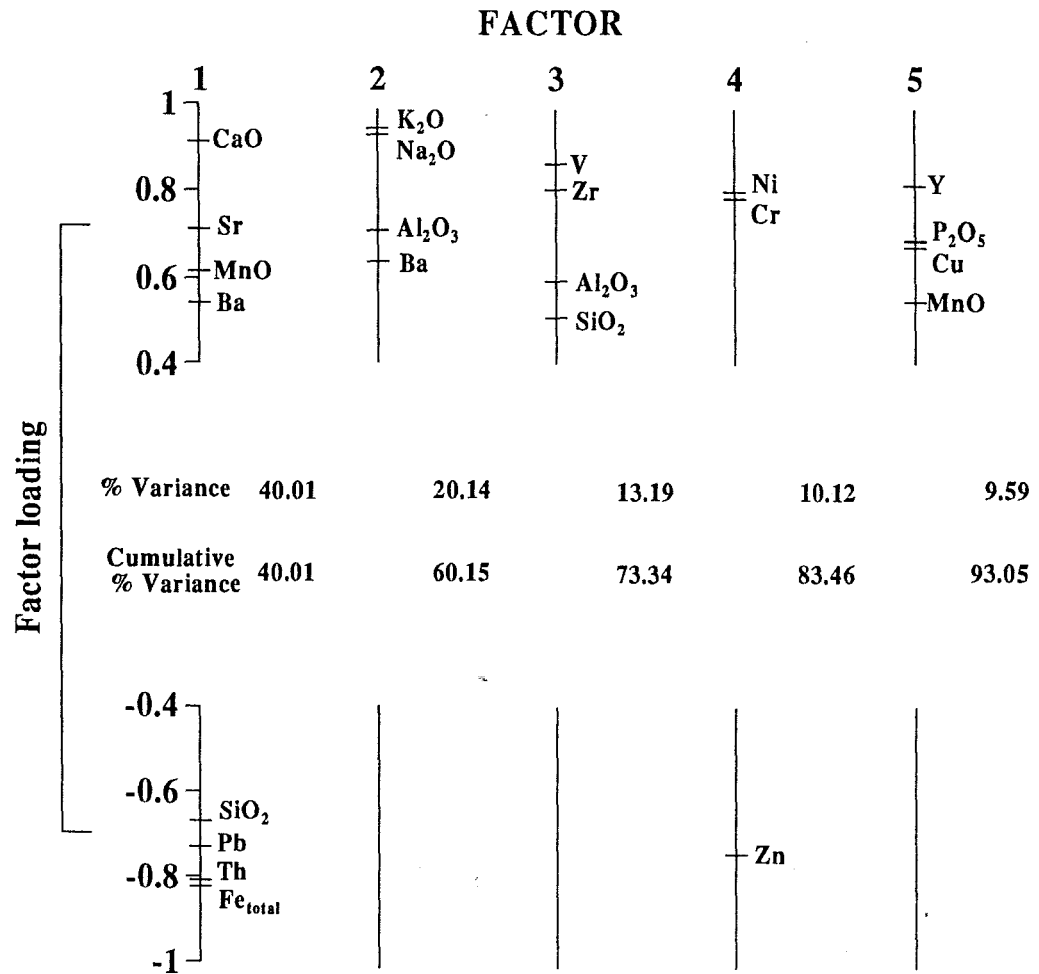


**Figure 3.9.** The five principal factors showing the factor loadings of the variables and their cumulative variance obtained in the principal components analysis of the pristine iron-formation.

The five factors identified for the altered iron-formation (Fig. 3.10) account for 79% of the variance, an indication of less well-constrained factors when compared to the ones obtained for the pristine iron-formation. Factor 1 accounts for 28.19% of the variance and corresponds to the “closure” factor for this sample group, with strong positive loadings for total Fe-oxide, Th, Ni and Pb, and negative loading for  $\text{SiO}_2$ . The antithetic correlation between quartz and Fe-oxide (now hematite) is thus readily apparent. Factor 2 suggests that small amounts of Sr and  $\text{Na}_2\text{O}$  (+Y) are now present in association with minor admixtures of acmite found in many of the samples, due to the respective positive loadings observed for those components. Factor 3 has positive loadings for  $\text{P}_2\text{O}_5$  and CaO which, in the absence of carbonates, implies that the limited remaining CaO is

now hosted almost exclusively in a phosphate mineral phase (apatite). Factor 4 has positive loadings for  $K_2O$ , Cu and  $Al_2O_3$ , an association related to a residual detrital (clay?) component in the samples, while factor 5 indicates an antithetic geochemical behaviour between V and Cr during alteration.

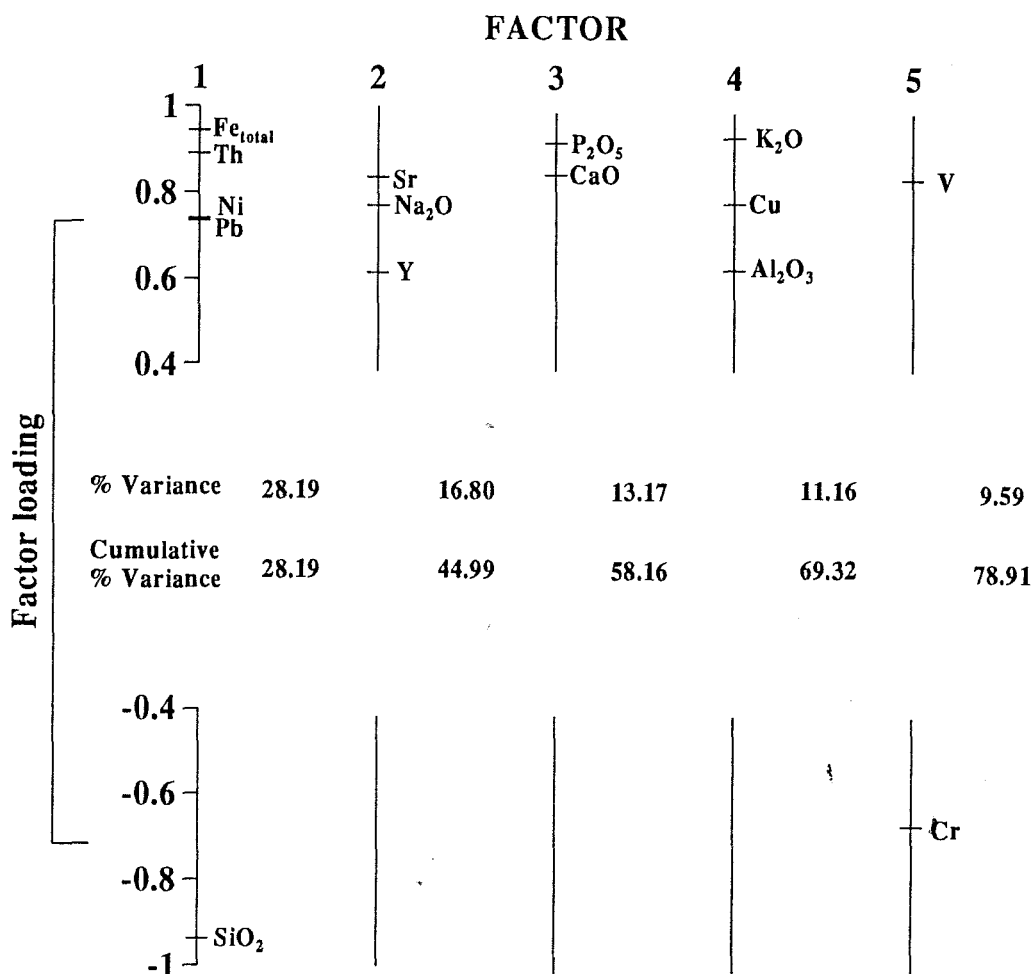


**Figure 3.10.** The five principal factors showing the factor loadings of the variables and their cumulative variance obtained in the principal components analysis of the altered iron-formation.

With regard to the oxidised iron-formation (Fig. 3.11), factor 1 accounts for almost 40% of the cumulative variance and shows positive loadings for Th, total Fe-oxide, Ni, Pb, Cu and Cr, and negative loadings for CaO and MgO. The “closure” effect in this group is demonstrated by a clear antithetic correlation between total Fe-oxide and associated transition elements, and the Mg-

enriched carbonate component of the rock. Positive loadings for MnO and Co and negative loading for SiO<sub>2</sub> in factor 2 indicate that limited amounts of Co-bearing Mn-oxide are present in the samples (possibly in association with Fe-oxide?) and correlate antithetically with the amount of chert present. Factor 3 is the terrigenous detrital factor with high positive loadings for Al<sub>2</sub>O<sub>3</sub>, Zr, V and Cr, while factor 4 shows positive loadings for P<sub>2</sub>O<sub>5</sub> and Y, corresponding again to a minor detrital/phosphate component. Finally, factor 5 has a positive loading for Sr and a negative loading for MgO which, in conjunction with factor 1 confirms earlier observations that a secondary, dolomitic carbonate is now the main carbonate phase, apparently replacing early Sr-bearing calcite of pristine iron-formation.

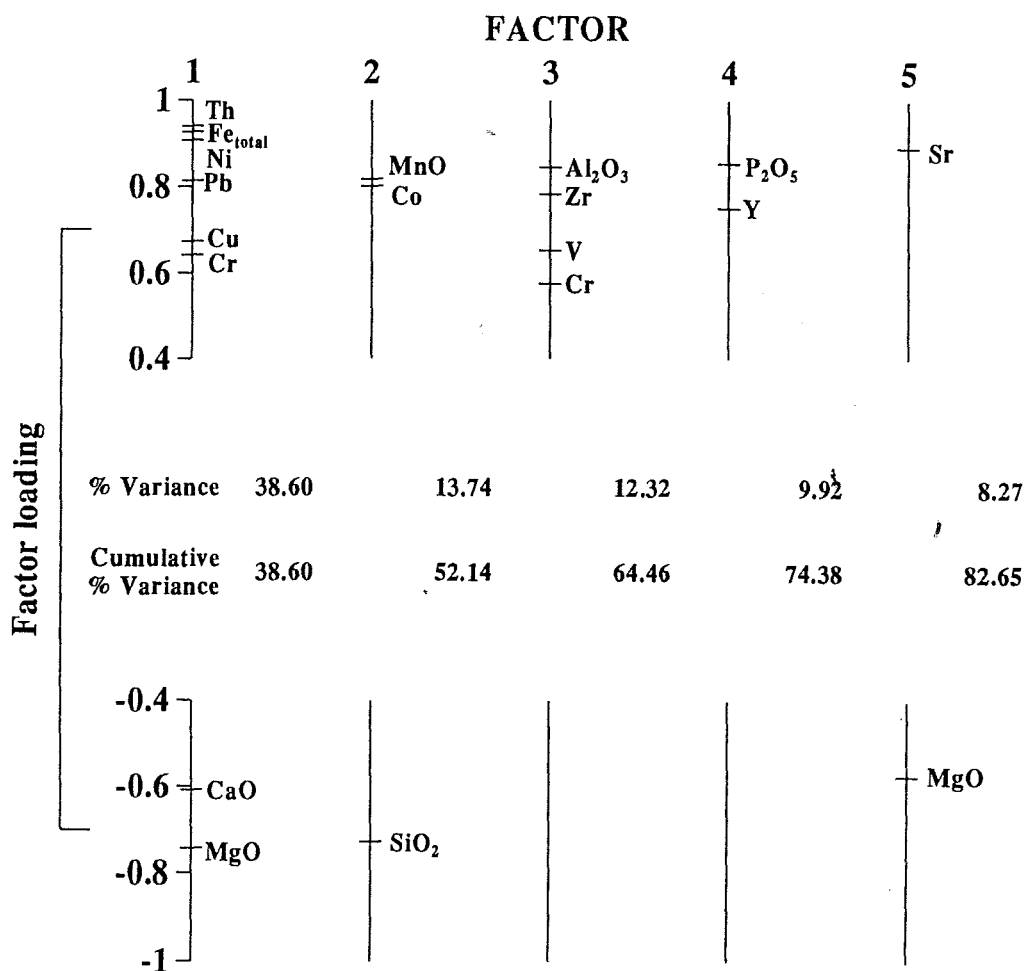


**Figure 3.11.** The five principal factors showing the factor loadings of the variables and their cumulative variance obtained in the principal components analysis of the oxidised iron-formation.

### 3.3.1.3. Inter-elemental relations

The results of principal component analysis proved to be particularly useful in highlighting the main mineralogical-geochemical associations that characterise the three iron-formation rock-types. In the light of this information, the selected major iron-formation datasets were further plotted on simple bivariate diagrams, with the purpose of providing a more detailed insight into the geochemical signatures of the individual iron-formation types. For the purpose of convenience, data from the individual types are represented on all graphs as filled circles (●) for the altered samples, filled triangles (▲) for the oxidised samples, and two symbols for the pristine samples, i.e. crosses (✚) for the carbonate-poor samples and open squares (□) for the carbonate-rich ones.

Figure 3.12 presents a summary of the major element geochemical relations developed in all three iron-formation groups, using as common attribute the main “closure” factor, that is, total Fe-oxide (as  $\text{Fe}_2\text{O}_3$ ). Graph 3.12a shows the relationship between total  $\text{Fe}_2\text{O}_3$  and  $\text{SiO}_2$  for all three groups. The antithetic correlation between the two components in the altered samples is clearly evident. On the other hand, data for the pristine and oxidised samples do not follow any specific trend and show substantial compositional overlap. A large proportion of carbonate-rich pristine samples obviously contain the lowest  $\text{SiO}_2$  and  $\text{Fe}_2\text{O}_3$  values relative to the carbonate-poor ones, resulting in a very broad positive trend. Also, oxidised samples exhibit the highest  $\text{Fe}_2\text{O}_3$  values for a significant proportion of the sample population.

The remaining plots of Figure 3.12, i.e.  $\text{Fe}_2\text{O}_3$  vs CaO, MgO and MnO, illustrate how the pristine and oxidised sample groups differ in terms of their carbonate-related components. Oxidised samples show relative enrichment in MgO and MnO and depletion in CaO compared to pristine samples. Antithetic relationships between total  $\text{Fe}_2\text{O}_3$  and CaO for pristine samples and between total  $\text{Fe}_2\text{O}_3$  and CaO/MgO for oxidised samples are indicative of closure between the carbonate and Fe-oxide mineralogy of the two iron-formation types. Most altered samples show very low CaO and MgO contents, commonly below the lower limit of detection.

Figure 3.13 shows plots of whole-rock CaO vs MnO, MgO, Sr and  $\text{P}_2\text{O}_5$ . Besides the distinct enrichment of oxidised samples in MnO and MgO relative to the pristine ones, the good positive

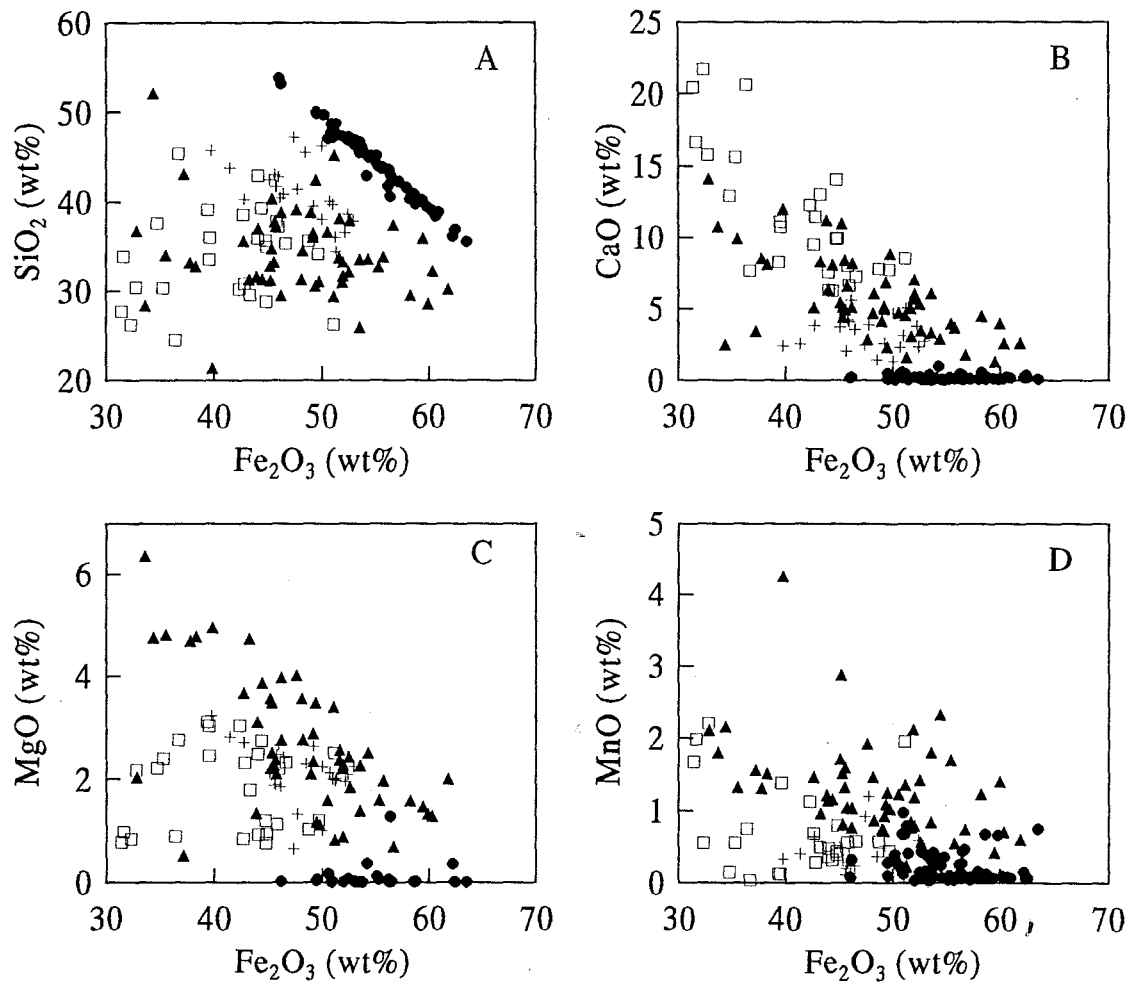


**Figure 3.12.** Major element characteristics of pristine (+: carbonate-poor; □: carbonate-rich), altered (●) and oxidised (▲) iron-formation as displayed on bivariate plots of total Fe-oxide concentrations (as  $\text{Fe}_2\text{O}_3$ ) versus whole-rock SiO<sub>2</sub> (a), CaO (b), MgO (c) and MnO (d).

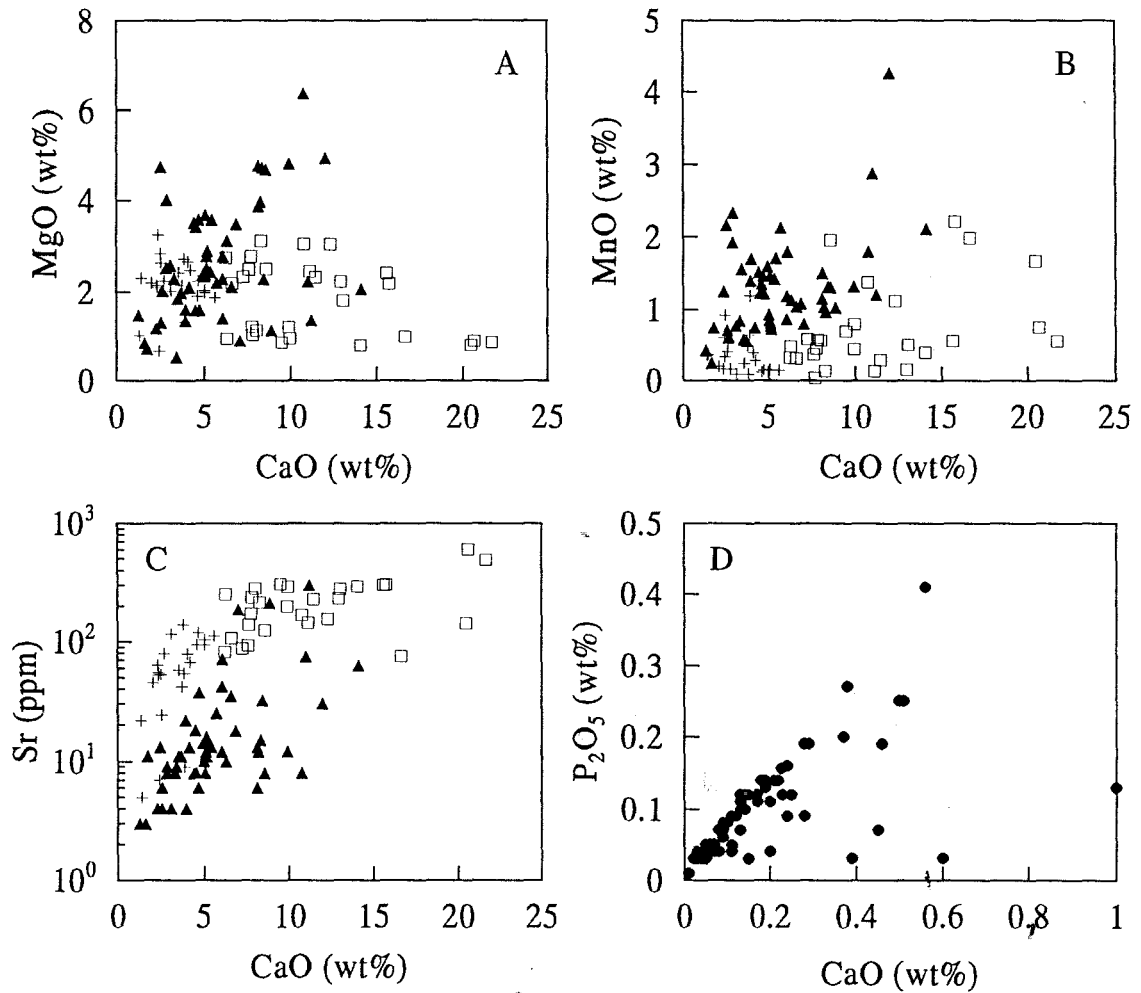


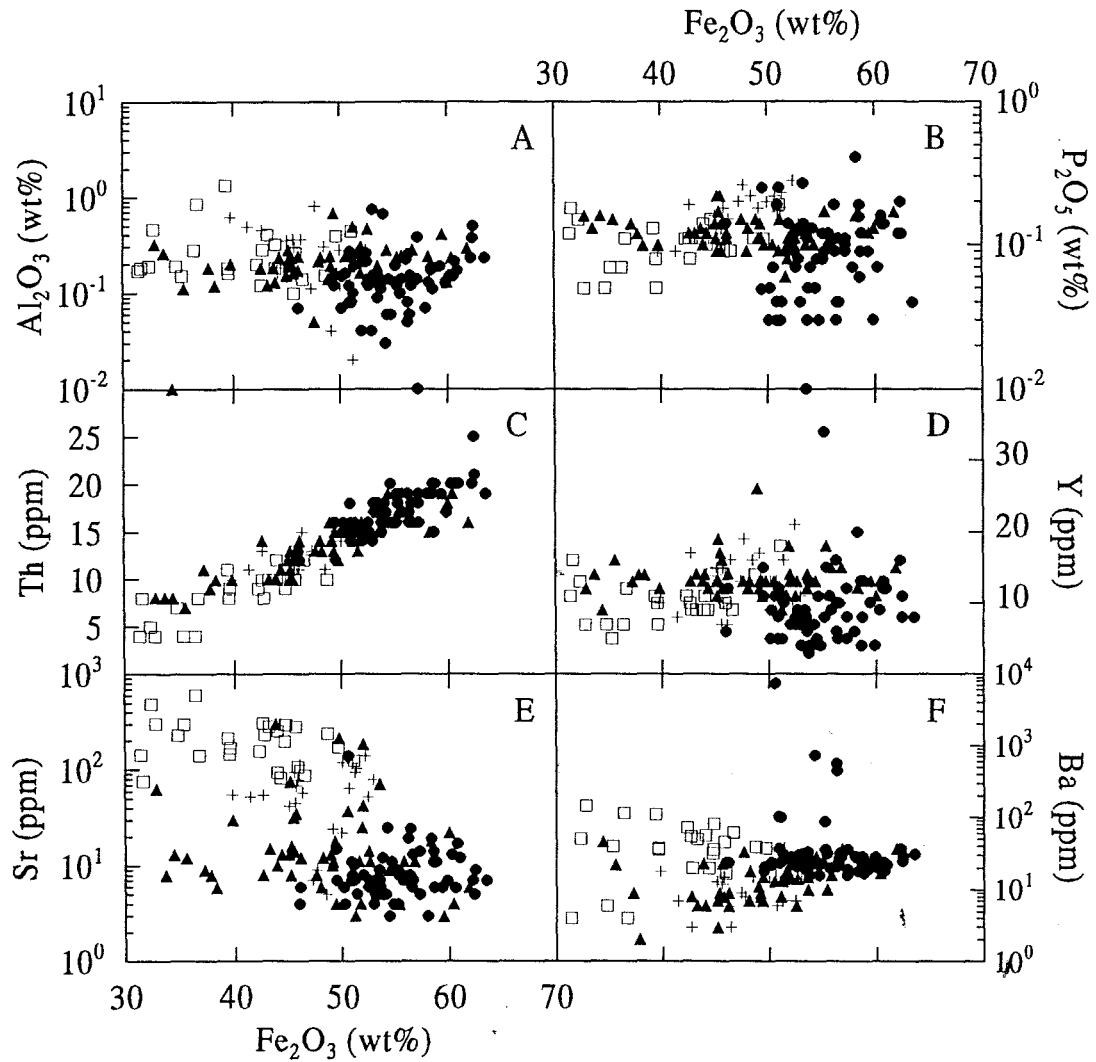
**Figure 3.13.** Bulk-rock carbonate geochemical signatures of selected samples from pristine (+: carbonate-poor; □: carbonate-rich), altered (●) and oxidised (▲) iron-formation, as displayed on bivariate plots of whole-rock CaO versus MgO (a), MnO (b), Sr (c) and P<sub>2</sub>O<sub>5</sub> (d).

correlation between CaO and MgO of Figure 3.13a supports previous petrographic observations that both components are hosted in the same carbonate phase, i.e. a dolomite/ankerite type carbonate with a MgO:CaO ratio of approximately 1:2. This is further confirmed in the CaO vs Sr graph of Fig. 3.13c where the pristine samples and particularly the carbonate-rich ones contain Sr on the order of several hundreds ppm, in association with calcite. Correlation coefficients for the two elements indicate that pristine samples correlate well (corr. coeff. = 0.78), while oxidised samples containing little or no calcite do not (corr. coeff. = 0.45). In the virtual absence of carbonate minerals in the altered iron-formation, the only Ca-bearing phase appears to be apatite with a CaO:P<sub>2</sub>O<sub>5</sub> ratio of approximately 3:2, as evidenced from the generally good positive correlation between these two components for most samples (corr. coeff. = 0.56; Fig. 3.13d).

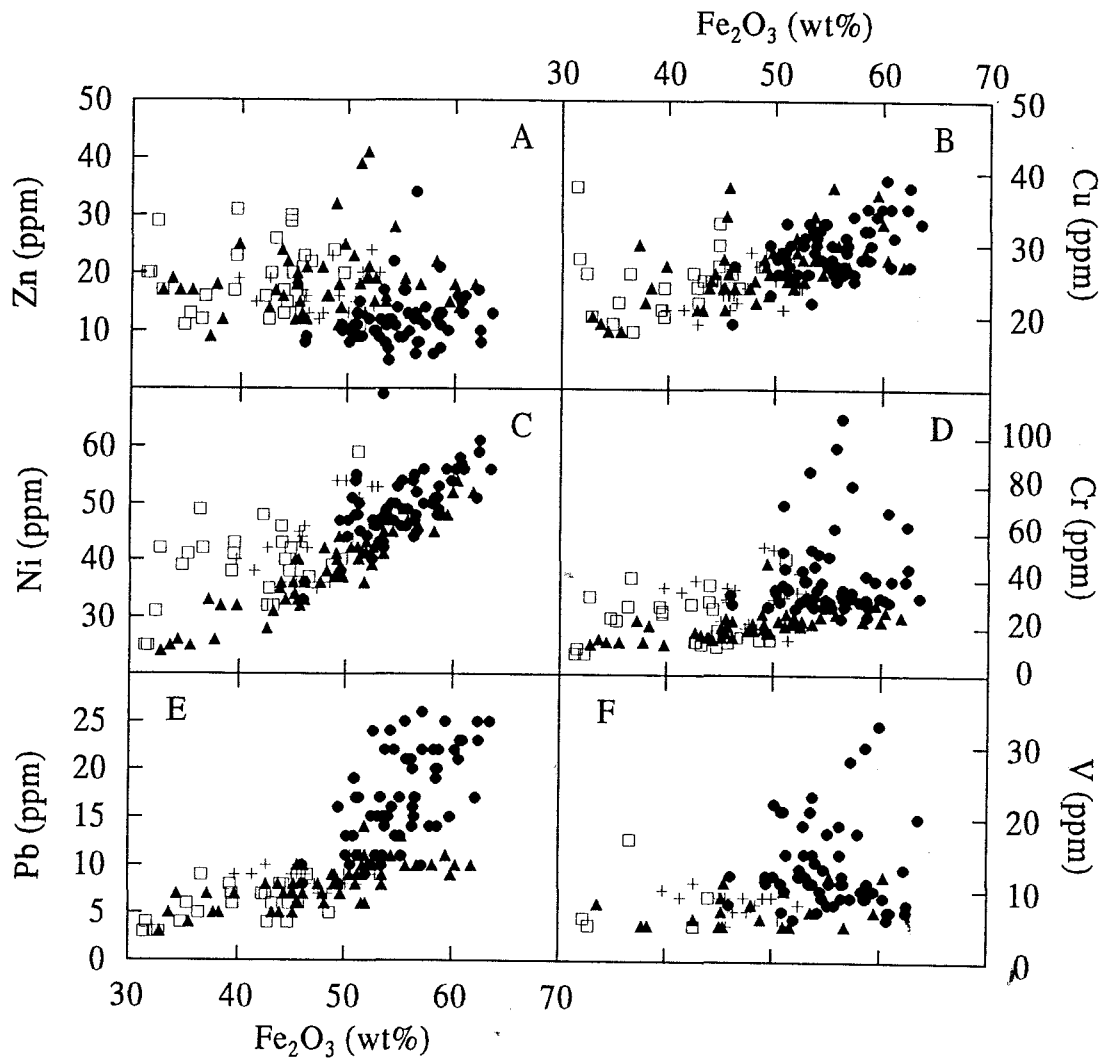
Figure 3.14a shows that Al<sub>2</sub>O<sub>3</sub> does not vary significantly in any sample group with increasing total Fe-content. Both P<sub>2</sub>O<sub>5</sub> and Y (Figs. 3.14b and d) however, show very broad positive trends from carbonate-rich to carbonate-poor pristine samples, while they also appear to suffer minor losses in altered samples with increasing total Fe-oxide. Sr values decrease markedly from the pristine to both the oxidised and the altered samples (Fig. 3.14e), while Ba shows a relative loss in all sample groups in relation to carbonate-rich, pristine iron-formation (Fig. 3.15f). The most remarkable positive geochemical correlation of Figure 3.14 is that of Th against Fe<sub>2</sub>O<sub>3</sub> (Fig. 3.14c). Th correlates linearly with total Fe-oxide in all sample groups (corr. coeff. = 0.89 for pristine samples, 0.90 for oxidised samples and 0.79 for altered samples), with altered iron-formation containing the highest absolute Th values.

Fig. 3.15a shows that Zn is the only element of the transition group where a decrease in absolute values is observed with increasing Fe-content from the pristine/oxidised to the altered samples. Cu (Fig. 3.15b) displays a generally positive trend with total Fe, especially in the oxidised samples (corr. coeff. = 0.57). Ni (Fig. 3.16c) exhibits broadly positive correlations with total Fe in the pristine and altered samples (corr. coeff. = 0.56 and 0.62 respectively) with the latter containing the highest absolute values, yet it shows a remarkably well-developed positive correlation in the oxidised samples (corr. coeff. = 0.93). As far as Cr, Pb and V are concerned (Figs. 3.15d, e and f) the highest contents are seen in the altered samples. Fairly good positive correlations are observed between Pb and total Fe in essentially all three sample groups (Fig. 3.15e), whereas Cr





**Figure 3.14.** Bivariate plots of total Fe-oxide (as  $\text{Fe}_2\text{O}_3$ ) versus  $\text{Al}_2\text{O}_3$  (a),  $\text{P}_2\text{O}_5$  (b), Th (c), Y (d), Sr (e) and Ba (f), for selected samples of pristine (+: carbonate-poor;  $\square$ : carbonate-rich), altered ( $\bullet$ ) and oxidised ( $\blacktriangle$ ) iron-formation.



**Figure 3.15.** Bivariate plots of total Fe-oxide (as  $\text{Fe}_2\text{O}_3$ ) versus Zn (a), Cu (b), Ni (c), Cr (d), Pb (e) and V (f), for selected samples of pristine (+:carbonate-poor; □:carbonate-rich), altered (●) and oxidised (▲) iron-formation.

shows a broadly positive correlation only in the oxidised group (corr. coeff. = 0.61).

#### 3.3.1.4. Summary of major geochemical affiliations

The main conclusions regarding the broad geochemical signatures of the three selected iron-formation types presented in the foregoing sections are summarised below:

- Pristine iron-formation is characterised by increased amounts of whole-rock CaO relative to other iron-formations, primarily in the form of calcite. These correlate antithetically with the amount of total Fe-oxide (mainly magnetite) present in the rock and constitute the main closure factor in this iron-formation type, as opposed to other typical iron-formations that contain SiO<sub>2</sub> and Fe-oxide as the only major constituents. Trace elements exhibiting geochemical affiliation with the Fe-oxide component are Pb, Th, and transition metals such as Ni, Cr and V, whereas carbonate-related constituents include Sr, Ba and MnO. Cu and Zn do not show any apparent geochemical affiliations, although a broadly negative relationship between the latter and Fe-oxide can be deduced.
- Altered iron-formation shows the strong antithetic correlation between SiO<sub>2</sub> and Fe-oxide in the complete absence of carbonate components in the rock. Elements such as Th, Ni and Pb appear to be directly related to the increased Fe-oxide fraction, while very small amounts of CaO and Na<sub>2</sub>O-Sr appear to be associated with minor to trace admixtures of phosphate (apatite) and acmite respectively.
- Oxidised iron-formation exhibits some important similarities with, and differences from pristine iron-formation. Closure is observed in relation to the carbonate and Fe-oxide components of the rock. The dolomite-dominated carbonate mineralogy of oxidised iron-formation is reflected in the positive correlations between CaO and MgO (+MnO), while a number of trace elements show distinct affiliation to the Fe-oxide component of the rock, including Th, Ni, Pb, and to a lesser extent Cu and Cr. In the virtual absence of calcite, the abundance of elements such as Sr and Ba is clearly reduced, and no direct geochemical association between these elements and whole-rock CaO is readily evident.

### 3.3.2. Mooidraai Formation

Bulk-rock geochemical data from ten samples of the Mooidraai Formation are presented as an essential supplement to the data presented for the Hotazel iron-formation. The Mooidraai Formation is developed over large parts of the KMF at the top of the Hotazel Formation and comprises primarily microcrystalline calcite along with small and variable amounts of quartz, magnetite and minor ferrous silicate minerals (mainly greenalite and minnesotaite; see also PART 2). Texturally, it resembles the Hotazel iron-formation from the point of view of its conspicuous compositional banding. Ten samples of the Mooidraai Formation, collected from borehole OLP7 (see Appendix I, Fig. A3) have been analysed for major and trace element compositions using standard XRF techniques, and the results are summarised below.

With regard to major element compositions (Fig. 3.16), the chief components besides CaO in the Mooidraai samples are SiO<sub>2</sub> (up to 15 wt%), Fe<sub>2</sub>O<sub>3</sub> (up to 25 wt%), MgO (0.5-2 wt%) and MnO (0.1-1.5 wt%), while most remaining major element components show very low values with little variation (e.g. TiO<sub>2</sub>, P<sub>2</sub>O<sub>5</sub>) or below the lower limit of detection (e.g. Na<sub>2</sub>O, K<sub>2</sub>O). As is expected, a strong linear antithetic correlation exists between CaO and both SiO<sub>2</sub> and Fe<sub>2</sub>O<sub>3</sub> (Figs. 3.16a,b) due to the antithetic mineralogical composition between CaCO<sub>3</sub> and Fe/Si-rich mineral phases. Of interest is the antithetic correlation between CaO and MgO (Fig. 3.16c) which, in the light of the complete absence of dolomite in the samples, suggests that MgO is not hosted in the structure of calcite but rather in a Mg-bearing silicate mineral phase (e.g. minnesotaite, greenalite). On the other hand, MnO does not show any clear correlation with CaO (Fig. 3.16d), implying that the former is either not associated with the carbonate fraction of the Mooidraai samples, or that it shows no regular distribution related to, for example, systematic substitution of Ca<sup>+2</sup> by Mn<sup>+2</sup>.

Antithetic correlations are seen between CaO and the transition metals Zn, Cu, and Ni (Figs. 3.17a,b, and f), suggesting a sympathetic relation of the latter with the silicate-Fe-oxide fraction of the samples. Sr and Ba values are in the range of several hundreds (800-1500) and tens (10-110) of parts per million respectively, but show a very erratic distribution when plotted against whole-rock CaO (Figs. 3.17c and d). This feature is in marked contrast to observations from the Hotazel iron-formation where good correlation exists between CaO and Sr, suggesting potential

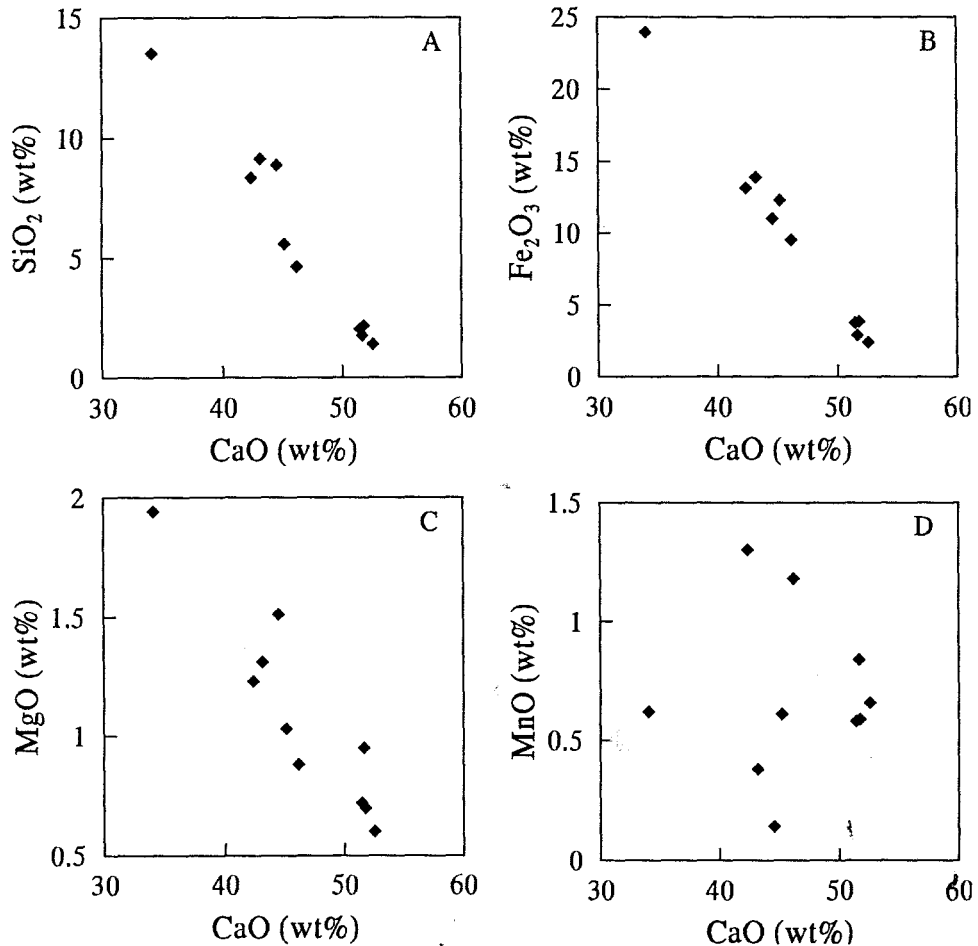


**Figure 3.16.** Major element signatures of the Mooidraai Formation as reflected on bivariate plots of whole-rock CaO versus SiO<sub>2</sub> (a), total Fe-oxide (as Fe<sub>2</sub>O<sub>3</sub>, b), MgO (c) and MnO (d), for ten selected samples.

differences between the origin of the Mooidraai calcite and that of Hotazel calcite. Al<sub>2</sub>O<sub>3</sub> appears to show a negative correlation with CaO for most samples (Fig. 3.17e), although this is obscured by the two samples with the highest Al<sub>2</sub>O<sub>3</sub> contents (>0.4 wt%). The remaining trace elements show statistically insignificant variations and/or very low absolute values.

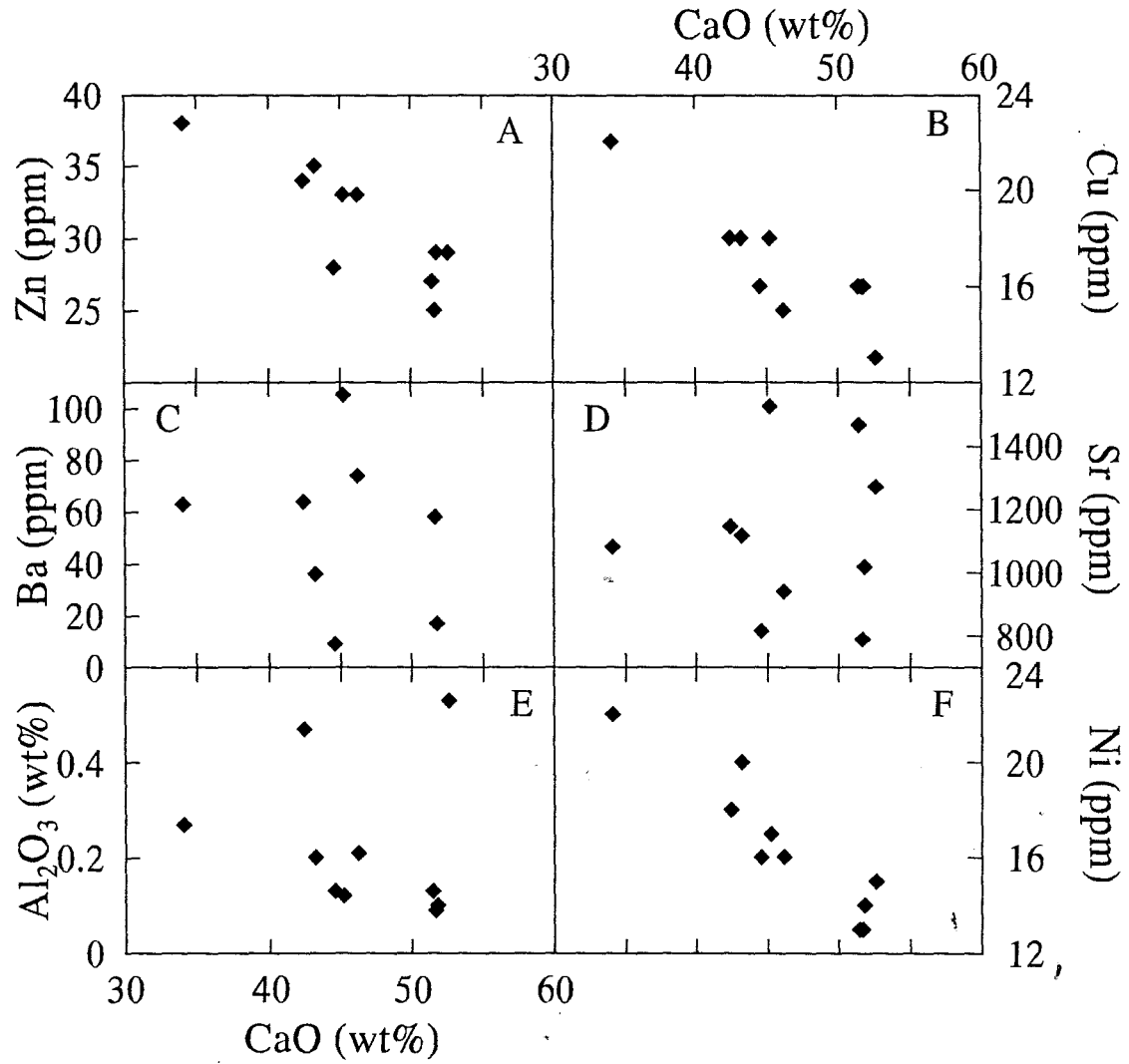


Figure 3.17. Bivariate plots of total CaO versus Zn (a), Cu (b), Ba (c), Sr (d), Al<sub>2</sub>O<sub>3</sub> (e) and Ni (f), for ten selected samples from the Moodraai Formation.

## Chapter 3.4: Geochemical evidence for secondary alteration

### 3.4.1. The isocon method

In 1967, Gresens introduced a comprehensive mathematical method to estimate composition-volume relationships in metasomatic systems. Gresens' approach was based on the equation:

$$\Delta c_i = f_v (p^A/p^O) c_i^A - c_i^O \quad (1)$$

where  $\Delta c_i$  = gain or loss of component (in wt %);

$c_i^A$  = concentration of component I in altered rock (in wt %);

$c_i^O$  = concentration of component I in original rock (in wt %);

$p^A$  = density of altered rock;

$p^O$  = density of original rock; and,

$f_v$  = volume factor

An alternative version of the original equation (1) was put forward by Grant (1986), who proposed a simple solution for both volume (or mass) and concentration changes during metasomatic alteration which requires no significant manipulation of analytical data and is readily accomplished graphically. Gresens' equation is rearranged by Grant (1986) into a linear relationship between the concentration of a component in the altered rock and that in the original rock. Simultaneous solutions of such equations for all "immobile" components, i.e. components that show no relative gain or loss of mass defines an "isocon". Grant's modified version of equation (1) effectively eliminates the term  $f_v(p^A/p^O)$  by replacing it with the ratio of equivalent concentration of a geochemically immobile element before and after alteration :

$$\Delta c_i = (c_x^O/c_x^A) c_i^A - c_i^O \quad (2)$$

where  $\Delta c_i$ ,  $c_i^A$ ,  $c_i^O$  as in equation (1);

$c_x^O$  = concentration of immobile component x in original rock; and,

$c_x^A$  = concentration of immobile component x in altered rock;

On a graph of the concentrations in the altered rock against those in the original, an isocon would be a straight line through the origin. The slope of the isocon defines the mass change in the alteration, and the deviation of a data point from the isocon defines the concentration change for the corresponding component (Grant, 1986).

Despite subsequent refinements (e.g. Baugmartner and Olsen, 1995), the isocon method will be applied in the following section as originally introduced by Grant (1986), in an exercise attempting to link the alteration histories of the altered and oxidised types of the Hotazel iron-formation in relation to the pristine iron-formation type. The exercise is based on selected geochemical data from a specific stratigraphic interval of the Hotazel Formation. Mass balance calculations are subsequently performed in an attempt to test further the validity of proposed models for metasomatic alteration in the northern KMF (Gutzmer and Beukes, 1997).

#### **3.4.2. The Hotazel exercise**

The isocon method was applied to 23 selected iron-formation samples corresponding to the three major iron-formation groups described earlier. Four boreholes were chosen for this purpose, i.e. GL26 (pristine iron-formation, n=6), MK3I/MK2G (altered iron-formation, n=8(4+4)), and BEL4C (oxidised iron-formation, n=9) (see also Appendix I, Figs. A1, A3, A4). Particular attention was placed on selecting samples from laterally correlative stratigraphic intersections. For that reason, all samples represent petrographically and geochemically homogeneous portions in all four boreholes, corresponding to intersections between the uppermost and middle Mn ore-units. Samples deviating strongly from the average compositions of the three groups were avoided, such as acmite-rich samples occurring immediately below the uppermost Mn-unit in boreholes MK3I/MK2G, as well as samples markedly enriched in carbonate component found immediately above the middle Mn-unit in boreholes GL26 and BEL4C. Figure 3.18 shows schematically the approximate stratigraphic location of all samples selected, while Table 3.7 contains average analytical data and standard deviations for selected major and trace elements from the three sample groups, as used in the isocon applications presented below. Figure 3.19 summarises the geochemical characteristics of the selected sample groups, in terms of major element compositions.



**Table 3.7:** Mean and standard deviation values for selected major and trace element data for iron-formation intersections from boreholes GL26, MK3I, MK2G and BEL4C, as used in applications of the isocon method.

	Factor	Pristine n=6	STD	Altered n=8	STD	Oxidised n=9	STD
<i>wt%</i>							
SiO <sub>2</sub>	0.5	36.18	1.56	39.98	2.26	34.17	3.26
Al <sub>2</sub> O <sub>3</sub>	10	0.19	0.10	0.21	0.11	0.19	0.05
Fe <sub>2</sub> O <sub>3</sub>	0.5	46.03	2.42	59.46	2.07	45.95	4.40
MnO	20	0.58	0.12	0.07	0.01	1.02	0.16
MgO	5	1.06	0.13	0.01	0.00	3.25	0.80
CaO	2.5	8.82	0.98	0.21	0.14	6.72	1.61
<i>ppm</i>							
Zn	1	21	5	13	4	17	4
Cu	0.5	27	3	34	3	24	3
Ni	0.1	37	3	54	4	35	5
Cr	0.5	15	2	35	5	18	3
Ba	0.1	49	16	29	22	10	7
Pb	1	6.5	1	22	2	6.4	1.3
Th	1	11	2	19	1	12	2
Y	1	13	2	15	8	14	2
Zr	1	4.8	0.4	6.6	0.7	5.2	0.8
Sr	0.1	248	50	12	4	13	3

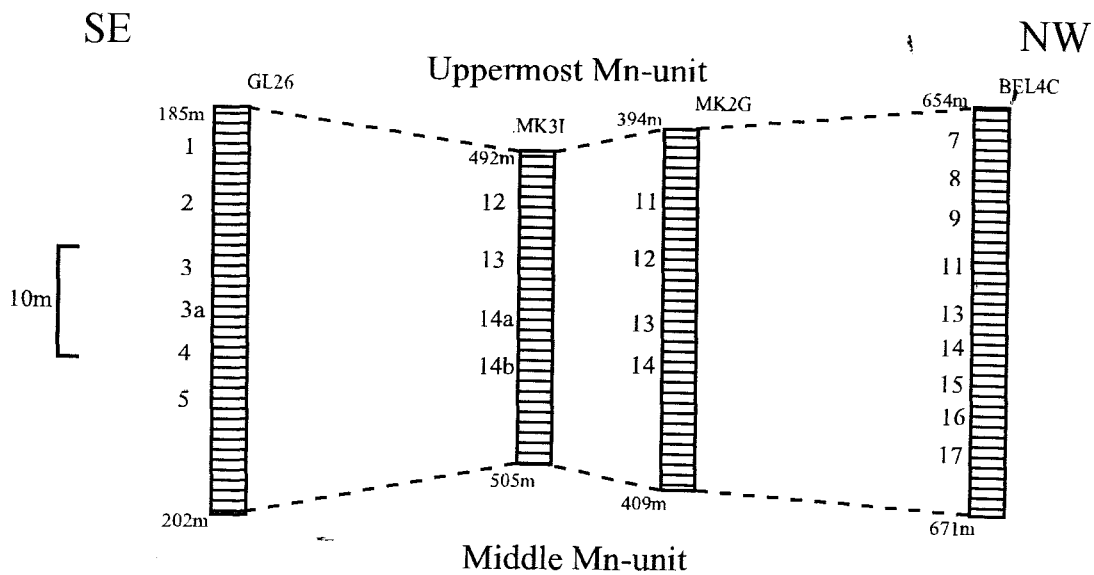


**Figure 3.18.** Simplified sketch illustrating borehole intersections and approximate stratigraphic locations of iron-formation samples selected for applications of the isocon method. Sketch is not drawn to scale, but true depths of all intersections are shown.

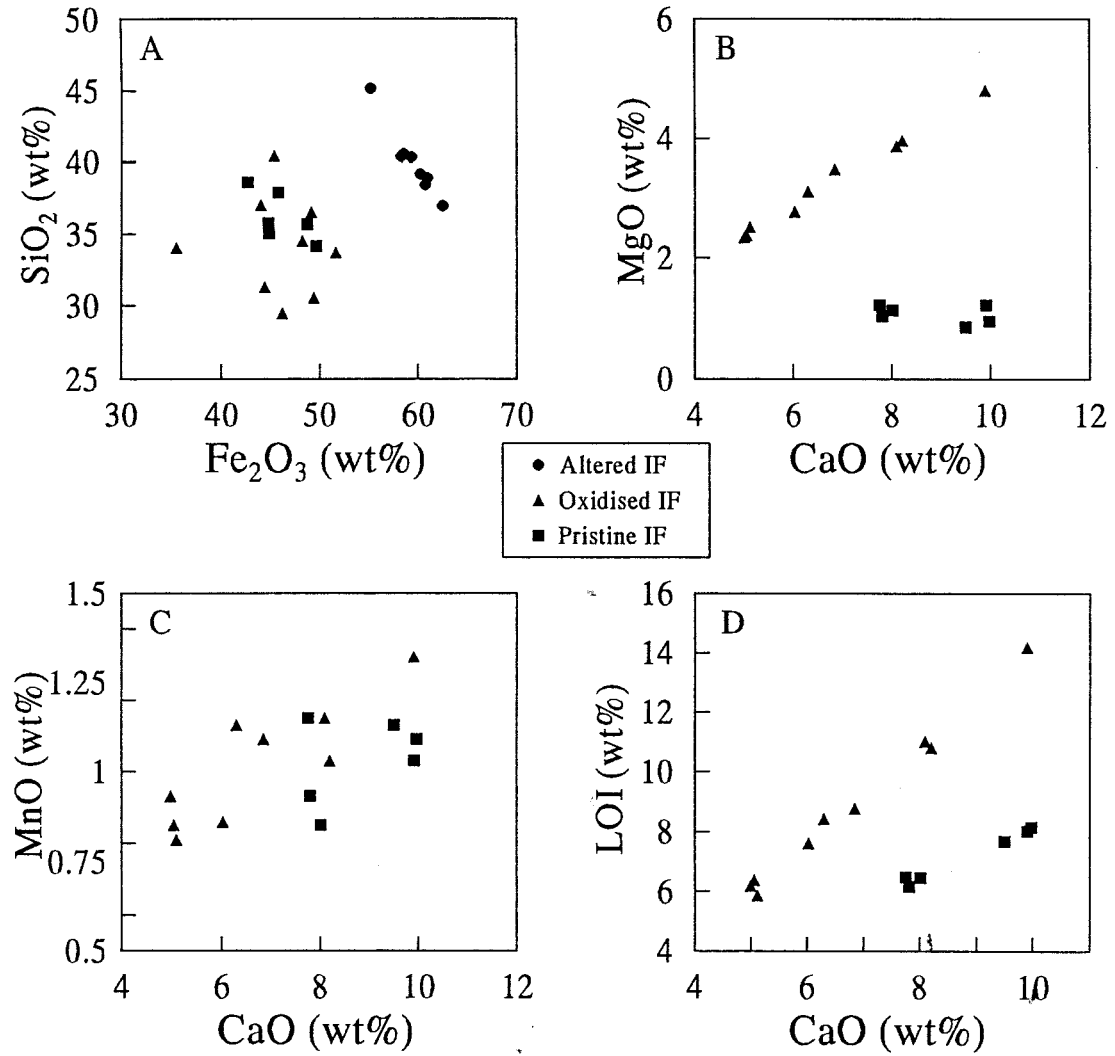


**Figure 3.19.** Bivariate plots of: (a) total Fe-oxide (as Fe<sub>2</sub>O<sub>3</sub>) vs SiO<sub>2</sub>; (b) CaO vs MgO; (c) CaO vs MnO; and (d) CaO vs LOI, for selected iron-formation samples from boreholes GL26, MK3I, MK2G and BEL4C.

The graphs b, c, and d of Figure 3.19 illustrate once again the most conspicuous geochemical differences between the pristine and oxidised iron-formation types, essentially all related to the carbonate petrography of the respective sample groups. Pristine iron-formation contains primarily calcite and, to a much lesser extent, ankerite as the main carbonate compounds. Oxidised iron-formation, on the other hand, contains one carbonate phase, a dolomite-type carbonate with a MgO:CaO ratio of 1:2. The linear correlations between CaO and MgO (Fig. 3.19b) and CaO vs LOI (loss on ignition; Fig. 3.19d) further establish the above. It should be pointed out that the LOI factor of graph 3.19d corresponds essentially to the CO<sub>2</sub> component in the samples, as the amount of water in both iron-formation types is minimal (little or no hydrous Fe-silicate minerals are observed). Also, the amount of Fe<sup>+2</sup> in the samples that would affect the determination of LOI during sample preparation and treatment (see Appendix II) is negligible, particularly in the oxidised samples.

The two isocon graphs of Figure 3.20 were constructed for 6 selected major element oxides and 10 trace element components of both the oxidised and altered iron-formation samples. Data have been plotted against compositions of the pristine iron-formation and have been conveniently scaled (see "Factor" column, Table 3.7) so that the plot axes are confined between the values 0 - 30.

Considering plot 3.20a first, the best-fit isocon for the selected data appears to coincide with that of constant mass, assuming that the oxidised iron-formation has been produced by alteration processes at the expense of a precursor which would have been chemically very similar to the pristine iron-formation. Based on the above assumption, the oxidised iron-formation shows significant relative gains for MgO and MnO and to a lesser extent Cr, and marked relative losses primarily for Sr, Ba, CaO and, to a lesser degree, Zn, Cu and SiO<sub>2</sub>. The remaining components plot essentially on or about the constant mass isocon and show small changes (<10 wt%) in their absolute concentrations.

It is important to note here that the constant mass isocon of Figure 3.20a is well defined by the distribution of commonly geochemically immobile components during low-temperature alteration processes, such as Al<sub>2</sub>O<sub>3</sub>, Zr and, for this particular example, Fe-oxide. This fact adds further

credibility to the assumption that no significant mass change may have taken place during alteration of pristine to oxidised iron-formation. Furthermore, if it is assumed that no major density changes have occurred during such an alteration event, the almost identical thicknesses of the selected iron-formation intersections in boreholes BEL4C and GL26 (Fig. 3.18) would support further the concept that changes in mass have been negligible, provided that primary lateral thickness variations were also insignificant.

The isocon graph of Figure 3.20b contains data from the pristine and altered iron-formation types and displays some important differences from graph 3.20a. Firstly, if the same immobile constituents were used to define a best-fit isocon (i.e.  $\text{Al}_2\text{O}_3$ , Zr and  $\text{Fe}_2\text{O}_3$ ), the latter would no longer correspond to the constant mass isocon as in Figure 3.20a. It thus becomes apparent that a significant change in mass must have taken place during alteration of a pristine precursor to produce the altered type observed in this study. Considering the petrography and thickness relations between intersection GL26 and MK31/MK2G, a substantial decrease in the thickness of the selected iron-formation intersection is observed from 17m, to 13m and 15m respectively. Assuming negligible effects of density changes, this thickness change would correspond to approximately 15-20% of mass loss during alteration, a loss which would correspond to the removal of the carbonate component from the system as documented from petrographic evidence (see PART 2).

These features are best demonstrated in Figure 3.20b when the two isocons corresponding to 15 and 20% mass loss are considered. The constituents that have been markedly lost from the system with reference to the field defined by these two isocons are CaO, MgO, MnO, Sr, Ba and Zn, all components previously associated with the carbonate fraction of pristine iron-formation. Elements that have been relatively enriched are Pb, Cr, Th and to a lesser extent Ni and Zr, while  $\text{Al}_2\text{O}_3$ , Y and Cu all plot on or about the field defined by the two isocons. V also shows relative enrichment, but its near detection limit values in pristine samples prevents it from being included in the graph. Based on the isocon plot of Figure 3.20a, should the oxidised iron-formation be chosen in place of the pristine iron-formation as a pre-alteration precursor, the geochemical changes observed would have been essentially the same.

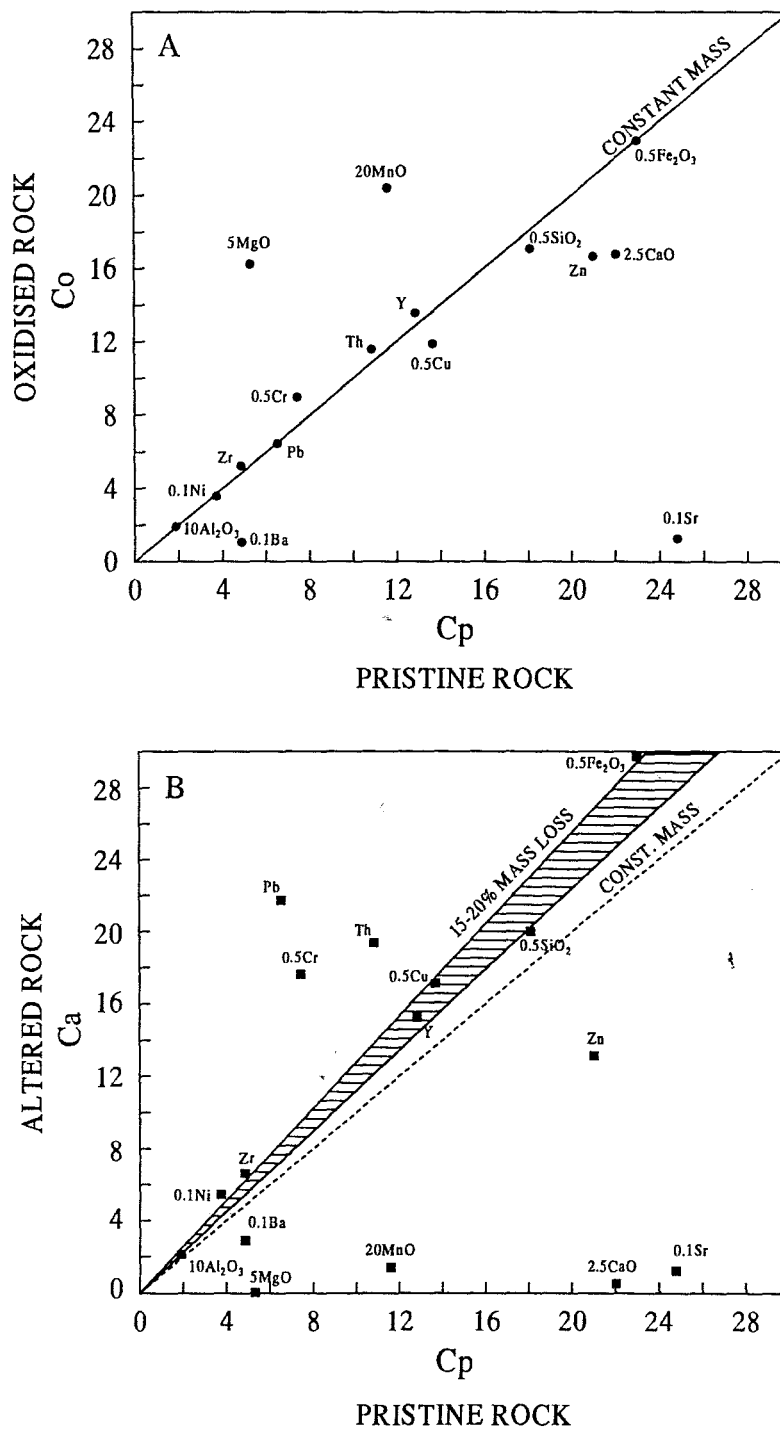


**Figure 3.20.** Isocon graphs displaying average bulk-rock geochemical relations between: (a) pristine and oxidised iron-formation; and (b) pristine and altered iron-formation. Isocons for constant mass are shown, whereas in graph (b) the field defined by the 15% and 20% mass loss is highlighted by a hatched fill.

### 3.4.3. Mass balance constraints

By combining information from the isocon graphs of Figure 3.20, some further conclusions can be drawn in the search for potential links between the altered and oxidised iron-formations in terms of the process/es involved in their development. In evaluating the data of Figure 3.20, there are two main alternatives likely to explain the geochemical characteristics of the oxidised and altered iron-formation types:

- (1) the oxidised iron-formation corresponds to an intermediate product of the alteration process which produced the altered type, and may thus be described as a partially altered rock;
- (2) the oxidised iron-formation shows no apparent relation to the altered one as part of a progressive alteration sequence. In this case, it should be pointed out that although the geochemical signatures of the two types are dissimilar, this by no means implies that the two iron-formation types are totally unrelated in terms of their post-depositional histories.

Considering case 1 above, one would expect that partial alteration of pristine iron-formation to form the oxidised member would generally involve a certain degree of loss of those components that are particularly mobile in the alteration environment, and are also effectively lost from the altered iron-formation. Columns 1 and 2 in Table 3.8 present the major relative gains and losses for the oxidised and altered iron-formation types assuming the above scenario. If the oxidised iron-formation is a partially altered lithology, substantial losses of 80-100 wt% are seen for the components Sr and Ba, and less so for CaO, Zn and Cu (10-30 wt%). Significant gains, however, are recorded for MgO and MnO (~200 and ~75 wt% respectively) and to a lesser extent for Cr (~20 wt%). The losses mentioned above would correspond readily to removal of calcite from the pristine rock, whereas the gains reflect the relative increase of a dolomite/ankerite-type carbonate based on the increased MgO and MnO contents. Altered iron-formation would have formed by essentially complete loss of all major carbonate-related components, (i.e. CaO, MgO, MnO), whereas others would have suffered further - though smaller - relative losses such as Zn and Sr (15-35%). Components showing marked enrichment include Pb (~200 wt%), V (not shown), Ba (~100 wt%), Cr and Th (50-70 wt%), and to a lesser extent Ni and Cu (20-30 wt%). Most of these elements would have been particularly immobile in low-temperature weathering environments that are characterised by large residual enrichments in Fe-oxides and hydroxides.

From the above, it becomes apparent that if partial alteration was responsible for the development of oxidised iron-formation *en route* to complete alteration forming the altered type, addition of MgO and MnO from an external source or redistribution of those components in a closed system would be required. These conditions would not apply if the carbonate mineralogy of the precursor material differed markedly from that observed in pristine iron-formation from the present study. There is, however, no available evidence that would support a primary lateral mineralogical and geochemical change in the Hotazel iron-formation between boreholes GL26 and BEL4C. Instead, the striking compositional similarities between the former and more distal borehole intersections such as those from the southern KMF, would suggest that this is a rather unlikely possibility.

The alternative case 2 proposed earlier in this section provides another potential scenario. The main assumption here is that the altered type derives from a complete alteration process which effectively removed the entire pre-existing carbonate component from the pristine rock, with subsequent compaction of the rock mass to approximately 80-85% of its original value. The associated geochemical changes presented in Figure 3.20b are comprehensively summarised in column 3 of Table 3.8, where it is clearly evident that the components CaO, MgO, Sr and MnO have now been entirely lost, along with lesser amounts of Ba and Zn (~50 wt%). Substantial gains are recorded for Pb, Cr, Th, Ni, Zr and V (not shown on Table 3.8), most of which would be affiliated to the residually enriched Fe-oxide.

Based on the above, the second alternative scenario would suggest that the carbonate component of the pre-alteration precursor has been entirely dissolved/mobilised, without necessarily any localised development of intermediate lithotypes. In this case, oxidised iron-formation may have been formed in favourable areas as a result of partial, localised re-deposition of solutes such as Mg and Mn derived from the leached component of altered iron-formation. In other words, oxidised rock would have formed locally as an “end-member” in the alteration process, under conditions preventing the complete outward loss of dissolved constituents and without the introduction of solutes from an external source being necessary.

With regard to total Fe<sub>2</sub>O<sub>3</sub> and SiO<sub>2</sub> contents, no marked changes would be required in both above processes apart from, perhaps, small enrichments in total Fe. The average compositions of

both these constituents, and particularly the ratio  $\text{Fe}_2\text{O}_3/\text{SiO}_2$  would thus be expected to remain effectively unchanged during alteration, with perhaps a slight shift towards higher  $\text{Fe}_2\text{O}_3/\text{SiO}_2$  values. When  $\text{Fe}_2\text{O}_3/\text{SiO}_2$  ratios are plotted on a histogram against the sample frequency for the entire Hotazel data set, the aforementioned shift from pristine to altered rock is clearly observed (Fig. 3.21). The oxidised iron-formation however, displays distinctly higher  $\text{Fe}_2\text{O}_3/\text{SiO}_2$  values for

**Table 3.8:** Relative gains and losses in wt% for selected major and trace elements during transformation of pristine to oxidised and altered iron-formation, for two potential alteration scenarios (see text for detailed discussion).

	Pristine n=6	Loss/gain Case 1(a) 1	Oxidised n=9	Loss/gain Case 1(b) 2	Altered n=8	Loss/gain Case 2 3
<i>wt%</i>						
MnO	0.58	75	1.02	>-90	0.07	>-90
MgO	1.06	>200	3.25	-100	0.01	-100
CaO	8.82	-25	6.72	-100	0.21	-100
<i>ppm</i>						
Zn	21.00	-20	16.67	-30~-35	13.13	-45~-50
Cu	27.33	-20~-25	23.78	20~25	34.25	
Ni	37.33		35.44	~30	54.25	20~25
Cr	14.83	20	17.89	65~70	35.25	~100
Ba	48.50	-80	10.44	>100	28.88	-50
Pb	6.50		6.44	~200	21.75	~200
Th	10.83		11.56	40~50	19.38	~50
Sr	247.83	-95	12.67	-22	12.38	~-95

a significant number of samples. In the light of the virtual absence of silicate compounds from the oxidised iron-formation, it appears that if the altered iron-formation has derived (partly or wholly) from complete oxidation/leaching of oxidised iron-formation (case 1) then a reverse, marginal shift should be expected towards lower  $\text{Fe}_2\text{O}_3/\text{SiO}_2$  ratios, presumably due to either reprecipitation of  $\text{SiO}_2$  and/or some remobilisation of Fe. The above renders the first alteration scenario less attractive in comparison with alternative case 2, whereby oxidised iron-formation would become further enriched in iron subsequent to the leaching processes responsible for the generation of altered iron-formation.



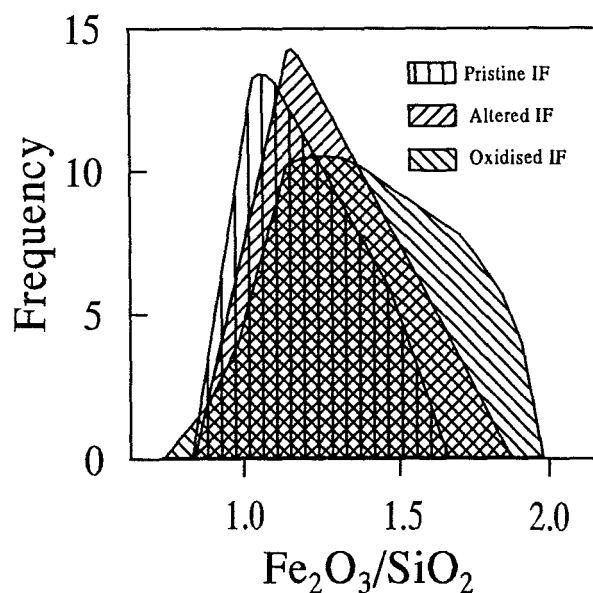


**Figure 3.21.** Histogram showing the distribution of  $\text{Fe}_2\text{O}_3/\text{SiO}_2$  ratios in pristine, altered and oxidised iron-formation. Note the higher values that characterise a significant proportion of the sample population of the oxidised group.

All foregoing information could be combined in the conceptual scheme of Figure 3.22 where the oxidised and altered iron-formations appear to have been sequentially formed by means of two major alteration pathways. The potential validity of each of the above schemes will be tested in the final part of this thesis (PART 5) in conjunction with available geological evidence. The important common aspect in both schemes, however, is that during the alteration process/es, the fluid agent/s involved may have caused redeposition of part of the dissolved load in favourable areas, depending primarily on the direction of fluid-flow and the physicochemical suitability of the encountered lithologies (permeability, composition etc.) for such a process to take place. It is thus possible that the MgO and MnO required for the development of oxidised iron-formation may in fact owe their origin to dissolution-mobilisation-precipitation processes operating on a broad geographical scale. If this is so, then the oxidised and altered iron-formation types may be closely interlinked, though on the basis of a system where not only outward mass transfer as previously proposed (Gutzmer and Beukes, 1997) but also partial redistribution of chemical constituents, have been equally important processes.

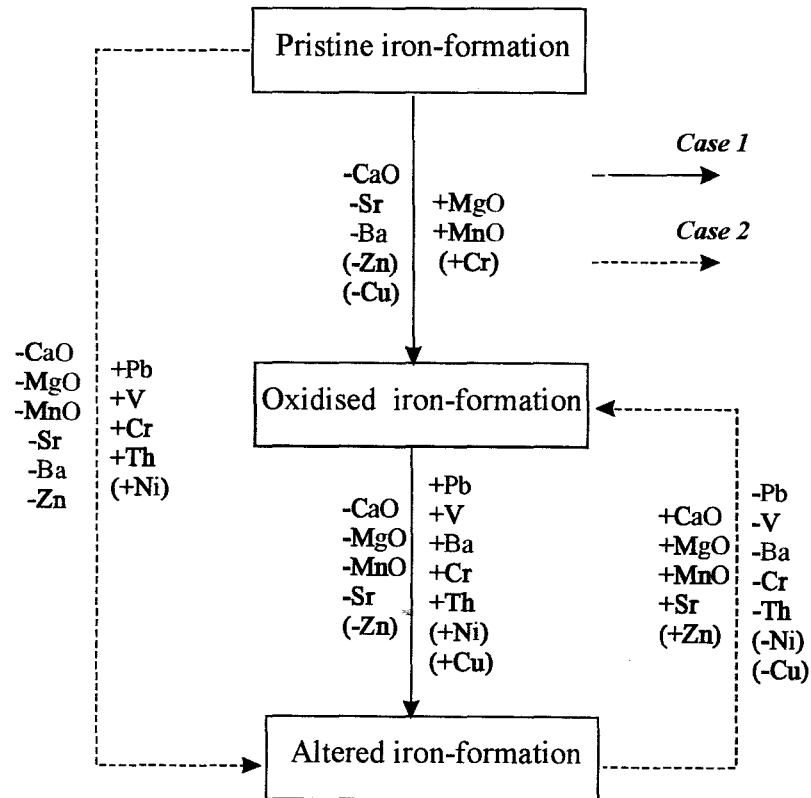


**Figure 3.22.** Conceptual diagram showing two alternative alteration pathways and associated geochemical changes, potentially responsible for the development of the oxidised and altered iron-formation types at the expense of a “pristine” precursor (see text for detailed discussion).

## Chapter 3.5: Rare-earth element geochemistry

### 3.5.1. Background

Many studies have been conducted on the rare-earth element (REE) systematics of iron-formations with the prime purpose of assessing potential sources not only for the REE but also, by extension, for the large amounts of coprecipitated iron that produced these unusually iron-enriched sediments. Most workers at present agree that the source for the REE, Fe and Si in iron formations must have been, at least partly, related to submarine hydrothermal activity (e.g. Jacobsen and Pimentel-Klose, 1988; Derry and Jacobsen, 1990). This concept has been shared particularly by researchers who have studied in detail various late Archaean iron-formation occurrences of India (Manikyamba et al., 1993; Gnaneshwar Rao and Naqvi, 1995; Khan and Naqvi, 1996), although proponents for a mixed terrigenous-hydrothermal source for the REE are not lacking (e.g. Alibert and McCulloch, 1993; Arora et al., 1995; Manikyamba and Naqvi, 1995).

Iron-formations of various ages may exhibit striking similarities in terms of REE geochemistry to the degree that no clear distinction can be made in terms of their genetic history (e.g. Graf, 1978; Appel, 1983). Recent investigations concentrating on evolutionary trends in positive Eu-anomalies in iron-formations, have suggested that Archaean iron-formations are characterised by REE compositions which derived from submarine hydrothermal input, whereas their Palaeoproterozoic counterparts have REE signatures indicative of low-temperature alteration (Danielson et al., 1992). It has also been suggested that a mixed origin for the REEs should be favoured, in the light of the stratified basinal settings postulated for the deposition of iron-formations. For example, Bau and Möller (1993) have proposed that submarine hydrothermal activity was dominant in controlling the REE character of bottom ocean waters, whereas riverine input was responsible for the REE signatures of shallow waters. Periodic mixing of those two components would have produced the REE patterns presently observed in iron-formations. Ultimately, many researchers now agree that bottom anoxic waters in the Precambrian must have carried at least a dilute, mid-ocean ridge-related hydrothermal component, which triggered the deposition of iron-formations with distinctly positive Eu-anomalies, as variously documented (e.g. Dymek and Klein, 1988; Klein and Beukes, 1989; Beukes and Klein, 1990a; Bau and Dulski, 1996).

### 3.5.2 Results

Analyses for rare-earth elements (REE) were performed on a total of 17 samples. Twelve of these come from the southern parts of the KMF and correspond to the sample group used in the comprehensive summary of the pristine Hotazel iron-formation presented in section 3.2.1. The remaining five samples come from the Mooidraai carbonate intersection in borehole OLP7, the general geochemistry of which was discussed earlier in section 3.3.2. The iron-formation samples were analysed by means of high-performance ion chromatography employing methods described by le Roex and Watkins (1990), while the five Mooidraai samples were analysed by ICP-MS techniques. All analyses were performed at the Department of Geological Sciences, University of Cape Town. Details of the analytical techniques used are summarised in Appendix II and analytical data are presented in Table 3.9.

**Table 3.9.** Rare-earth element data for selected Hotazel iron-formation and Mooidraai carbonate samples

Sample	La	Ce	Pr	Nd	Sm	Eu	Gd	Tb	Dy	Ho	Er	Tm	Yb	Lu
<i>ppm</i>														
<b>Mooidraai</b>														
OLP-1	2.09	2.04	0.31	1.32	0.24	0.076	0.36	0.058	0.41	0.11	0.37	0.055	0.34	0.061
OLP-3	2.53	2.59	0.34	1.43	0.24	0.069	0.34	0.054	0.38	0.10	0.33	0.05	0.32	0.055
OLP-5	2.69	3.11	0.41	1.69	0.30	0.083	0.42	0.072	0.52	0.14	0.48	0.075	0.50	0.089
OLP-8	0.66	0.74	0.092	0.36	0.067	0.019	0.091	0.015	0.12	0.036	0.13	0.021	0.14	0.028
OLP-10	0.60	0.61	0.085	0.36	0.071	0.022	0.11	0.018	0.14	0.043	0.15	0.024	0.17	0.032
<b>Hotazel IF</b>														
R65-2	1.85	2.12	0.23	1.09	0.26	0.062	0.33	lld	0.49	nd	0.42	nd	0.45	nd
R65-3	2.49	3.18	0.34	1.84	0.36	0.09	0.48	0.077	0.70	nd	0.65	nd	0.58	nd
R59-3	4.59	5.00	lld	2.60	0.48	0.10	0.57	lld	0.76	nd	0.63	nd	0.58	nd
R63-5	3.65	3.99	0.54	2.30	0.39	0.14	0.56	lld	0.84	nd	0.69	nd	0.74	nd
R59-9	3.26	2.49	0.43	1.85	0.30	0.063	0.42	lld	0.56	nd	0.43	nd	0.38	nd
R63-8	2.59	2.96	0.34	1.62	0.35	0.059	0.38	0.065	0.53	nd	0.43	nd	0.36	nd
R70-13	1.91	2.48	lld	1.08	0.21	0.039	0.20	lld	0.30	nd	0.13	nd	0.17	nd
R59-15	8.83	13.30	1.34	5.94	1.25	0.33	1.48	0.22	1.58	nd	0.99	nd	1.00	nd
R70-17	3.20	4.41	lld	2.32	0.39	0.11	0.54	lld	0.97	nd	0.78	nd	0.83	nd
R70-18	5.45	9.25	lld	4.11	0.94	0.28	1.13	lld	1.33	nd	0.84	nd	0.90	nd
R65-20	7.18	13.10	1.76	6.66	1.48	0.46	1.82	lld	2.48	nd	1.60	nd	1.75	nd
R65-30	3.19	3.17	0.39	1.69	0.31	0.088	0.36	lld	0.52	nd	0.41	nd	0.36	nd

nd = not determined; lld=lower limit of detection

Results for all samples analysed are graphically presented in the plots of Figure 3.23. Data have been normalised against the North American Shale Composite (NASC; Gromet et al., 1984) and

have been separated into three distinct groups on the basis of the bulk mineralogical composition of the individual samples. Figure 3.23a shows normalised REE patterns for carbonate samples, i.e. the five samples from the Mooidraai Formation and sample R59-9 corresponding to a Fe-Mn-rich carbonate unit from the Hotazel iron-formation. Figures 3.23b and c present similar REE patterns for carbonate-rich and carbonate-poor Hotazel iron-formation samples respectively.

REE patterns for all 17 samples (Fig. 3.23) are very similar, with the main characteristic being a distinct depletion in light-REE (La-Sm) relative to heavy-REE (Gd-Lu). In terms of absolute REE concentrations, the lowest values are observed in two Mooidraai samples carrying the lowest amounts of Fe and Si admixtures, i.e. they are the “purest” carbonate samples selected (Fig. 3.23a, samples OLP-8, OLP-10; see also Appendix III). The remaining Mooidraai samples (including sample R59-9) are clearly more enriched in total REE (Fig. 3.23a) and compare particularly well with samples from the carbonate-rich iron-formation (Fig. 3.23b). REE patterns for carbonate-poor iron-formation samples also agree fairly well with those of carbonate-rich ones, with the exception of sample R70-13 whose pattern appears much “flatter” (Fig. 3.23c). With regard to absolute REE values, at least three carbonate-poor samples (ie. R65-20, R59-15 and R70-18) appear to be distinctly more enriched than all remaining samples selected.

A very consistent feature in all patterns of Fig. 3.23 is the behaviour of Ce. Ce is the only other REE besides Eu for which anomalies due to redox reactions can be observed in aqueous solutions and their precipitates. For example, ferrömanganese nodules and crusts in modern basins show a strong positive Ce-anomaly, while recent seawater has a pronounced negative Ce-anomaly, both as a result of oxidation of trivalent Ce to Ce<sup>+4</sup> and subsequent decoupling of Ce from the other REEs due to formation of less soluble Ce(IV) species (Elderfield, 1988). It could be argued that REE data for all samples plotted in Figure 3.23 exhibit apparent negative Ce anomalies. This feature, however, appears to be influenced by the abundances of La which are clearly more enriched than one would expect by back-extrapolation from Sm over Nd and Pr, on the assumption that no chemical reason exists for anomalous behaviour of the latter two rare earths. Such anomalous La abundances have been reported for both ancient and recent metalliferous sediments (Barrett et al., 1988; Bau et al., 1996) as well as some high-temperature hydrothermal fluids at mid-ocean ridges (Klinkhammer et al., 1994), and commonly pose significant

complications in interpreting the behaviour of Ce in marine precipitates (Bau and Dulski, 1996).

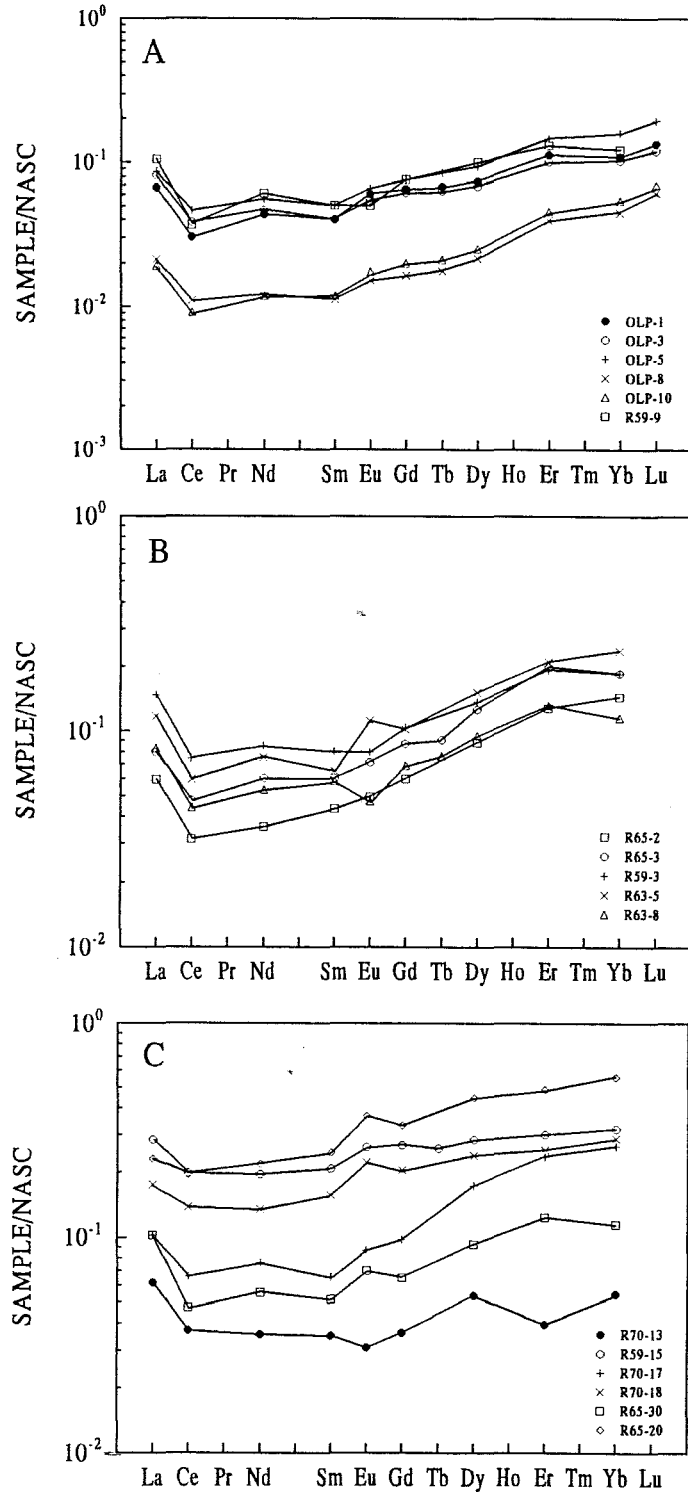


Figure 3.23. NASC-normalised, REE geochemical patterns for five Moodraai and one Hotazel Fe-bearing limestone samples (a) as well as five carbonate-rich (b) and six carbonate-poor (c) iron-formation samples.

Another characteristic of the REE patterns of Figure 3.23 is the inconsistency in the behaviour of Eu. Carbonate-poor samples generally have small - though distinct - positive Eu anomalies, with the exception of one sample which has a slightly negative anomaly (R70-13). On the other hand, carbonate-rich iron-formation samples display a fairly variable behaviour for Eu, with two samples having negative Eu anomalies (R63-8 and R59-3), one showing positive Eu anomaly (R63-5) and two having no anomalies at all (R65-2, R65-3). Carbonate-rich samples from the Mooidraai Formation show effectively very weakly positive to indistinct Eu anomalies, whereas sample R59-9 from the Fe-Mn-rich Hotazel carbonate unit has a negative Eu anomaly. The behaviour of Eu and its implications are discussed in more detail in the following section.

### 3.5.3. Comparisons with ancient and modern equivalents

In order to facilitate comparisons between the REE signatures of the Hotazel-Mooidraai samples with similar data from modern and ancient metalliferous precipitates, data presented in the previous section have been conveniently averaged into four main types, i.e. Hotazel iron-formation (n=12), carbonate-poor iron-formation (n=6), carbonate-rich iron-formation (n=6) and Mooidraai Formation (n=5). NASC-normalised, average REE patterns for the carbonate-poor and carbonate-rich iron-formation samples and the Mooidraai Formation have been plotted in Figure 3.24a, along with data from major iron-formation occurrences such as the Brockman iron-formation, Hamersley Group, Western Australia (Klein and Beukes, 1992), the Ouplaas and Danielskuil Members of, respectively, the Kuruman and Griquatown iron-formations of the Transvaal Supergroup (Beukes and Klein, 1990a; Klein and Beukes, 1992), and Rapitan iron-formations of Canada (Klein and Beukes, 1993). In addition, average values for the entire Hotazel iron-formation (n=10, samples R59-5 and R65-30 excluded) and the Mooidraai Formation (n=5) are shown along with modern metalliferous precipitates from the TAG hydrothermal field, 26° N Mid-Atlantic ridge (Mills and Elderfield, 1995) as well as with average shallow-level (<100m) seawater (Elderfield and Greaves, 1982; see Fig. 3.24b).

Figure 3.24b illustrates the relation between average REE patterns of the Hotazel iron-formation and Mooidraai carbonate, with those for modern seawater and Fe-rich, submarine metalliferous deposits in the immediate proximity to hydrothermal vents. There is a striking similarity between

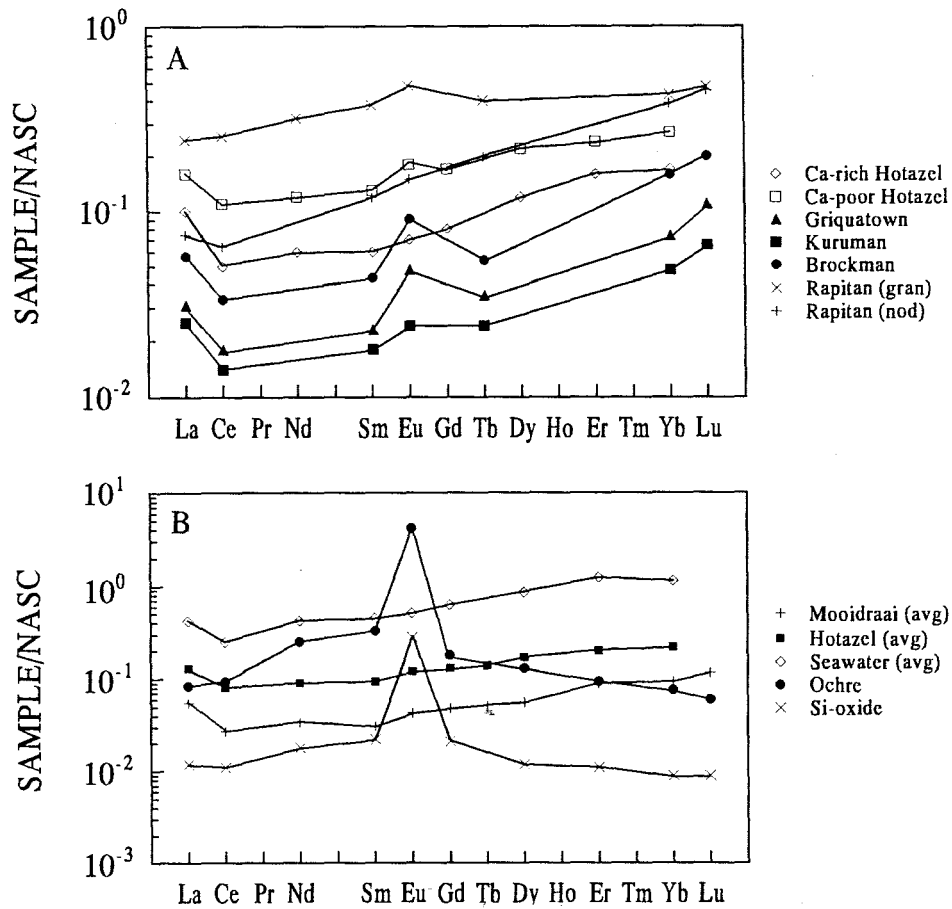


**Figure 3.24.** (a) Comparisons between averaged, NASC-normalised, REE signatures of carbonate-poor and carbonate-rich Hotazel iron-formation, and respective data from the Brockman, Ouplaas, Danielskuil and Rapitan-type iron-formation (data from Beukes and Klein, 1990; and Klein and Beukes, 1992, 1993). (b) NASC-normalised, average REE geochemical patterns of Hotazel iron-formation and Mooidraai limestone, in relation to modern, shallow-level seawater (average based on data by Elderfield and Greaves, 1982) and Fe-rich hydrothermal precipitates from the TAG hydrothermal field (data from Mills and Elderfield, 1995).

the REE patterns of both Hotazel and Mooidraai averages and that of modern seawater, while the hydrothermal precipitates show clearly very flat patterns with characteristically pronounced positive Eu anomalies. These patterns suggest that proximal hydrothermal activity does not constitute a very plausible mechanism as a source for REE in the Hotazel iron-formation. In contrast, it appears likely that the REE, and potentially the Fe and Si in the Hotazel iron-formation were intrinsic constituents of the ambient waters, and that, if a hydrothermal source is invoked, this would have been a distal one, both geographically and temporally. This conclusion



comes in direct contrast to the suggestion of Cornell and Schütte (1995) that the Hotazel sediments are products of volcanic-exhalative mechanisms that formed as a result of rapid precipitation in the immediate vicinity of a mid-ocean ridge setting.

The REE patterns of the Brockman, Kuruman and Griquatown iron-formations of Figure 3.24a show distinct similarities with all REE averages of this study, particularly with regard to their relative heavy REE enrichment and anomalously positive La values. The main difference observed is that of the positive Eu anomaly for primarily the Brockman and Danielskuil averages and, to a lesser extent, the Ouplaas average. Beukes and Klein (1990a) explained the Eu anomalies in the Kuruman and Griquatown iron-formations as evidence for a dilute hydrothermal input in the deeper, anoxic waters of the depositional environment. The difference in the intensities of these anomalies has been attributed to differences in depth of formation of these iron-formations, with the Danielskuil Member having formed in deeper waters with more pronounced hydrothermal signature, as opposed to the more shallower water equivalent represented by the Ouplaas Member. Based on the above, the carbonate-poor, REE-enriched iron-formation facies of the Hotazel Formation would also correspond to a deeper-water sediment due to the small positive Eu anomaly observed in its average REE pattern. In contrast, the seawater-like REE patterns with essentially no Eu-anomalies and lower absolute REE values for both the carbonate-rich iron-formation facies and ultimately for the Mooidraai limestone, are explained as a result of deposition in a shallower environment characterised by increased marine carbonate precipitation, gradually evolving into a carbonate platform. Furthermore, the similarities between the Hotazel and Rapitan-type iron-formations (Klein and Beukes, 1993; see Fig. 3.24a) in terms of the behaviour of Eu, would suggest that the Hotazel iron-formation is probably closer to the Rapitan- than the Superior-type, an observation which bears important genetic implications for the Hotazel rocks. Rapitan-type iron-formations are commonly developed stratigraphically above glacial deposits, and are believed to have formed during periglacial episodes of oxygenation of Fe-rich marine reservoirs, containing a very weak hydrothermal signal (Klein and Beukes, 1993). The presence of the glacial Makganyene Diamictite Formation below the Hotazel rocks (see Part 2, Table 2.1) would imply that processes similar to those involved in the development of Rapitan iron-formations, may also have played a critical role in the formation of the Hotazel Fe-Mn rocks. The significance of this observation will be discussed further in the final part (PART 5) of this thesis.

## **PART 4: STABLE ISOTOPE GEOCHEMISTRY**

Part 4 deals with applications of stable isotope systematics in the study of the Hotazel iron-formation and associated manganese ores. Investigations of this kind usually deal with the isotopic variations of two elements, that is, C and O (e.g. Baur et al., 1985; Kaufman et al., 1990; Beukes et al., 1990). Such variations have been used in the past as evidence of isotopic variations in primary/early diagenetic environments, isotopic compositions of depositional waters, as well as isotopic exchange reactions during post-depositional processes such as prograde metamorphism and/or low-temperature retrograde effects (e.g. Gregory et al., 1990; Kaufman et al., 1990; Winter and Knauth, 1992). In cases where there is sufficient evidence for the existence of isotopic equilibrium, the application of stable isotope geothermometry may prove viable and temperatures of deposition, diagenesis and/or metamorphism may be inferred from the isotopic composition of suitable mineral pairs (e.g. Perry and Bonnicksen, 1966).

Mineral phases in iron-formations that commonly constitute candidates for stable-isotope studies can be grouped into two main categories: (1) Fe-carbonate minerals, present usually as ankerite and siderite and commonly in coexistence with calcite/dolomite; (2) silicate-oxide pairs, of which quartz-magnetite and quartz-hematite are the ones most commonly used. In cases where manganese carbonate ores have been the object of stable isotope investigations, the carbonate minerals analysed include a complete range of Mn-bearing phases, that is, Mn-bearing calcite, kutnahorite and rhodochrosite.

This part consists of two main chapters on the basis of the aforementioned categories. The first chapter deals with carbon and oxygen isotope variations of carbonate minerals from the entire Voëlwater Subgroup as it develops in the southern and central parts of the KMF. These include iron-formation and Mn ore carbonates from the Hotazel Formation as well as  $\text{CaCO}_3$  developed in ferriferous limestone of the overlying Mooidraai Formation. The second chapter focuses on stable isotope systematics of quartz-Fe-oxide pairs from two mineralogically and petrographically diverse borehole intersections of the Hotazel Formation from the northern parts of the KMF. The importance of these studies with regard to the primary/early diagenetic and alteration/metasomatic environments is discussed in the two chapters respectively.

According to convention, carbon isotope variations are reported as  $\delta^{13}\text{C}$  values, defined by the relation:

$$\delta^{13}\text{C}_{\text{mineral}} = [({}^{13}\text{C}/{}^{12}\text{C})_{\text{mineral}} - ({}^{13}\text{C}/{}^{12}\text{C})_{\text{PDB}}] / ({}^{13}\text{C}/{}^{12}\text{C})_{\text{PDB}} \quad (1)$$

Similarly, oxygen isotope variations are reported as  $\delta^{18}\text{O}$  values, according to the equation:

$$\delta^{18}\text{O}_{\text{mineral}} = [({}^{18}\text{O}/{}^{16}\text{O})_{\text{mineral}} - ({}^{18}\text{O}/{}^{16}\text{O})_{\text{SMOW}}] / ({}^{18}\text{O}/{}^{16}\text{O})_{\text{SMOW}} \quad (2)$$

In equation (1), PDB is the acronym for the Pee Dee Belemnite, a Cretaceous belemnite sample which, although long exhausted, is still widely used for palaeotemperature determinations (Hoefs, 1987). In equation (2), SMOW stands for Standard Mean Ocean Water, a hypothetical standard which has approximately the oxygen isotope composition of modern ocean water (Gonfiantini, 1978).

## Chapter 4.1: Carbon and oxygen isotope geochemistry of Voëlwater carbonates

### 4.1.1. Background

A number of studies have been conducted on the stable-isotope geochemistry of carbonate minerals in both iron-formations and carbonate-bearing manganese ores. The prime objective of these studies has been to obtain information on several attributes pertaining to the genesis of such rocks, namely:

- (i) isotopic composition of depositional waters overlying iron- and/or manganese-rich sediments;
- (ii) variations in the chemical composition of primary and diagenetic carbonates;
- (iii) oxygen-isotopic exchange between carbonates and coexisting mineral phases, and;
- (iv) post-depositional processes such as metamorphism and/or oxidation of organic carbon in the presence of ferric iron and/or tetravalent Mn-oxide.

#### 4.1.1.1. Iron-formations

Essentially all major iron-formation occurrences of the Palaeoproterozoic have been investigated in terms of the C and O isotopic character of their contained carbonates. The results have shown that carbonate minerals from essentially all these occurrences exhibit marked C-isotopic depletion as compared to coeval marine carbonates. According to most authors, two key processes may have been involved in variable degrees towards producing such depletions (e.g. Baur et al., 1985; Kaufman et al., 1990; Beukes et al., 1990): (i) coupled organic carbon oxidation - Fe<sup>+3</sup>-reduction during diagenesis/ metamorphism; (ii) precipitation from a stratified water column with the bottom parts enriched in light C due to submarine hydrothermal activity.

Baur et al. (1985) investigated millimetre-scale variations in C and O isotopes in the Marra Mamba iron-formation, Western Australia, and concluded that there is a close association between isotopic depletion in carbonates and the amount of magnetite present in the rock. The main point in Baur et al. (1985) is that such variations cannot result from metamorphism, but are probably due to fermentative metabolism or anaerobic respiration during which an initial Fe<sup>3+</sup>-bearing precursor acted as electron acceptor during oxidation of organic matter. Similar conclusions were also reached by Kaufman et al. (1990) in studies of the isotopic compositions of carbonate microbands from the Dales Gorge Member, Brockman iron-formation, W. Australia. Isotopic depletion in primary siderite ( $\delta^{13}\text{C} \sim -5\text{‰}$ ) is believed to be associated with precipitation from an anoxic water column depleted in <sup>13</sup>C, whereas additional depletion of <sup>13</sup>C is associated with co-precipitation of Fe-oxides and organic C during diagenesis. Kaufman et al. (1990) also support the concept that millimetre-scale isotopic variations in abundances of <sup>13</sup>C and <sup>18</sup>O are associated with diagenetic replacement of primary siderite by secondary ankerite and/or magnetite, and cannot be ascribed to open-system isotopic exchange reactions during burial metamorphism.

Carrigan and Cameron (1991) examined the C and O isotopic composition of carbonates from the Gunflint iron-formation, USA, and suggested that deposition took place in a stratified ocean with the bottom waters being anoxic and containing dissolved Fe and Si from a distal hydrothermal source. Heaviest C-isotope values for siderite and dolomite are attributed to input from normal seawater. Isotopic depletions in <sup>13</sup>C up to -7‰ are due to oxidation of organic matter during

diagenesis, whereas values lighter than these are the result of metamorphism. Heaviest  $\delta^{18}\text{O}$  values for siderite and ankerite (25.2‰, 24.4‰ and 23.8‰ vs SMOW for siderite, ankerite and calcite respectively) are considered to represent the original marine composition. Lighter values (up to 13.5‰) represent isotopic exchange reactions at higher temperature and/or isotopic exchange with  $^{18}\text{O}$ -depleted meteoric  $\text{H}_2\text{O}$ .

Winter and Knauth (1992) discount decarboxylation or anaerobic oxidation of organic matter as potential causes of  $^{13}\text{C}$ -depletion in the Gunflint iron-formation and propose that the latter precipitated in a layered ocean with respect to C-isotopes. According to these authors, depletion of deep-water siderites in  $^{13}\text{C}$  ( $\delta^{13}\text{C}$ : -6.0 to -2.6‰) is attributed to hydrothermal input, whereas shallow-water, shale-facies siderites ( $\delta^{13}\text{C}$ : -2.5 to 0.5‰) may have precipitated from a near-shore water mass which was marginally more enriched in  $^{13}\text{C}$  relative to deep-water. Later siderites and ankerites have similar  $\delta^{13}\text{C}$  to "earlier" shale-facies siderites, implying that shallow seawater was a major component of the diagenetic fluid.  $\delta^{18}\text{O}$  values of carbonates are more variable (13.8-22.5‰), indicating exchange during neomorphism with burial waters depleted in  $^{18}\text{O}$ . The small range in  $\delta^{18}\text{O}$  values of co-existing chert (21.3 to 24.7‰) suggests that silicification, lithification and conversion to quartz from a hydrous silica precursor occurred close to the sediment-water interface.

Beukes et al. (1990) investigated the transition from the Campbellrand carbonates to the Kuruman iron-formation of the Transvaal Supergroup in terms of carbonate petrography, kerogen distribution and carbon-oxygen isotopic variations. They noted that oxide-facies iron-formation carbonates are more depleted in  $^{13}\text{C}$  than those in siderite-facies iron-formation, whereas the kerogens in oxide iron-formation are more enriched. This was used as a strong indication that siderite-rich iron-formation was not derived from oxide-rich iron-formation through reduction of ferric iron by organic matter. Such a process, however, brought about a decrease in the abundance of kerogen in oxide-rich iron-formation and led to the formation of isotopically very light sparry carbonates. Siderite and calc-microsparite represent primary precipitates deposited in a stratified ocean, with the siderites having precipitated from a deeper water mass depleted in  $^{13}\text{C}$  as reflected by their lower  $\delta^{13}\text{C}$  values relative to the calc-microsparites. Such isotopic depletion has been linked to hydrothermal activity due to the very low organic matter supply, as postulated by the

low kerogen contents in the deeper-water siderite-facies iron-formation (Beukes et al., 1990).

Finally, Horstmann (1996) obtained limited isotopic data from siderite and ankerite of the Kuruman and Griquatown iron-formations and suggested that  $^{13}\text{C}$  and  $^{18}\text{O}$  isotopic depletion in early diagenetic siderite from oxide-rich BIF is attributed to incorporation of oxidised organic matter in the presence of ferric iron. Such depletion occurs in addition to an already isotopically depleted signature inherited from a water mass carrying a certain degree of hydrothermal input. Higher  $\delta^{13}\text{C}$  and  $\delta^{18}\text{O}$  values for ankerite are explained by means of later diagenetic shifts in the presence of an evolved pore-fluid.

#### 4.1.1.2. Manganese ores

Carbon and oxygen isotope data of manganiferous carbonates have been obtained from predominantly Mesozoic Mn-carbonate ores such as those of Molango, Mexico (Okita et al., 1988; Okita, 1992; Okita and Shanks, 1992), Ürkút, Hungary (Polgari et al., 1991), Taojiang, China (Okita and Shanks, 1992), and southwestern Taurides, Turkey (Öztürk and Hein, 1997). The results have shown that Mn-carbonates exhibit negative  $\delta^{13}\text{C}$  values which vary depending on the kind of carbonate: Mn-bearing calcites have  $\delta^{13}\text{C}$  values near 0‰ whereas  $\delta^{13}\text{C}$  values of kutnahorites are negative and become progressively lower as the Mn-content in the kutnahorite molecule increases. Invariably, pure rhodochrosites represent the lowest end of the spectrum by having the most negative  $\delta^{13}\text{C}$  values.

Such depletions are explained in a manner similar to the one presented earlier for isotopic depletions in iron-formation carbonates, i.e. as the result of diagenetic reactions involving reduction of higher valence Mn-oxide and coupled oxidation of organic matter. It has been proposed that isotopically depleted, carbonate-rich Mn-deposits may have formed at the margins of dysaerobic to anoxic marine basins, with  $\text{Mn}^{2+}$  preserved in oxygen-deficient bottom basinal waters. Eh fluctuations according to the transgression-regression model of Frakes and Bolton (1984) and Force and Cannon (1988) have been used in order to explain the common cyclicity between carbonates, carbonate-rich manganese ores, and/or chert and black shales as has been documented from the majority of such deposits.

#### 4.1.1.3. Carbonates

Veizer et al. (1992) have demonstrated that several important occurrences of Palaeoproterozoic carbonates such as the Malmani Dolomite, South Africa, the Duck Creek Dolomite, Australia, and the Bruce "Limestone" Member, Canada, have  $\delta^{13}\text{C}$  signatures similar to their Phanerozoic counterparts and are commonly characterised by enrichments in Fe and Mn. Furthermore, an important suggestion regarding the isotopic evolution of Palaeoproterozoic carbonates was put forward by Karhu and Holland (1996). These authors compiled a large dataset of C isotope data from carbonates and to a lesser extent iron-formations of the Palaeoproterozoic, and concluded that, around about 2.2 Ga, a positive carbon-isotopic excursion of approximately 10‰ took place. Karhu and Holland (1996) suggest that this excursion is strong evidence that during the same period, the level of atmospheric oxygen rose significantly as a result of increased rates of organic carbon burial. The excursion is believed to be comparable with other lines of evidence suggesting a sudden oxygenation of the Palaeoproterozoic atmosphere at that time, including changes in the oxidation levels of palaeosols, changes in the geochemistry of uranium as well as the first appearance of red beds (e.g. Krupp et al., 1994).

#### 4.1.2. Sample selection and analytical procedures

The mixed lithologic nature of the Voëlwater Subgroup comprising iron-formation, carbonate-rich Mn ore and limestone provides an excellent opportunity where the stable-isotope characteristics of a diverse group of chemical sediments can be investigated as part of the same stratigraphic succession. For that reason, twenty-six quartered-core samples of Hotazel iron-formation and Mn ore and 10 carbonate samples from the Mooidraai Formation were selected for isotopic analyses from six boreholes drilled through the Voëlwater stratigraphy in the southern and central parts of the KMF (Appendix I, Figs. A1, A2, A3). Care was taken with regard to homogeneity of the sample material and frequency of sample selection across the stratigraphy. In most cases, core samples of no more than 15cm in length, taken approximately every 3-5 metres, were sufficiently homogeneous and representative for a whole-rock analytical approach.

Carbon and oxygen isotopic compositions were determined by mass spectroscopic analyses, using

a Finnigan MAT 252 mass spectrometer in the Department of Geological Sciences, University of Cape Town. Carbon dioxide was evolved from whole-rock powder samples by treatment with 100%  $\text{H}_3\text{PO}_4$  (Appendix II). The results are presented in Table 4.1 and are complemented by corresponding partial whole-rock geochemical data for each sample. The major element compositional fields of the selected sample groups are shown schematically on the ternary graph of Figure 4.1.

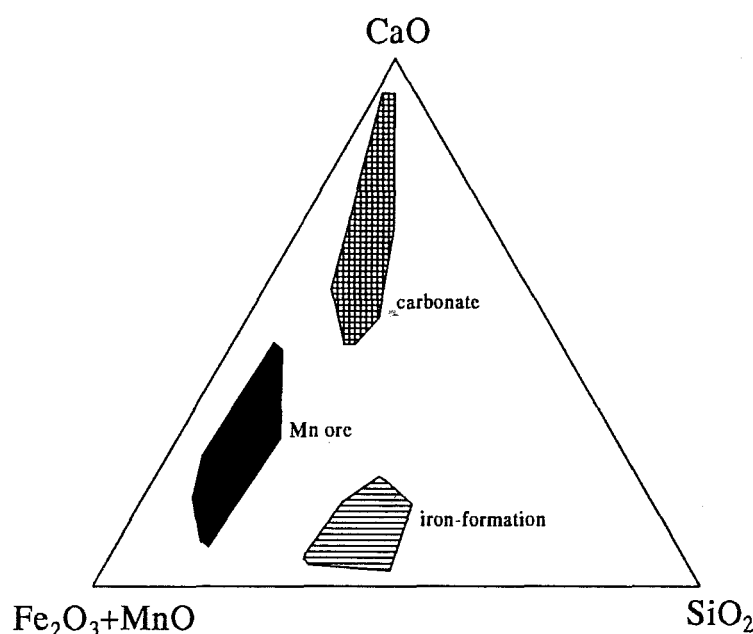


**Figure 4.1.** Ternary plot showing the compositional fields of Hotazel iron-formation, Kalahari Mn ore, and Mooidraai carbonate, as defined by whole-rock data for the selected samples presented in Table 4.1.

Chemical separation techniques for coexisting carbonates in iron-formation and Mn ore were used as described by Al-Aasm et al. (1990) for coexisting calcite, dolomite and siderite. Iron-formation samples were reacted in evacuated Y-tubes at  $25^\circ\text{C}$  for 4 hours and the  $\text{CO}_2$  extracted was labelled "calcite". The unreacted portion of the samples was then reacted at  $50^\circ\text{C}$  for a minimum of 18-20 hours and the  $\text{CO}_2$  yielded corresponded to ankerite. This was done on the assumption that reaction times for ankerites are effectively similar to those of dolomite. For ankerite/dolomite-free samples such as those from the Mooidraai Formation and two samples from a Fe/Mn-bearing carbonate unit occurring in the Hotazel Formation, the above stage was omitted.



The manganese samples posed certain difficulties. With all samples containing a mixture of Mn-calcite and kutnahorite, it was observed that no effective fractionation of respective CO<sub>2</sub> yields could be obtained, as both phases exhibit reactivities intermediate between pure calcite and dolomite. This is clearly demonstrated on a plot of  $\delta^{13}\text{C}$ - $\delta^{18}\text{O}$  vs time for one manganese sample treated at 25°C over periods of 30 minutes, 1, 2, 4 and 6 hours (Fig. 4.2). A similar problem has been reported previously by Okita et al. (1988) on mixed Mn-carbonate samples from Molango, Mexico, and it may be due to the fact that the kutnahorite present may possibly represent an example of disordered kutnahorite ("pseudokutnahorite") without any dolomite-type ordering (Mucci, 1988). Since no effective chemical separation was possible, an alternative method was employed. Approximately 25mg of each Mn sample were reacted at 25°C for one hour and the CO<sub>2</sub> yielded was attributed to Mn-calcite proper. Subsequently, the samples were reacted for an additional 3 hours at 25°C, degassed, and transferred to a 50°C water bath for further reaction for approximately 12 hours. The CO<sub>2</sub> evolved through that process was labelled "kutnahorite". Given its apparent limitations, the above technique served as a crude attempt in order to eliminate, as much as possible, any effects of cross-contamination between the coexisting Mn-carbonates in the Mn ore-units.

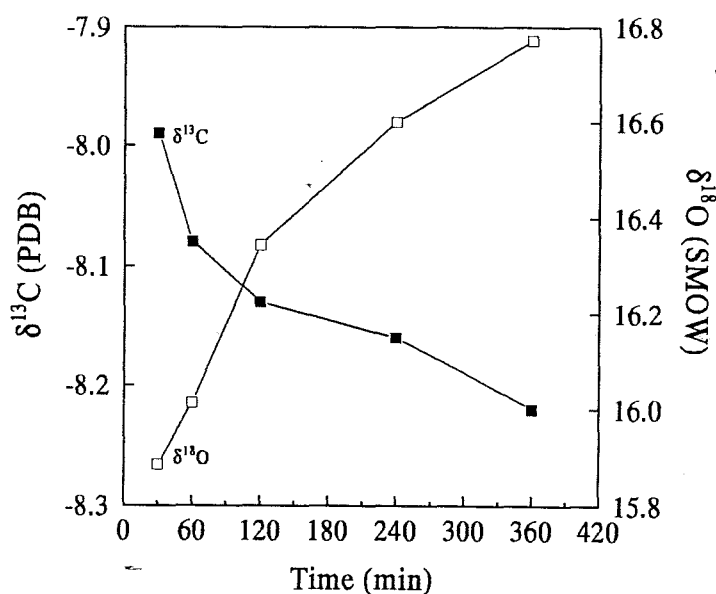


**Figure 4.2.** Plot of time (in minutes) versus  $\delta^{13}\text{C}$  and  $\delta^{18}\text{O}$ , showing variations in isotopic determinations at different reaction times for one manganese ore sample (R70-23).

### 4.1.3. Petrographic descriptions

#### 4.1.3.1. Hotazel Formation

Mineralogically and texturally, the 26 samples from the Hotazel Formation cover the entire range of lithotypes present in the Hotazel stratigraphy from the southernmost KMF (Kleyenstüber, 1984; Nel et al., 1986; Tsikos and Moore 1997; see also PART 2). Samples 11-16, 19 and 25-26 correspond to the carbonate-rich iron-formation (Tsikos and Moore 1997; see also PART 2), with bulk mineralogy dominated by chert, magnetite, calcite, ankerite, stilpnomelane, minnesotaite, minor greenalite, and traces of pyrite. Banding is generally in the order of 1mm to 1cm and is commonly characterised by sharp or diffuse contacts and soft sediment deformation structures, almost exclusively associated with carbonate-bearing chert. A characteristic textural feature in the carbonate-rich iron-formation is the almost perfect development of ankerite rhombohedra disseminated in microcrystalline chert, with occasional minnesotaite occurring in the form of dispersed laths, sheaves and “bow-tie” textures. Microprobe analyses obtained from a number of ankerites (see also Table 2.2, PART 2), indicated a composition approximated by the formula  $\text{CaFe}_{0.65}\text{Mg}_{0.30}\text{Mn}_{0.05}(\text{CO}_3)_2$  (Tsikos, 1994). The ankerite-bearing bands alternate with magnetite-bearing ones, as well as with banded concentrations of calcite admixed with acicular stilpnomelane and magnetite.

Samples 27-29 represent the carbonate-poor iron-formation (Tsikos and Moore 1997). These samples exhibit rhythmic banding, with individual bands rarely exceeding 1cm in thickness. All samples are characterised by the development of very fine-grained, greenalite-bearing chert containing occasional minnesotaite and very small amounts of carbonate in the form of finely disseminated ankerite blebs. X-ray diffraction studies did not verify the presence of any siderite in the samples, although dark, cryptocrystalline micro-granular structures within the greenalite-chert assemblage were occasionally observed, resembling siderites described from iron-formations elsewhere (Beukes et al., 1990; Kaufman et al., 1990). The chert-greenalite bands are commonly replaced by coarser minnesotaite and alternate rhythmically with thin, essentially pure magnetite. Calcite-stilpnomelane(-magnetite) laminae are very sporadically present.

Sample 36 corresponds to the oxide-rich iron-formation (Tsikos and Moore 1997) and contains chert bands impregnated with cryptocrystalline, “dusty” hematite, macroscopically reflected by a characteristic red appearance. Magnetite occurs as thin monomineralic bands, and in the form of fine, subhedral disseminated grains overprinting the chert-hematite assemblage. The total carbonate content in this sample is small, corresponding to minor amounts of interstitial calcite and fine, dispersed ankerite.

Samples 20 and 21 correspond to the thin (1-1.5m) ferromanganiferous carbonate unit enclosed within the BIF between the middle and upper manganese beds (Tsikos and Moore 1997). Here, sparry calcite is the sole carbonate phase and is associated with dusty hematite containing a small amount of chert. Minor stilpnomelane, riebeckite and pyrite may also be present.

Samples 17-18, 22-24 and 30-35 are from the three manganese units interbedded with the iron-formation. The mineralogy of the Mn ore is fairly consistent in all units and it comprises essentially very fine-grained braunite-kutnahorite-hematite assemblages, containing pinkish-white laminae and ovoids of Mn-calcite/kutnahorite. Kutnahorites from the lowermost Mn-unit have an average formula  $\text{CaMn}_{0.7}\text{Mg}_{0.3}(\text{CO}_3)_2$ , while Mn-calcites contain up to 10 wt% MnO (Kleyenstüber, 1984; Nel et al., 1986). Variations in the relative proportions of Mn-carbonate, braunite and hematite are responsible for the overall variations in Mn content and Mn/Fe ratios of the samples. Hausmannite and jacobsonite, occasionally present in the Mn ores (Kleyenstüber, 1984; Nel et al., 1986), were not observed in the selected samples.

#### 4.1.3.2. Mooidraai Formation

Samples 1-10 are from the Mooidraai Formation immediately overlying the Hotazel Formation (Appendix I, Fig. A3) and are characterised by the abundance of microcrystalline calcite. The rock appears banded/laminated and resembles strikingly the underlying iron-formation. The calcite is very fine-grained and is commonly associated with chert-magnetite-bearing bands containing dispersed minnesotaite needles. Thin magnetite laminae are present in substantial amounts in some of the samples. Although a considerable range in bulk chemical compositions exists amongst the selected samples, the simple carbonate mineralogy and low Fe content (<15 wt%) suggests that

the Mooidraai Formation is in fact a Fe-bearing limestone (see PART 2), in contrast to previous descriptions (Beukes, 1983).

#### 4.1.4. Results

##### 4.1.4.1. Isotopic compositions

C and O isotopic results presented in Table 4.1 reveal a general depletion in both  $^{13}\text{C}$  and  $^{18}\text{O}$  in iron-formation and Mn ore carbonates relative to normal marine carbonate isotopic signatures. This is in good agreement with published data from other important occurrences of Palaeoproterozoic iron-formation (Baur et al., 1985; Kaufman et al., 1990; Beukes and Klein, 1990; Beukes et al., 1990; Carrigan and Cameron, 1991; Winter and Knauth, 1992; Horstmann, 1996), and Mn-carbonate ores of Mesozoic age (Okita et al., 1988; Polgari et al., 1991; Okita and Shanks, 1992; Öztürk and Hein, 1997). Also, the isotopic composition of the Mooidraai carbonates is very similar to other Palaeoproterozoic carbonates (Baur et al., 1985; Carrigan and Cameron, 1991) which are believed to have formed via direct precipitation from seawater. Figure 4.3 demonstrates comparisons between the isotopic range of values observed in the Voelwater sediments, and variations in the isotopic composition of other Palaeoproterozoic iron-formations, carbonates and Mn ores according to published data from important occurrences worldwide.

Calcites from the carbonate-rich iron-formation samples have  $\delta^{13}\text{C}$  values ranging between -4.2 and -7.8‰, whereas coexisting ankerites are more depleted in  $^{13}\text{C}$  with values ranging from -5.9 to -9.5‰.  $\delta^{18}\text{O}$  in calcite exhibits a fairly narrow range of values between 17.4 and 19.8‰, while respective ankerites vary more widely (14.7-19.8‰). The two samples from the carbonate unit have  $\delta^{13}\text{C}$  values of 3.3 and 3.9‰, and  $\delta^{18}\text{O}$  values of 18.3 and 19.6‰ for samples 20 and 21 respectively; these are comparable to the isotopically lightest calcites from the carbonate-rich iron-formation (Table 4.1).

Particularly strong depletion in  $^{13}\text{C}$  is observed in the carbonate-poor and oxide-rich iron-formation samples, with values between -13.3 and -18.2‰ for calcite and -14.8 and -17.9‰ for ankerite. Carbonates from the carbonate-poor iron-formation are also depleted in terms of

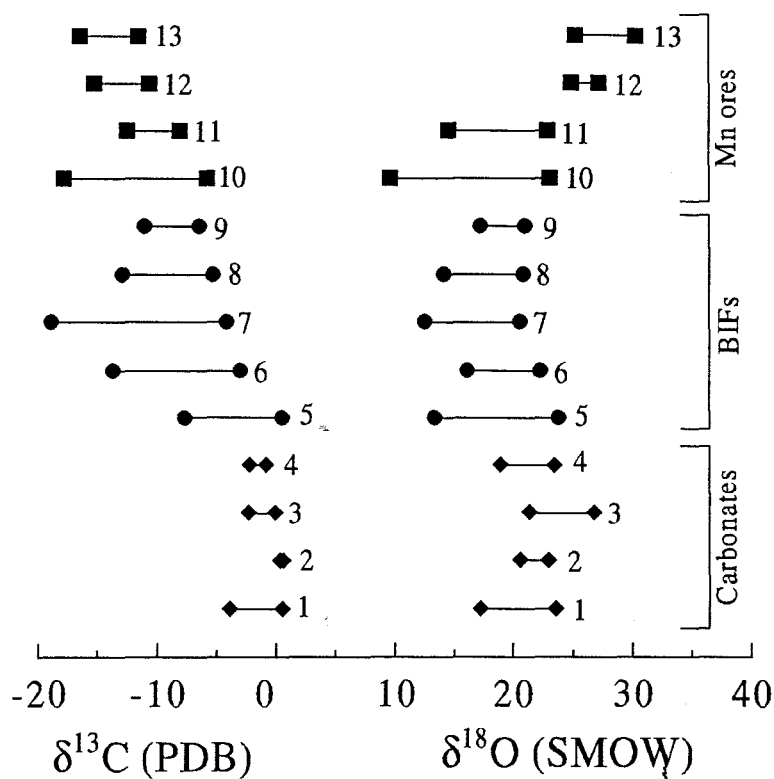


**Figure 4.3.** Variations in the C- and O-isotopic compositions of carbonate minerals from the Voëlwater Subgroup (this study), worldwide iron-formations/carbonate rocks of Palaeoproterozoic age, and carbonate-rich manganese deposits of various ages. Locations and data sources: (1) Gunflint carbonates, N. America (Winter and Knauth, 1992); (2) Wittenoom Dolomite, W. Australia (Baur et al., 1985); (3) Campbellrand Dolomite, Transvaal Supergroup, S. Africa (Beukes et al., 1990); (4) Mooidraai limestone (this study); (5) Gunflint IF, N. America (Carrigan and Cameron, 1991; Winter and Knauth, 1992); (6) Asbesheuwels IF, Transvaal Supergroup, S. Africa (Beukes et al., 1990); (7) Hotazel IF (this study); (8) Marra Mamba IF, W. Australia (Baur et al., 1985); (9) Brockman IF, W. Australia (Kaufman et al., 1990); (10) Taojiang Mn ore, China (Okita and Shanks, 1992); (11) Kalahari Mn ore (this study); (12) Ulukent Mn ore, Turkey (Öztürk and Hein, 1997); (13) Molango Mn ore-district, Mexico (Okita et al., 1988; Okita and Shanks, 1992).

$\delta^{18}\text{O}$ , with values ranging from 15.6 to 20.6‰ for calcite and 12.5 to 19.4‰ for ankerite. The carbonate-poor iron-formation carbonates, and particularly ankerite, are clearly more depleted in  $^{18}\text{O}$  as compared with the carbonate-rich samples, whereas the oxide-rich sample 36 appears relatively enriched in  $^{18}\text{O}$  ( $\delta^{18}\text{O} = 20.6\text{‰}$  for calcite and 19.4‰ for ankerite) which is comparable to  $\delta^{18}\text{O}$  values of carbonate-rich samples.

Mn-calcites and kutnahorites from the three Mn ore-units in the Hotazel Formation display a narrow range in  $\delta^{13}\text{C}$  between -8.1 and -10.9‰, and -8.3 and -12.5‰ respectively (Table 4.1). Kutnahorites are always more depleted in  $^{13}\text{C}$  than coexisting Mn-calcites, similar to calcites and ankerites from the iron-formation units. Although there is essentially no significant variation in  $\delta^{13}\text{C}$  values amongst samples from the three units, the lowest ones appear exclusively in the lowermost Mn unit for both carbonates.

In terms of  $\delta^{18}\text{O}$ , Mn-calcites from five out of the six samples from the lower Mn-unit range between 16 and 17.9‰, and kutnahorites between 14.5 and 18.6‰ (Table 4.1). The lowermost sample from this unit differs in that it shows heavier  $\delta^{18}\text{O}$  values for both carbonates, which compare well with the samples from the middle and upper Mn-units ( $\delta^{18}\text{O}$ : 20.9 and 21.6‰ for Mn-calcite, and 20.3 and 22.5‰ for kutnahorite).

Calcites from the 10 Mooidraai samples exhibit a narrow variation in both  $\delta^{13}\text{C}$  and  $\delta^{18}\text{O}$  values, i.e. -2.2 to -0.8‰ and 19.5 to 23.4‰ respectively. The isotopically more depleted samples appear to be related to correspondingly increased amounts of quartz and magnetite.

All above observations are comprehensively illustrated in the  $\delta$ - $\delta$  plots of Figure 4.4. Discriminations between the various sample groups are demonstrated on  $\delta^{13}\text{C}$ - $\delta^{18}\text{O}$  plots for calcite and ankerite respectively (Figs. 4.4c,d), primarily on the basis of variations in  $\delta^{13}\text{C}$ , i.e.:

- carbonate-poor iron-formation samples exhibit strong depletions in  $^{13}\text{C}$ ;
- limestone samples show normal “marine”  $\delta^{13}\text{C}$  signatures ( $\sim 0\text{‰}$ );
- carbonate-rich iron-formation samples (including the two Fe/Mn-rich carbonates) have values intermediate between normal limestone and carbonate-poor iron-formation;
- manganese ore samples are intermediate between carbonate-rich and carbonate-poor

**Table 4.1:** Partial whole-rock and stable isotope data of 36 samples from the Voëlwater Subgroup.

Sample	SiO <sub>2</sub>	CaO	Fe <sub>2</sub> O <sub>3</sub>	MnO	δ <sup>13</sup> C <sub>cc</sub>	δ <sup>18</sup> O <sub>cc</sub>	δ <sup>13</sup> C <sub>ank/kutn</sub>	δ <sup>18</sup> O <sub>ank/kutn</sub>
1 (OLP-1)	4.63	46.18	9.50	1.18	-1.3	21.6		
2 (OLP-2)	8.35	42.40	13.14	1.30	-1.4	21.4		
3 (OLP-3)	8.88	44.55	10.97	0.14	-1.2	20.9		
4 (OLP-4)	9.15	43.17	13.89	0.38	-1.5	19.8		
5 (OLP-5)	13.50	34.07	23.92	0.62	-2.2	19.5		
6 (OLP-6)	1.76	51.64	2.89	0.84	-1	22.8		
7 (OLP-8)	2.02	51.43	3.74	0.58	-0.9	23.4		
8 (OLP-9)	1.39	52.56	2.42	0.66	-0.8	23.3		
9 (OLP-10)	2.15	51.78	3.83	0.59	-1.1	22.2		
10 (OLP-11)	5.57	45.18	12.29	0.61	-1.7	18.9		
11 (R65-2)	37.66	12.95	34.79	0.15	-4.1	19.6	-5.9	18.9
12 (SM31-2)	30.86	11.46	42.80	0.29	-5.8	19	-7.1	18.2
13 (SM31-3)	37.20	6.61	45.90	0.31	-6.8	19.4	-9.2	14.7
14 (R65-3)	35.97	7.58	43.97	0.37	-7.6	19.8	-9.5	15.5
15 (SM31-5)	35.40	7.23	46.55	0.58	-6.7	19.1	-7.3	17.9
16 (R59-3)	30.38	15.77	32.81	2.21	-5.9	18.8	-7.6	19.8
17 (R65-7)	7.44	13.12	9.21	49.98	-8.1	20.7	-8.3	21.8
18 (R59-5)	7.60	12.85	15.35	42.21	-8.3	21.6	-9.1	22.5
19 (R63-5)	33.50	10.74	39.60	1.38	-3.4	18.1	-5.2	17.6
20 (SM31-10)	7.73	36.66	10.39	9.75	-3.3	18.3		
21 (R59-9)	12.96	33.69	10.87	7.17	-3.9	19.6		
22 (R59-11)	7.93	15.24	12.56	28.84	-9.5	21.6	-10	20.3
23 (R70-10)	6.76	16.27	22.13	25.41	-9.8	21.5	-10.2	21.1
24 (R63-7)	10.50	18.98	14.69	23.18	-8.8	20.9	-10.1	21.2
25 (R63-8)	30.30	15.62	35.32	0.55	-6	17.5	-9.1	17.3
26 (SM31-15)	29.52	13.04	43.23	0.50	-7.8	17.4	-8.9	15.9
27 (R70-13)	43.15	4.60	45.58	0.12	-13.3	17.8	-15.9	12.5
28 (SM31-17)	34.47	5.06	51.38	0.15	-15.9	17.8	-17.1	16.3
29 (SM31-18)	42.59	3.74	45.08	0.49	-18.2	15.6	-17.9	16.2
30 (R70-20)	4.85	28.29	9.62	20.50	-8.1	16	-9.4	14.5
31 (R70-21)	5.05	19.05	16.62	33.16	-8.4	17.2	-8.6	18.6
32 (R70-23)	5.14	22.19	6.37	38.41	-8.2	16.4	-9.3	16.7
33 (R63-15)	5.50	16.78	7.17	45.02	-10.2	17.9	-10.4	17.4
34 (R63-17)	5.19	17.49	5.61	45.55	-10.5	17.6	-11.9	15.2
35 (R59-24)	11.34	6.94	20.82	39.93	-10.9	22.8	-12.5	21.2
36 (R65-30)	28.63	4.44	48.14	5.24	-13.9	20.6	-14.8	19.4

Total Fe as Fe<sub>2</sub>O<sub>3</sub>; Total Mn as MnO

SiO<sub>2</sub>, CaO, Fe<sub>2</sub>O<sub>3</sub> and MnO values presented in wt%

δ<sup>13</sup>C and δ<sup>18</sup>O values normalized to PDB and SMOW respectively

Abbreviations: ank: ankerite; cc: calcite; kutn: kutnahorite

iron-formation, in terms of  $\delta^{13}\text{C}$ . Discrimination between Mn ore samples from the lowermost Mn-unit and the middle/uppermost units can be obtained from their respective differences in  $\delta^{18}\text{O}$ .

A feature that deserves particular reference is the good linear correlation in Fig. 4.4a between  $\delta^{13}\text{C}$  values of calcite and those of ankerite/kutnahorite (corr. coeff. = 0.91). Such a trend can be taken as a potential indication of relatively constant C-isotope fractionation between the two co-existing carbonates in both the iron-formation and the Mn ore. Such fractionation, however, does not necessarily imply that crystallisation took place under conditions of isotopic equilibrium, attained during diagenesis/very low grade metamorphism. In fact,  $\Delta_{\text{ank-cc}}$  values for both C and O are practically all negative, a fact which renders meaningless the use of such data as temperature indicators according to published fractionation curves for dolomite-calcite pairs (Sheppard and Schwarz, 1970; in Friedman and O'Neil, 1977).

It is thus possible that the constant C-isotope variations in the two carbonates has resulted from an early diagenetic mechanism that caused relative  $^{13}\text{C}$ -depletions in a uniform fashion throughout the depositional history of the Hotazel Formation. On the other hand, reasons for the poorer correlation in the  $\delta^{18}\text{O}$  values between calcite and ankerite and the very broad correlation between calcite and kutnahorite as seen in Figure 4.4b, should be sought in: i. uncertainties regarding effective chemical separation of the Mn-carbonates during sample treatment, and/or: ii. diagenetic exchange reactions involving carbonates and other mineral phases present in the sediments (e.g. Fe-Mn-oxides, Fe-silicates, etc.).

#### 4.1.4.2. Isotopic compositions vs bulk-rock CaO - chemostratigraphy

In a chemically simple rock such as the Hotazel iron-formation, the major constituents, that is,  $\text{SiO}_2$ , total Fe-oxide and CaO, are all clearly interrelated with one another. Figure 4.5 demonstrates the distinct negative correlation between whole-rock CaO and the sum Fe/Mn-oxide+ $\text{SiO}_2$  in the Voëlwater sediments, suggesting that any increase in the carbonate component invariably coincides with a corresponding decrease in both Fe-compounds and quartz in the iron-formation, and in braunite and hematite in the manganese ore-units. Since Fe and Mn are hosted in a variety of mineral phases, whole-rock CaO values can serve as a common denominator for



both sample groups. It is thus convenient to place particular emphasis on the relation between whole-rock CaO contents and variations in C- and O-isotopic compositions.

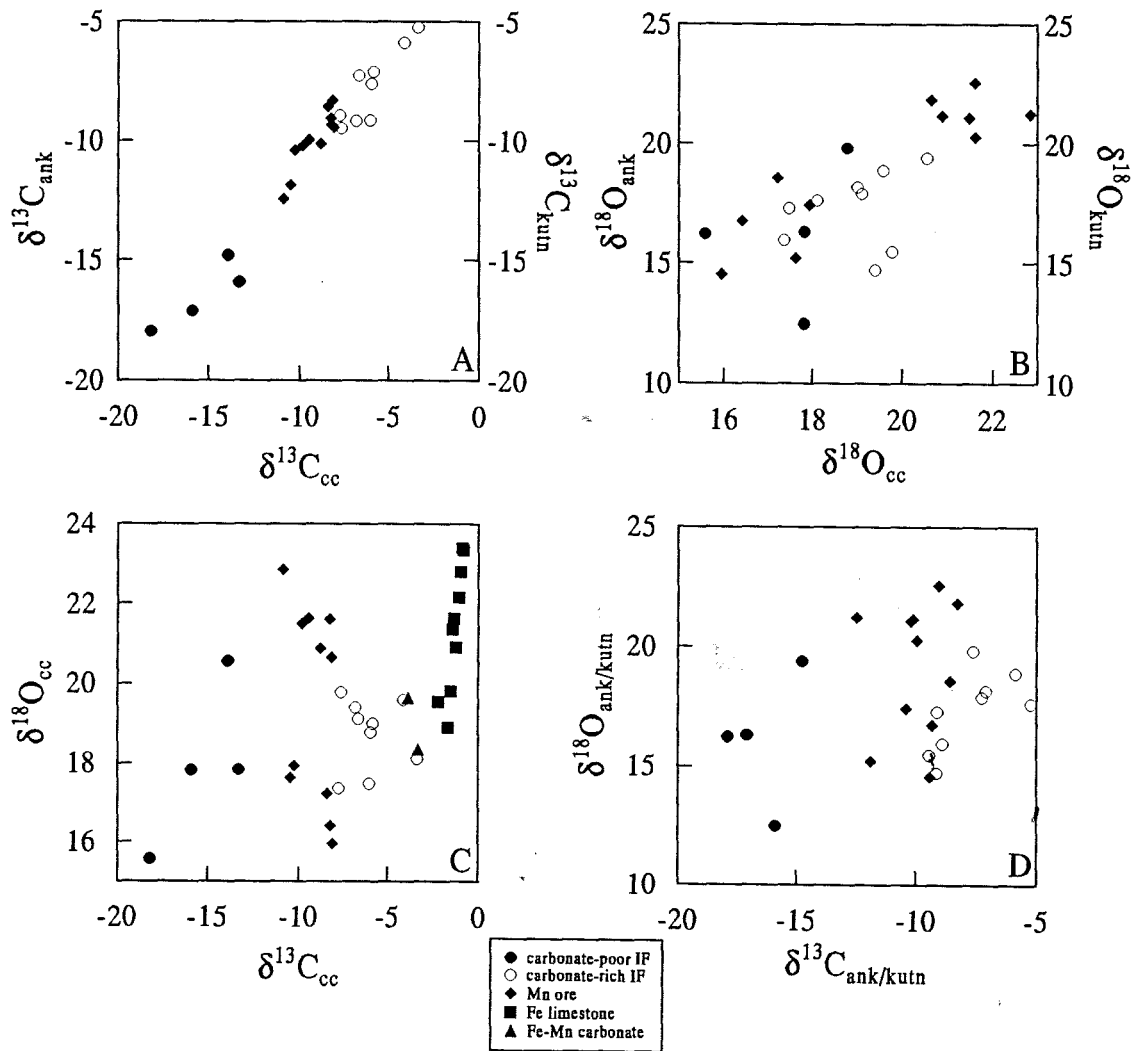


Figure 4.4. Bivariate  $\delta$ - $\delta$  plots of carbonate minerals from selected samples of Hotazel iron-formation, Mn ore and Moodraai limestone.

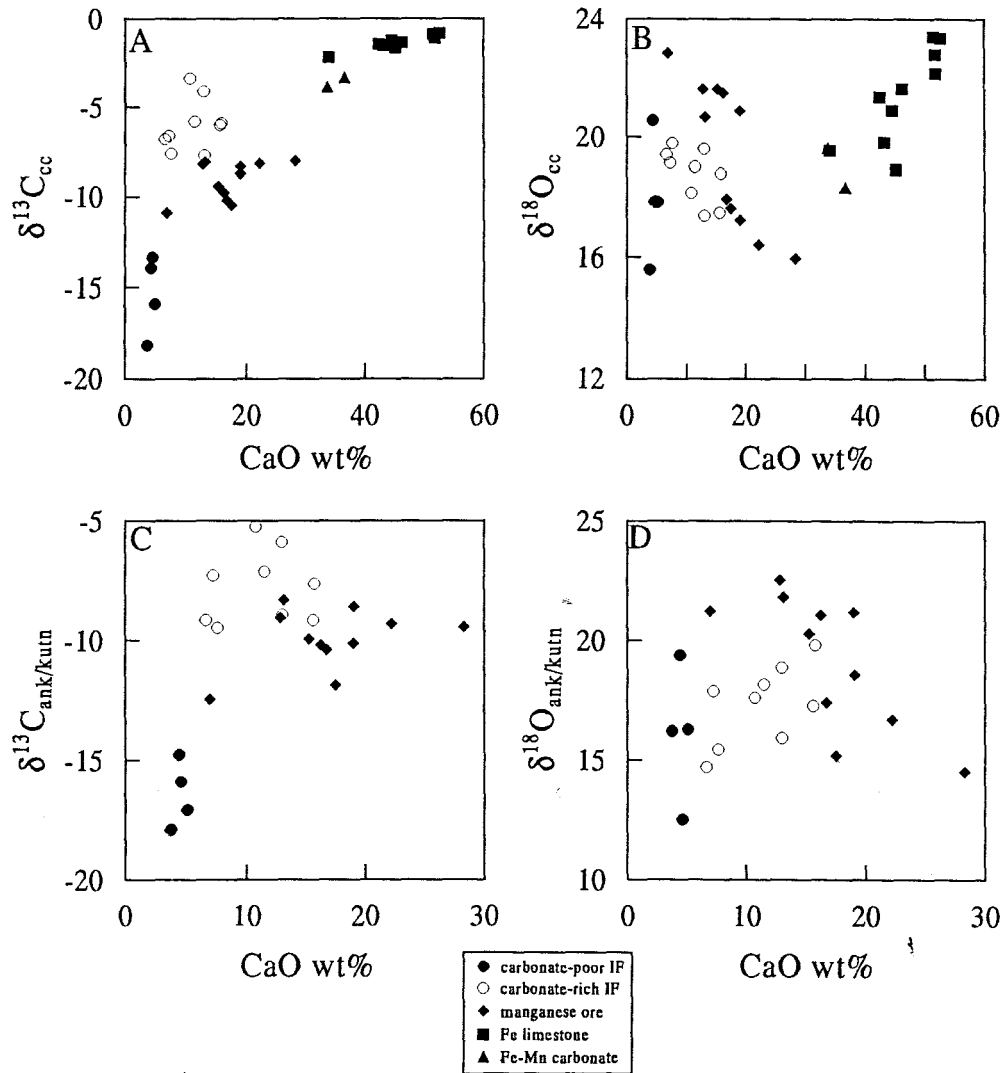
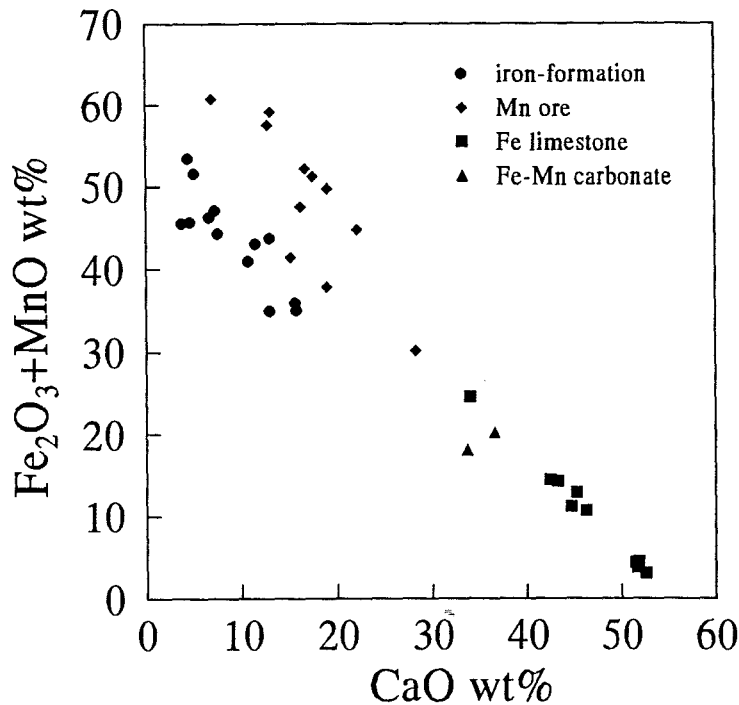


Figure 4.6. Bivariate plots of whole-rock CaO versus  $\delta^{13}C$ - $\delta^{18}O$  for iron-formation, Mn ore and Moodraai limestone samples analysed in this study.



**Figure 4.5.** Bivariate plot of whole-rock CaO versus the sum of total Fe- and Mn-oxide for all samples selected for C- and O-isotope analyses from this study.

Figure 4.6 shows the relations between stable isotope data and corresponding whole-rock CaO values of all samples analysed in the form of simple  $\delta$ -CaO plots. In Figures 4.6a and c, a clear “hyperbolic” pattern is observed, linking the various sample groups and demonstrating a progression in more  $^{13}\text{C}$ -enriched carbonates with increasing total carbonate content in the following manner:

*carbonate-poor IF → carbonate-rich IF → Fe-Mn-bearing carbonate → Mooidraai limestone*

The exception in this trend corresponds to the behaviour of the Mn ore samples which maintain a clearly more depleted C-isotope character with increasing CaO. The CaO- $\delta^{18}\text{O}$  plots of Figure 4.6 do not seem to establish any statistically important correlations, except for a rather clear separation of the various sample groups in distinct “clusters”, particularly with respect to the manganese ore samples from the lowermost and middle/uppermost units (Fig. 4.6b).

Figure 4.7 shows variations in whole-rock CaO and  $\delta^{13}\text{C}$  and  $\delta^{18}\text{O}$  values for carbonate minerals from all samples analysed, against a simplified stratigraphic profile of the Voëlwater Subgroup. There are essentially three pronounced features on these variation plots that deserve particular consideration:

(i) A distinct, gradual positive isotopic excursion of approximately 10‰ is observed in the  $\delta^{13}\text{C}$  values of calcite and ankerite over the transition from carbonate-poor to carbonate-rich iron-formation. This transition coincides with a corresponding, though more sudden, increase in the total carbonate content of the rock as reflected in the geochemical profile of whole-rock CaO values (Fig. 4.7);

(ii) The threefold cyclic nature of the Hotazel Formation is clearly documented by the distinct differences in the isotopic values between iron-formation carbonates and Mn carbonates. Furthermore, there is a very smooth upward progression in the  $\delta^{13}\text{C}$  - and to a lesser extent  $\delta^{18}\text{O}$  - profiles of the iron-formation (particularly in the case of calcite) towards more enriched values, with the Mooidraai carbonates providing the upper limit. The same situation applies to carbonates from the interbedded Mn-units, where a progression towards slightly more  $^{13}\text{C}$ -enriched values is observed between the lowermost and the middle/uppermost units.

(iii) There is a marked difference between the  $\delta^{18}\text{O}$  of Mn-carbonates between the lowermost and middle/uppermost Mn-units, that is, below and above the isotopic excursion observed in the iron-formation. Mn-carbonates from the middle and uppermost beds are significantly more enriched in  $^{18}\text{O}$  than those from their lowermost counterpart, and compare well with those of the Mooidraai limestone.

As stated earlier, positive C-isotopic excursions of approximately 10‰ have been reported from various Palaeoproterozoic carbonate sequences and have been interpreted as a result of a sudden rise in atmospheric oxygen levels at approximately 2.2 Ga (Karhu and Holland, 1996). The Voëlwater succession is believed to have been deposited during this time interval, on the basis of age data for the underlying Ongeluk lavas (approximately 2.2 Ga; Cornell et al., 1996). Although a sudden rise in available oxygen cannot be readily deduced from the Hotazel-Mooidraai transition, the isotopic excursion observed in the transition from carbonate-poor to carbonate-rich iron formation could be taken as partial evidence for a localised rise in atmospheric oxygen levels. Similar positive excursions were recently reported from lithological units of the Pretoria Group,

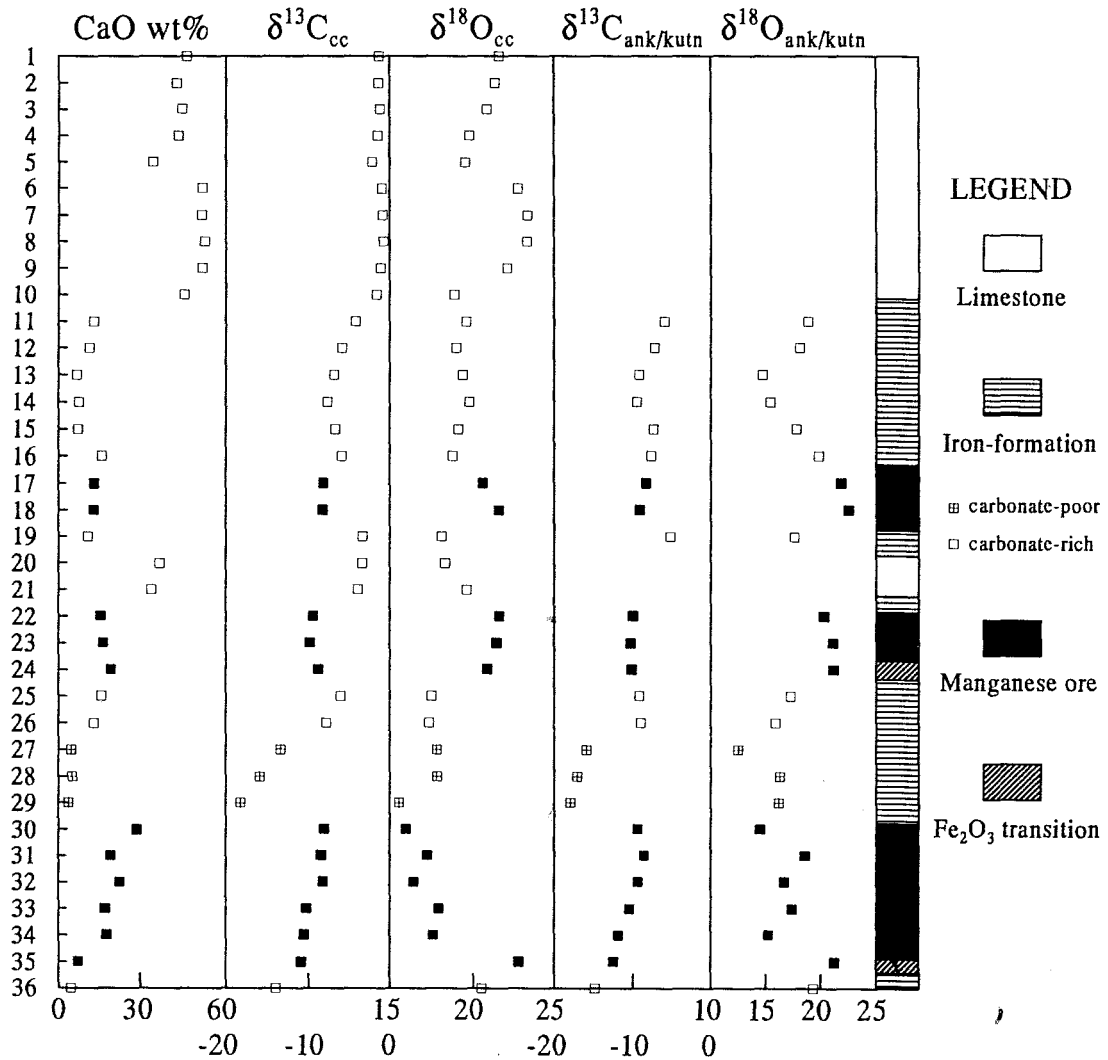


**Figure 4.7.** Stratigraphic variation plots of whole-rock CaO contents and  $\delta^{13}\text{C}$ - $\delta^{18}\text{O}$  values for both calcite and ankerite/kutnahorite from all samples from the Hotazel/Mooidraai succession. Stratigraphic column is not drawn to scale, but exhibits crude relative thickness relations between iron-formation, Mn ore and Mooidraai limestone, as well as the approximate stratigraphic location of the selected samples.

Transvaal Supergroup (Buick et al., 1998), parts of which are regarded as chronostratigraphic correlatives to the Voëlwater Subgroup. Alternatively, one could assume that this transition coincides with a progressive change in the conditions of precipitation imposed by a shallowing-upwards trend, due to build-up of sediment in the palaeodepository and “crossing” of a critical zone in the water column (lysocline?) above which precipitation of marine carbonate was favoured. Factors promoting this increased carbonate precipitation would include primarily increases of the pH and temperature levels of the ambient waters, which would further imply a likely change towards warmer climatic conditions at the time of deposition. A shift towards higher oxygen fugacity values may only have been marginal, as is suggested by whole-rock Fe# values of selected iron-formation samples across the Hotazel stratigraphy (Fig. 4.8; see also PART 3, and Tsikos and Moore, 1997). Hence, a dramatic rise in atmospheric oxygen levels may, in fact, not be required.

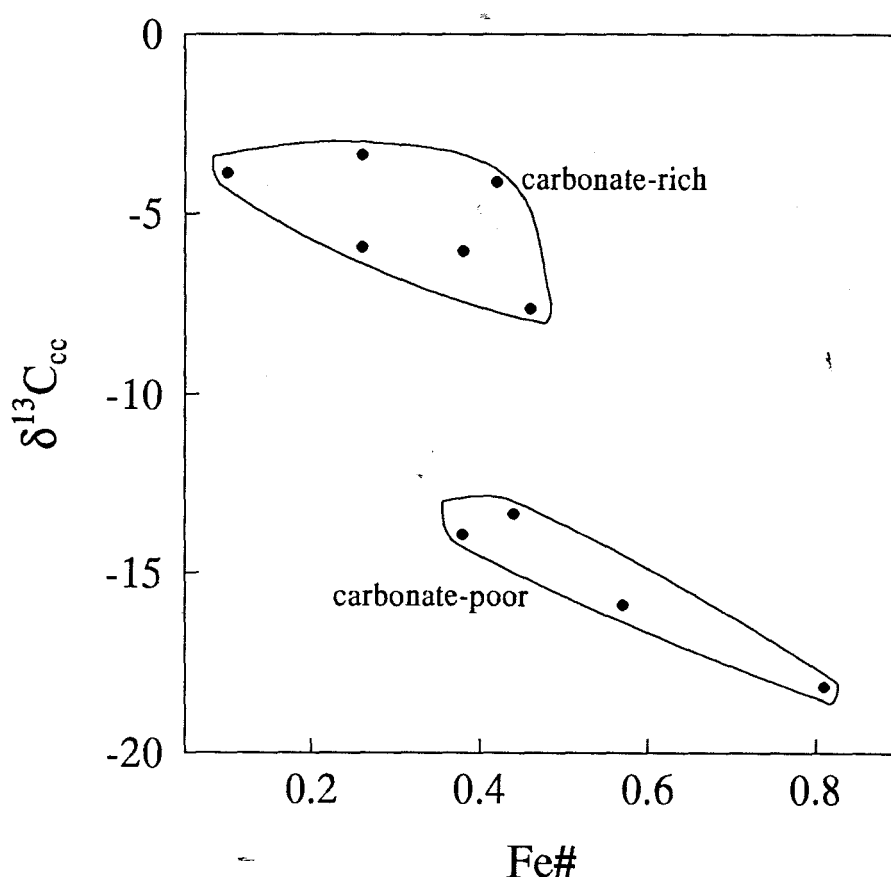


Figure 4.8. Bivariate plot of Fe# ( $FeO/FeO+Fe_2O_3$ ) vs  $\delta^{13}C$  of calcites from carbonate-poor and carbonate-rich Hotazel iron-formation. Note the clear discrimination between the two groups and the roughly negative trend in data distribution, suggesting an antithetic relation between C-isotopic depletion in calcites and the valence state of total Fe-content in the samples (Fe# values correspond to those presented in Table 3.1).

The progressive enrichment in heavy C and bulk-rock CaO in iron-formation carbonates across the stratigraphy culminating in the near-zero  $\delta^{13}\text{C}$  values observed in the Mooidraai limestone, constitutes good evidence for a generally shallowing-upward sedimentary sequence. Should the three episodes of Mn-ore deposition be ignored, the complete transition from carbonate-poor through carbonate-rich iron-formation to finally pure Mooidraai carbonate can be manifested from the  $\delta^{13}\text{C}$  isotopic profiles. This rather ideal pattern is disrupted by essentially one feature, that is, the development of the three Mn ore-units which were accompanied by sudden, positive  $\delta^{18}\text{O}$  excursions. The formation of manganese sediment would thus require some kind of episodic changes in a stratified depositional setting with a bottom anoxic, carbonate-depleted layer separated from a shallower, oxygenated, carbonate-enriched one through a chemocline. Such changes could have been brought about as a result of sea-level fluctuations in response to either climatic changes and/or geotectonic processes operating on a broad geographical scale.

Further evidence in support of the above may be found in the more enriched  $\delta^{18}\text{O}$  values higher in the stratigraphy. Although both calcite and ankerite show textural features of diagenetic growth, the  $\delta^{18}\text{O}$  data could be used as indicators of more oxygenated conditions at higher stratigraphic levels, as long as it is assumed that the isotopic composition of the diagenetic fluids was controlled primarily by the isotopic composition of the overlying water mass. The characteristic calcite-stilpnomelane-(magnetite) and chert-ankerite bands observed in the Hotazel iron-formation are thus likely to represent the early diagenetic products of short (seasonal?) episodes of iron-formation precipitation characterised by atypical enrichment in terms of their carbonate component.

The marginally more depleted, in terms of its stable isotope composition, lowermost Mn-ore unit, appears to have formed before the positive C-isotopic excursion occurred that brought about the change from carbonate-poor to carbonate-rich iron-formation. It appears that this early and most extensive Mn-ore forming event took place in conditions mildly more reducing than those that formed the middle and uppermost Mn-units. This is demonstrated in Fig. 4.9 where the  $\delta^{18}\text{O}$ -isotopic compositions of all Mn-carbonates are plotted against the ratio  $\text{CaO}/\text{SiO}_2$ . In the light of the complete absence of quartz from the Mn-ores (Miyano and Beukes, 1987), the above ratio reflects the relative amounts of Mn-carbonate vs Si-bearing Mn-oxide (braunite) in the samples.

The plot shows that samples from the lowermost Mn-ore unit contain more Mn-carbonate relative to braunite (higher CaO/SiO<sub>2</sub> ratio) and are more depleted in <sup>18</sup>O than the samples from the middle and upper units, which are relatively richer in braunite and hematite and are also more enriched in <sup>18</sup>O. This change may be the reflection of the general change in the depositional environment induced by the aforementioned isotopic excursion, and particularly of the postulated increase in Eh levels.

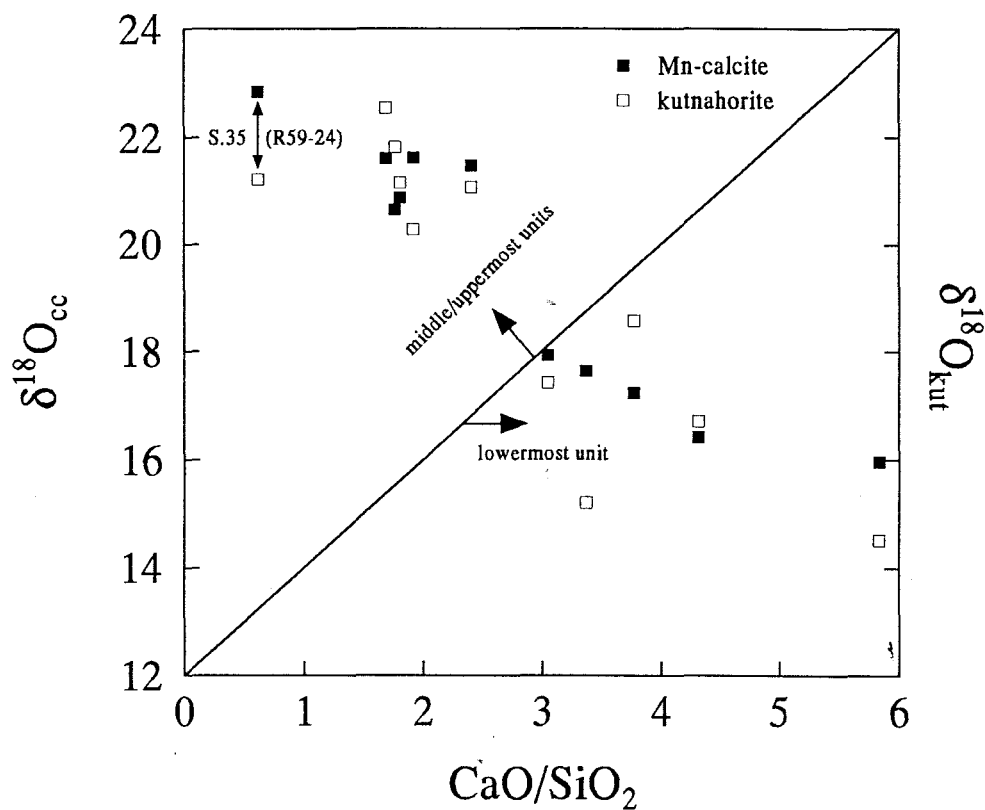


**Figure 4.9.** Bivariate plot of whole-rock CaO/SiO<sub>2</sub> ratios versus δ<sup>18</sup>O values for Mn-ore carbonates (calcite-kutnahorite). Apart from one hematite-enriched sample from the lowermost Mn unit (R59-24), the data are well-separated into two groups corresponding to samples from the lowermost and middle/uppermost units.



#### 4.1.5. Isotopic depletion - causes and constraints on genesis

As stated in the beginning of this chapter, depletion in  $^{13}\text{C}$  in iron-formation and Mn-bearing carbonates may be related to a variety/combination of processes, i.e. introduction of mantle-derived carbon via submarine hydrothermal activity, metamorphic alteration/recrystallisation involving Fe/Mn-oxides admixed with preserved organic carbon, and/or early diagenetic oxidation of organic matter in the presence of ferric iron and/or higher Mn-compounds. The importance of each of the above mechanisms has been assessed largely in the context of relatively simple depositional systems involving either iron-formation or Mn-rich carbonate deposits alone. In the case of the Voëlwater rocks, the mixed chemical sedimentary nature of the succession lends itself for an all-inclusive approach in the search for causes of isotopic depletion in these sediments.

##### 4.1.5.1. Metamorphism

The studies of Baur et al. (1985) and Kaufman et al. (1990) on millimetre-scale variations in  $\delta^{13}\text{C}$  values of carbonates from the Marra Mamba and Brockman iron-formations respectively, suggest that carbon isotope depletions in iron-formations cannot be the result of metamorphic processes involving ferric iron-oxide and preserved organic carbon. The lack of band-to-band isotopic data from this study would not allow for the metamorphic scenario to be discounted on purely isotopic grounds. However, mineralogical evidence in support of clear-cut metamorphism in the Voëlwater Subgroup is lacking. The mineral assemblages that constitute the Hotazel iron-formation and Mn-ores, and particularly the absence of grunerite in the iron-formation, are regarded as indicative of a late diagenetic to very-low grade metamorphic environment, commonly related to normal burial processes (see PART 2). Despite the unsuitability of C- and O-isotope data from coexisting calcite-ankerite pairs for applications in geothermometry, the presence of minnesotaite in many of the selected samples suggests maximum temperatures in the region of 250–300°C (Klein, 1983). This is further supported by the observed textures and particularly the microcrystalline nature of most mineral phases present. Evidence for a diagenetic overprint in the Voëlwater sequence comes primarily from the abundance of relatively coarse magnetite and carbonate in the rocks, and particularly the euhedral development of ankerite in carbonate-rich iron-formation and the abundance of carbonate ovoids/laminations in the Mn ore-units.

#### 4.1.5.2. Organic carbon oxidation - ferric iron reduction

Several studies have focused on the documentation, modelling and importance of organic carbon oxidation in the diagenesis of modern pelagic sediments (e.g. Suess, 1979; Fröelich et al., 1979; Emerson et al., 1980; Klinkhammer, 1980; Boudraeu, 1987; Rabouille and Gaillard, 1991). Particular emphasis has been placed on environments lacking free oxygen, where organic matter oxidation is induced by means of the consumption of a series of suitable electron acceptors. This process would progress on the basis of a respective series of reactions whereby organic matter oxidizes by coupled reduction of the oxidant yielding the greatest free energy change per mole of organic carbon oxidised. Upon depletion of this oxidant, oxidation will proceed utilising the next most efficient oxidant etc, until either all oxidants are consumed or oxidisable organic matter is depleted. Amongst the various electron acceptors oxidising organic matter in modern anoxic basinal environments are high-valence oxides of iron and manganese.

The antithetic correlation between  $^{13}\text{C}$  depletion and abundance of Fe-oxide documented from earlier studies on isotopic depletions in iron-formation carbonates (Baur et al. 1985; Kaufman et al., 1990) suggests that a ferric oxide precursor acted as an electron acceptor during the oxidation of organic matter to produce isotopically light carbonate. In a similar fashion to modern environments, this process is believed to have taken place at very early stages during diagenesis, and would have involved interactions between essentially three components, i.e.;

- (i) a (hydrous?) ferric oxide precursor precipitated during periodic upwelling and photosynthetic oxidation of  $\text{Fe}^{2+}$ -laden bottom basinal waters;
- (ii) co-precipitated particulate organic matter; and;
- (iii) an early diagenetic fluid with composition controlled largely by the composition of waters above the sediment-water interface.

Lovley and Phillips (1988) observed that the product of microbially-mediated organic matter oxidation in the presence of ferric oxide in natural environments is microcrystalline magnetite. This observation has born significant implications concerning the origin of the abundant magnetite in Precambrian iron-formations. It is important to note that Lovley and Philips (1988) did not observe any concomitant precipitation of Fe-carbonate (e.g. siderite), and also, that dissimilatory

reduction of ferric iron becomes sluggish and finally ceases once microcrystalline  $\text{Fe}_3\text{O}_4$  has formed, which implies that complete reduction of  $\text{Fe}^{+3}$  is not normally attained.

According to Morris (1993), crude band-to-band variations in the mineralogical composition of iron-formations from Fe-poor to Fe-rich compositions, is a reflection of periodic changes in the physicochemical conditions in the environment of deposition. Fe-enriched bands would form during seasonal storm mixing of bottom, Fe-enriched basinal waters with shallower, mildly oxygenated waters which are normally characterised by evaporitic precipitation of chert and carbonate. Paucity of such cycles due to Fe-replenishment in the shallow waters, would reverse the character of deposition to precipitation of Fe-poor, cherty sediment. Early, suboxic diagenetic processes involving organic carbon oxidation - coupled Fe-reduction would tend to modify these "primary" compositional variations, yielding the mineral assemblages observed at present. The stability and preservation of individual  $\text{Fe}^{2+}$ -bearing mineral phases would depend upon primarily two factors:

(i) the composition and Eh conditions of the bottom waters, and by extension, the pore-fluids incorporated in the precursor sediments (Brookins, 1988);

(ii) the amount of organic carbon deposited, which would have had an effect on the type of Fe-bearing minerals that form in the diagenetic environment: the more reduced species would precipitate in concert with increasing supply of organic carbon (Walker, 1984).

The two carbonate minerals in the Hotazel iron-formation are associated with dissimilar assemblages occurring on a band-to band scale. Calcite is present in close association with Fe-rich bands containing abundant magnetite and stilpnomelane, while ankerite develops in Fe-poor bands along with microcrystalline chert, occasional minnesotaite and minor magnetite. The above assemblages would correspond to diagenetic products of original precursor materials as suggested by their petrographic signatures. Based on earlier suggestions, it is possible that calcite growth has involved incorporation of isotopically light  $\text{CO}_2$  produced during diagenetic oxidation of organic carbon (average  $\delta^{13}\text{C} \sim -30$ ), along with a "primary"  $\text{CaCO}_3$  component of normal marine isotopic signature ( $\delta^{13}\text{C} \sim 0$ ). Contemporaneous formation of an early magnetite precursor would also have occurred as a result of partial reduction of a  $\text{Fe}^{+3}$ -rich precipitate.

A similar process would have caused the systematically stronger depletion in  $^{13}\text{C}$  in the ankerites relative to calcites. In this case, however, precipitation of ferric compounds relative to both organic carbon and marine bicarbonate must have been significantly subdued. Organic carbon oxidation would have been driven by reactions which were able to reduce essentially the entire  $\text{Fe}^{3+}$ -bearing component, so that a more depleted, Ca- $\text{Fe}^{+2}$ -bearing carbonate species (ankerite) would have formed in equilibrium. Such a process may have taken place in the presence of a somewhat more reducing pore-fluid compared to the one present during the formation of the  $\text{Fe}^{+3}$ -enriched, calcite-stilpnomelane-magnetite microbands, as suggested by the consistently lower  $\delta^{18}\text{O}$  values in ankerites relative to calcites. However, the likelihood of such depleted isotopic values being amplified due to further depletion during later exchange with other mineral phases and/or  $^{18}\text{O}$ -depleted meteoric waters cannot be discounted.

The carbonate-poor and oxide-rich iron formation samples contain very low amounts of carbonate and are markedly depleted in  $^{13}\text{C}$ . Such depletions would have been the result of deposition in parts of the stratified basin well below the chemocline where conditions may have been particularly anoxic and contributions of marine bicarbonate to the formation of the small amounts of calcite and ankerite were minimal. Consequently,  $\delta^{13}\text{C}$  values in the latter reflect comparatively low marine bicarbonate/organic carbon ratios. In this case, the virtual absence of marine carbonate and the clearly more reduced conditions have resulted in organic carbon oxidation coupled with the extensive formation of a completely reduced Fe-compound, in this case, the Fe-silicate greenalite. The possibility that some mantle-derived carbon was present in the ambient waters cannot be rejected, particularly in the light of REE data from the carbonate-poor samples (Tsikos and Moore, 1997; see also PART 3, Chapter 3.5) which suggest the existence of a small, dilute hydrothermal component in the deeper waters of the palaeodepository. Hydrothermal activity, however, cannot be regarded as the sole controlling factor towards producing such marked isotopic depletions as those observed in the silicate-oxide facies samples, as mantle-derived  $\text{CO}_2$  would be expected to have had an isotopic composition not lower than  $\delta^{13}\text{C} \sim -6\text{‰}$ .

#### 4.1.5.3. Organic matter oxidation - manganese reduction

Manganese-rich sediments are known to form in conditions at least mildly more oxidizing than

those favouring precipitation of Fe-bearing mineral species. Assuming the existence of sufficiently oxidizing conditions in the Palaeoproterozoic atmosphere, the oxidation of  $Mn^{+2}$  in the palaeodepositional basin would have been attained during periods of episodic oxygenating (regression?) events. Such conditions would have promoted the pronounced precipitation of Mn-rich sediment, provided that the basinal waters had been supersaturated with respect to Mn. The fact that deposition of the Voëlwater sediments was preceded by a glacial event as indicated by the widespread occurrence of the Makganyene diamictites below the Ongeluk formation (see Part 1, Table 1.1), suggests that climatic conditions may have played a critical role in enhancing preservation of Mn in the wider depositional setting. High rates of precipitation of Mn-oxide compounds would have effectively curtailed any contemporaneous deposition of Fe-oxide and silica.  $Mn^{+2}$  is also known to be an important inhibitor of  $CaCO_3$ -precipitation (Sumner and Grotzinger, 1996) which would have ensured only a small dilution of Mn-sediment by contemporaneous calcite deposition.

The depleted C-isotope signatures of Mn-calcites and kutnahorites in the three Mn ore-units (Fig. 4.6), and particularly the more depleted isotopic character of the Mn-carbonates relative to carbonate-rich calcite and ankerite could be explained in a similar fashion to iron-formation carbonates. As has been suggested by Lovley and Philips (1988), coupled organic carbon oxidation-dissimilatory reduction of higher Mn-oxide produces Mn-carbonate. During this process, reduction of higher Mn oxide is complete and formation of a mixed Mn-Ca carbonate phase is favoured in equilibrium with a diagenetic fluid (Mucci, 1988), despite the fact that the latter may have been supersaturated with respect to calcite (Emerson et al., 1980; Boudreau, 1987). In addition, the fact that appreciable amounts of hematite are present in the ores suggests that conditions were probably too oxidizing for  $Fe^{+3}$ -reduction to be the dominant reaction oxidizing organic matter. This relative inhibition of  $CaCO_3$  precipitation during diagenetic growth of Ca-Mn-carbonate would imply a more decreased contribution of marine bicarbonate and thus explain not only the somewhat stronger C-isotopic depletion of the Mn-carbonates than carbonate-rich ankerite and calcite of the Hotazel Formation, but also the generally more depleted C-isotopic character observed in Mn ore carbonates relative to iron-formation carbonates (see also Fig. 4.3).

## Chapter 4.2. Oxygen isotope systematics of silicate - Fe-oxide pairs

### 4.2.1. General

Precambrian iron-formations are amongst the most suitable sedimentary rock-types for the study of  $\delta^{18}\text{O}$  systematics of mineral pairs for a number of reasons: (1) unlike most sedimentary rocks such as cherts and carbonates which contain effectively one mineral phase (quartz and carbonate respectively), iron-formations contain multi-phase mineral assemblages, thus bearing greater potential for palaeoclimatological considerations; (2) the oxygen in iron-formations is represented almost entirely in quartz and iron-oxide phases, both of which are stable over a wide range of pressures and temperatures; (3) the conspicuous banding of iron-formations results in a wide range of individual layer bulk  $\delta^{18}\text{O}$  compositions; and (4) the silica and iron-oxide precursors from a given deposit may have precipitated at a relatively constant temperature from an isotopically uniform reservoir of surface water, which would imply that the initial  $\delta^{18}\text{O}$  values of the mineral phases would have been very uniform (Gregory, 1986).

The span of  $\delta^{18}\text{O}$  values from the principal iron-formation components quartz and magnetite, are shown in Figure 4.10, in comparison with other important oxygen-containing compounds (Hoefs, 1987). Although no whole-rock  $\delta^{18}\text{O}$  data from iron-formations are available in the literature, the range presented in Figure 4.10 constitutes a reasonable approximation, since it derives from  $\delta^{18}\text{O}$  values of quartz-magnetite pairs from essentially unmetamorphosed iron-formation occurrences of North America, South Africa and Australia, which would yield the largest fractionation in  $\delta^{18}\text{O}$ . Diagenetic and very low-grade metamorphic minerals commonly coexisting with quartz and magnetite such as iron-bearing silicates (greenalite, minnesotaite) and carbonates (calcite, ankerite, siderite) would, on the grounds of crystal-chemical relationships, be expected to have  $\delta^{18}\text{O}$  values intermediate between those of quartz and magnetite. Any higher-grade metamorphic process would be expected to shift the  $\delta^{18}\text{O}$  values of both the quartz and the magnetite towards the area defined by the broken lines in Figure 4.10, provided that the rock has attained closed-system isotopic equilibrium.

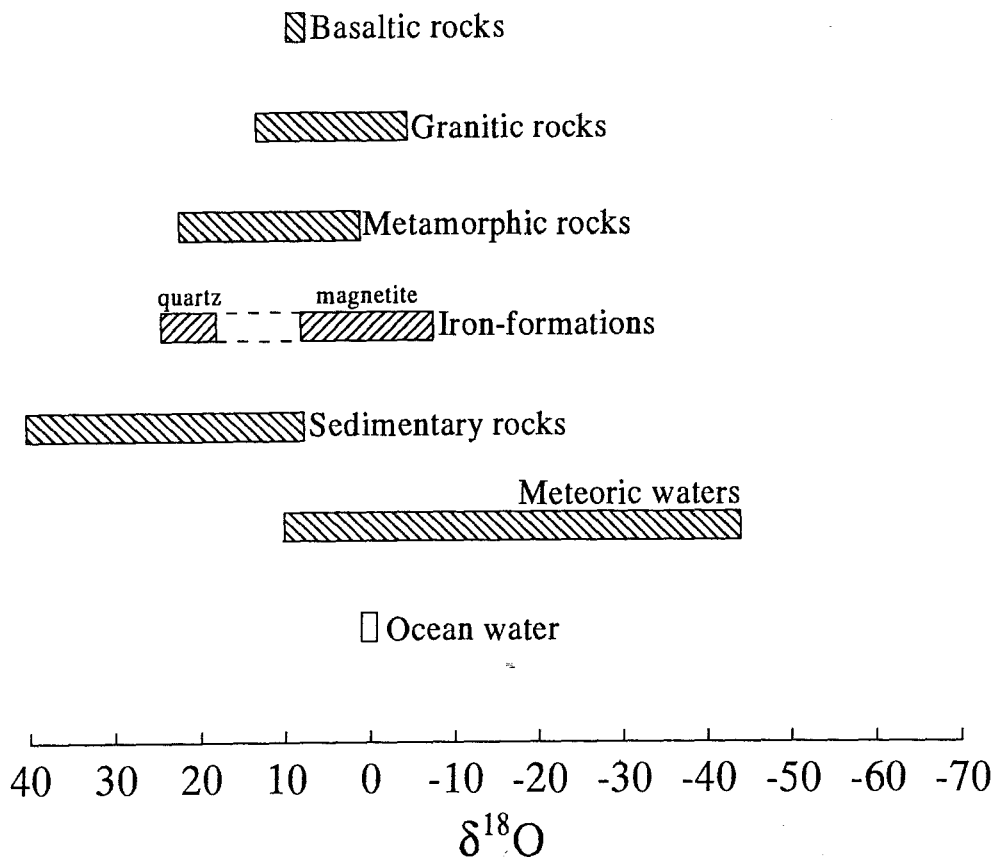


**Figure 4.10.** Comparisons between the O-isotope compositional ranges of major rock types, meteoric and ocean waters (Hoefs, 1987), and Palaeoproterozoic iron-formations. Iron-formation data are from quartz-magnetite pairs analysed in this study, and from Perry et al, 1973 and Perry and Tan, 1973 (Biwabik iron-formation, North America), Perry and Ahmad, 1980 (Kuruman iron-formation, Transvaal Supergroup, South Africa) and Becker and Clayton, 1976 (Brockman iron-formation, Western Australia)

#### 4.2.1.1. Quartz-magnetite

Studies on the  $\delta^{18}\text{O}$  systematics of coexisting quartz and magnetite have been carried out on several important iron-formation occurrences worldwide. The results have been used to address problems such as the degree of equilibration, temperatures of equilibration and whether the rock mass has behaved as a closed or open system. The majority of earlier studies were conducted by E.C. Perry and co-workers on a number of both unmetamorphosed and metamorphosed iron-formation occurrences such as: (1) the Biwabik iron-formation (Perry and Tan 1973; Perry et al.,

1973) and its metamorphosed equivalent in the contact aureole of the Duluth igneous complex, Minnesota (Perry and Bonnichsen, 1966); (2) Archaean iron-formation from Isukasia, W. Greenland (Perry et al., 1978); (3) the Kuruman iron-formation, South Africa (Perry and Ahmad, 1980); and (4) the Krivoy-rog iron-formation, former USSR (Perry and Ahmad, 1981). In addition to the above studies, Becker and Clayton (1976) provide a detailed treatise of  $\delta^{18}\text{O}$  measurements from quartz-magnetite pairs and other iron-formation minerals from the Dales Gorge Member, Hamersley Group, Western Australia. Data from the above studies form essentially the backbone in the existing literature of  $\delta^{18}\text{O}$  data from quartz-magnetite pairs in iron-formations, as recent studies are very scarce (e.g. Kaufman et al., 1990).

The results of the studies by Perry and co-workers are summarised in a review paper dealing with major iron-formations of the Precambrian (Perry, 1983, p. 359-371). Interpretations derive mostly from a specific scientific approach which is essentially based on plots of  $\delta^{18}\text{O}$  data in  $\Delta_{\text{QM}}-\delta$  space (Fig. 4.11), where  $\Delta_{\text{QM}}$  represents the difference between the  $\delta^{18}\text{O}$  values of quartz and coexisting magnetite:

$$\Delta_{\text{QM}} = \delta^{18}\text{O}_{\text{quartz}} - \delta^{18}\text{O}_{\text{magnetite}}$$

The good linear correlations produced in a  $\Delta_{\text{QM}}-\delta$  graph for datasets from quartz-magnetite pairs from the Biwabik (Perry et al., 1973) and Brockman (Becker and Clayton, 1976) iron-formations have been taken as strong indications for isotopic exchange in a closed and largely homogeneous system. Extrapolation of the trend lines of Figure 4.11, intersect at  $\Delta_{\text{QM}}$  values which would correspond to an upper limit to ocean temperature at the time of deposition of these iron formations, as  $\Delta$  is a temperature-dependent function that is virtually independent of pressure (Bottinga and Javoy, 1973). Absolute temperature values can be obtained using published oxygen isotope fractionation curves for quartz-magnetite pairs constructed using the general equation:

$$\Delta_{\text{QM}} = \delta_{\text{Q}} - \delta_{\text{M}} \approx 10^3 \ln \alpha_{\text{Q-M}} = A10^6/T^2 + B$$

where A, B are constants and T is temperature in degrees Kelvin. Figure 4.12 shows fractionation



curves for quartz-magnetite pairs for a wide range of metamorphic temperatures (Becker and Clayton, 1976) and for low temperature (<250°C) systems (Blattner et al., 1983), along with fractionation curves for low-temperature quartz-hematite (Yapp, 1990b) and quartz-calcite pairs (Friedman and O'Neil, 1977; based on expressions of O'Neil et al., 1969, and Bottinga and Javoy, 1973, for calcite-water and quartz-water respectively).

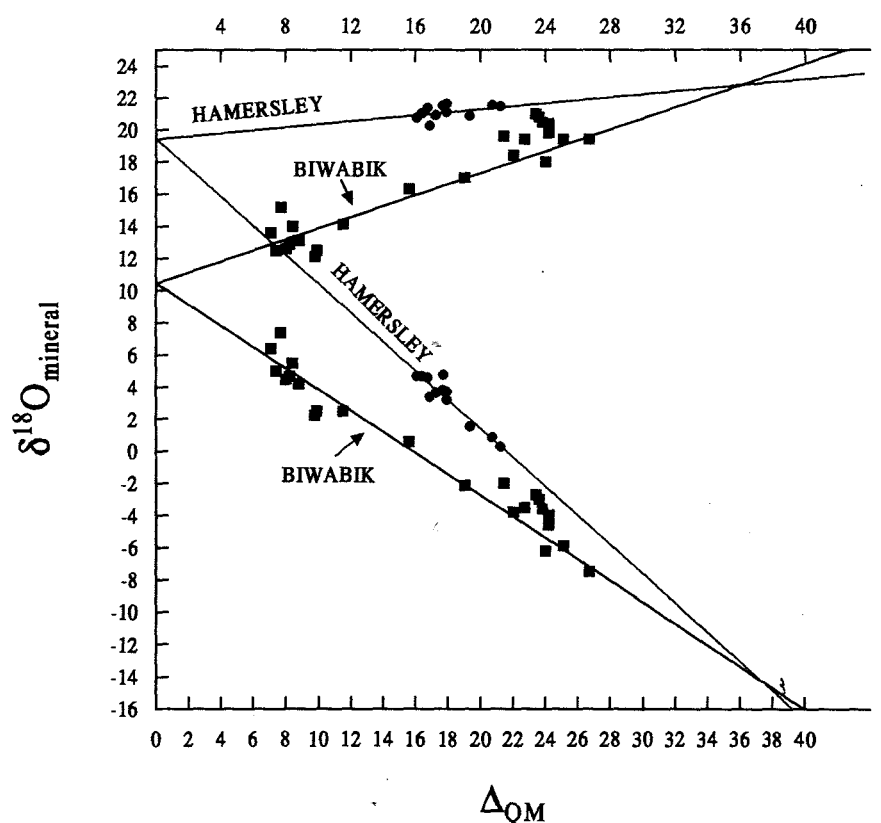


**Figure 4.11.** Representative example of the use of  $\Delta$ - $\delta$  plots for O-isotope data of the Brockman (Hamersley Group, W. Australia) and Biwabik (N. America) iron-formations. The two legs of each of the curves shown, represent trend lines for quartz and magnetite, and have been used as indications of equilibrium O-isotope fractionation in essentially closed, homogeneous systems (modified after Perry, 1983; see text for discussion).

The main conclusion of Perry (1983) is that many Proterozoic iron-formations such as the Biwabik and Brockman iron-formations, may have behaved as essentially closed systems. Any observed variations in  $\Delta_{QM}$  values in smaller subsystems within a given deposit may have been the

result of isotopic exchange reactions ceasing at different stages of diagenesis/metamorphism due to localised differences in porosity and permeability. Perry (1983) also suggests that maximum  $\delta^{18}\text{O}$  values of quartz from those iron-formations may well approximate the primary  $\delta^{18}\text{O}$  of  $\text{SiO}_2$  deposited from Precambrian sea water at the time of sedimentation.

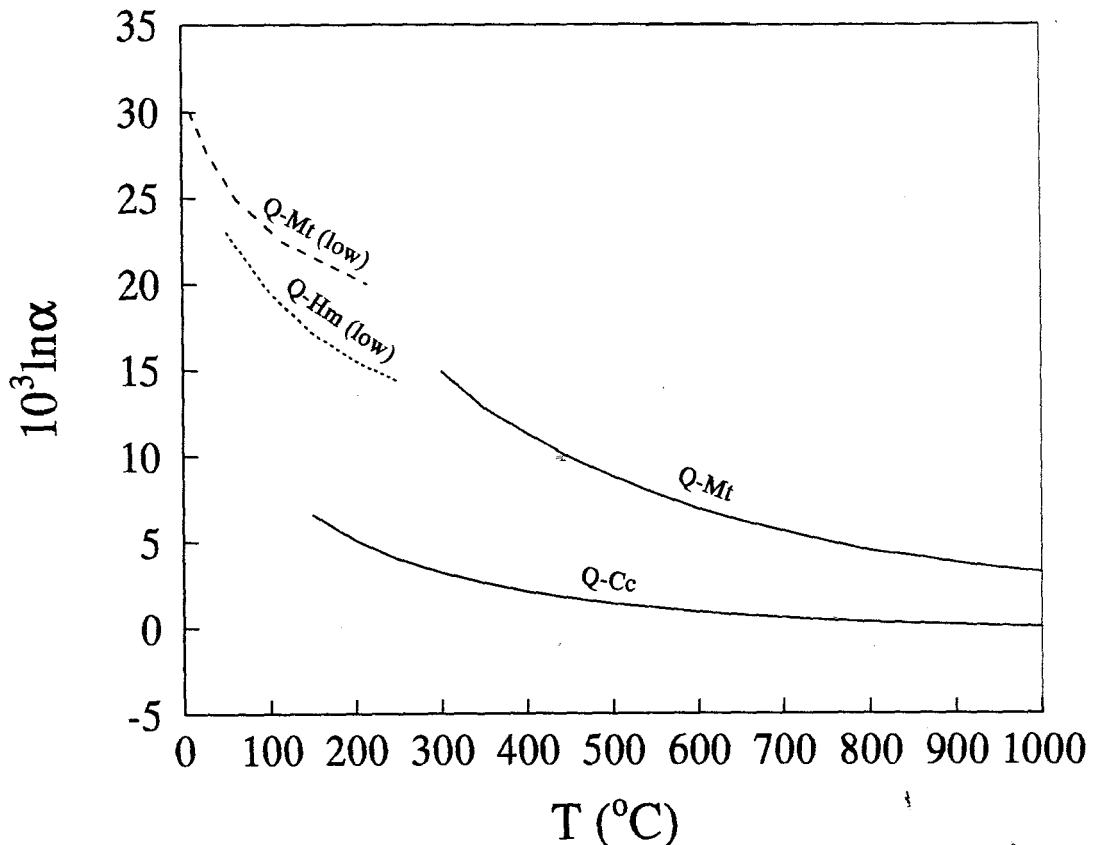


**Figure 4.12.** Fractionation curves for the mineral pairs: quartz-calcite (Friedman and O'Neil, 1977), quartz-magnetite (Becker and Clayton, 1976; low temperature curve from Blattner et al., 1983) and quartz-hematite (Yapp, 1990b).

It was soon after the review paper by Perry (1983) that an extensive evaluation of the already existing oxygen isotope database for iron-formations was conducted by Gregory (1986, 1990) and Gregory et al. (1989). These authors presented a substantially different approach towards the interpretation of  $\delta^{18}\text{O}$  data for quartz-magnetite pairs from iron-formations, as compared to the one employed previously by Perry and co-workers. Gregory et al. (1989) strongly criticised the interpretation of  $\delta^{18}\text{O}$  data on the basis of  $\Delta_{\text{QM}}-\delta$  plots, stressing that such plots can be very misleading, particularly if the modal mineralogy of individual samples is not taken into account.

Gregory et al. (1989) note that  $\Delta_{\text{QM}}-\delta$  plots present visually good correlations simply because the isotopic data are constrained to lie within a relatively narrow  $45^\circ$  angle, in contrast to  $\delta-\delta$  plots which allow data to spread over  $90^\circ$ . They point out that such “forced” correlations bear very little validity in the absence of comprehensive modal mineralogical data. In fact, no linear correlation of  $\delta^{18}\text{O}$  should be expected in mineral pairs that are not characterised by uniform modal abundance.

According to Gregory (1986, 1990) and Gregory et al. (1989),  $\delta^{18}\text{O}$  data from quartz-magnetite pairs should be plotted on simple  $\delta-\delta$  plots. On such plots, the distribution of data would allow a sufficient estimate as to whether the rock has behaved as a closed or open system. Specifically, in the case of closed system isotopic exchange between quartz and magnetite, data would, upon equilibrium, map out  $\sim 45^\circ$  arrays of equal  $\Delta_{\text{QM}}$ , which essentially correspond to lines of equal temperature (isotherms). In such systems, the accessible space for quartz-magnetite pairs during prograde diagenesis/metamorphism will be constrained by the 100% quartz and magnetite vectors emanating from an initial point corresponding to the initial isotopic composition of the system (Fig. 4.13). These vectors will be parallel to the  $\delta^{18}\text{O}$  axes for quartz and magnetite respectively, and will intersect the isotherm corresponding to the final equilibration temperature of the system. The spread of data along this isotherm would correspond to the  $\Delta$  values of quartz-magnetite pairs as reflected by the relative modal abundances of the two minerals in each sample. It is apparent that such systems are particularly suitable for application of isotope geothermometry, so long as no retrograde effects have isotopically “reset” the mineral pair at lower temperatures. Hence, the quartz-magnetite pair in iron-formations has so far been one of the most widely used mineral pairs for estimations of metamorphic temperatures.

If a fluid phase was present in the rock during prograde metamorphism, additional parameters are introduced such as fluid/rock ratios, relative rates of isotopic exchange of the selected mineral-pair with the coexisting fluid, as well as the initial isotopic composition of the fluid phase. In this case, the system is generally described as open, and the suitability of the chosen mineral-pair as a geothermometer depends upon the magnitude of one or more of the above-mentioned factors. If, for example, the one mineral has exchanged rapidly with the fluid phase while the other has

remained relatively inert, the validity of deduced temperatures is highly doubtful; furthermore, in those cases where the isotopic composition of the fluid was substantially different from the  $\delta^{18}\text{O}$  of the initial rock, the temperatures obtained would be effectively unrealistic (Gregory, 1986).

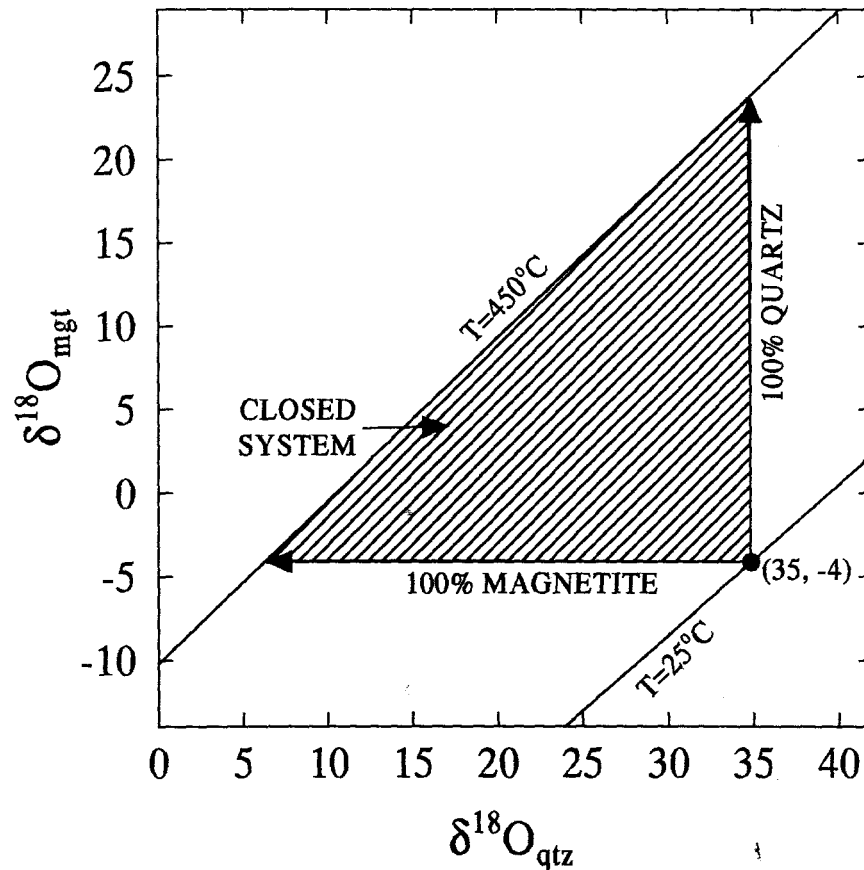


**Figure 4.13.**  $\delta^{18}\text{O}$  magnetite versus  $\delta^{18}\text{O}$  quartz diagram illustrating closed-system behaviour for mineral pairs precipitated from a seawater reservoir at low temperatures (35, -4). The prograde field is shown for an initial point that lies along the 25°C isotherm. Emanating from the initial point (35, -4) are the 100% magnetite and quartz vectors, respectively, that represent the legs of a right triangle that bounds the field of accessible  $\delta$  space for prograde closed-system diagenesis/metamorphism. The intersection of the vectors with the  $T=450^\circ\text{C}$  isotherm defines the mineral  $\delta^{18}\text{O}$  heterogeneity that would be observed if all mineral pairs (in separate sedimentary layers, each of which with a different modal composition) behaved as closed systems. Note that along the isotherm, the mole fraction of quartz will increase monotonically as  $\delta^{18}\text{O}$  increases (modified after Gregory, 1986).

Data from such systems would plot on steep, nearly positive arrays on  $\delta$ - $\delta$  plots, which, as will be demonstrated later on, is commonly the case in quartz-magnetite pairs from essentially unmetamorphosed iron-formations. On the other hand, for a mineral-pair where the relative exchange rate of the two phases with the fluid approaches unity, data would lie along  $\sim 1$  slopes

or “pseudo-isotherms”, which would correspond to underestimates of temperature during prograde metamorphism and overestimates during retrograde metamorphism (Gregory, 1986). Such “apparent” temperatures should always be evaluated in the context of other lines of evidence such as textural equilibration and homogeneity of mineral chemistry. A comprehensive treatment of oxygen isotopic exchange kinetics between minerals and water in fluid-bearing systems is provided by Criss et al. (1987).

#### 4.2.1.2. Quartz-hematite

Studies on the O-isotope geochemistry of hematite-rich iron-formations and hematitic iron-ores have been conducted in various areas of the world where hematite is the dominant (or only) Fe-oxide species. In such iron-formations, the hematite may be regarded as either primary/early diagenetic, or as a product of higher grade metamorphic/metasomatic processes. The iron-ores from the Iron Quadrangle, Brazil (Hoefs et al., 1982), constitute a good example where multiple deformation and associated metamorphism have been the chief processes in the development of these hematitic deposits. Despite several limitations concerning the existence of isotopic equilibria (e.g. likelihood of retrograde isotopic re-equilibration),  $\delta^{18}\text{O}$  measurements of quartz-hematite pairs from those ores were extensively used by Hoefs et al. (1982) as potential monitors of “temperatures of formation”, in relation to the multi-stage deformational history of the host-rock. On the other hand, examples where  $\delta^{18}\text{O}$  measurements of quartz-hematite pairs have been used as “proxies” for early diagenetic to very-low-grade metamorphic environments include iron-formations from the Kushtagi Belt, Archaean Dharwar Craton, India (Khan and Naqvi, 1996) and Rapitan-type Fe-Mn formations from the Urukum District, Brazil (Hoefs et al., 1987).

One of the problems frequently encountered in isotopic determinations of coexisting quartz and hematite in iron-formations, is the extremely fine-grained and texturally complex nature of the latter. Hoefs et al. (1987), in their study of the Urukum deposits, attempted to overcome this obstacle by obtaining  $\delta^{18}\text{O}$  values for hematite and quartz from  $\delta^{18}\text{O}$  measurements on samples containing practically pure, binary quartz-hematite mixtures. They did so by plotting the “mixed”  $\delta^{18}\text{O}$  values against the relative proportions of hematite in each sample. Yapp (1990c) pointed out the importance of such extrapolations being performed against the mole fraction of oxygen in the

component of interest (hematite or quartz) so that accurate data could be confidently deduced. In his re-evaluation of the data of Hoefs et al. (1987), Yapp (1990c) used the general formula (assuming  $^{18}\text{O} \ll ^{16}\text{O}$ ):

$$\delta^{18}\text{O}_{\text{mixture}} = \delta^{18}\text{O}_2 + (\delta^{18}\text{O}_1 - \delta^{18}\text{O}_2)X(\text{O})_1 \quad (3)$$

where  $\delta^{18}\text{O}_1$ ,  $\delta^{18}\text{O}_2 = \delta^{18}\text{O}$  of pure component 1 and 2, respectively;

$$X(\text{O})_1 = n(\text{O})_1 / [n(\text{O})_1 + n(\text{O})_2]$$

and  $n(\text{O})_1$ ,  $n(\text{O})_2 =$  moles of oxygen in components 1 and 2 respectively.

The above method yielded results which are somewhat different from the values presented in the original paper by Hoefs et al. (1987) and has found application in subsequent studies of O-isotopes of very fine-grained two-component systems, such as Phanerozoic ironstone from the Neda Formation, Wisconsin (Yapp, 1993) and Archaean iron-formation from the Kushtagi belt, India (Khan et al., 1996). As it will be demonstrated in the following paragraphs, the approach of Yapp (1990c) has been of great use in considerations regarding the Hotazel iron-formation.

#### 4.2.2. Oxygen isotope systematics of the Hotazel iron-formation

In the light of the literature information presented above, an oxygen isotope investigation of co-existing quartz-iron-oxide pairs from the Hotazel iron-formation was undertaken as part of this project. The main objectives of such an investigation are to obtain an understanding of a variety of processes that are currently believed to have affected the iron-formation and associated manganese ore-units. These include diagenesis-very low grade metamorphism characterising the central and southern parts of the KMF (Nel et al., 1986; Tsikos and Moore, 1997) and hydrothermal alteration-metasomatism, affecting parts of the northernmost segment of the field (Kleyenstüber, 1984, 1985; Dixon 1985; Gutzmer and Beukes, 1995; Gutzmer, 1996).

##### 4.2.2.1. Sample selection and description

Samples for isotopic analyses were selected from two representative borehole intersections out of the 15 used in this study (Appendix I, Fig. A1). The boreholes come from the northern parts of the KMF and are relatively closely-spaced. The first intersection (GL26) was drilled on the

farm Gloria, more specifically to the west of the underground Gloria mine, the only underground operation currently exploiting low-grade Mn ore in the KMF. The second borehole (MK3I) was drilled on the farm Mukulu situated to the west of farm Gloria and to the south of farm N'chwaning, the latter being the locality of one of the two major mines where underground exploitation of high-grade Mn ore is being carried out at present.

Samples from both intersections were selected across a largely homogeneous portion of the Hotazel iron-formation, in accordance with the mineralogical and whole-rock geochemical compositions observed. Emphasis was placed on selecting samples that would ensure macroscopic homogeneity and exhibit mineralogical compositions containing the fewest components possible. Details with regard to the stratigraphic locations of the selected samples is comprehensively presented in Appendix I (Figs, A3, A4).

The two iron-formation intersections display striking differences on both a macro- and a micro-scale. Intersection GL26 contains pristine iron-formation identical to the one encountered in the southernmost parts of the KMF, with chert, magnetite and carbonate being the major mineral constituents. Chert-carbonate-dominated bands alternate rhythmically with magnetite-dominated ones through generally diffuse contacts. The most abundant carbonate mineral in all samples is calcite, while ankerite is present in much lesser amounts, usually undetectable by means of x-ray diffraction in the selected samples (modal abundance <5%). With regard to iron-silicates, greenalite is the most important phase and is present in small amounts, predominantly in the lower parts of the sampled portion of the Hotazel iron-formation (modal abundance 5-10%; samples GL26-3a, 4, 5 and 6) where trace minnesotaite is also present. Band thicknesses range generally between 1mm and 1 cm, while features such as podding and cross-bedding are occasionally seen.

In contrast, intersection MK3I shows clear features suggesting a later alteration overprint. The rock contains no magnetite or carbonate and consists almost exclusively of rhythmic, alternating laminations (1-5mm) of hematite and hematite-bearing chert. The very fine banding, reduced overall stratigraphic thickness and striking red colouration observed in this iron-formation suggests that the rock has suffered a severe oxidation-compaction effect, with all iron-bearing components having been converted to fine-grained hematite while carbonate phases have been

effectively leached out (see also PARTS 2 and 3). These observations apply to essentially the entire upper and middle portion of the Hotazel iron-formation in this borehole and agree well with a model proposed recently for the northernmost parts of the KMF, whereby the alteration of the Hotazel Formation was accompanied by significant loss of chemical constituents and marked reduction in volume of the original, pre-alteration package (Gutzmer and Beukes, 1997).

A small portion of the iron-formation intersection immediately below the uppermost Mn-unit in borehole MK3I, although macroscopically very similar to the rest of the iron-formation, shows marked differences in terms of mineralogy and bulk chemistry. The principal components in this part of the stratigraphy are essentially acmitic pyroxene and hematite, both particularly fine-grained and admixed with negligible amounts of chert. Similar acmite occurrences have also been reported from the Cuyuna Range, Minnesota (Grout, 1946; McSwiggen et al., 1994) and have been described as products of hydrothermal Na-metasomatism of iron-formation (see PART 2). In order to shed some light on the conditions behind the development of acmite in the Hotazel iron-formation, the two acmite-bearing samples were also selected for isotopic analyses.

#### 4.2.2.2. *Methods*

Due to the extremely fine-grained nature of essentially all mineral constituents in the selected iron-formation samples, mechanical separation of individual mineral phases was generally not feasible. For that reason, a wet chemical technique was employed in order to selectively separate individual phases and/or binary mixtures. The method is described in detail below and was used for the seven pristine, multi-phase samples of iron-formation from borehole GL26, as well as for three samples from the oxidised iron-formation of borehole MK3I.

With regard to the pristine iron-formation samples, the method involved two stages of chemical separation using the same agent, i.e. hydrochloric acid (HCl). During the first stage, 10-12g of finely powdered samples were treated with cold, dilute hydrochloric acid (5%) for approximately six hours; this allowed complete dissolution of the carbonate component of the samples (calcite+minor ankerite). The undissolved portions were then rinsed several times with 1% HCl and distilled water and allowed to dry at room temperatures. The samples were subsequently

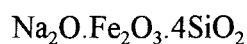


analysed by means of x-ray diffraction and x-ray fluorescence procedures in order to determine their modal mineralogical composition. As was expected, the residual samples contained essentially binary mixtures of quartz and magnetite corresponding very closely to the original quartz-magnetite relative proportions, assuming complete absence of carbonate. Any Fe-silicate component (greenalite, minnesotaite) that may have been present in the original samples, was now undetectable with x-ray diffraction, which allows the assumption that the weak acid probably caused decomposition of most of the hydrous Fe-silicates, leaving behind an essentially SiO<sub>2</sub>-bearing residue.

Subsequently, 3-4 grams of the quartz-magnetite mixtures were treated with hot, concentrated HCl (32%) for approximately 12-18 hours. During this stage, magnetite dissolved slowly in the acid, leaving behind a white residue which corresponded to the chert-component of the original sample. After this treatment, the separated powders were washed with cold, weak HCl and distilled water, and dried thoroughly at room temperatures. The white powders were subsequently analysed by means of x-ray diffraction which confirmed that the sole remaining phase was SiO<sub>2</sub>. This SiO<sub>2</sub> was labelled "quartz", assuming negligible input of SiO<sub>2</sub> by any decomposed Fe-silicate.

The same technique was applied on three selected samples of the hematite-rich iron-formation of borehole MK3I. Dissolution of hematite in hot, concentrated HCl took place at almost the same rate as the magnetite in the unaltered iron-formation samples. The resultant residue was again assigned the name "quartz".

Due to uncertainties regarding the behaviour of acmite in the presence of HCl, the two hematite-acmite samples were not treated by means of the chemical separation described above. Instead, conventional handpicking of macroscopically pure chips of acmite-rich laminae was performed on finely crushed material, and the purity of the acmite separate was attested by means of x-ray diffraction and x-ray fluorescence procedures (see also PART 2 Table 2.3.). Comparisons of the above data with literature information (Grout, 1946), suggest that the mineral is indeed the pure Na-end member of the aegirine-augite series, i.e. it is composed entirely of Na<sub>2</sub>O, Fe<sub>2</sub>O<sub>3</sub> and SiO<sub>2</sub>, corresponding to the formula:



Oxygen for isotope analysis was liberated from quartz, acmite, as well as quartz-magnetite, quartz-hematite and hematite-acmite mixtures by the  $\text{ClF}_3$  technique described by Borthwick and Harmon (1982) and was converted to carbon dioxide by reaction with hot graphite (Appendix II).  $\text{CO}_2$  was also evolved from calcite from 7 untreated samples of borehole GL26, using methods described earlier in this chapter (see also Appendix II). Analyses for O and C isotopes were performed using a Finnigan MAT 252 mass spectrometer at the Department of Geological Sciences, University of Cape Town.  $\delta^{18}\text{O}$  values for magnetite and hematite were calculated from corresponding values of their binary mixtures using equation (3) (Yapp 1990c). Analytical data are presented in Tables 4.2a and 4.2b.

#### 4.2.2.3. Limitations

It is important to stress here that the data presented in Tables 4.2.a and 4.2.b suffer from a number of obvious limitations, which stem from the chemical separation technique used. Quantitative oxygen yields from the 10 “quartz” samples were always >94% which is in support of the fact that the samples consisted of essentially pure  $\text{SiO}_2$ . The slightly lower yields could be explained by the existence of negligible admixtures of undissolved magnetite and/or contamination of samples by admixed Fe-silicate compounds. Also, the two acmite samples had oxygen yields slightly above 100% which implies minor admixtures of quartz in the handpicked separates. The errors, however, introduced by both quartz and acmite yields, fall well into the range of analytical error.

The main uncertainties arise in relation to the pre-existing Fe-silicate component of the samples and particularly the effect of the decomposed greenalite in 4 out of the 7 samples of borehole GL26. Specifically, three samples (GL26-1, 2, and 3) contain very little (<5%) or no greenalite while the remaining four samples (GL26-3a, 4, 5, and 6) contain relatively higher amounts of greenalite (5-10%) which, as stated earlier, apparently decomposed during treatment with cold, dilute HCl. Assuming that all the Fe-component of the greenalite went into solution, the corresponding  $\text{SiO}_2$  would be expected to “contaminate” the quartz separates, even more so after the second acidification stage which would have brought about an increase in the relative contents of greenalite-hosted  $\text{SiO}_2$  in the “quartz” residues, as compared to the true quartz fractions.

In order to test the above statements,  $\delta^{18}\text{O}$  values for the “quartz” separates were plotted against the relative difference in total  $\text{SiO}_2$  wt% values between the 7 untreated samples of borehole GL26 and the corresponding “quartz”-magnetite separates (Fig. 4.14). Such differences would be related to a respective loss of Fe-oxide component from the samples, largely due to the decomposition of greenalite. A difference in the  $\delta^{18}\text{O}$  values of “quartz” by approximately 0.5‰ can be seen in the samples containing little or no greenalite as compared to the greenalite-bearing ones. This would be readily attributed to contamination by the original greenalite component, the  $\delta^{18}\text{O}$  of which would be expected to be lower than the one for quartz on the grounds of crystal-chemical relationships (Hoefs, 1987). Hence, it would be reasonable to assume that the  $\delta^{18}\text{O}$  values of true quartz could be expected to be marginally higher and perhaps comparable to the values of the three samples containing negligible greenalite. It should be also noted that such limitations are not expected to impact significantly on the hematite values deriving from the three quartz separates of borehole MK3I, as no silicate phase is present in these samples.

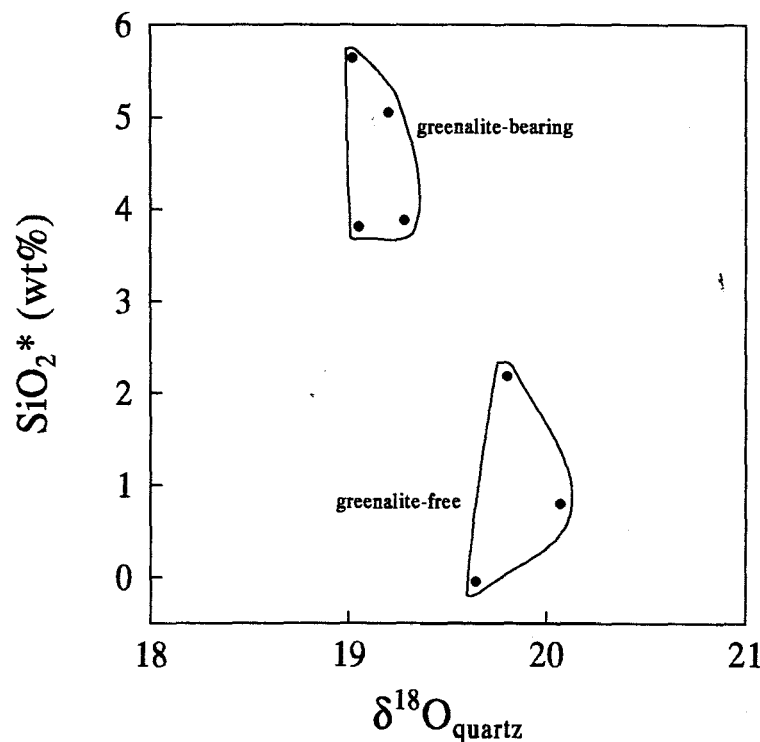


**Figure 4.14.** Bivariate plot of  $\delta^{18}\text{O}$  versus  $\text{SiO}_2^*$  (“quartz”) contents as determined by XRF of seven selected samples of carbonate-free, pristine iron-formation. Note the separation into two distinct “clusters”, as a result of the relative amounts of greenalite in the samples prior to HCl-treatment (see text for discussion).

Quantitative yields from the quartz-magnetite and quartz-hematite mixtures ranged between 90 and 99%, as a result of either incomplete reaction of the slowly reacting phase (i.e. iron-oxide), or due to small sample losses caused by loading of very-fine grained sample material. These uncertainties would increase the potential of error in the calculated  $\delta^{18}\text{O}$  values of the magnetite and hematite using the method of Yapp (1990c). According to the yields of the quartz-oxide mixtures and all uncertainties regarding the determination of the  $\delta^{18}\text{O}$  values for the quartz and acmite separates, these errors should be expected to fall within the region of  $\pm 1\%$ .

#### 4.2.3. Results

Bearing in mind the analytical drawbacks outlined above, distributions of the  $\delta^{18}\text{O}$  values for all minerals are shown in Figure 4.15. Quartz (quartz 1) and calcite from the seven unaltered iron-formation samples of borehole GL26 lie within relatively narrow limits. On the other hand, magnetite values as calculated from the seven quartz-magnetite mixtures show a wider range of  $\delta^{18}\text{O}$  values. A similar situation applies to the  $\delta^{18}\text{O}$  range of the three quartz samples from the hematitic iron-formation of borehole intersection MK3I (quartz 2) and the respective hematite  $\delta^{18}\text{O}$  values calculated from the corresponding hematite-quartz mixtures (hematite 1). The two acmite samples have very similar  $\delta^{18}\text{O}$  values which are substantially lower than those observed for quartz and calcite from the pristine and oxidised samples.  $\delta^{18}\text{O}$  values for hematites calculated from the two hematite-acmite mixtures (hematite 2) compare well with those of magnetites and hematites from Fe-oxide - quartz iron-formation samples.

##### 4.2.3.1. Diagenesis-metamorphism

A  $\delta$ - $\delta$  plot for quartz-magnetite pairs from the seven selected samples of borehole GL26 is shown in Figure 4.16. For comparative purposes, the Hotazel data have been plotted along with the fields defined by isotopic data from other major iron-formation occurrences, namely the Brockman iron-formation, Hamersley Group, (Becker and Clayton, 1976), the Kuruman iron-formation, S. Africa (Perry and Ahmad, 1980) and the Biwabik iron-formation, Minnesota (Perry and Bonnicksen, 1966; Perry et al., 1973). A first obvious feature in Figure 4.16 is the similarity in data distribution

between the Hotazel samples and iron-formations which have suffered little or no metamorphism (Hamersley, Kuruman, unmetamorphosed Biwabik). The Hotazel data plot as a steep ( $\sim 90^\circ$ ) non-equilibrium array with  $\delta^{18}\text{O}$  values for magnetite showing a fairly wide variation, while corresponding values for quartz range within very narrow limits. Such distribution is a strong indication of open-system isotopic exchange whereby the Fe-oxide phase (in this case magnetite) has exchanged more rapidly with a pore fluid during diagenesis/low-grade metamorphism, while quartz would have remained essentially inert.

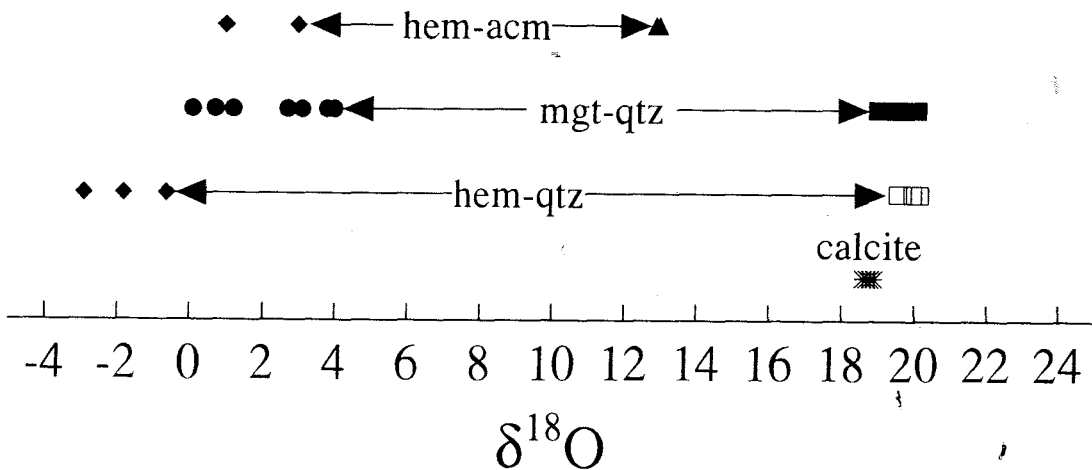


**Figure 4.15.** Ranges of  $\delta^{18}\text{O}$  values for quartz, hematite, magnetite, calcite and acmite for selected samples from the Hotazel iron-formation.

**Table 4.2a:** Stable isotope compositions of quartz, magnetite and calcite from pristine Hotazel iron-formation.

	$\delta^{18}\text{O}_{\text{mgt+qtz}}$	$\delta^{18}\text{O}_{\text{mgt}}$	$\delta^{18}\text{O}_{\text{qtz}}$	$\delta^{18}\text{O}_{\text{cc}}$	$\delta^{13}\text{C}_{\text{cc}}$
GL26-1	13.2	3.1	19.6	18.8	-9.5
GL26-2	13.3	0.7	20.1	18.6	-10
GL26-3	13.7	4	19.8	18.7	-9.3
GL26-3a	13.5	2.7	19.3	18.6	-9.4
GL26-4	13	0.1	19.2	18.9	-10
GL26-5	14.6	3.8	19	18.6	-8.8
GL26-6	12.8	1.2	19.1	18.7	-8.6
<i>Mean</i>	13.5	2.2	19.5	18.7	-9.4
<i>STD</i>	0.6	1.3	0.4	0.1	0.5

**Table 4.2b:** Stable isotope compositions of quartz, hematite and acmite from altered Hotazel iron-formation.

	$\delta^{18}\text{O}_{\text{hem+qtz}}$	$\delta^{18}\text{O}_{\text{hem}}$	$\delta^{18}\text{O}_{\text{qtz}}$	$\delta^{18}\text{O}_{\text{acm+hem}}$	$\delta^{18}\text{O}_{\text{acm}}$
MK3I-3	11.8				
MK3I-4	9.7				
MK3I-5	11.4				
MK3I-6	11.6	-1.8	20		
MK3I-7	11.4				
MK3I-8	10.2	-2.9	20.2		
MK3I-10		3		9.3	13
MK3I-11		1		8.7	12.9
MK3I-12	10.6				
MK3I-13	10.2	-0.6	19.6		
MK3I-14a	10.5				
MK3I-14b	9.9				
<i>Mean</i>	10.7	-0.3	19.9	9	12.95
<i>STD</i>	0.7	1.6	0.3	0.3	0.05

 $\delta^{18}\text{O}$  vs SMOW;  $\delta^{13}\text{C}$  vs PDB

STD: Standard deviation

**Abbreviations:** qtz: quartz; hem: hematite; mgt: magnetite; cc: calcite; acm: acmite

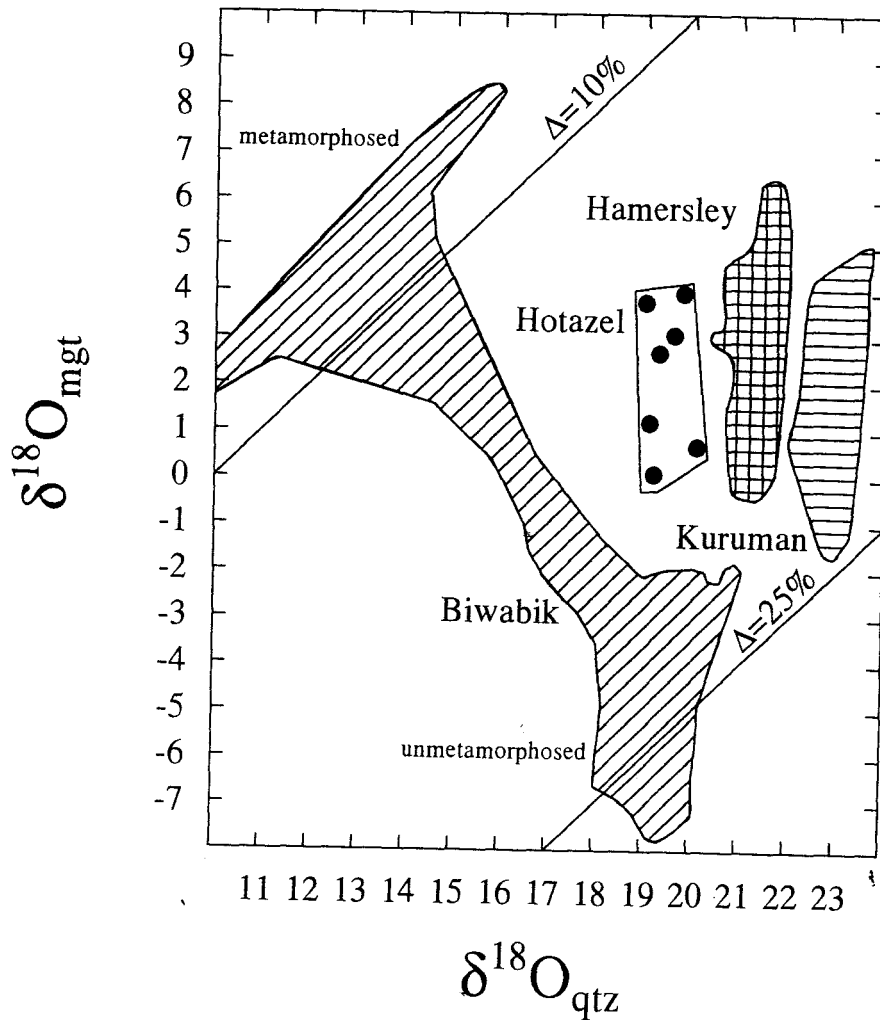


**Figure 4.16.**  $\delta$ - $\delta$  plot showing the distribution of  $\delta^{18}\text{O}$  data for quartz-magnetite pairs from the Hotazel iron-formation. For comparative purposes, the data have been plotted along with the fields defined by similar data from the Biwabik (Perry and Bonichsen, 1966; Perry et al., 1973), Kuruman (Perry and Ahmad, 1983) and Brockman (Becker and Clayton, 1976) iron-formations (based on an original graph by Gregory et al., 1989).

Reasons for such a dissimilar behaviour between quartz and magnetite during isotopic exchange may lie in mineral transformation processes linking primary precursor materials with the minerals presently observed. It has been suggested that magnetite probably originates from some sort of a primary precursor (hydrated iron-oxide?) which would have exchanged more readily than the magnetite itself (Gregory et al., 1989). Coexisting quartz, on the other hand seems to have remained isotopically unchanged, which suggests that its isotopic composition prior to the open-system event that caused the variation in  $\delta^{18}\text{O}$  values for magnetite must have been very uniform at  $\sim+19$  to  $\sim+20\text{‰}$ . This relative uniformity in the isotopic values of quartz does not preclude the possibility that an earlier event has shifted the  $\delta^{18}\text{O}$  of the quartz or its precursor phase (e.g. amorphous/opaline silica?) and of the entire system for that matter. The rather low  $\delta^{18}\text{O}$  values of quartz could be attributed to a number of reasons, namely diagenetic/metamorphic effects, primary deposition of the Hotazel iron-formation from low- $\delta^{18}\text{O}$  meteoric or marine waters, and/or warmer surface temperatures in the Paleoproterozoic. The latter possibility carries important implications, if one considers the clearly smaller degree of fractionation of the Hotazel quartz-magnetite pairs compared to those from the Kuruman iron-formation. These two iron-formation occurrences are developed respectively above and below a Palaeoproterozoic glacial diamictite (Makganyene Formation), hence it is possible that they may have been deposited under contrasting surface temperatures.

Mineralogical and petrographic evidence suggests that the Hotazel Formation has suffered a diagenetic to very low-grade metamorphic overprint on the basis of the stability environments of minerals such as greenalite and minnesotaite (Klein, 1983; see also Fig. 2.2, PART 2). This, in conjunction with the very fine-grained nature of the iron-formation points towards conditions not exceeding the domain of very low greenschist facies metamorphism. Similar evidence is also available from the manganese ores which contain abundant diagenetic Mn-carbonate ovoids in a very fine-grained matrix of Mn-oxide (braunite) and carbonate (Kleyenstüber, 1984; Nel et al., 1986).

As mentioned earlier, quartz-magnetite pairs from iron-formations that have suffered open-system isotopic exchange do not satisfy equilibrium conditions and are thus not suitable for applications of stable isotope geothermometry. Apparent "temperatures" estimated by quartz-magnetite pairs



from the seven unaltered, Hotazel iron-formation samples range between 220°C and 300°C. It is perhaps somewhat surprising that the “temperatures” obtained from the quartz-magnetite pairs are well within the temperature range of crystallisation of the Hotazel mineral assemblages as postulated on petrographic grounds (<300°C). The rather realistic range of “temperatures” obtained from the quartz-magnetite pairs is perhaps a good indication that quartz is not “primary” in terms of isotopic composition, but has probably also undergone a certain degree of isotopic exchange with a fluid during diagenetic conversion of an original amorphous or opaline precursor (Gregory, 1986). This phase transition is expected to have taken place at an early stage during burial (early diagenesis), while magnetite would have continued to exchange with more evolved diagenetic fluids and/or other mineral phases at later prograde stages of diagenesis-very low grade metamorphism, as evidenced from the coarser-grained textures of magnetite relative to quartz.

It is important to consider here the  $\delta^{18}\text{O}$  composition of calcite in relation to quartz and magnetite, and its potential applicability in terms of geothermometry. Calcite from the pristine iron-formation has  $\delta^{18}\text{O}$  values that vary within a particularly narrow range (18.6-18.9), substantially smaller even when compared to the range observed for quartz. By using published fractionation curves for quartz-calcite pairs (Fig. 4.12), “temperatures” obtained for the Hotazel Formation would fall in the region of 580-790°C. Although this range of temperatures is largely the result of the gentle slope of the quartz-calcite fractionation curve at higher temperatures, rather than due to different fractionations from one sample to another, the minimum temperature values obtained are unreasonably high and thus geologically meaningless. As was demonstrated in Chapter 4.1, C and O isotope data from calcite-ankerite pairs suggest negative  $\Delta_{\text{cc-ank}}$  values which, in the light of published fractionation curves for a wide range of metamorphic conditions (Friedman and O’Neil, 1977) are also unrealistic. The above would support the concept that closed-system isotopic equilibrium was not attained between calcite and quartz and that the two minerals have probably been characterised by diverse isotopic exchange histories, closely linked to the processes that led to their formation.

It has been noted that the carbonate minerals in the Hotazel rocks exhibit textures indicative of late diagenetic crystallisation, which would imply that O-isotopic re-equilibration has accompanied sub- to euhedral growth. In spite of the variation in the magnetite  $\delta^{18}\text{O}$  values, comparison

between the calcite-quartz and magnetite-quartz fractionation curves of Figure 4.12 suggests that the “apparent temperatures” deduced from calcite-magnetite fractionations during diagenesis would fall well below the range predicted from respective quartz-magnetite pairs, and thus correspond more closely to a late diagenetic environment. Therefore, it appears likely that during diagenetic organic matter oxidation and subsequent development of calcite and magnetite, the isotopic composition of quartz had already been “locked in”. Although the very small range in isotopic values of calcite suggests that the mineral formed in almost complete equilibrium with a diagenetic fluid, the variation in the magnetite values would suggest that the latter mineral may not owe its origin entirely to processes of organic-matter oxidation - Fe-reduction, but it may have also formed partially as a result of later replacement mechanisms at the expense of pre-formed minerals which would have allowed for further open system exchange reactions. The main conclusion from the above is that under favourable circumstances where a closely interlinked diagenetic history for both calcite and magnetite is supported, selected co-existing magnetite-calcite pairs in unmetamorphosed iron-formations may potentially constitute more reliable geothermometers than quartz-magnetite pairs.

#### 4.2.3.2. Alteration-metasomatism

$\delta^{18}\text{O}$  isotopic results from 10 mixed quartz-hematite samples of iron-formation from borehole MK3I have been plotted in Fig. 4.17 against the molar fraction of hematite-hosted oxygen in each sample. The distribution of data approximates a linear array with regression correlation coefficient ( $r$ ) of -0.91, which would allow for a reasonable extrapolation of end-member quartz and hematite  $\delta^{18}\text{O}$  values corresponding to  $X(\text{O})_{\text{hem}}$  values of 0 and 1 respectively. These end-member values are approximately -1 for hematite and 20 for quartz. In order to establish a rough constraint on the margin of error in the values for quartz and hematite, chemically separated quartz residues from three out of the ten selected samples were analysed for their oxygen isotopic compositions (see Table 4.2b). The values determined for quartz were then used in equation (3) (Yapp, 1990c) in order to determine the corresponding  $\delta^{18}\text{O}$  values for coexisting hematite from the already analysed quartz-hematite mixtures. As stated earlier, the three hematite samples show a wider isotopic variation compared to co-existing quartz. Figure 4.17 demonstrates that end-member values for the ten quartz-hematite samples would be expected to lie within the range represented

by the spread in pure hematite and quartz  $\delta^{18}\text{O}$  values of the three selected samples.

An important aspect of the quartz-hematite isotope data concerns correlations with respective quartz-magnetite data from unaltered iron-formation, as presented in the foregoing paragraphs. Quartz  $\delta^{18}\text{O}$  values are very similar between pristine and altered iron-formation ( $\sim 20\text{‰}$ ), while hematite ( $\sim 1\text{‰}$ ) is significantly more depleted in terms of  $\delta^{18}\text{O}$  than magnetite ( $\sim 2\text{‰}$ ). The shift in the Fe-oxide isotopic values by approximately 2-3 per mil can be used as a strong indication of low-temperature oxidation process(es) involving a low- $\delta^{18}\text{O}$  fluid, possibly of meteoric origin ( $\delta^{18}\text{O} \sim 0\text{‰}$ ). This would involve transformation of magnetite and any Fe-silicate compounds into hematite, accompanied by leaching/removal of all carbonate components and preservation of silica in the form of microcrystalline  $\text{SiO}_2$ . Similar isotopic exchange processes have also been documented in the laboratory during the solid-state, closed-system transformation of goethite into hematite (Yapp, 1990a). Quartz  $\delta^{18}\text{O}$  values indicate that the mineral remains essentially isotopically unexchanged during this process, suggesting that temperatures of alteration must have been substantially low. Although the quartz-hematite pair suffers from the same limitations as the quartz-magnetite pair in terms of geothermometry (open-system isotopic exchange, larger isotopic variation in the Fe-oxide than in the quartz), "apparent" temperatures obtained using the quartz-hematite fractionation curve of Yapp (1990c; see Fig. 4.12), suggest that this alteration may have taken place at temperatures as low as  $50^\circ\text{C}$ . Under such conditions, O-isotope fractionation between hematite and water is very small and equilibrium isotopic exchange between the two minerals is usually attained, resulting in O-isotope compositions of natural hematite approaching very closely those of coexisting natural waters (Bao and Koch, 1999).

The limited isotopic data available from the acmite-bearing samples of borehole MK3I cannot, in principle, be used alone as evidence for the conditions of formation of this assemblage. The two acmite separates gave  $\delta^{18}\text{O}$  values of approximately  $13\text{‰}$ , while coexisting hematite is depleted in terms of  $\delta^{18}\text{O}$  with values that are only slightly heavier than those of hematites from oxidised iron-formation ( $1\text{-}3\text{‰}$ ). One can assume that the formation of acmite would have been promoted in a rock containing abundant iron present exclusively in the trivalent state, along with free  $\text{SiO}_2$ ; therefore, it is reasonable to postulate that acmite formation has taken place at some point during

or after oxidation of the original iron-formation assemblage, as long as Na-rich fluids from a yet unidentified source were able to infiltrate the system. If it is assumed that hematite and acmite represent an equilibrium pair, then temperatures of approximately 250°C would be derived by combining the expressions for acmite-water by Zheng (1992) and for hematite-water by Yapp (1990b). However, the similarity of the hematite isotopic values between acmite-hematite and acmite-free, quartz-hematite samples, implies that hematite has suffered minimal isotopic changes during the formation of acmite, a fact which would cast doubt on any assumptions regarding isotopic equilibrium, and thus reduce the validity of the deduced temperatures to a minimum.

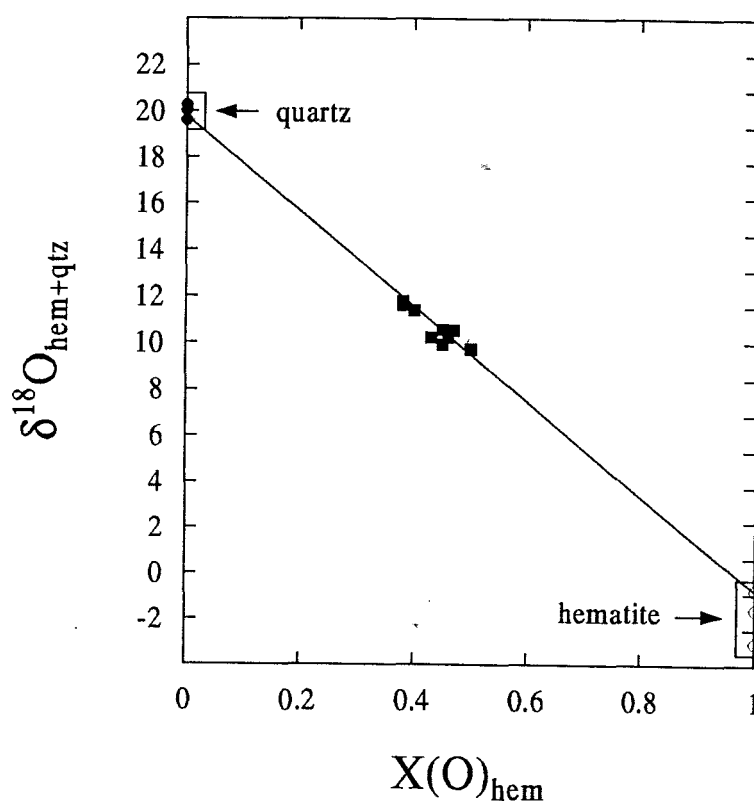


**Figure 4.17.** Bivariate plot of  $\delta^{18}O$  values for binary quartz-hematite mixtures against the molar fraction of oxygen in hematite, for the 10 selected samples of altered Hotazel iron-formation.

All above uncertainties are amplified if one considers the large spectrum of environments regarding temperatures of formation of acmite as reflected in a number of earlier studies. Pyroxenes of the aegirine-augite group are common constituents of fenites, with the more pure

Na-end member (i.e. acmite) occurring preferentially in the peripheral zones of alkaline intrusions as temperature decreases (Sutherland, 1969). Pure acmite occurrences have also been reported from hematitic iron-formation of the Cuyuna Range, Minnesota (Grout, 1946; McSwiggen et al., 1994) and are believed to have formed as a result of hydrothermal activity involving NaCl-enriched fluids at temperatures that depend on the amount of dissolved salts. Also, the complex mineral assemblages locally developed in the Mn-ore from the northern segment of the KMF (Dixon, 1985) contain acmite as an important constituent, and are believed to have formed at temperatures in the region of 400-600°C.

The general perception that acmite in iron-formation would be expected to form at medium- to high temperatures stems from the common association of the mineral with certain igneous rocks and fenites. The occurrence, however, of authigenic acmite in trona deposits of the unmetamorphosed Green River Formation, Wyoming (Milton and Eugster, 1959; Milton et al., 1960; Bradley and Eugster, 1969), adds another perspective to the lower stability limits of acmite in natural environments. As Milton et al. (1960) state: "if such minerals (e.g. acmite) form under conditions such as prevailed during lacustrine sedimentation and a subsequent 'normal' (that is, non-magmatic, non-hydrothermal) history of the lake deposits, then we must either drastically revise downwards our notions of what constitutes magmatic or hydrothermal conditions, or agree that the minerals in question formed in nature under a surprisingly varied range of geological conditions".

From the foregone, it becomes clear that acmite alone cannot be used as a clear-cut indicator of temperatures of alteration in the Hotazel rocks. In fact, any isotopic information on the apparently complex nature of the alteration process/es that enriched the Hotazel Formation in Fe and Mn ought to be interpreted along with other lines of evidence presented in other parts of this thesis. This aspect will be investigated further in the final synthesis, in conjunction with other geological evidence.

## PART 5: SYNTHESIS

### Chapter 5.1: Origin of iron-formations

#### 5.1.1. Palaeoenvironment and source of Fe and Si

It has been widely proposed that iron-formations were deposited in relatively shallow-water marine settings, and probably in partly barred, stable, continental-shelf basins of original dimensions that may have been highly variable from place to place (e.g. Trendall, 1973a,b,c,d; Beukes, 1973; Drever, 1974; Loughheed, 1983; Garrels, 1987). Proposed depositional settings span over a wide range, including open palaeo-oceans (Button et al., 1982), barred lagoonal environments (Dimroth, 1975; Chauvel and Dimroth, 1974), fresh-water lakes (Govett, 1966) and playa-lake complexes (Eugster and Chou, 1973). The fact that clastic terrestrial input is strikingly absent in iron-formations (e.g. Gross, 1980; Beukes, 1983; Morris and Horwitz, 1983; Holland, 1984; Simonson, 1985) suggests that deposition is likely to have taken place in a polar or desert environment (James and Trendall, 1982). The suggestion that iron-formations have formed in evaporitic settings has remained rather controversial over the years, with various authors being in favour of it (e.g. Dimroth, 1976; Garrels, 1987), while others have strongly disputed it on sedimentological grounds (e.g. James and Trendall, 1982; Morris and Trendall, 1988).

The source of Fe and Si in iron-formations has not been clearly established and previous researchers are divided into essentially two schools of thought, i.e. those who advocate a terrigenous origin and those who are in favour of a submarine volcanic-exhalative source. Proponents of a terrigenous origin propose that the Fe and Si may have derived from a large landmass comprising predominantly basaltic material, under conditions of mature weathering and lateritisation. The two elements would have been transported to the depositional basin(s) through well-developed drainage systems, possibly in the form of organometallic colloidal complexes (e.g. Gruner, 1922; Sakamoto, 1950; Govett, 1966; Lepp and Goldich, 1959, 1964; Pride and Hagner, 1972; Garrels et al., 1973; Drever, 1974; Hålbich et al., 1993).

Holland (1973, 1984) argues that a terrigenous source would require unusually large drainage systems in the Precambrian, coupled with unrealistic efficiency to dissolve and carry the necessary

amounts of iron and silica in order to precipitate iron-formations. Although Holland (1984) supports the concept that the Precambrian oceans may well have been characterised by intrinsically high amounts of dissolved Fe and Si, the volcanogenic source is certainly the most strongly favoured alternative (van Hise and Leith, 1911; Goodwin, 1956; Gross, 1965; Trendall and Blockley, 1970; Kimberley, 1979, 1989a,b; Morris and Horwitz, 1983). Particularly in recent years, genetic models for iron-formations invoke the contemporaneous operation of mid-ocean ridge activity similar to modern marine environments, accompanied by large-scale delivery of volcanogenic Fe to the oceans in the form of massive hydrothermal plumes (e.g. Klein and Beukes, 1989; Morris, 1993; Isley, 1995). Although the volcanogenic source seems more feasible than the terrigenous one in terms of the migration of Fe and Si in the Precambrian oceans (Mel'nik, 1982), direct evidence concerning large-scale volcanic activity at the time of, or prior to the formation of large iron-formations of the world is markedly lacking. The Hotazel Formation underlain by Ongeluk lavas is the most notable exception to the above (Beukes, 1983; Cornell and Schütte, 1995), along with the sparse presence of pyroclastic material and/or variolites in certain iron-formation occurrences worldwide (e.g. LaBerge, 1966a,b; Brooks, 1977).

### **5.1.2. Genetic modelling**

Irrespective of the apparent lack of consensus, genetic models variously proposed for the deposition of iron-formations (e.g. Drever, 1974; Button et al., 1982; François, 1986; Klein and Beukes, 1989; Carrigan and Cameron, 1991; Morris, 1993) share some common important characteristics. The model of Morris (1993) on the giant iron-formations of the Hamersley Group, Western Australia, provides a conceptual genetic framework where most of the characteristics encountered in worldwide iron-formations, are comprehensively described (Fig. 5.1).

Essentially all authors agree that the existence of a stratified depositional environment is required for the extensive deposition of iron-formation, whereby basinal waters were separated by a wide chemocline zone characterised by a linear decrease of temperature with depth. The chemocline essentially corresponds to a redox boundary, separating a bottom anoxic water layer with the capacity to preserve effectively large amounts of iron (and possibly manganese) in solution, with mildly oxygenated (suboxic) surface waters which would have been saturated with respect to Si.

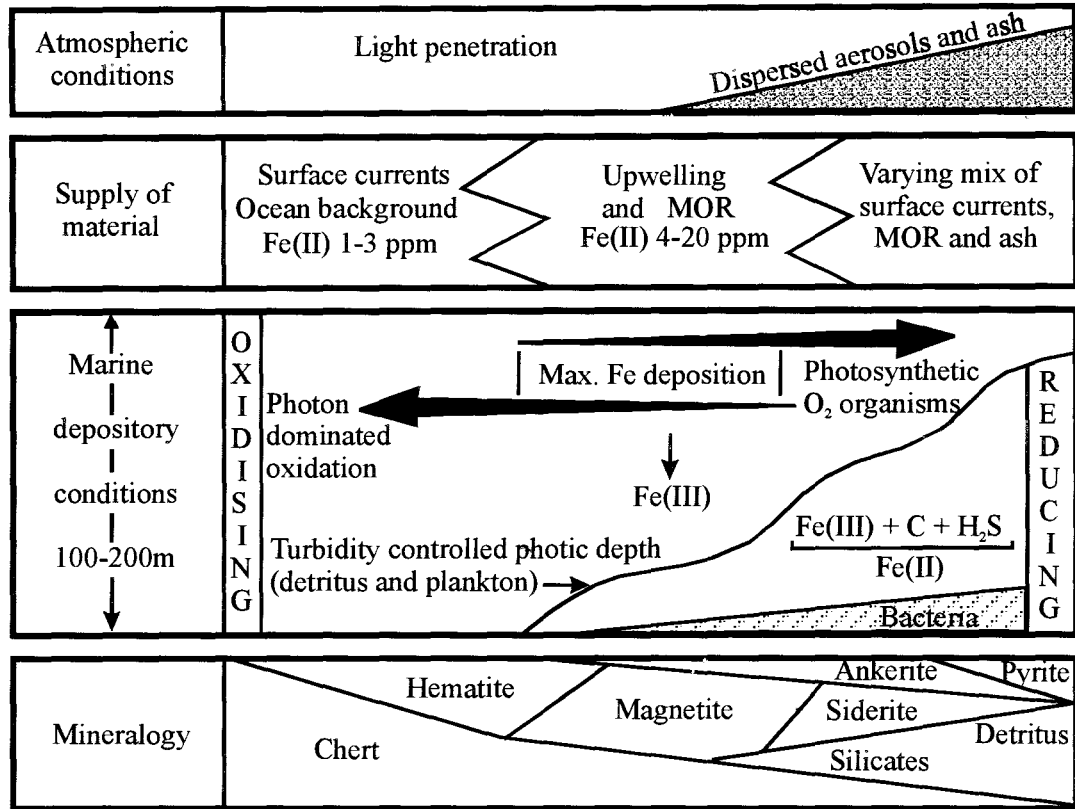


**Figure 5.1.** A summary of the main features of the genetic model for iron-formation in the Hamersley Group. Atmospheric conditions are modified by volcanic emissions. Supply of materials is (1) from surface ocean currents, giving rise to hematite varves, interrupted periodically by (2) high iron supply from upwelling currents and MOR hydrothermal output, both modified by (3) fine ash from distal sources. Photic depths are controlled by seasonal changes and turbidity in the water and atmosphere. Precipitation of iron is primarily by oxidation in the photic zone, and the precipitate consolidates as ferric oxide; or is modified by partial reduction to form magnetite (2 ferric/1 ferrous); or is substantially reduced, dependant on the organic supply, augmenting iron in the sub-photic zone and leading to the precipitation of ferrous-rich compounds. The mineralogical distributions are qualitative (modified after Morris, 1993).

According to Morris (1993), the characteristic banded nature of iron-formations would be explained as a result of alternate precipitation of Fe-rich and Si-rich layers on a mm-scale, such



as the “varves” (mm-scale microbands) of Trendall (1973b,d) and Trendall and Blockley (1970). Such periodicity would have been caused by the interaction of seasonal storm-mixing of bottom, Fe-rich waters with surface Si-saturated waters, periodically coupled with upwelling processes induced by mid-ocean ridge (MOR) or hot spot activity.

One of the long-standing debates in the earth sciences concerns the question whether the Palaeoproterozoic atmosphere was anoxic or, at least, poorer in oxygen content in comparison with the present (e.g. Cloud, 1968, 1972, 1973; Dimroth and Kimberley, 1976; Walker, 1977; Towe, 1983; Holland, 1984; Kasting, 1987; Holland and Beukes, 1990; Kirkham and Roscoe, 1993; Krupp et al., 1994; Ohmoto, 1996, 1997). In accordance with most genetic models, the widespread deposition of iron-formation in the Palaeoproterozoic would require that at least the deeper parts of the depositories were anoxic. Precipitation of the Fe-rich layers would also require that rapid oxidation of upwelled Fe took place in the surface waters. Irrespective of whether free oxygen was available in the atmosphere during Palaeoproterozoic times, alternative oxidation mechanisms have been proposed, including O<sub>2</sub>-production by means of photosynthetic activity, as well as oxidation by sunlight (photo-oxidation and/or photolytic dissociation; see Cairns-Smith, 1978, and Braterman et al., 1983). The latter mechanism has been particularly favoured on the grounds of the absence of manganese in iron formations (Kump and Holland, 1992; Anbar and Holland, 1992), although the abundance of manganese ore in the Hotazel Formation has added an important dimension contradicting that theory.

In addition, reasons are sought for the mineralogy of worldwide iron-formation occurrences that do not show any effects of regional or contact metamorphism (e.g. Klein, 1983). Assuming that the original precursor materials consisted of a combination of ferric iron-enriched compounds, the Fe<sup>2+</sup>-dominated iron-formations suggest that major redox changes to their sedimentary precursors occurred shortly after precipitation i.e. during diagenesis. In this regard, it is important to stress the potential significance of bacterial metabolism and its contribution towards the reduction of ferric iron in the diagenetic environment (e.g. Walker, 1984; Lovley et al., 1987; Myers and Nealson, 1988a,b; Nealson and Myers, 1990), which is essentially translated into processes of coupled organic C oxidation - ferric iron reduction as described earlier in this thesis (for details, see PART 4, section 4.1.5.2).

## Chapter 5.2: Genesis of the Hotazel Formation

In order to shed light on the processes of formation of the Hotazel sediments, the discussion that follows will concentrate on three major aspects, namely:

- (i) review of previous models for the genesis of the Kalahari manganese deposits;
- (ii) proposed mechanisms for development of the Hotazel Fe-Mn cycles; and,
- (iii) regional significance of the Voëlwater Subgroup (Hotazel/Mooidraai Formations).

### 5.2.1. Previous genetic models

Although the sedimentary character of the vast majority of commercial manganese deposits is not generally disputed, proposed genetic models variously emphasise the importance of additional processes (for example, sea-floor volcanic exhalative activity, sea-level fluctuations, climatic changes, biological productivity) as critical in the development of large accumulations of manganiferous sediment in depositional environments of various ages (Frakes and Bolton, 1992). The relative importance of any of the above-mentioned processes with regard to the Kalahari example can, in theory, be determined by examining a variety of well-preserved geological attributes such as stratigraphy, structure, sedimentology, mineralogy and geochemistry of the ore and host-rocks. Irrespective of its origin, however, the sheer volume of the KMF renders it an undisputed enigma in the geological record. As a direct consequence, the question concerning potential source/s for the massive amounts of manganese sediment deposited in close stratigraphic association with the Hotazel iron-formation has remained one of the most contentious issues in recent years.

The two main genetic models previously proposed for the Kalahari manganese deposits postulate diverse metallogenic processes, namely:

- *epigenetic replacement* whereby Kalahari manganese ore was formed as a result of hypogene replacement mechanisms at the expense of a suitable protolith (De Villiers, 1983, 1992);
- *volcanic-exhalative*, involving interaction between mid-ocean ridge-type submarine volcanism and rapid precipitation of Mn- and Fe-rich compounds in the form of volcanogenic-sedimentary cycles (Cornell and Schütte, 1995).

A characteristic common to the above models is that they focus on a particular aspect of the Hotazel Formation and/or country rocks, to the virtual exclusion of all else. As a result, a substantial degree of debate has emerged amongst the various schools of thought (De Villiers, 1986, 1992; Kleyenstüber, 1986; Beukes, 1992; Beukes and Gutzmer, 1996; Cornell and Schütte, 1996), although none of the above models needs be totally exclusive of the others.

The epigenetic model describes the genesis of the Kalahari manganese deposits as a result of large-scale replacement of a carbonate-rich protolith by Mn-rich hypogene fluids (De Villiers, 1983). The model is based almost exclusively on mineralogical evidence from manganese ore from the KMF and suggests a close link with similar ores from the neighbouring Postmasburg manganese field. One of the main shortcomings of this model is that it does not take into account several features unique to the KMF, such as the stratigraphic constancy and striking cyclic character of the Hotazel Formation, and particularly the gradational nature of the contacts between iron-formation and Mn ore (Kleyenstüber, 1984; Nel et al., 1986; Tsikos and Moore, 1997). It also requires the operation of an epigenetic mechanism of unusual spatial extent, which finds little validity in the light of the pronounced differences in the geological settings of the Kalahari and Postmasburg fields as documented in recent studies (e.g. Plehwe-Leisen and Klemm, 1995; Gutzmer and Beukes, 1996b). Hence, although the epigenetic model of De Villiers (1983) may find application in those parts of the KMF where late alteration processes have been prominent, it is unlikely that it was the prime mechanism in producing these very extensive stratiform manganese deposits.

The volcanic-exhalative model (Cornell and Schütte 1995) attributes a great degree of significance to the directly underlying andesitic Ongeluk lavas in the generation of the Hotazel Formation and its contained manganese ores. The model suggests that the Kalahari manganese ores and associated iron-formation were deposited as an immediate result of sea-floor volcanic exhalative processes operating in close proximity to a mid-ocean ridge setting. Alteration features observed in Ongeluk lavas from the Kalahari area have been interpreted as being the result of such hydrothermal activity.

The model of Cornell and Schütte (1995) fails to explain several petrographic, geochemical and

sedimentological features of the Hotazel Formation as discussed at length by Beukes and Gutzmer (1996). An important weakness of this model is the lack of any information on the associated iron-formations and particularly on the cyclic development of iron-formation and manganese ore as evident from investigations in this study and elsewhere (e.g. Beukes 1983; Kleyenstüber, 1984, 1985; Nel et al., 1986; Tsikos and Moore, 1997). Cornell and Schütte (1995) have overlooked the fact that the Hotazel iron-formation is mineralogically and chemically a typical example of a Superior-type iron-formation and thus bears essentially no resemblance to rocks that are common hosts to volcanogenic Mn deposits, such as radiolarian cherts, jaspers and jaspilites (Roy, 1981; see Fig. 5.2). Moreover, Superior-type iron-formations are classic examples of stratigraphically monotonous sedimentary sequences, conspicuously lacking any mafic volcanic sequences and/or syngenetic manganese ore deposits in close stratigraphic association. It is of note that most other manganese deposits known to be hosted within iron-formations such as those in the Cuyuna Range, Minnesota (Morey and Southwick, 1993) and in Rooinekke, South Africa (Dirr and Beukes, 1990; Beukes, 1993), are regarded as clearly supergene in origin.

In addition to the above, manganese deposits of undisputed volcanogenic origin are usually small in size and economically unviable. In Phanerozoic assemblages, such deposits occur sporadically as small, irregular bodies and they are invariably associated with structurally chaotic ophiolite sequences (melanges) (e.g. Bonatti et al., 1976; Roy, 1981; Crerar et al., 1982). Furthermore, volcanogenic manganese deposits are rich in  $\text{SiO}_2$  (contents up to 40 wt% in cases: Crerar et al., 1982; Peters, 1988) and commonly contain no carbonate minerals. In contrast, the Kalahari manganese deposit is exceptionally voluminous (approximately 50% of the world's total land-based resources; see Laznicka, 1992), comprising three structurally undisturbed laminar beds of braunite/Mn-carbonate ore lacking any free quartz (Nel et al., 1986). Moreover, the underlying Ongeluk lavas are not typical MOR-type ophiolites but rather basaltic andesite flows of tholeiitic character (Schütte, 1992; Cornell et al., 1996) that overlie continental basement rocks (essentially platform sediments deposited on a craton).

On the basis of mass balance constraints alone, the hypothesis of Cornell and Schütte (1995) that the manganese in the Kalahari ores has derived from submarine hydrothermal leaching of Ongeluk lava would appear only remotely conceivable, given the relative volumes of Mn sediment, the

continental setting and restricted lateral extent of the Ongeluk Formation and the required efficiency of the leaching process invoked. On these grounds, it could be argued that the only link between the Kalahari manganese deposits and marine volcanism is one of geographical coincidence with an underlying thick succession of continental-type basaltic andesite flows, which have suffered a certain degree of normal sea-floor alteration/weathering.

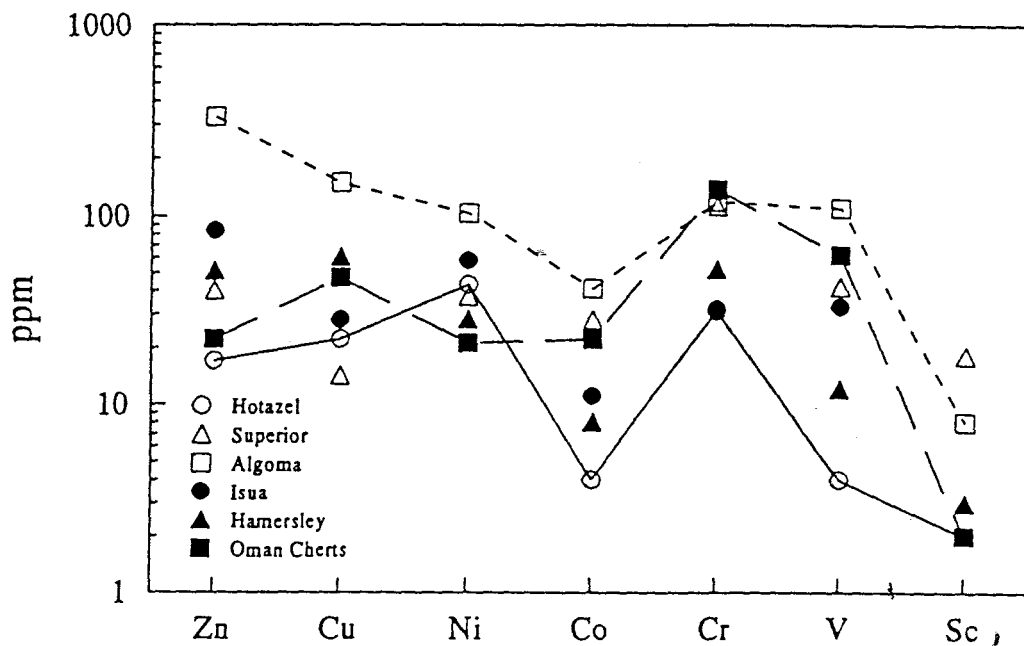


**Figure 5.2.** Plot of average transition metal values of pristine Hotazel iron-formation, Algoma- and Superior-type iron-formations of Canada, (Gross and McLeod, 1980), Archaean iron-formation of Isua, W. Greenland (Dymek and Klein, 1988), Palaeoproterozoic iron-formations of the Hamersley Group, W. Australia (Davy, 1983) and Mesozoic manganese-rich Oman cherts (Peters, 1988). Note the depleted transition-metal character of the Hotazel iron-formation, relative to the volcanogenic, Algoma iron-formations and Oman cherts.

The role of submarine volcanism in the genesis of the Hotazel Formation was also previously emphasised by Beukes (1983), Beukes et al. (1983) and Kleyenstüber (1985) in the context of a

volcanogenic-sedimentary model. This model proposes that the Ongeluk volcanic episode has had a distal influence on the precipitation of the Hotazel sediments, in combination with fluctuations in sea-level, thus producing the three discrete iron-formation - manganese cycles. Although the volcanogenic-sedimentary model was proposed in a tentative fashion, no follow-up investigations were conducted in order to establish further the significance of Ongeluk volcanism in promoting the genesis of the Kalahari deposits. The fact that some of the authors who advocated the volcanogenic-sedimentary scenario (e.g. Beukes, 1983) subsequently opposed very strongly the volcanic-exhalative model of Cornell and Schutte (1995) (Beukes and Gutzmer, 1995), leads to the conclusion that the former model has probably been abandoned as a potential genetic mechanism for the KMF.

### 5.2.2. Development of the Hotazel Fe-Mn cycles

Given the absence of direct evidence for a major volcanogenic influence on the genesis of the Hotazel Fe/Mn Formation, it is possible that a rather unusual confluence of processes must have operated in that particular place in space and time. Deciphering the nature of these processes is no easy task, but the results of this study provide some important constraints.

Mineralogical and geochemical data from pristine iron formation (PARTS 2 and 3) have shown that the latter is a typical example of the Superior-type iron-formation. Besides the presence of the interbedded Mn units, the important feature that distinguishes this particular iron-formation from other, well-studied worldwide occurrences, is the relative enrichment in whole-rock carbonate and total Fe-oxide components in the uppermost parts of the Hotazel succession. This upward increase in modal carbonate is regarded as a prelude to the change in the depositional character from mixed iron-manganese deposition to the formation of Fe/Si-bearing limestone of the Mooidraai Formation. Although in terms of quantitative carbonate precipitation this change appears to be rather abrupt, C and O isotopic evidence from the entire Voëlwater stratigraphy suggests a more gradational shift from a typical stratified depositional environment to a shallow carbonate platform (Fig. 5.3). This shallowing-upwards sedimentary trend is also evident from a general decrease in whole-rock Fe# values of Hotazel iron-formation samples across the stratigraphy, the occasional presence of a Fe-Mn-bearing carbonate unit, and the change in the

textural signatures of the iron-formation from rhythmically banded in the lower parts, to ones characterised by clear effects of agitated deposition (e.g. soft-sediment deformation structures) stratigraphically higher in the succession.

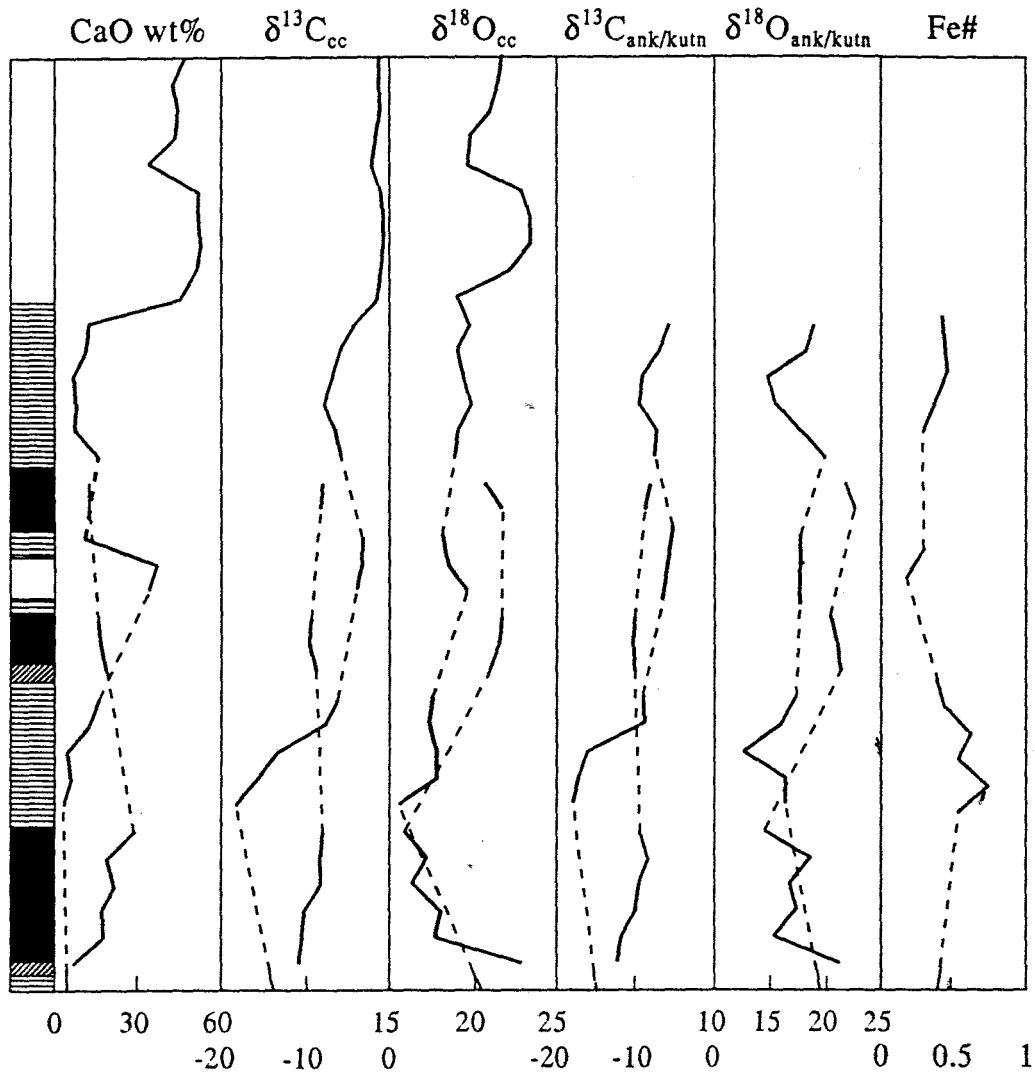


**Figure 5.3.** Summary of whole-rock CaO, Fe# ( $\text{FeO}/\text{FeO}+\text{Fe}_2\text{O}_3$ ) and C and O isotope chemostratigraphic signatures in the Voelwater Subgroup. Note the gradual transition towards heavier  $\delta^{13}\text{C}$  for iron-formation and Mooidraai calcites upward in the stratigraphy, reflecting a general shallowing-upwards pattern. Distinct isotopic excursions between the iron-formation and manganese ore-units would correspond to transgression-regression cycles. Abbreviations: cc=calcite (manganiferous in Mn-units); ank=ankerite; kutn=kutnahorite.

The deposition of manganese in three distinct sedimentary episodes appears to coincide with fairly sharp C and O isotopic excursions in the Hotazel carbonate constituents (Fig. 5.3). Although the behaviour of  $\delta^{13}\text{C}$  across the entire stratigraphy is highly dependent on processes of organic matter oxidation - Fe/Mn-reduction (see PART 4), positive O-isotope excursions between iron-formation and manganese ore-beds would point towards corresponding subtle redox changes, potentially related to climatically- and/or tectonically-driven fluctuations in sea-level. Models involving sea level changes in a stratified depositional environment (Frakes and Bolton, 1984, Force and Cannon, 1988) have been widely used in interpretations of the genesis of sedimentary manganese deposits of various ages and settings (e.g. Okita and Shanks, 1992; Öztürk and Hein, 1997; Gutzmer and Beukes, 1998). Applications of a transgression-regression model for the episodic development of the three iron-formation-manganese cycles of the Hotazel Formation have already provided a genetic framework (Beukes et al., 1982; Beukes, 1983), though in direct connection with volcanogenic-exhalative processes directly related to the submarine extrusion of the Ongeluk lavas.

Assuming no direct influence of the Ongeluk volcanic episode with regard to the deposition of the Hotazel sediments, a conceptual genetic model is presented schematically in Figure 5.4. The first three stages correspond to respective intervals of the depositional history of the Hotazel Formation in relative chronological order, as directly documented by lithostratigraphic, petrographic and geochemical information. The fourth stage represents the culmination of the above cyclic depositional scheme as reflected by the transition between the Hotazel iron-formation and the overlying Mooidraai carbonate succession.

The onset of major manganese precipitation occurred during a first regressive cycle following a gradual transition from iron oxide-rich iron-formation through a hematite - Mn carbonate-rich transitional zone (Fig. 5.4). The oxide-rich iron-formation would have been the product of precipitation of largely Fe-oxide compounds, with subordinate amounts of chert and carbonate material. Rapid precipitation of this unusually Fe/Mn-enriched iron-formation would require the lack of a well-established stratified basinal environment during early depositional stages. Continuous decrease in sea-level and shift of the redox regime towards more oxidising conditions, would have brought about a corresponding increase in the precipitation of manganese-rich



sediment in close association with marine bicarbonate. Relative depositional rates of silica and iron would have been curtailed, resulting in the formation of a hematite-bearing, mixed manganese carbonate/oxide unit, characterised by the development of isotopically light carbonate minerals and the lack of free  $\text{SiO}_2$ . Such conditions appear to have been ideal for the development of a particularly thick accumulation of Mn-rich sediment, hence the significant primary thicknesses of the lowermost manganese ore-unit from the southernmost KMF (see also Appendix I, Fig. A1).

Subsequently, marine transgression inhibited manganese precipitation and led to the establishment of a chemocline separating bottom, anoxic, Fe/Mn-rich waters from surface, oxygenated waters. Conditions would have been anoxic enough for precipitation of typical, Mn-free, Superior-type iron-formation in the form of alternating microcycles of mixed chert-greenalite-magnetite bands. Marine carbonate precipitation during this interval was significantly suppressed, resulting in strongly depleted isotopic signatures in the precipitated carbonate component, mainly due to processes of coupled ferric Fe-reduction - organic carbon oxidation during early diagenesis.

Progressive shallowing related to a second regressive stage would have brought about an increase in the relative amounts of marine carbonate precipitation, resulting in the deposition of carbonate-rich iron-formation with isotopic signatures substantially more enriched in the heavier isotopes of C and O, due to the introduction of more marine carbonate in the diagenetic environment (Fig. 5.4). Redox conditions favouring the development of a second, brief carbonate-rich manganese cycle were progressively reached, and ceased as a consequence of a second transgressive event.

From that point on, conditions at depth were insufficiently reducing for carbonate-poor iron-formation to form. Deposition of carbonate-rich iron-formation gradually led into a third cycle of manganese precipitation, and continued subsequent to a third and last transgressive event, with only mild fluctuations in the relative amount of carbonate deposited (Fig. 5.4). Episodic precipitation of a thin Fe-Mn bearing carbonate unit enriched in isotopically heavy marine calcite ( $\delta^{13}\text{C} \sim -3$ ) occurred between the second and third cycle, indicating an environment approaching at times that of a typical carbonate platform. Ultimately, sediment consisting almost exclusively of calcium carbonate precipitated (Mooindraai Formation), characterised by typically marine C-isotope signatures ( $\delta^{13}\text{C} \sim 0$ ) and reduced deposition of chert and Fe-compounds.

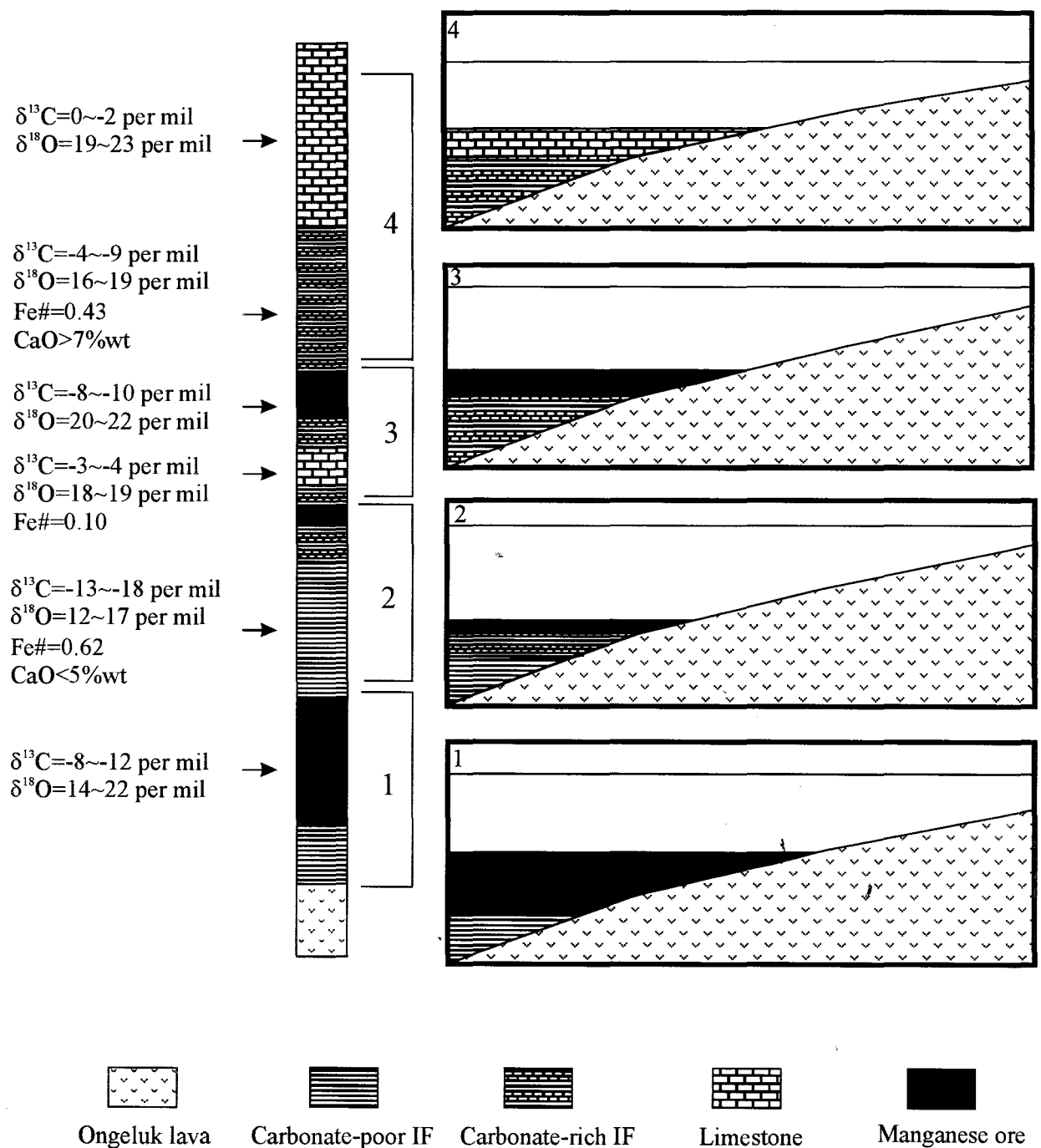


**Figure 5.4.** Schematic diagram illustrating the deposition of the Hotazel and Mooidraai Formations in four distinct stages, corresponding to respective transgression-regression cycles. Each stage corresponds to a complete depositional interval following a major transgressive event. Averaged geochemical and isotopic data for the Hotazel and Mooidraai sediments are also shown adjacent to a representative stratigraphic profile from the southernmost part of the KMF. The diagram and profile are not drawn to scale, but relative thickness relations between the individual lithologic units are crudely displayed.

Had deposition of the Voëlwater sediments have remained undisturbed by major sea-level changes, it is likely that dilute incorporation of manganese into various carbonate phases would have taken place for large parts of the succession under syn-diagenetic conditions (e.g. Force and Cannon, 1988; Pratt et al., 1991). In that case, formation of economic manganese mineralisation would not have occurred. The postulated transgression-regression cycles resulted in the depletion of dissolved manganese from the ambient waters, to a degree that fractionation between Fe and Mn during deposition of the iron-formation remained as effective as has been observed in other Palaeoproterozoic iron-formations worldwide.

### 5.2.3 Regional stratigraphy and implications

The conceptual model presented above places particular emphasis on the intimate association between iron-formation and Mn ore in the KME. The whole succession is seen as an inclusive and inseparable unit, so that the unusual existence of manganese within the Hotazel iron-formation can be duly accommodated. In the search for potential driving mechanisms for the formation of this unusual association, attention is drawn to the symmetrical nature of the Transvaal Supergroup in the Northern Cape, with platform carbonate - BIF associations symmetrically arranged above and below a central diamictite-andesitic lava association (Fig. 5.5). Removal of the lavas from this equation as an incidental volcanic episode, would place the diamictite unit (Makganyene Formation) at the centre of this symmetry. The Makganyene diamictite is believed to correspond to a Palaeoproterozoic low-latitude glacial event (Evans et al., 1997), comparable in many respects to the Huronian glaciation (Frakes, 1979). Currently, there are two contrasting hypotheses attempting to explain the causes of these glaciations, namely the "snow-ball Earth" phenomenon (Hoffman et al., 1998), whereby it is postulated that polar ice-caps in the Precambrian extended well down into the tropics, and the "high-obliquity" hypothesis (Williams et al., 1998) which proposes that low-latitude glaciations in Precambrian times were a consequence of high planetary obliquity.

Although the generally held opinion is that a major unconformity exists between the Makganyene diamictite and underlying rocks (Beukes and Smit, 1987), this does not appear to be universally valid based on field studies currently in progress, in which diamictite, sandstone and conglomerate

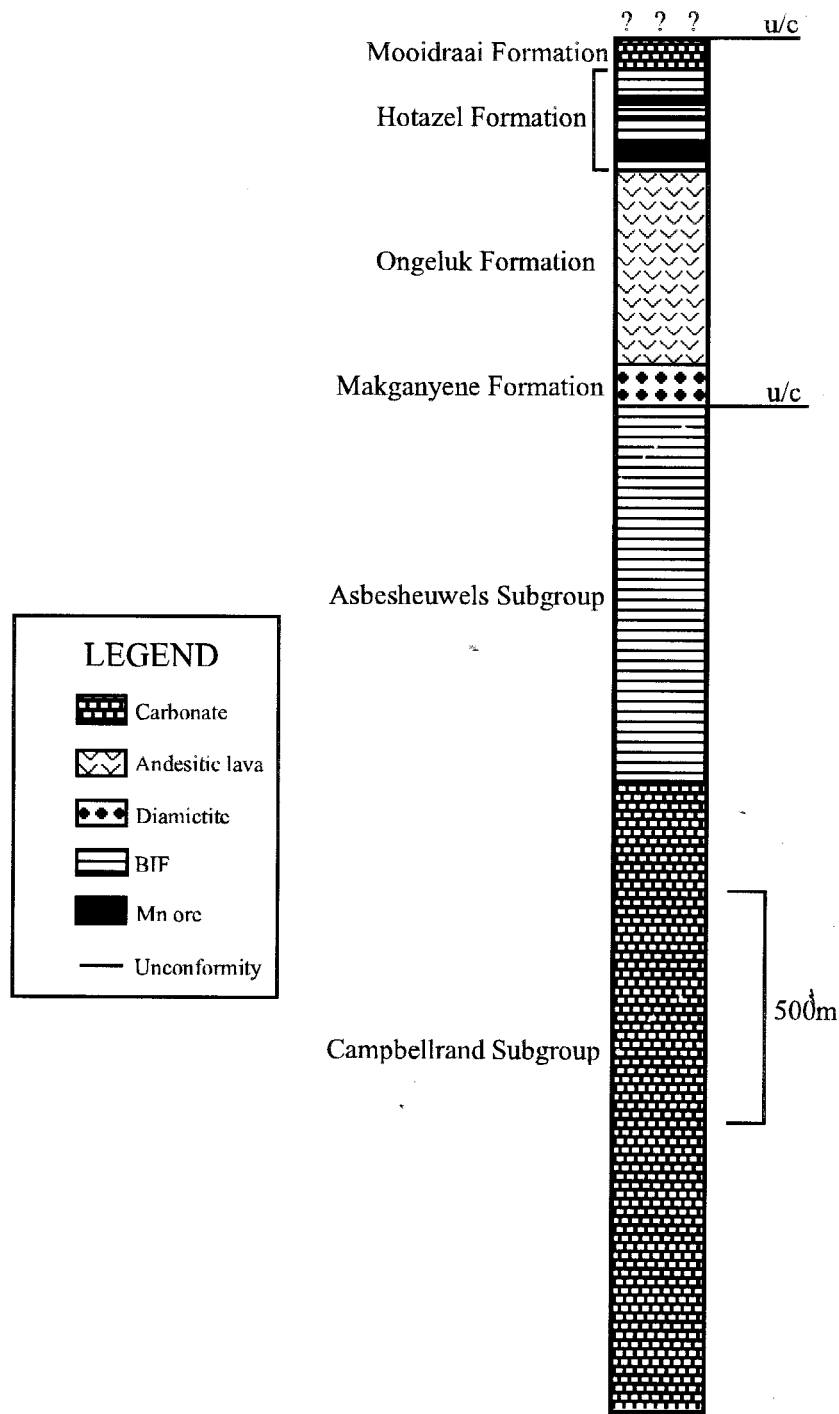


Figure 5.5. Simplified stratigraphic profile of the Palaeoproterozoic Transvaal Supergroup in the Northern Cape Province, displaying major lithological units and positions of regional unconformities (modified after Beukes and Smit, 1987).

are intercalated with iron-formation at the basal contact (Polteau and Moore, 1999). The absence of a significant time gap between the diamictite and the underlying sediments, would emphasise the potential role of climatic changes in regional sedimentation patterns of the Transvaal Supergroup in the Northern Cape. In this regard, it is important to consider current theories regarding the origin of Neoproterozoic Fe-Mn-formations of the so-called "Rapitan type" (e.g. Klein and Beukes, 1993). The development of such formations in several parts of the world including Canada, southern Africa and Brazil (Bühn et al., 1992; Urban et al., 1992; Klein and Beukes, 1993) has been closely related to glacial events, whereby preservation of Fe (and perhaps Mn) in oceanic water would be attained in essentially anoxic basinal settings capped by extensive ice-sheets. Precipitation of Fe- and Mn-rich sediments would then follow due to warming (and oxygenation?) of the ambient waters during periglacial periods. Whether or not such a mechanism has been partly or wholly responsible for large-scale conservation of Mn in oceanic water and subsequent formation of the deposits of the KMF is certainly debatable at this stage. Such a process, however, would remove the necessity for a volcanic driving mechanism such as the Ongeluk lavas, by focusing the attention on the significance that Palaeoproterozoic glaciation may have had in terms of large-scale metallogenic processes producing primary manganese carbonate ores.

## **Chapter 5.3. Alteration of the Hotazel Formation**

### **5.3.1. Previous models**

A comprehensive model was recently proposed to account for the processes involved in the alteration and economic upgrading of manganese ore from the northernmost parts of the KMF (Gutzmer and Beukes, 1993, 1995; Beukes et al., 1995). The specific area where alteration is observed is confined to approximately 3-5% of the overall area occupied by the field (Fig. 5.6). The boundary between the altered and unaltered domains has been arbitrarily placed by previous authors along a NE-SW trend (e.g. Kleyenstüber, 1984; Nel et al., 1986; Gutzmer and Beukes, 1995). According to Figure 5.6, this trend would show a potential relation to two features, namely (page 178):

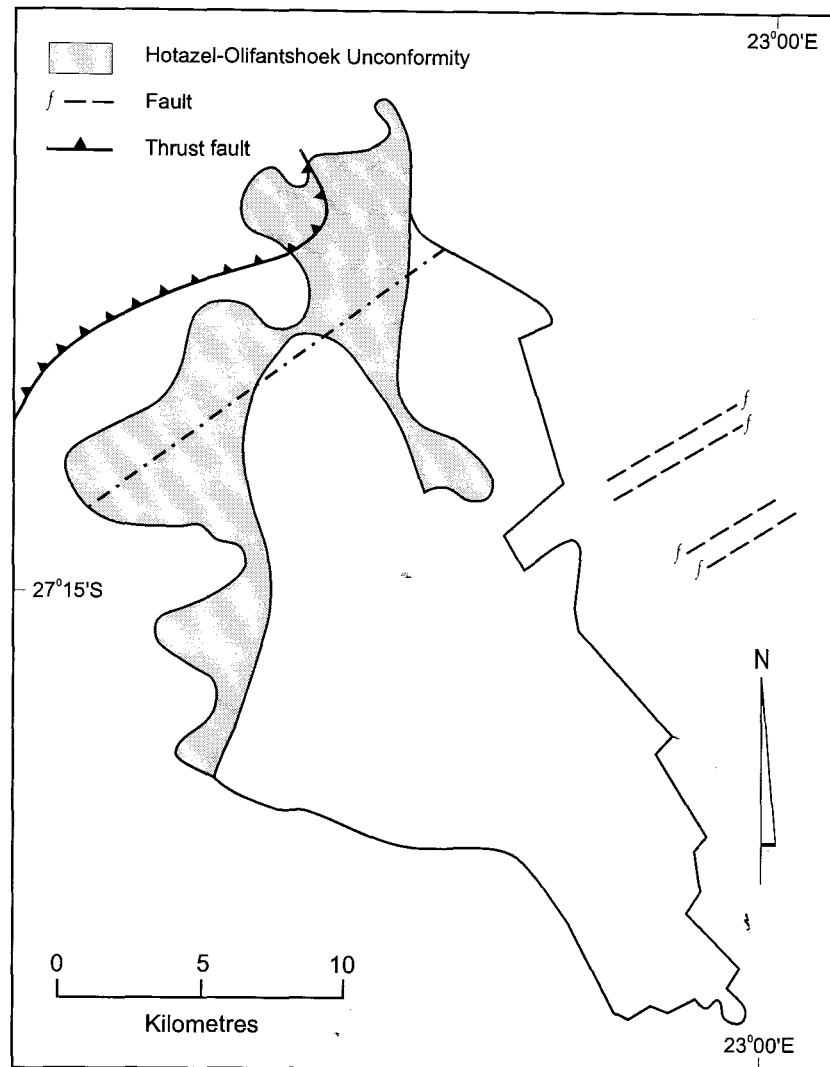


**Figure 5.6.** Simplified map of the KMF showing major structural features, the spatial distribution of the Hotazel-Olifantshoek unconformity and the postulated boundary separating the northernmost, altered portions of the Hotazel Formation from the remaining parts of the field.

- (i) thrusting, as manifested in the north-westernmost portion of the KMF (Black Rock);
- (ii) the southward outline of the area where the Hotazel Formation is directly overlain by rocks of the Olifantshoek Group.

A potential relation could thus be deduced between fluid-dominated alteration processes and thrust plane/s, and/or the Hotazel-Olifantshoek unconformity.

Gutzmer and Beukes (1995) describe alteration processes in the northernmost KMF as a result of fault-related hydrothermal circulation. The area is characterised by north-trending normal faults which intersect both the Hotazel Formation and unconformably overlying strata of the Palaeoproterozoic Olifantshoek Group (Grobbelaar et al., 1995). According to Gutzmer and Beukes (1995) the faults have acted as fluid channels, causing progressive alteration laterally into the Mn ore-beds (Fig. 5.7). The degree of alteration decreases away from the faults and low-grade unaltered manganese ore is preserved in the core of faulted blocks of Hotazel Formation. Enrichment in manganese is manifested by the development of hausmannite-braunite II-bixbyite dominated assemblages, lacking any quartz or carbonate compounds. The model applies not only to the N'chwaning area from which borehole material was selected for the purposes of this study, but also to the Wessels area further to the north of the N'chwaning mine (Beukes et al., 1995), hence the term "Wessels-type alteration".

Subsequent to publication of the above, Gutzmer and Beukes (1997) introduced some further refinements to their original model by highlighting mass balance relations between altered (enriched) manganese ore and unaltered ore as it develops in the largest part of the KMF. Gutzmer and Beukes (op. cit.) point out that fault-related alteration was accompanied by effective loss of Ca, Mg and CO<sub>2</sub>, i.e. elements primarily related to the pre-existing carbonate component of the ores. This resulted in significant volume loss and compaction of the ore-units (particularly the lowermost and most extensively studied) to approximately two-thirds of their original thickness. Such thickness relations have also been proposed by Gutzmer and Beukes (1997) as a potential exploration tool for the discovery of further high-grade manganese ore reserves in the KMF.

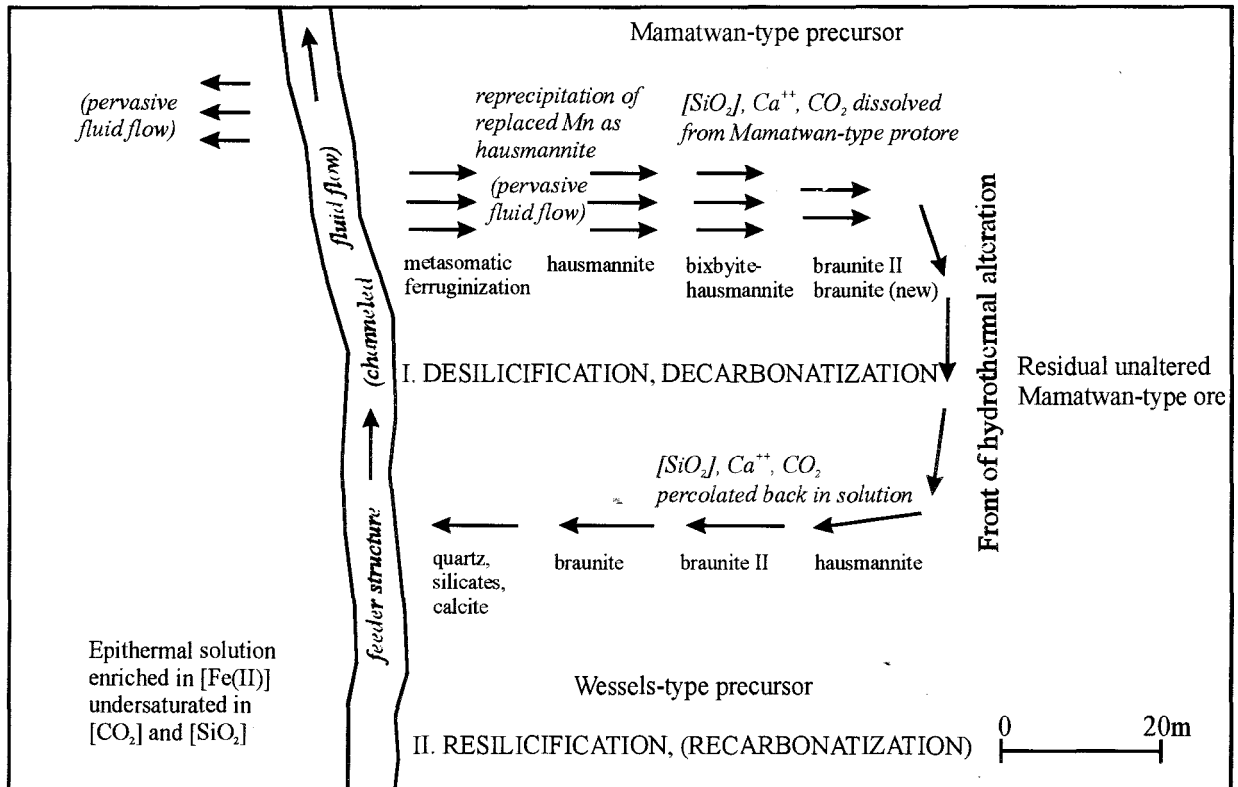


**Figure 5.7.** Conceptual model of a closed hydrothermal system responsible for alteration and ferruginization of Mn ores in the KMF. Fluid flow symmetrical to that of the central fluid feeder, only right half of fluid flow scheme is displayed. Scale only approximate (after Gutzmer and Beukes, 1995).

### 5.3.2. Appraisal

#### 5.3.2.1. Evaluation of geological evidence

Available geological information from the northernmost KMF can assist in reviewing the existing alteration model of Gutzmer and Beukes (1995, 1997). Although the area is almost entirely



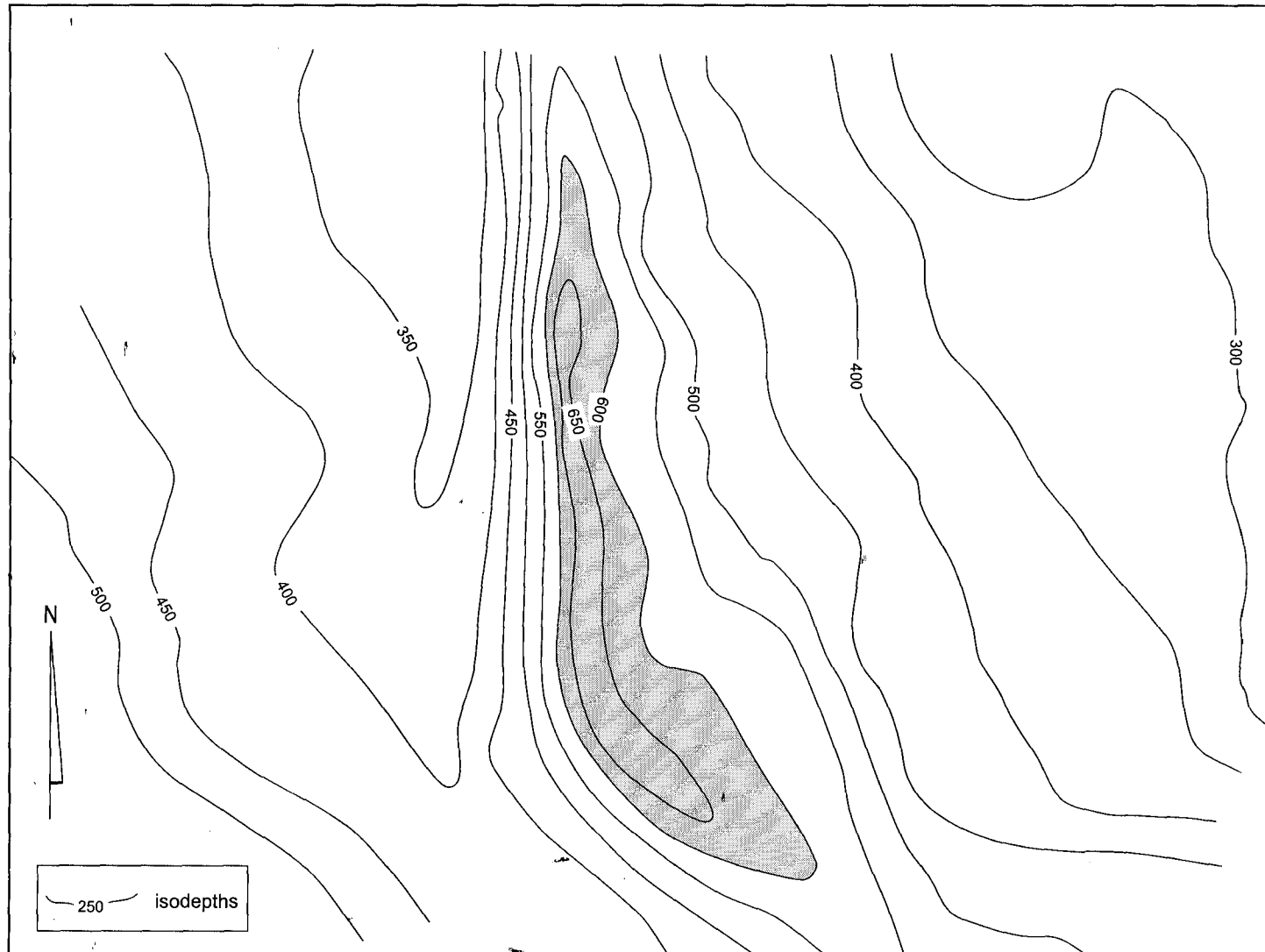
covered by a thick, Tertiary sand/calcrete cover (Kalahari Formation), compilation of existing borehole-log information as presented below\*, reflects some important geological features.

Figure 5.8 shows the general structure of the sub-surface geology of the Hotazel Formation in the area occupied by the farm N'chwaning and adjoining farms (see Appendix I), as reflected on an isodepth map. The contours correspond to lines of equal depth from the present surface, of a critical contact selected between the uppermost manganese ore-unit and the underlying iron-formation. Figure 5.8 shows that the Hotazel Formation dips gently to the West by 5-10°, except for a portion characterised by normal, essentially N-S-trending faulting, corresponding to the graben structure reported by Grobbelaar et al. (1995). Faults of that nature are regarded by Gutzmer and Beukes (1995) as important conduits for fluid-flow and subsequent alteration of the Hotazel rocks laterally away from the faults.

Figure 5.9 shows an isopach map of the N'chwaning area where each contour corresponds to a portion of the Hotazel Formation of equal stratigraphic thickness. The specific portion selected for constructing this map corresponds to the iron-formation intersection between the lower contact of the uppermost manganese ore unit and the upper contact of the lowermost manganese ore-unit, in order to avoid any thickness variations related to the basal contact of the Hotazel Formation with the Ongeluk lavas and to pre-Olifantshoek erosion. In Figure 5.9, areas where the selected Hotazel portion attains maximum and minimum thicknesses are respectively highlighted with vertical and inclined line-fills. Based on descriptions from the previous section, areas of minimum thickness would correspond to areas where altered iron-formation and enriched manganese ore are developed and *vice versa*. It becomes apparent that domains of thick, unaltered Hotazel Formation are distributed roughly along a NE-SW trend. Studies of borehole material from these domains (e.g. N91B) have shown that the iron-formation developed is of the oxidised type. In the immediate vicinity of the faulted zone of Figure 5.8, portions of thin, altered Hotazel iron-formation are seen, implying the presence of high-grade manganese mineralisation.

---

\* Due to a confidentiality agreement with ASSMANG LTD, the author is not at liberty in disclosing any information regarding borehole localities or any borehole-log data without prior permission from the company's management.



**Figure 5.8.** Plan view of the N'chwaning mine area and environs showing the general structure of the Hotazel Formation as reflected on an isodepth contour map (for details on general locality of the area, see APPENDIX, Fig A1). Contours correspond to the depths below the surface of the contact between the uppermost Mn ore-unit and the underlying iron-formation. The shaded area corresponds to the half-graben structure of Grobelaar et al., (1995).

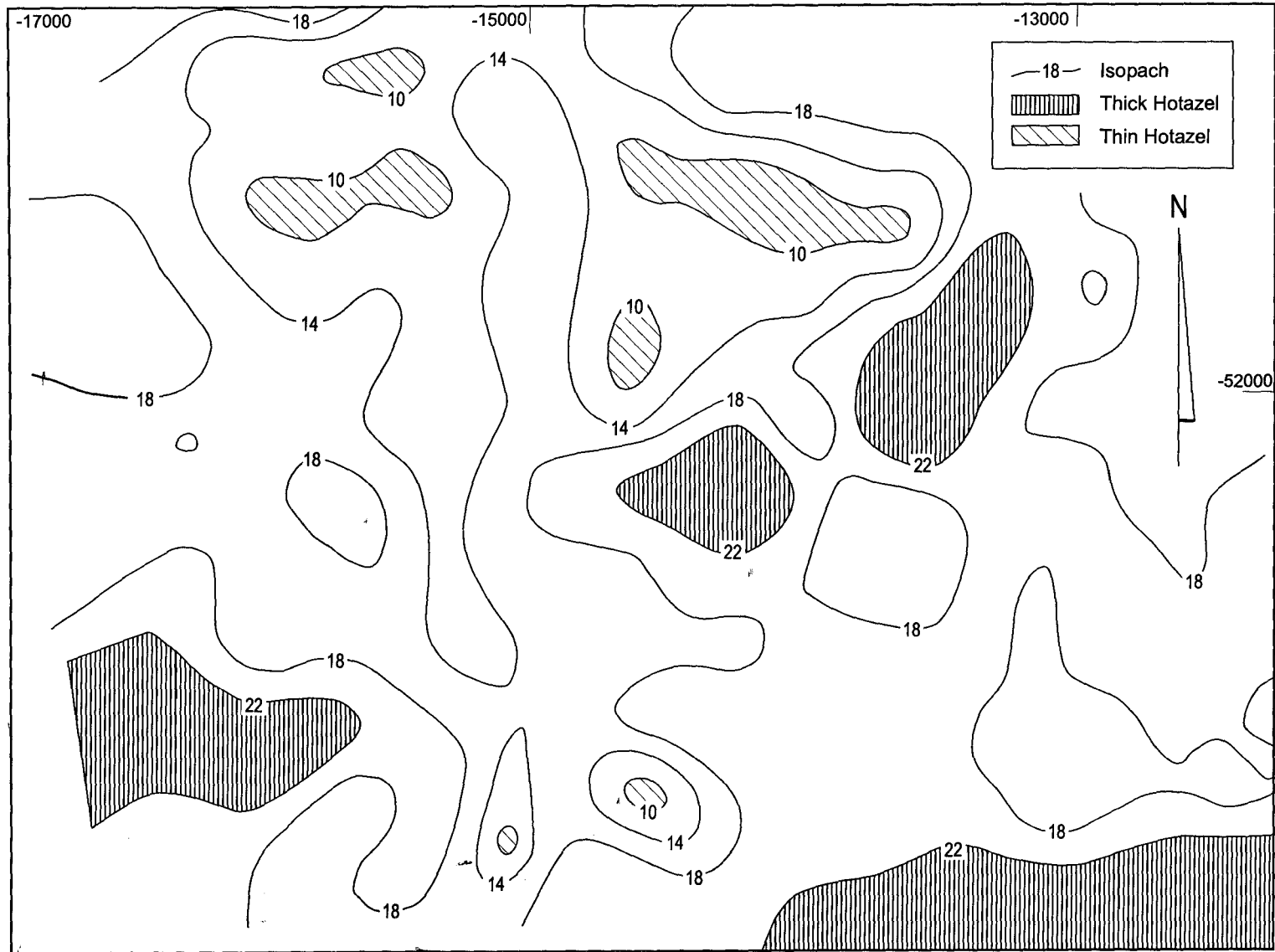


**Figure 5.9.** Plan view of the N'chwaning mine area and environs displaying an isopach contour map of the portion of the Hotazel Formation enveloped between the uppermost and lowermost Mn-ore-units (for details on general locality, see APPENDIX, Fig A1). The distribution of domains where this specific portion attains maximum (>22m) and minimum (<10m) thickness is shown as vertical and inclined line-fills respectively.

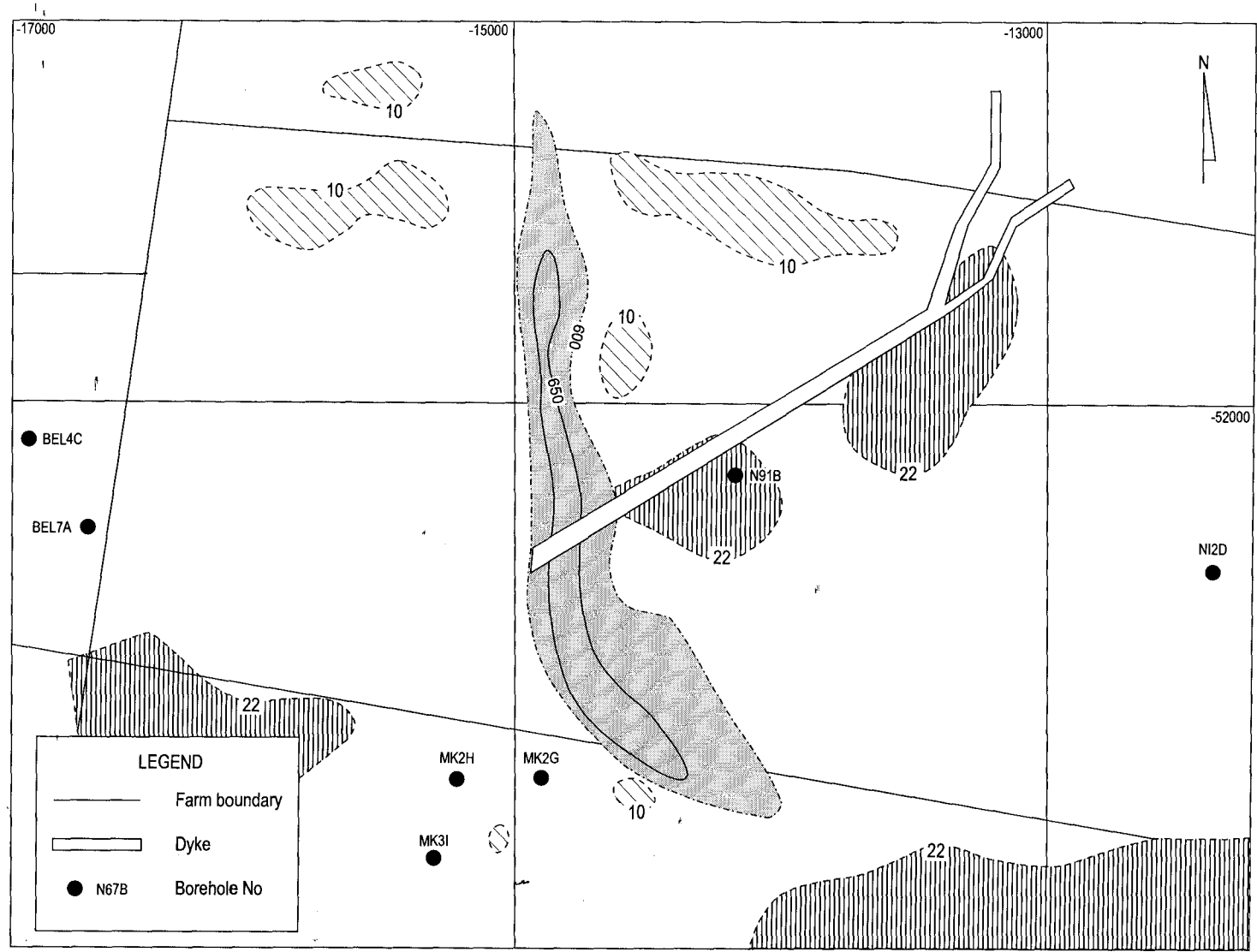


**Figure 5.10.** Plan view of the N'chwaning mine area showing the localities of boreholes selected for this study, farm boundaries, and location of a major dyke. Superimposed on the map is selected information regarding major structural features (graben, shaded) and areas of the Hotazel Formation attains minimum (inclined line-fill) and maximum (vertical line-fill) thicknesses (see also Figs 5.8, 5,9). Note the asymmetric distribution of thick, "oxidised" Hotazel iron-formation in the immediate vicinity to the dyke.

Figure 5.10 shows a simple pre-Olifantshoek geological map of the N'chwaning area which includes information from Figures 5.8 And 5.9. The map also contains the location of the seven boreholes selected for this project from that area, as well as an intrusive dyke trending NE-SW. This dyke intersects the entire Hotazel Formation and is unconformably overlain by shales of the Olifantshoek Group (Grobbelaar et al., 1995), implying that the intrusion took place in pre-Olifantshoek times. It is important to note that although the distribution of altered iron-formation shows a distinct association with the recognised fault structure, thick iron-formation is distributed along a trend similar to the dyke, in an asymmetric fashion. The bearing that these features have on modelling the alteration in the northernmost KMF is discussed in the following section.

#### *5.3.3.2. Constraints from the present study*

In reviewing the model of Gutzmer and Beukes (1995), it is necessary to place the history of the alteration process/es in the context of a hypothetical sequence of geological events that occurred subsequent to the deposition and diagenesis of the Hotazel Formation, and are documented from the northernmost KMF. These events can be grossly classified relative to the deposition of the Olifantshoek sediments into:

- (1) Pre-Olifantshoek weathering, intrusion of dykes and (possibly) faulting/fracturing;
- (2) Post-Olifantshoek development (rejuvenation?) of normal, N-S-trending faults and thrusting.

In terms of relative timing of some of these events (i.e. faulting, intrusion of dykes), information derives mostly from field observations and the paper by Grobbelaar et al. (1995). Due to the absence of absolute geochronological constraints, this relative chronological order does not necessarily provide a unique interpretation of the geological history of the northernmost parts of the KMF, but it facilitates the discussion that follows.

#### Pre-Olifantshoek processes

Mineralogical and geochemical data from samples collected a few tens of centimetres below the Hotazel-Olifantshoek unconformity, have been regarded as indicative of surface weathering

processes that occurred prior to the deposition of the Olifantshoek sediments (see PART 2), as they reflect strong enrichments in Fe (hematite), Mn (Mn-oxide) and Al (as very fine-grained mica) and depletions in silica, Ca and Mg. These features, however, are not extensively developed in terms of stratigraphic depth, which implies that pre-Olifantshoek surface processes *sensu-stricto* were probably not critical in terms of large-scale alteration and economic upgrading of the Hotazel deposits. Below this surface-enriched zone however, variable degrees of alteration are manifested in three different ways in the selected borehole intersections:

- (i) massive hematite developed above altered iron-formation (boreholes MK2H, N12D);
- (ii) development of altered iron-formation essentially throughout the Hotazel stratigraphy (boreholes MK3I, MK2G);
- (iii) altered iron-formation developed stratigraphically above oxidized iron-formation (boreholes, N91B, BEL4C, BEL7A).

This vertical “zonation” of iron-formation types would suggest that alteration may have been controlled by *per-descendum* movement of fluids of meteoric origin, as in the case of a low-temperature weathering profile (Fig. 5.11). The most elevated portions of the succession would have been characterised by vigorous leaching of carbonate material and chert, resulting in the development of residual massive hematite. Below, leaching of carbonate would be the dominant effect, causing complete remobilisation of Ca, Mg, Sr, Ba (and possibly some Fe and Mn) and residual enrichment in quartz and isotopically light ( $\delta^{18}\text{O} \sim -1$ ), secondary hematite, along with trace elements which would have been immobile in a low-temperature environment, such as Cr, Ni, V, Pb and Th. Depending on palaeotopography and position of the palaeo-water table, (partial?) reprecipitation of solutes would have occurred at depth in the form of Mg/Mn-enriched dolomite-type carbonate, accompanied by incipient oxidation of pre-existing Fe-bearing phases and, possibly, reprecipitation of further amounts of hematite. The appearance of pristine rock in the lowermost parts of certain boreholes containing oxidised iron-formation (e.g. BEL7A), suggests that the weathering profile would have developed down to stratigraphic depths of approximately 100m, assuming a low-angle dipping palaeotopography.

The relative timing of the above process is particularly important. If vertical faults/fractures had been present during alteration, gravity-driven movement of fluids would have been further

enhanced. This would have promoted intense band-to-band alteration close to the faults and subsequent diffusion laterally and/or in a down-dip direction, so long as the general attitude of the Hotazel strata (5~10° to the west) had, by that stage, already been established. On the other hand, the role of dykes is still somewhat unclear. Previous authors agree that their influence in terms of metasomatic processes in the surrounding Hotazel sediments is minimal (e.g. Dixon, 1985). Nevertheless, the information presented in Figures 5.9 and 5.10 suggests that the presence of at least one of these dykes must have had an indirect, yet important, control in the development and relative distribution of domains characterised by dissimilar degrees of alteration. It is thus possible, that the dyke/s may have acted as impermeable “barriers” during movement of the alteration fluids. If the *per-descendum* model is valid and it operated on a gently dipping stratigraphy, one would expect that down-dip flow along banding would have driven modified fluids at deeper levels, and would have potentially re-precipitated part of the dissolved solutes in the periphery of the impermeable dyke. The above features are presented in the schematic diagram of Figure 5.11, which corresponds roughly to a pre-Olifantshoek, E-W cross-section from the portion of the N’chwaning area to the east of the graben as shown in Figure 5.10.

#### Post-Olifantshoek processes

It was shown earlier (Figure 5.8) that normal, NS-trending faulting is another important geological process in the northernmost KMF. According to Grobbelaar et al. (1995),<sup>1</sup> this faulting would have taken place subsequent to the deposition of the Olifantshoek strata, as the faults cut through the Olifantshoek rocks. The model of Gutzmer and Beukes (1995), proposes that alteration of the Hotazel Formation would have taken place subsequent to the faulting, since the faults are believed to have acted as channels for the fluids that induced the alteration processes laterally into the Hotazel rocks. This conceptual model is presented in a highly schematic three-dimensional fashion in Figure 5.12. Application of the model in an ideal situation where no other post-diagenetic effects have been involved prior or subsequent to the fault-controlled alteration, would require that alteration decreased laterally away from the faults and hence blocks of unaltered rock would be expected to develop along a trend similar to the one observed for the faults, i.e. roughly N-S. The spatial extent of these unaltered portions would depend upon the scale of the alteration process which would, in turn, be related to the distribution of faults in space

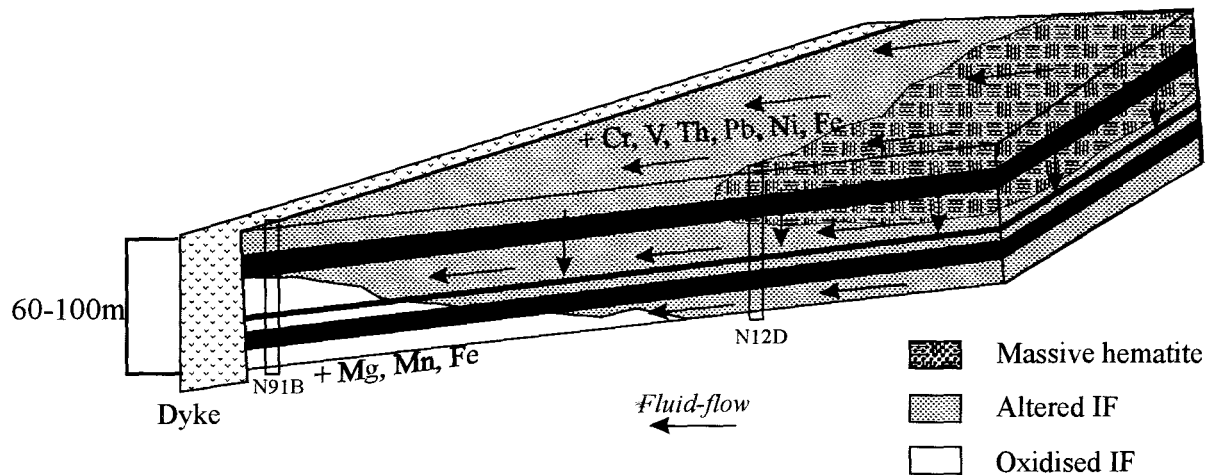


**Figure 5.11.** Conceptual schematic diagram (not to scale) showing the development of altered and oxidized iron-formation as a result of low-temperature weathering processes induced by descending meteoric fluids. The model assumes that alteration and leaching of the Hotazel Formation took place at pre-Olifantshoek times, subsequent to gentle tilting of the strata to the west. The most elevated portions would have suffered intense alteration and development of residual, massive hematite. Lower in the stratigraphy, leaching of carbonate material led to residual enrichment of Fe, Si and other elements (e.g. Ni, Cr, V, Pb, Th) in the iron-formation, and development of altered iron-formation. Down-dip transport of solutes from dissolution of pre-existing carbonates (e.g. Mg, Mn, Fe, and possibly some Ca), gave rise to dolomite/ankerite-rich, oxidised iron-formation, by means of (partial) re-deposition and incipient oxidation at depth, adjacent to dykes. Potentially suitable borehole locations for the Hotazel stratigraphy as developed in intersections N12D and N91B, are shown.

assuming that the Hotazel iron-formation behaved largely as a homogeneous medium in terms of its pre-alteration physicochemical properties (mineralogical/chemical composition, porosity-permeability, etc).



It becomes apparent that the model of Gutzmer and Beukes (1995) cannot explain an important feature, namely, the origin and asymmetric distribution of oxidised iron-formation in the vicinity of the dyke. This aspect depends largely on the scale of the postulated fault-controlled alteration process. Specifically, if the graben structure acted as the main fluid conduit for lateral, pervasive alteration away from the faults, one would expect that highly altered iron-formation would occur away from the faults for appreciable lateral distances, while pristine iron-formation would have been expected to develop in those areas where oxidised iron-formation is now seen, assuming that the dyke acted as an impermeable fluid barrier. On the other hand, had fluid-flow been promoted at a smaller scale along every normal fault and/or fracture zone present in the mine area, there would be no apparent reason for the specific distribution of oxidised iron-formation as presently observed. It appears therefore, that although faulting may have had a role to play in the alteration process, it was not necessarily the sole or most important mechanism. In fact, it is likely that fault-controlled alteration may have happened at any stage in the geological history of the Kalahari ores, effectively overprinting and/or obliterating earlier alteration features.

The potential role of thrusting as an important attribute in the alteration process/es has also been considered previously (e.g. Kleyenstüber, 1985). Thrusting is believed to be related to the Kheis orogenic event at 1.8-1.9 Ga (Beukes and Smit, 1987), the manifestations of which in the KMF are the major thrust structures observed in the Black Rock area to the west of the N'chwaning mine. Thrust planes commonly act as important aquifers along which ascending, tectonically driven fluids from deeply-buried adjacent areas would pass. Fluids of such nature are usually in the form of Cl-rich, metal-laden brines derived from processes of basin dewatering. Continental-scale fluid-flow systems of this kind are currently believed to be responsible for the development of major stratabound mineral deposits, ranging from the world-class iron-ore districts of the USA (e.g. Morey, 1999) and Australia (e.g. Oliver et al., 1998, Powell et al., 1999), to the famous metallogenic provinces of Mississippi Valley-type (MVT) deposits of North America (e.g. Garven et al., 1993). Examples of MVT deposits of similar origin in the Transvaal Supergroup in the Northern Cape Province include the Pering Zn-Pb deposit (Wheatley et al., 1986) whereas the iron-ore deposit of Sishen (van Schalkwyk and Beukes, 1986) is regarded as a product of leaching of iron-formation in the presence of highly alkaline groundwater solutions.

The possibility that alteration in the northernmost portions of the KMF is related to thrust-driven fluid-flow processes cannot be discounted. The conspicuous occurrence of acmite in parts of the Hotazel stratigraphy, in conjunction with the complex metasomatic mineral occurrences in parts of the northernmost KMF (see also PART 2), point towards the likely operation of a strongly alkaline metasomatic-hydrothermal system. From the distribution of the metasomatic assemblages alone, the scale of this event appears to be rather small and essentially localised. In addition, the development (at least) of the acmite would be promoted if the precursor material contained binary mixtures of hematite and quartz, presumably derived from an earlier oxidation-leaching process at the expense of pristine iron-formation (PART 2, section 2.2.2.3). Although the stratigraphically well-confined distribution of acmite-rich assemblages remains an enigma, it is believed that Na-metasomatism was an unimportant process in terms of large-scale alteration and economic upgrading of the Hotazel iron-formation and Mn ores.

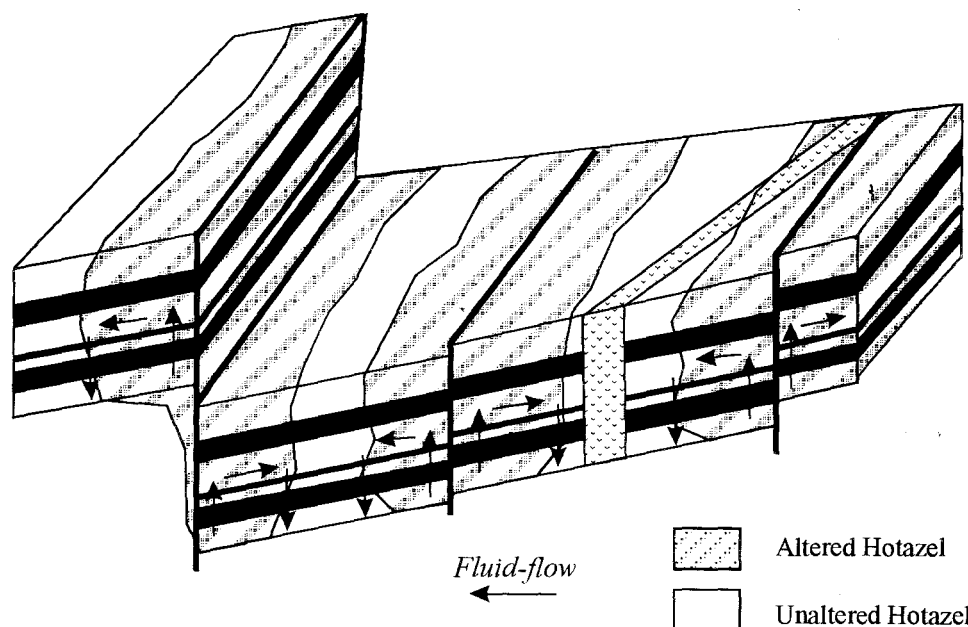


**Figure 5.12.** Simplified diagram showing the expected distribution of altered and unaltered Hotazel iron-formation and Mn ore on the basis of the fault-controlled alteration model of Gutzmer and Beukes (1995).

## Chapter 5.4: Conclusions - suggestions for further study

The results of this study have provided some important new information concerning the genesis and post-depositional history of the Hotazel Fe-Mn Formation. For the first time, the focus of attention was withdrawn from the Kalahari manganese deposits and was placed instead on the mineralogical and geochemical characteristics of the host iron-formation.

In the largest part of the KMF, the Hotazel iron-formation exhibits strong similarities with other worldwide occurrences of Superior-type iron-formation. The rock appears devoid of metamorphic or supergene alteration effects. Relative to other iron-formations, the Hotazel iron-formation contains a lower amount of chert and a higher amount of total Fe (as Fe-oxide), primarily present as magnetite and to a lesser extent Fe-silicate compounds (mainly greenalite, minnesotaite and stilpnomelane). An important characteristic of the Hotazel iron-formation is its increased levels of carbonate constituents, in the form of coexisting calcite and ankerite. Isotopic compositions, and particularly their relation with whole-rock CaO contents of the rock, indicate a mixed origin for these carbonates, involving marine bicarbonate ( $\delta^{13}\text{C} \sim \text{O}\%$ ) and isotopically light carbon and related to processes of organic carbon oxidation - ferric iron reduction. As a result, iron-formation carbonates have low isotopic signatures ( $\delta^{13}\text{C} = -4 \sim -18\%$  vs PDB;  $\delta^{18}\text{O} = 12 \sim 19\%$  vs SMOW), which compare well with similar data from the literature.

Isotopic depletion is particularly prominent in carbonate-poor iron-formation, suggesting deposition of the latter in the deeper parts of the palaeodepository. Higher in the stratigraphy and closer to the transition with overlying ferriferous limestone of the Moodraai Formation ( $\delta^{13}\text{C} = -2 \sim 0\%$ ;  $\delta^{18}\text{O} = 19 \sim 23\%$ ), the bulk carbonate content increases and the isotopic values for the iron-formation become substantially heavier, indicating a progressive shallowing-upwards trend. This trend was periodically interrupted by the episodic deposition of carbonate-rich mangiferous sediment, with C isotope values slightly more depleted than those of iron-formation carbonates ( $\delta^{13}\text{C} = -8 \sim -12\%$ ) and O-isotope values somewhat more variable and generally heavier ( $\delta^{18}\text{O} = 14 \sim 22\%$ ). These cycles are attributed to corresponding fluctuations in sea level, whereas the Mn-carbonate isotope signatures probably owe their origin to processes similar to the ones postulated

for the iron-formation, i.e. coupled organic C oxidation and reduction of higher valence Mn-oxide precursors.

$\delta^{18}\text{O}$  data from quartz, magnetite and calcite in iron-formation confirm petrographic observations that the rock has suffered a burial (very low-grade metamorphic) effect, and point towards an open-system environment characterised by disequilibrium isotopic exchange with diagenetic fluid/s, with different minerals obtaining their isotopic character at different stages of their diagenetic history. Such data cannot, in principle, be used as indicators of temperatures of formation. However, isotopic fractionations between magnetite and both quartz and calcite, suggest that the commonly selected quartz-magnetite pair may not necessarily represent the most reliable pair in terms of geothermometry, and that mineral-pair selection should be carefully constrained on the basis of the diagenetic history of the rock as derived from petrographic studies.

Rare-earth element data for selected iron-formation and Moidraai limestone samples suggest a hydrogenous origin, with the ambient waters containing a dilute hydrothermal component. Comparisons with rare-earth element data from modern hydrothermal precipitates of Fe in the proximity of submarine hydrothermal vents, suggest that a volcanic-exhalative origin for the Hotazel rocks is doubtful, and that only a distal volcanogenic influence may be invoked. This, in conjunction with field relations, the volume of the Kalahari Mn deposits and the mineralogical and geochemical character of the iron-formation, cast doubt on volcanic-exhalative models proposed previously. Similarities between the Hotazel REE signatures and Neoproterozoic, glaciogenic iron-formations of the Rapitan type, have shifted the attention to Palaeoproterozoic glaciation as reflected by the occurrence of the Makganyene Formation, and the potential role of regional climatic trends in the deposition of the mixed, Fe/Mn-rich Hotazel Formation

In the northernmost parts of the KMF, the Hotazel iron-formation exhibits severe oxidation and leaching effects. The rock appears to have lost its entire carbonate component (mainly Ca, Mg, Sr, and possibly some Fe and Mn hosted in pre-existing carbonates) and shows substantial mass loss of 15-20%, accompanied by residual enrichments in Fe, Si and trace elements such as Cr, Ni, V, Th, and Pb. Oxygen isotope compositions from the essentially only two main mineral constituents, i.e. chert and hematite, indicate that the former remained isotopically unexchanged

during alteration, whereas the latter shows clear depletion ( $\delta^{18}\text{O} \sim -1\%$ ) relative to its main precursor magnetite ( $\delta^{18}\text{O} \sim -2\%$ ) from unaltered iron-formation. This isotopic shift would have been the result of the action of low-temperature, isotopically light meteoric waters ( $\delta^{18}\text{O} \sim 0\%$ ). It is therefore believed that low-temperature supergene processes that occurred prior to deposition of the Olifantshoek rocks were primarily responsible for the alteration and economic upgrading of the Hotazel iron-formation and Mn ores. Also, the antithetic thickness-grade relation has been previously proposed on the basis of data from the Mn ores, and was further verified as a useful exploration tool in this thesis. Therefore, borehole-log thickness measurements and mere macroscopic observations of newly-obtained borehole-core material, can offer an adequate estimation of the expected quality of manganese ores in future prospecting.

It is of note that certain geological features (e.g. dyke intrusives) seem to have had a much more significant effect on the distribution and degree of alteration/upgrading of the deposits than others (e.g. normal faults). The recognition of a Mg/Mn/Fe-enriched iron-formation in close proximity to the dykes would suggest that, in such areas, re-precipitation of solutes derived from intensive leaching of the Hotazel rocks is likely to have taken place. This may provide a useful exploration tool in the northernmost KMF in the delineation of further areas containing high-grade and low-grade manganese mineralisation. Finally, the localised occurrence of acmite-rich iron-formation is regarded as a later metasomatic event of little significance with respect to the main alteration process that economically upgraded the Kalahari Mn-ores.

The data presented in this thesis will hopefully constitute at least a useful framework for future research in the KMF, as potential prospects for further study are far from exhausted. Rare-earth element studies across the Hotazel stratigraphy in areas where incipient and/or intense alteration occurs, have the potential of generating further geochemical evidence on the physicochemical attributes of the alteration process/es. Also, stable isotope studies of carbonate minerals from unaltered iron-formation and manganese ore have shed further light on the deposition and diagenesis of the Hotazel succession, and they could be substantially expanded with Sr-isotopic studies and, possibly, Pb-Pb and U-Pb isotope systematics.

Underground traverse sampling of iron-formation in areas adjacent to dykes would provide an

ideal platform upon which the controlling factors, lateral extent and spatial geochemical signatures of alteration could be further evaluated and interpreted by means of standard petrographic and bulk geochemical studies. Stable isotope investigations of oxidised iron-formation may also supply additional information with respect to later alteration processes, as long as the isotope signatures of carbonates from such rocks are not “buffered” by earlier events (e.g. diagenesis). Furthermore, despite apparent limitations posed by the particularly fine-grained nature of the Hotazel rocks, O-isotope investigations of co-existing Mn-oxides may prove useful in unravelling further the alteration history and associated economic upgrading of manganese ore from the northern parts of the KMF.

It is the author’s main intention to follow up on at least some of the above-mentioned aspects shortly after the completion of this thesis. The widely acclaimed perception amongst many that the chief aim of a PhD project of this nature is to provide long-awaited solutions and hard-sought answers, has once again been defeated. What this study has definitely achieved, is to profoundly prove that research in a specific field does not end with a Doctoral thesis, and that by breaking new grounds more prospects will naturally emerge. Invariably, many aspects concerning the origin of the KMF shall remain enigmatic, and future research studies in conjunction with the results of this work will certainly provide further valuable insight. It is hoped that this remarkable deposit will soon be converted into a constant source of information on the evolutionary processes of the early earth, and how these may have yielded some of the richest mineral resources the modern world is privileged to exploit.

## PART 6: REFERENCES

- Al-Aasm, I.S., Taylor, B.E., and South, B., 1990**, Stable isotope analysis of multiple carbonate samples using selective acid extraction: *Chem. Geol. (Isot. Geosc. Sect.)*, v. 80, p. 119-125.
- Alibert, C., and McCulloch, M.T., 1993**, Rare earth element and neodymium isotopic compositions of the banded iron-formations and associated shales from Hamersley, western Australia: *Geoch. Cosm. Acta*, v. 57, p. 187-204.
- Altermann, W., and Hälbich, I.W., 1990**, Thrusting, folding and stratigraphy of the Ghaap Group along the south-western margin of the Kaapvaal Craton: *S. Afr. J. Geol.*, v. 93, p.556-616.
- Altermann, W., and Hälbich, I.W., 1991**, Structural history of the southwestern corner of the Kaapvaal Craton and the adjacent Namaqua realm: new observations and a reappraisal: *Prec. Res.*, 52, p. 133-166.
- Anbar, A.D., and Holland, H.D., 1992**, The photochemistry of manganese and the origin of banded iron-formations: *Geoch. Cosm. Acta*, v. 56, p. 2595-2603.
- Appel, P.W.U., 1983**, Rare-earth elements in the Early Archaean Isua iron-formation, West Greenland: *Prec. Res.*, v. 20, p. 243-258.
- Arora, M., Govil, P.K., Charan, S.N., Uday Raj, B., Balaram, V., Manikyama, C., Chatterjee, A.K., and Naqvi, S.M., 1995**, Geochemistry and origin of Archaean banded iron-formation from the Bababudan schist belt, India: *Econ. Geol.*, v. 90, p. 2040-2057.
- Astrup, J., and Tsikos, H., 1998**, Manganese, in: Mineral resources of southern Africa, eds, Wilson, M.J., and Anhaeusser, C.R: *Handbook 16, Council for Geoscience*, Pretoria, South Africa, p. 450-460.
- Banerji, A.K., 1977**, On the Precambrian iron-formations and the manganese ores of the Singhbhum Region, Eastern India: *Econ. Geol.*, v. 72, p. 90-98.
- Bao, H., and Koch, P.L., 1999**, Oxygen isotope fractionation in ferric oxide-water systems: low temperature synthesis: *Geoch. Cosm. Acta*, v. 63, p. 599-613.
- Barrett, T.J., Fralick, P.W., and Jarvis, I., 1988**, Rare-earth element geochemistry of some Archaean iron-formations north of Lake Superior, Ontario: *Can. J. Earth Sci.*, v. 25, p. 570-580.
- Bau, M., and Möller, P., 1993**, Rare-earth element systematics of the chemically precipitated component in Early Precambrian iron-formations and the evolution of the terrestrial atmosphere-hydrosphere-lithosphere system: *Geoch. Cosm. Acta*, v. 57, p. 2239-2249.

- Bau, M., and Dulski, P., 1996**, Distribution of yttrium and rare-earth elements in the Penge and Kuruman iron-formations, Transvaal Supergroup, South Africa: *Prec. Res.*, v. 79, p. 37-56.
- Bau, M., Koschinsky, A., Dulski, P., and Hein, J.R., 1996**, Comparison of the partitioning behaviours of yttrium, rare-earth elements, and titanium between hydrogenetic marine ferromanganese crusts and seawater: *Geoch. Cosm. Acta*, v. 60, 1709-1725.
- Baumgartner, L.P., and Olsen, S.N., 1995**, A least-squares approach to mass transport calculations using the isocon method: *Econ. Geol.*, v. 89, p. 1261-1270.
- Baur, M.E., Hayes, J.M., Studley, S.A., and Walter, M.R., 1985**, Millimeter-scale variations of stable isotope abundances in carbonates from banded iron-formations in the Hamersley Group, Western Australia: *Econ. Geol.*, v. 80, p. 270-282.
- Becker, R.H., and Clayton, R.N., 1972**, Carbon isotopic evidence for the origin of a banded iron-formation in Western Australia: *Geoch. Cosm. Acta*, v. 36, p. 577-595.
- Becker, R.H., and Clayton, R.N., 1976**, Oxygen isotope study of a Precambrian banded iron-formation, Hamersley Range, West. Australia: *Geoch. Cosm. Acta*, v. 40, p. 1153-1165.
- Beukes, N.J., 1973**, Precambrian iron-formations of Southern Africa: *Econ. Geol.*, v. 68, p. 960-1004.
- Beukes, N.J., 1978**, Die karbonaatgesteendes en ysterformasies van die Ghaap-Groep van die Transvaal-Supergroep in Noord-Kaapland: *Unpublished PhD thesis*, Rand Afrikaans Univ., Johannesburg, 580 p.
- Beukes, N.J., 1980a**, Lithofacies and stratigraphy of the Kuruman and Griquatown iron-formations, Northern Cape Province, South Africa: *Trans. Geol. Soc. S. Afr.*, v. 83, p. 69-86.
- Beukes, N.J., 1980b**, Suggestions towards a classification of, and nomenclature for iron-formation: *Trans. Geol. Soc. S. Afr.*, v. 83, p. 285-290.
- Beukes, N.J., 1983**, Palaeoenvironmental setting of iron-formations in the depositional basin of the Transvaal Supergroup, South Africa, in: Iron-formations: facts and problems, eds., Trendall, A.F., and Morris, R.C.: *Developments in Precambrian Geology 6*, Elsevier Sci. Pbl., p. 131-209.
- Beukes, N.J., 1984**, Sedimentology of the Kuruman and Griquatown iron-formations, Transvaal Supergroup, Griqualand West, South Africa: *Prec. Res.*, v. 24, p. 47-84.
- Beukes, N.J., 1986**, The Transvaal Sequence in Griqualand West, in: Mineral deposits of southern Africa, eds., C.R. Anhaeusser, and S. Maske: *Geol. Soc. S. Afr.*, v. I, p. 819-828.
- Beukes, N.J., 1992**, Some comments on the view by J.E. de Villiers that the Griqualand West



manganese and iron-ore deposits are of hydrothermal origin: *S. Afr. J. Sci.*, v. 88, p. 15-17.

**Beukes, N.J., 1993**, A review of manganese deposits associated with the Early Proterozoic Transvaal Supergroup in Northern Cape province, South Africa: *Extended abstracts, 16th Colloquium of African Geology, Swaziland*, v. I, p. 37-39.

**Beukes, N.J., and Dreyer, C.J.B., 1986**, Crocidolite deposits of the Pomfret Area, Griqualand West, in: Mineral deposits of Southern Africa, eds., Anhaeusser, C.R., and Maske, S.: *Geol. Soc. S. Afr.*, v. I, p. 911-921.

**Beukes, N.J., and Smit, C.A., 1987**, New evidence for thrust faulting in Griqualand West, South Africa: implications for stratigraphy and the age of red beds: *S. Afr. J. Geol.*, v. 90(4), p. 378-394.

**Beukes, N.J., and Klein, C., 1990**, Geochemistry and sedimentology of a facies transition-from microbanded to granular iron-formation-in the Early Proterozoic Transvaal Supergroup, South Africa: *Prec. Res.*, v. 47, p. 99-139.

**Beukes, N.J., and Gutzmer, J., 1996**, A volcanic-exhalative origin for the world's largest (Kalahari) Manganese field: A discussion of a paper by D.H. Cornell and S.S. Schütte: *Mineral. Dep.*, v. 31, p. 242-245.

**Beukes, N.J., Kleyenstüber, A., and Nel, C., 1982**, Volcanogenic-sedimentary cycles in the Kalahari manganese field: *Abstracts, Sedimentology '82, Geol. Soc. S. Afr.*, p. 93-97.

**Beukes, N.J., Klein, C., Kaufman, A.J., and Hayes, J.M., 1990**, Carbonate petrography, kerogen distribution, and carbon and oxygen isotope variations in an Early Proterozoic transition from limestone to iron-formation deposition, Transvaal Supergroup, South Africa: *Econ. Geol.*, v. 85, p. 663-690.

**Beukes, N.J., Burger, A.M., and Gutzmer, J., 1995**, Fault-controlled hydrothermal alteration of Palaeoproterozoic manganese ore in Wessels mine, Kalahari manganese Field: *S. Afr. J. Geol.*, v. 98(4), p. 430-451.

**Blake, R.L., 1965**, Iron phyllosilicates of the Cuyuna district in Minnesota: *Amer. Min.*, v. 50, p. 148-169.

**Blattner, P., Braithwaite, W.R., and Glover, R.B., 1983**, New evidence on magnetite oxygen isotope geothermometers at 175° and 112°C in Wairakei steam pipelines (New Zealand): *Chem. Geol. (Isot. Geosc. Sect.)*, v. 1, p. 195-204.

**Boardman, L.G., 1941**, The Black Rock manganese deposit in the south-eastern Kalahari: *Trans. Geol. Soc. S. Afr.*, v. 44, p. 51-60.

- Boardman, L.G., 1964**, Further geological data on the Postmasburg and Kuruman manganese ore-deposits, Northern Cape Province, in: *The Geology of some ore deposits in Southern Africa*, ed., Haughton, S.H.: *Geol. Soc. S. Afr.*, v. II, p. 415-440.
- Bonatti, E., Zerbi, M., Kay, R., and Rydell, H., 1976**, Metalliferous deposits from the Apennine ophiolites: Mesozoic equivalents of modern deposits from oceanic spreading centers: *Geol. Soc. Am. Bull.*, v. 87, p. 83-94.
- Borthwick, J., and Harmon, R.S., 1982**, A note regarding  $\text{ClF}_3$  as an alternative to  $\text{BrF}_3$  for oxygen isotope analysis: *Geoch. Cosm. Acta*, v. 46, p. 1665-1668.
- Bottinga, Y., and Javoy, M., 1973**, Comments on oxygen isotope geothermometry: *Earth Plan. Sci. Let.*, v. 20, p. 250-265.
- Boudraeu, B.P., 1987**, A steady-state diagenetic model for dissolved carbonate species and pH in the porewaters of oxic and suboxic sediments: *Geoch. Cosm. Acta*, v. 51, p. 1985-1996.
- Bradley, W.H., and Eugster, H.P., 1969**, Geochemistry and paleolimnology of the trona deposits and associated authigenic minerals of the Green River Formation of Wyoming: *U.S. Geol. Sur. Prof. Pap. 496-B*, 71 p.
- Braterman, P.S., Cairns-Smith, A.G., and Sloper, R., 1983**, Photo-oxidation of hydrated  $\text{Fe}^{2+}$  - significance for banded iron formations: *Nature*, v. 303, p. 163-164.
- Brookins, D.G., 1988**, Eh-pH diagrams for geochemistry: *Springer-Verlag*, 176 p.
- Brooks, C., 1977**, Archaean variolites: Source of iron in the Precambrian environment?: *Can. J. Earth Sci.*, v. 14, p. 511-513.
- Bühn, B., Stanistreet, I.G., and Okrusch, M., 1992**, Late Proterozoic outer shelf manganese and iron deposits at Otjosondu (Namibia) related to the Damaran oceanic opening: *Econ. Geol.*, v. 87, p. 1393-1411.
- Buick, I.S., Uken, R., Gibson, R.L., and Wallmach, T., 1998**, High- $\delta^{13}\text{C}$  Paleoproterozoic carbonates from the Transvaal Supergroup, South Africa: *Geol.*, v. 26, p. 875-878.
- Burger, A.M., 1994**, Fault-controlled hydrothermal alteration of Palaeoproterozoic manganese ore in Wessels mine, Kalahari manganese field: *Unpublished MSc thesis, Rand Afrikaans Univ., Johannesburg*, 138 p.
- Button, A., 1986**, The Transvaal sub-basin of the Transvaal sequence, in: *Mineral deposits of Southern Africa*, eds., C.R. Anhaeusser, and S. Maske: *Geol. Soc. S. Afr.*, v. I, p. 811-817.
- Button, A., Brock, T.D., Cook, P.J., Eugster, H.P., Goodwin, A.M., James, H.L., Margulis,**

- L., Neelson, K.H., Nriagu, J.O., Trendall, A.F., and Walter, M.R., 1982, Sedimentary iron deposits, evaporites and phosphorites-state of the art report, in: Mineral deposits and the evolution of the biosphere (Dahlem Konferenzen), eds., H.D. Holland, and M. Schidlowski: *Springer-Verlag*, p. 259-273.
- Cairns-Smith, A.G., 1978, Precambrian solution photochemistry, inverse segregation and banded iron-formations: *Nature*, v. 276, p. 807-808.
- Carrigan, W.J., and Cameron, E.M., 1991, Petrological and stable isotope studies of carbonate and sulfide minerals from the Gunflint iron-formation, Ontario: evidence for the origin of Early Proterozoic iron-formation: *Prec. Res.*, v. 52, p. 347-380.
- Catuneanu, O., and Eriksson, P.G., 1999, The sequence stratigraphic concept and the Precambrian rock record: an example from the 2-7-2.1 ga Transvaal Supergroup, Kaapvaal Craton. *Prec. Res.*, in press.
- Chauvel, J.J., and Dimroth E., 1974, Facies types and depositional environment of the Sokoman iron-formation, central Labrador Trough, Quebec, Canada: *J. Sed. Petr.*, v. 44, #2, p.299-327.
- Cheney, E.S., and Winter, H. de la R., 1995, The late Archaean to Mesoproterozoic major unconformity-bounded units of the Kaapvaal of southern Africa: *Prec. Res.*, v. 74, p. 203-223.
- Clendenin, C.W., Charlesworth, E.G., and Maske, S., 1988a, An early Proterozoic three-stage rift system, Kaapvaal Craton, South Africa: *Tectonophysics*, v. 145, p. 73-86.
- Clendenin, C.W., Charlesworth, E.G., and Maske, S., 1988b, Tectonic style and mechanism of early Proterozoic successor basin development, southern Africa: *Tectonophysics*, v. 156, p. 275-291.
- Cloud, P., 1968, Atmospheric and hydrospheric evolution of the primitive Earth: *Science*, v. 160, p. 729-736.
- Cloud, P., 1972, A working model of the primitive earth: *Am. J. Sci.*, v. 272, p. 537-548.
- Cloud, P., 1973, Paleoecological significance of the banded iron-formation: *Econ. Geol.*, v. 68, p. 135-1143.
- Coplen, T.B., Kendall, C., and Hopple, J., 1983, Comparison of stable isotope reference samples: *Nature*, v. 302, p. 236-238.
- Cornell, D.H., and Schütte, S.S., 1995, A volcanic exhalative model for the world's largest (Kalahari) Manganese field: *Mineral. Dep.*, v.30, p.146-151.

- Cornell, D.H., and Schütte, S.S., 1996**, Reply to the discussion by N.J. Beukes and J. Gutzmer: *Mineral. Dep.*, v. 31, p. 246-247.
- Cornell, D.H., Schütte, S.S., and Eglington, B.L. 1996**, The Ongeluk basaltic andesite formation in Griqualand West, South Africa: submarine alteration in a 2222 Ma Proterozoic sea. *Prec. Res.*, v. 79, p. 101-124.
- Cornell, D.H., Armstrong, R.A., and Walraven, F., 1998**, Geochronology of the Proterozoic Hartley Basalt Formation, South Africa: constraints on the Kheis tectogenesis and the Kaapvaal Craton's earliest Wilson Cycle: *J. Afr. Earth Sci.*, v. 26, pp. 5-27.
- Crerar, D.A., Namson, J., Chyi, M.S., Williams, L., and Feigenson, M.D., 1982**, Manganiferous cherts of the Franciscan assemblage: I. General geology, ancient and modern analogues, and implications for hydrothermal convection at oceanic spreading centers: *Econ. Geol.*, v. 77, p. 519-540.
- Criss, R.E., Gregory, R.T., and Taylor, H.P.Jr, 1987**, Kinetic theory of oxygen isotopic exchange between minerals and water: *Geoch. Cosm. Acta*, v. 51, p. 1099-1108.
- Danielson, A., Möller, P., and Dulski, P., 1992**, The Europium anomalies in banded iron-formations and the thermal history of the oceanic crust: *Chem. Geol.*, v. 97, p. 89-100.
- Davy, R., 1983**, A contribution on the chemical composition of Precambrian iron-formations, in: Iron-formations: facts and problems, eds., Trendall, A.F., and Morris, R.C.: *Developments in Precambrian Geology 6, Elsevier Sci. Pbl.*, p. 325-343.
- Derry, L.A., and Jacobsen, S.B., 1990**, The chemical evolution of Precambrian seawater: evidence from REE in banded iron-formations: *Geoch. Cosm. Acta*, v. 54, p. 2965-2977.
- De Villiers, J., 1960**, The manganese deposits of the Union of South Africa: *S. Afr. Geol. Sur., Handbook 2*, 280 p.
- De Villiers, P.R., 1970**, The geology and mineralogy of the Kalahari manganese field north of Sishen, Cape Province: *S. Afr. Geol. Sur. Mem. 59*, 65 p.
- De Villiers, J.E., 1943a**, A preliminary description of the new mineral partridgeite: *Amer. Min.*, v. 28, p. 336-338.
- De Villiers, J.E., 1943b**, Gamagarite, a new vanadium mineral from the Postmasburg manganese deposits: *Amer. Min.*, p. 28, p. 329-335.
- De Villiers, J.E., 1945a**, Some minerals occurring in South African manganese deposits: *Trans. Geol. Soc. S. Afr.*, v. 48, p. 17-25.

- De Villiers, J.E., 1945b**, Lithiophorite from the Postmasburg manganese deposits: *Amer. Min.*, v. 30, p. 629-634.
- De Villiers, J.E., 1983**, The manganese deposits of Griqualand West, South Africa: some mineralogical aspects: *Econ. Geol.*, v. 78, p. 1108-1118.
- De Villiers, J.E., 1986**, "The mineralogy of the manganese-bearing Hotazel formation, of the Proterozoic Transvaal Sequence in Griqualand West, South Africa"-discussion: *Trans. Geol. Soc. S. Afr.*, v. 89, p. 421-423.
- De Villiers, J.E., 1992**, On the origin of the Griqualand West manganese and iron deposits: *S. Afr. J. Sci.*, v. 88, p. 12-15.
- Dimroth, E., 1975**, Paleoenvironment of iron-rich sedimentary rocks: *Geol. Rud.*, v. 64, p. 751-767.
- Dimroth, E., 1976**, Aspects of the sedimentary petrology of cherty iron-formation, in: Handbook of strata-bound and stratiform ore-deposits, ed., Wolf, K.H.: *Elsevier Sci. Pbl.*, v. 7, 656 p.
- Dimroth, E., and Chauvel, J.J., 1973**, Petrography of the Sokoman iron-formation in part of the central Labrador Trough, Quebec, Canada: *Geol. Soc. Am. Bull.*, v. 84, p. 111-134.
- Dimroth, E., and Kimberley, M.M., 1976**, Precambrian atmospheric oxygen: evidence in the sedimentary distributions of carbon, sulfur, uranium, and iron: *Can. J. Earth Sci.*, v. 13, #9, p. 1161-1185.
- Dirr, H.V.D., and Beukes, N.J., 1990**, Sedimentology and geochemistry of mangiferous marls, stromatolitic carbonates and banded iron-formation, Transvaal Supergroup, Griqualand West: *Abstracts, Geocongress '90, Geol. Soc. S. Afr.*, p. 127-130.
- Dixon, R., 1985**, Sugilite and associated minerals from Wessels mine, Kalahari manganese field: *Trans. Geol. Soc. S. Afr.*, v. 88, p. 11-17.
- Dixon, R., 1989**, Sugilite and associated metamorphic silicate minerals from Wessels mine, Kalahari manganese field: *Dep. Min. En. Aff., Geol. Surv. S. Afr.*, Bull. 93, 47 p.
- Dorr, J.V.N., 1973a**, Iron-formation and associated manganese in Brazil, in: Genesis of Precambrian iron and manganese deposits: *Proc. Kiev Symposium 1970, UNESCO Paris*, p. 105-113.
- Dorr, J.V.N., 1973b**, Iron-formation in South America: *Econ. Geol.*, v. 68, p. 1005-1022.
- Drever, J.I., 1974**, Geochemical model for the origin of Precambrian banded iron-formations: *Geol. Soc. Am. Bull.*, v. 85, p. 1099-1106.

- Dunn, P.J., Brummer, J.J., and Belsky, H., 1980**, Sugilite, a second occurrence: Wessels mine, Kalahari manganese field, Republic of South Africa: *Can. Min.*, v. 18, p. 37-39.
- Dymek, R.F., and Klein, C., 1988**, Chemistry, petrology and origin of banded iron-formation lithologies from the 3800 ma Isua supracrustal belt, West Greenland: *Prec. Res.*, v. 39, p. 247-302.
- Elderfield, H., 1988**, The oceanic chemistry of the rare-earth elements. *Philos. Trans. R. Soc. London*, v. A325, p. 105-126.
- Elderfield, H., and Greaves, M.J., 1982**, The rare earth elements in seawater: *Nature*, v. 296, p. 214-219.
- Emerson, S., Jahnke, R., Bender, M., Froelich, P., Klinkhammer, G., Bowser, C., and Setlock, G., 1980**, Early diagenesis in sediments from the eastern equatorial Pacific, I. Pore water nutrient and carbonate results: *Earth Plan. Sci. Lett.*, v. 49, p. 57-80.
- Eugster, H.P., and Ming Chou, I., 1973**, The depositional environments of Precambrian banded iron-formations: *Econ. Geol.*, v. 68, p. 1144-1168.
- Evans, D.A., Beukes, N.J., and Kirschvink, J.L., 1997**, Low-latitude glaciation in the Palaeoproterozoic era: *Nature*, v. 386, p. 262-266.
- Ewers, W.E., and Morris, R.C., 1981**, Studies of the Dales Gorge member of the Brockman iron-formation, Western Australia: *Econ. Geol.*, v. 76, p. 1929-1953.
- Fetherston, J.M., 1990**, Manganese, in: Geology and mineral resources of Western Australia: *Geol. Sur. W. Austr.*, Mem. 3, p. 693-694.
- Floran, R.J., and Papike, J.J., 1975**, Petrology of the low-grade rocks of the Gunflint iron-formation, Ontario-Minnesota: *Geol. Soc. Am. Bull.*, v. 86, p. 1169-1190.
- Floran, R.J., and Papike, J.J., 1978**, Mineralogy and petrology of the Gunflint iron-formation, Minnesota-Ontario: Correlation of compositional and assemblage variations at low to moderate grade: *J. Petr.*, v. 19, p. 215-288.
- Force, E.R., and Cannon, W.F., 1988**, Depositional model for shallow-marine manganese deposits around black shale basins: *Econ. Geol.*, v. 81, p. 93-117.
- Frakes, L.A., 1979**, Climates throughout geologic time: *Elsevier Sci. Publ.*, 310 p.
- Frakes, L.A., and Bolton, B.R., 1984**, Origin of manganese giants: Sea-level change and anoxic-oxic history: *Geol.*, v. 12, p. 83-86.
- Frakes, L.A., and Bolton, B.R., 1992**, Effects of ocean chemistry, sea level, and climate on the

- formation of primary sedimentary manganese ore-deposits: *Econ. Geol.*, v. 87, p. 1207-1217.
- François, L.M., 1986**, Extensive deposition of banded iron-formation was possible without photosynthesis: *Nature*, v. 320, p. 352-354.
- Frankel, J.J., 1958**, Manganese ores from the Kuruman district, Cape Province, South Africa: *Econ. Geol.*, v. 53, p. 577-597.
- French, B.M., 1968**, Progressive contact metamorphism of the Biwabik iron-formation, Mesabi Range, Minnesota: *Minn. Geol. Sur. Bull.*, v. 45, 103 p.
- French, B.M., 1973**, Mineral assemblages in diagenetic and low-grade metamorphic iron-formation: *Econ. Geol.*, v. 68, p. 1063-1074.
- Friedman, I., and O'Neil, J.R., 1977**, Compilation of stable isotope fractionation factors of geochemical interest: *Data of Geochemistry, 6th ed., Geol. Sur. Prof. Pap., Washington, 440-KK*, 49 fig.
- Fröelich, P.N., Klinkhammer, G.P., Bender, M.L., Luedtke, N.A., Heath, G.R., Cullen, D., Dauphin, P., Hammond, D., Hartman, P., and Maynard, V., 1979**, Early oxidation of organic matter in pelagic sediments of the eastern equatorial Atlantic: suboxic diagenesis: *Geoch. Cosm. Acta*, v. 43, p. 1075-1090.
- Garrels, R.M., 1987**, A model for the deposition of the microbanded Precambrian iron-formations: *Am. J. Sci.*, v. 287, p. 81-106.
- Garrels, R.M., Perry, E.A., and Mackenzie, F.T., 1973**, Genesis of Precambrian iron-formations and the development of atmospheric oxygen: *Econ. Geol.*, v. 68, p. 1173-1179.
- Garven, G., Person, M.A., and Sverjensky, D.A., 1993**, Genesis of stratabound ore deposits in the midcontinent basins of North America. 1. The role of regional groundwater flow: *Am. J. Sci.*, v. 293, p. 497-568.
- Gnaneshwar Rao, T., and Naqvi, S.M., 1995**, Geochemistry, depositional environment and tectonic setting of the BIF's of the late Archaean Chitradurga Schist Belt, India: *Chem. Geol.*, v. 121, p. 217-243.
- Gole, M.J., 1980**, Mineralogy and petrology of very low-metamorphic grade Archaean banded iron-formations, Weld Range, Western Australia: *Am. Min.*, v. 65, p. 8-25.
- Gole, M.J., 1981**, Archaean banded-iron formations, Yilgarn Block, Western Australia: *Econ. Geol.*, v. 76, p. 1954-1974.
- Gole, M.J., and Klein, C., 1981**, Banded iron-formations through much of Precambrian time:

*J. Geol.*, v. 89, p. 169-183.

**Gonfiantini, R., 1978**, Standards for stable isotope measurements in natural compounds: *Nature*, v. 271, p. 534-536.

**Goodwin, A.M., 1956**, Facies relations in the Gunflint iron-formation: *Econ. Geol.*, v. 51, p. 565-595.

**Govett G.J.S., 1966**, Origin of banded iron-formations: *Geol. Soc. Am. Bull.*, v. 77, p. 1191-1212.

**Graf, J.L.Jr., 1978**, Rare-earth elements, iron-formations and sea-water: *Geoch. Cosm. Acta*, v. 42, p. 1845-1850.

**Grant, J.A., 1986**, The isocon diagram—a simple solution to Gresens' equation for metasomatic alteration: *Econ. Geol.*, v. 81, p. 1976-1982.

**Gregory, R.T., 1986**, Oxygen isotope systematics of quartz-magnetite pairs from Precambrian iron-formations: evidence for fluid-rock interaction during diagenesis and metamorphism, in: Fluid-rock interactions during metamorphism, eds., Walther, J.V., and Wood, B.J.: *Adv. in Phys. Geochem.*, v. 5, Springer-Verlag, p. 132-153.

**Gregory, R.T., 1990**, Mineral pairs as stable isotopic monitors of fluid-rock interaction in the lithosphere, in: Stable isotopes and fluid processes in mineralization, eds., Herbert, H.K., and Ho, S.E.: *Geol. Dep. & Univ. Ext., Univ. of Western Australia, publication No. 23*, p. 177-203.

**Gregory, R.T., Criss, R.E., and Taylor, H.P.Jr., 1989**, Oxygen isotope exchange kinetics of mineral pairs in closed and open systems: applications to problems of hydrothermal alteration of igneous rocks and Precambrian Iron Formations: *Chem. Geol.*, v. 75, p. 1-42.

**Gresens, R.L., 1967**, Composition-volume relationships of metasomatism: *Chem. Geol.*, v. 2, p. 47-65.

**Grobbelaar, W.S., Burger, M.A., Pretorius, A.I., Marais, W., and van Niekerk, I.J.M., 1995**, Stratigraphic and structural setting of the Griqualand West and the Olifantshoek Sequences at Black Rock, Beeshoek and Rooinekke Mines, Griqualand West, South Africa: *Mineral. Dep.*, v. 30, p. 152-161.

**Gromet, L.P., Dymek, R.F., Haskin, L.A., and Korotev, R.L., 1984**, The "North American Shale Composite": its compilation, major and trace element characteristics: *Geoch. Cosm. Acta*, 48, p. 2469-2482.

**Gross, G.A., 1965**, Geology of iron Deposits in Canada: general geology and evaluation of iron



- deposits: *Dep. of Mines and Tech. Surveys, Econ. Geol. rep.* #22, v. I, 173 p.
- Gross, G.A., 1972**, Primary features in cherty iron-formations: *Sed. Geol.*, v. 7, p. 241-261.
- Gross, G.A., 1973**, The depositional environment of principal types of Precambrian iron-formations, in: Genesis of Precambrian iron and manganese deposits: *Proc. Kiev Symposium 1970, UNESCO Paris*, p. 15-21.
- Gross, G.A., 1980**, A classification of iron-formations based on depositional environments: *Can. Min.*, v. 18, p. 215-222.
- Gross, G.A., 1983**, Tectonic systems and the deposition of iron-formation: *Prec. Res.*, v. 20, p. 171-187.
- Gross, G.A., 1990**, Geochemistry of iron-formation in Canada, in: Ancient banded iron-formations (regional presentations): *Theophrastus publ., Athens*, p. 3-26.
- Gross, G.A., and McLeod, C.R., 1980**, A preliminary assessment of the chemical composition of iron-Formations in Canada: *Can. Min.*, v. 18, p. 223-229.
- Gross, G.A., and Zajac, I.S., 1983**, Iron-formation in fold belts marginal to the Ungava Craton, in: Iron-formations: Facts and problems, eds., Trendall, A.F., and Morris, R.C.: *Developments in Precambrian Geology 6, Elsevier Sci. Pbl.*, p. 253-294.
- Grout, F.F., 1946**, Acmite occurrences on the Cuyuna Range, Minnesota: *Am. Min.*, v. 31, p. 125-130.
- Gruner, J.W., 1922**, The origin of sedimentary iron-formations-the Biwabik formation of the Mesabi range: *Econ. Geol.*, v. 17, #6, p. 407-460.
- Gruner, J.W., 1936**, The structure and chemical composition of greenalite: *Am. Min.*, v. 21, p. 449-455.
- Gruner, J.W., 1937**, Composition and structure of stilpnomelane: *Am. Min.*, v. 22, p. 912-925.
- Gruner, J.W., 1944a**, The structure of stilpnomelane re-examined: *Am. Min.*, v. 29, p. 291-298.
- Gruner, J.W., 1944b**, The composition and structure of minnesotaite, a common iron-silicate in iron-formations: *Am. Min.*, v. 29, p. 363-372.
- Gutzmer, J., 1996**, Genesis and alteration of the Kalahari and Postmasburg manganese deposits, Griqualand West, South Africa: *Unpubl. PhD thesis, Rand Afrikaans Univ., Johannesburg, South Africa*, 266 p.
- Gutzmer, J., and Beukes, N.J., 1992**, Fault-controlled hematitization and hydrothermal alteration from low-grade to high-grade manganese ore, Nchwaning mine, Kalahari Manganese

Field: *Unpublished report, Rand Afrikaans Univ., Johannesburg, South Africa*, 152 p.

**Gutzmer, J., and Beukes, N.J., 1993**, Fault zone-controlled hematitization and upgrading of manganese ores in the Kalahari manganese field, South Africa: *Extended abstracts, 16th Colloquium of African Geology, Swaziland*, vol. I, p. 139-142.

**Gutzmer, J., and Beukes, N.J., 1995**, Fault-controlled metasomatic alteration of early Proterozoic sedimentary manganese ores in the Kalahari manganese field, South Africa: *Econ. Geol.*, v. 90, p. 823-844.

**Gutzmer, J., and Beukes, N.J., 1996a**, Mineral paragenesis of the Kalahari manganese field, South Africa: *Ore Geol. Rev.*, v. 11, p. 405-428.

**Gutzmer, J., and Beukes, N.J., 1996b**, Karst-hosted, fresh water, Paleoproterozoic manganese deposits, Postmasburg, South Africa: *Econ. Geol.*, v. 91, p. 1435-1454.

**Gutzmer, J., and Beukes, N.J., 1997**, Effects of mass transfer, compaction and secondary porosity on hydrothermal upgrading of Paleoproterozoic sedimentary manganese ore in the Kalahari manganese field, South Africa: *Mineral. Dep.*, v. 32, p. 250-256.

**Gutzmer, J., and Beukes, N.J., 1998a**, Earliest laterites and possible evidence for terrestrial vegetation in the early Proterozoic: *Geol.*, v. 26, p. 263-266.

**Gutzmer, J., and Beukes, N.J., 1998b**, The manganese formation of the Neoproterozoic Penganga Group, India-revision of an enigma: *Econ. Geol.*, v. 93, p. 1091-1102.

**Gutzmer, J., Beukes, N.J., and Yeh, H.-W. 1997**, Fault-controlled metasomatic alteration of early Proterozoic sedimentary manganese ore at Mamatwan mine, Kalahari manganese field, South Africa: *S. Afr. J. Geol.*, v. 100, p. 53-71.

**Hälbich, I.W., Scheepers, R., Lamprecht, D., van Deventer, J.L., and De Kock, N.J., 1993**, The Transvaal-Griqualand West banded iron-formation: geology, genesis, iron exploitation: *J. Afr. Earth Sci.*, v. 16, p. 63-120.

**Heinrich, K.F.J., 1996**, X-ray absorption uncertainty, in: *The electron microprobe*, eds., Macinley, T.D., Heinrich, K.F.J., and Wittry, D.B.: *John Wiley and Sons, New York*, p. 269-377.

**Hoefs, J., 1987**, Stable isotope geochemistry: *Springer-Verlag*, 241 p.

**Hoefs, J., Müller, G., and Schuster, A.K., 1982**, Polymetamorphic relations in iron ores from the iron quadrangle, Brazil: the correlation of oxygen isotope variations with deformation history: *Con. Min. Pet.*, v. 79, p. 241-251.

**Hoefs, J., Müller, G., Schuster, and Walde, D., 1987**, The Fe-Mn ore deposits of Urucum,

Brazil: an oxygen isotope study: *Chem. Geol.*, v. 65, p. 311-319.

**Hofmann, P.F., Kaufman, A.J., Halverson, G.P., and Schrag, D.P., 1998**, A Neoproterozoic snowball Earth: *Science*, v. 281, p. 1342-1346.

**Holland, H.D., 1973**, The oceans: a possible source of iron in iron-formations: *Econ. Geol.*, v. 68, p. 1169-1172.

**Holland, H.D., 1984**, The chemical evolution of the atmosphere and oceans: *Princeton, N.J., Princeton Univ. Press*, 582 p.

**Holland, H.D., and Beukes, N.J., 1990**, A palaeoweathering profile from Griqualand West, South Africa: evidence for a dramatic rise in atmospheric oxygen between 2.2 and 1.9 BYBP: *Am. J. Sci.*, v. 290-A, p. 1-34.

**Horstmann, U.E., 1996**, C and O isotopic composition of Fe-carbonates from oxide-rich banded iron-formation of the Griqualand West Sequence, Northern Cape Province, South Africa: *Z. Geol. Wiss.*, v. 24, p. 687-698.

**Horstmann, U.E., and Hälbich, I.W., 1995**, Chemical composition of banded iron-formations of the Griqualand West Sequence, Northern Cape Province, South Africa, in comparison with other Precambrian iron-formations: *Prec. Res.*, v. 72, p. 109-145.

**Immega, I.P., and Klein, C., 1976**, Mineralogy and petrology of some metamorphic Precambrian iron-formations in Southwestern Montana: *Am. Min.*, v. 61, p. 1117-1144.

**Isley, A.E., 1995**, Hydrothermal plumes and the delivery of iron to banded iron-formation: *J. Geol.*, v. 103, p. 169-185.

**Jacobsen, S.B., and Pimentel-Klose M.R., 1988**, A Nd isotopic study of the Hamersley and Michipicoten banded iron-formations: the source of REE and Fe in Archaean oceans: *Earth Plan. Sci. Lett.*, v. 87, p. 29-44.

**James, H.L., 1954**, Sedimentary facies of iron-formation: *Econ. Geol.*, v. 49, p. 235-293.

**James, H.L., and Trendall, A.F., 1982**, Banded-iron formation: distribution in time and palaeoenvironmental significance, in: Mineral deposits and the evolution of the biosphere (Dahlem Konferenzen), eds., H.D. Holland and M. Schidlowski: *Springer-Verlag*, p. 199-218.

**JCPDS - Joint Committee on Powder Diffraction Standards (1st edition), 1974**, Selected powder diffraction data for minerals: *Philadelphia, USA*, 833 p.

**JCPDS - Joint Committee on Powder Diffraction Standards, (Search Manual), 1980**: *International centre for diffraction data, USA*, 484 p.

- Kaiser, H.F., 1958**, The varimax criteria for analytical relation in factor analysis: *Psychology*, v. 23, p. 187-200.
- Karhu, J.A., and Holland, H.D., 1996**, Carbon isotopes and the rise of atmospheric oxygen: *Geol.*, v. 24, p. 867-870.
- Kasting, J.F., 1987**, Theoretical constraints on oxygen and carbon dioxide concentrations in the Precambrian atmosphere: *Prec. Res.*, v. 34, p. 205-229.
- Kaufman, A.J., Hayes, J.M., and Klein, C., 1990**, Primary and diagenetic controls of isotopic compositions of iron-formation carbonates: *Geoch. Cosm. Acta*, v. 54, p. 3461-3473.
- Khan, R.M.K., and Naqvi, S.M., 1996**, Geology, geochemistry and genesis of BIF of Kushtagi schist belt, Archaean Dharwar Craton, India: *Mineral. Dep.*, v. 31, p. 123-133.
- Kimberley, M.M., 1978**, Palaeoenvironmental classification of iron-formations: *Econ. Geol.*, v. 73, p. 215-229.
- Kimberley, M.M., 1979**, Geochemical distinctions among environmental types of iron-formations: *Chem. Geol.*, v. 25, p. 185-212.
- Kimberley, M.M., 1989a**, Nomenclature for iron-formations: *Ore Geol. Rev.*, v. 5, p. 1-12.
- Kimberley, M.M., 1989b**, Exhalative origins of iron-formations: *Ore Geol. Rev.*, v. 5, p. 13-145.
- Kirkham, R.V., and Roscoe, S.M., 1993**, Atmospheric evolution and ore deposit formation: *Res. Geol. Sp. Issue*, #15., p. 1-17.
- Klein, C., 1966**, Mineralogy and petrology of the metamorphosed Wabush iron-formation, southwestern Labrador: *J. Petr.*, v. 7, p. 246-305.
- Klein, C., 1973**, Changes in mineral assemblages with metamorphism of some banded Precambrian iron-formations: *Econ. Geol.*, v. 68, p. 1075-1088.
- Klein, C., 1974**, Greenalite, stilpnomelane, minnesotaite, crocidolite and carbonates in a very low-grade metamorphic Precambrian iron-formation: *Can. Min.*, v. 12, p. 475-498.
- Klein, C., 1978**, Regional metamorphism of Proterozoic iron-formation, Labrador Trough, Canada: *Am. Min.*, v. 63, p. 898-912.
- Klein, C., 1983**, Diagenesis and metamorphism of Precambrian banded iron-formations, in: Iron-formations: Facts and problems, eds., Trendall, A.F., and Morris, R.C.: *Developments in Precambrian Geology 6*, Elsevier Sci. Pbl., p. 417-469.
- Klein, C., and Fink, R.P., 1976**, Petrology of the Sokoman iron-formation in the Howells River area, at the western edge of the Labrador Trough: *Econ. Geol.*, v. 71, p. 453-487.

- Klein, C., and Bricker, O.P., 1977**, Some aspects of the sedimentary and diagenetic environment of Proterozoic banded iron-formation: *Econ. Geol.*, v. 72, p. 1457-1470.
- Klein, C., and Gole, M.J., 1981**, Mineralogy and petrology of parts of the Mara Mamba iron-formation, Hamersley Basin, Western Australia: *Am. Min.*, v. 66, p. 507-525.
- Klein, C., and Beukes, N.J., 1989**, Geochemistry and sedimentology of a facies transition from limestone to iron-formation deposition in the Early Proterozoic Transvaal Supergroup, South Africa: *Econ. Geol.*, v. 84, p. 1733-1774.
- Klein, C., and Beukes, N.J., 1992**, Time distribution, stratigraphy, sedimentological setting, and geochemistry of Precambrian iron-formations, in: The proterozoic biosphere: A multidisciplinary study, eds, Schopf, J.W., and Klein, C.: *Cambridge, Cambridge Univ. Press*, p. 139-146.
- Klein, C., and Beukes, N.J., 1993**, Sedimentology and geochemistry of the glaciogenic Late Proterozoic Rapitan iron-formation in Canada: *Econ. Geol.*, v. 88, p. 542-565.
- Kleyenstüber, A.S.E., 1979**, n' Mineralogiese ondersoek van hoetemperatuur-reduksieprodukte van mangaanerts vanuit die Mamatwanmyn, Kalaharimangaanveld. *Unpublished MSc thesis, Rand Afrikaans Univ., Johannesburg, South Africa*, 125 p.
- Kleyenstüber, A.S.E., 1984**, The mineralogy of the manganese-bearing Hotazel Formation of the Proterozoic Transvaal Sequence in Griqualand West, South Africa: *Trans. Geol. Soc. S. Afr.*, v. 87, p. 257-272.
- Kleyenstüber, A.S.E., 1985**, A regional mineralogical study of the manganese-bearing Voëlwater Subgroup in Northern Cape Province: *Unpublished PhD thesis, Rand Afrikaans Univ., Johannesburg, South Africa*, 328 p.
- Kleyenstüber, A.S.E., 1986**, "The mineralogy of the manganese-bearing Hotazel formation, of the Proterozoic Transvaal Sequence in Griqualand West, South Africa" - author's reply to discussion: *Trans. Geol. S. Afr.*, v. 89, p. 423-425.
- Klinkhammer, G., 1980**, Early diagenesis in sediments from the eastern equatorial Pacific, II. Pore water metal results: *Earth Plan. Sci. Lett.*, v. 49, p. 81-101.
- Klinkhammer, G., Elderfield, H., Edmond, J.M., and Mitra, A., 1994**, Geochemical implications of rare-earth element patterns in hydrothermal fluids from mid-ocean ridges: *Geoch. Cosm. Acta*, v. 58, p. 5105-5113.
- Krupp, R., Oberthür, T., and Hirdes, W., 1994**, The Early Precambrian atmosphere and hydrosphere: thermodynamic constraints from mineral deposits: *Econ. Geol.*, v. 89, p. 1581-

1598.

**Kump, L.R., and Holland, H.D., 1992**, Iron in Precambrian rocks: implications for the global oxygen budget of the ancient earth: *Geoch. Cosm. Acta*, v. 56, p. 3217-3223.

**LaBerge, G.L., 1966a**, Altered pyroclastic rocks in South African iron-formation: *Econ. Geol.*, v. 61, p. 572-581.

**LaBerge, G.L., 1966b**, Altered pyroclastic rocks in iron-formations in the Hamersley Range, Western Australia: *Econ. Geol.*, v. 61, p. 147-161.

**Lambert, R.St.J., Winchester, J.A., and Holland, J.G., 1981**, Comparative geochemistry of pelites from the Moinian and Appin Group (Dalradian) of Scotland: *Geol. Mag.*, v. 118, p. 477-490.

**Lambert, R.St.J., Holland, J.G., and Winchester, J.A., 1982**, A geochemical comparison of the Dalradian Level schists and the Grampian Division Monadhliath schists of Scotland: *J. Geol. Soc. Lond.*, v. 139, p. 71-84.

**Laznicka, P., 1992**, Manganese deposits in the global lithogenetic system: quantitative approach: *Ore Geol. Rev.*, v. 7, p. 279-356.

**le Maitre, R.W. 1982**, Numerical Petrology: Statistical interpretation of geochemical data: *Developments in Petrology*, 8, Elsevier Sci. Pub., Amsterdam, 281 p.

**Lepp, H., and Goldich, S.S., 1959**, Chemistry and origin of iron formation: *Geol. Soc. Am. Bull.*, v. 70, p. 1637.

**Lepp, H., and Goldich, S.S., 1964**, Origin of the Precambrian iron-formations: *Econ. Geol.*, v. 59, p. 1025-1060.

**le Roex, A., and Watkins, M., 1990**, Analysis of rare-earth elements in geological samples by gradient ion chromatography: An alternative to ICP and INAA. *Chem. Geol.*, v. 88, p. 152-162.

**Leshner, C.M., 1978**, Mineralogy and petrology of the Sokoman iron-formation near Ardua Lake, Quebec: *Can. J. Earth Sci.*, v. 15, p. 480-500.

**Lougheed, M.S., 1983**, Origin of Precambrian iron-formations in the Lake Superior region: *Geol. Soc. Am. Bull.*, v. 94, p. 325-340.

**Lovley, D.R., and Phillips, E.J.P., 1988**, Novel mode of microbial energy metabolism: organic carbon oxidation coupled to dissimilatory reduction of iron and manganese: *App. Envir. Microb.*, v. 54, No.6, p. 1472-1480.

**Lovley, D.R., Stolz, J.F., Nord, G.L.Jr, and Phillips, E.J.P., 1987**, Anaerobic production of

magnetite by a dissimilatory iron-reducing microorganism: *Nature*, v. 330, p. 252-253.

**Manikyamba, C., and Naqvi, S.M., 1995**, Geochemistry of Fe-Mn formations of the Archaean Sandur schist belt, India-mixing of clastic and chemical processes at a shallow shelf: *Prec. Res.*, v. 72, p. 69-95.

**Manikyamba, C., Balaram, V., and Naqvi, S.M., 1993**, Geochemical signatures of polygenetic origin of a banded iron-formation (BIF) of the Archaean Sandur greenstone belt (schist belt) Karnataka nucleus, India: *Prec. Res.*, v. 61, p. 137-164.

**Marriott, F.H.C., 1974**, The interpretation of multiple observations: *Academic Press, London*, 117p.

**Maynard, B.J., 1983**, Geochemistry of sedimentary ore deposits: Springer-Verlag, New York Inc., 305 p.

**McCrea, J.M., 1950**, On the isotopic chemistry of carbonates and a palaeotemperature scale: *J. Chem. Phys.*, v. 18, p. 849-857.

**McSwiggen, P.L., Morey, G.B., and Cleland, J.M., 1994**, The origin of aegirine in iron formation of the Cuyuna Range, Minnesota: *Can. Min.*, v. 32, p. 589-598.

**Mel'nik, Y.P., 1982**, Precambrian banded iron-formations: physicochemical conditions of formation: *Developments in Precambrian Geology 5, Elsevier Sci. Pbl.*, 310 p.

**Milton, C., Chao, E.C.T., Fahey, J.J., and Mrose, M.E., 1960**, Silicate mineralogy of the Green River Formation of Wyoming, Utah, and Colorado: *Int. Geol. Congr., Proc. Sect. 21, Copenhagen, Denmark*, p. 171-184.

**Milton, C., and Eugster, H.P., 1959**, Mineral assemblages of the Green River Formation, in: *Researches in geochemistry*, ed. Abelson, P.H.: *New York, John Wiley and Sons*, p. 118-150.

**Mills, R.A., and Elderfield, H., 1995**, Rare earth element geochemistry of hydrothermal deposits from the active TAG Mound, 26°N Mid-Atlantic Ridge: *Geoch. Cosm. Acta*, v. 59, p. 3511-3524.

**Miyano T., 1982**, Stilpnomelane, iron-rich mica, K-feldspar and hornblende in banded iron-formation assemblages of the Dales Gorge Member, Hamersley Group, W. Australia: *Can. Min.*, v. 20, p. 189-202.

**Miyano, T., 1987**, Diagenetic to low-grade metamorphic conditions of Precambrian iron-formations, in: *Precambrian iron-formations*, eds., Appel, P.W.U., and LaBerge, G.L.: *Theophrastus publ., Athens*, p. 155-186.

- Miyano T., and Miyano, S., 1982**, Ferri-annite from the Dales Gorge Member iron-formations, Wittenoom area, Western Australia: *Am. Min.*, v. 67, p. 1179-1194.
- Miyano T., and Klein, C., 1983a**, Conditions of riebeckite formation in the iron-formations of the Dales Gorge Member, Hamersley Group, Western Australia: *Am. Min.*, v. 68, p. 517-529.
- Miyano T., and Klein, C., 1983b**, Phase relations of orthopyroxene, olivine, and grunerite in high-grade iron-formations: *Am. Min.*, v. 68, p. 699-716.
- Miyano T., and Beukes N.J., 1984**, Phase relations of stilpnomelane, ferri-annite, and riebeckite in very low-grade metamorphosed iron-formations: *Trans. Geol. Soc. S. Afr.*, v. 87, p. 111-124.
- Miyano T., and Beukes N.J., 1987**, Physicochemical environments for the formation of quartz-free manganese oxide ores from the Early Proterozoic Hotazel Formation, Kalahari manganese field, South Africa: *Econ. Geol.*, v. 82, p. 706-718.
- Miyano, T., and Klein, C., 1989**, Phase equilibria in the system  $K_2O$ -FeO-MgO- $Al_2O_3$ - $SiO_2$ - $H_2O$ - $CO_2$  and the stability limit of stilpnomelane in metamorphosed Precambrian iron-formations: *Con. Min. Pet.*, v. 102, p. 478-491.
- Miyano, T., Beukes, N.J., and van Reenen, D.D., 1987**, Metamorphic evidence for early post-Bushveld sills in the Penge iron-formation, Transvaal Sequence, Eastern Transvaal: *S. Afr. J. Geol.*, v. 90(1), p. 37-43.
- Moore, J.M., 1989**, A comparative study of metamorphosed supracrustal rocks from the Western Namaqualand metamorphic complex: Precambrian Research Unit, Univ. of Cape Town, 370 p.
- Morey, G.B., 1983**, Animikie Basin, Lake Superior Region, U.S.A., in: Iron-formations: facts and problems, eds. Trendall, A.F., and Morris, R.C.: *Developments in Precambrian Geology 6*, Elsevier Sci. Pbl., p. 13-67.
- Morey, G.B., 1999**, High-grade iron ore deposits of the Mesabi Iron Range, Minnesota-product of a continental-scale Proterozoic ground-water flow system: *Econ. Geol.*, v. 94, p. 133-141.
- Morey, G.B., and Southwick, D.L., 1993**, Stratigraphic and sedimentological factors controlling the distribution of epigenetic manganese deposits in iron-formation of the Emily District, Cuyuna Iron Range, east-central Minnesota: *Econ. Geol.*, v. 88, p. 104-122.
- Morris, R.C., 1980**, A textural and mineralogical study of the relationship of iron-ore to banded iron-formation in the Hamersley Iron Province of western Australia: *Econ. Geol.*, v. 75, p. 184-209.
- Morris, R.C., 1993**, Genetic modelling for banded iron-formation of the Hamersley Group,



- Pilbara Craton, Western Australia: *Prec. Res.*, v. 60, p. 243-286.
- Morris, R.C., and Horwitz, R.C., 1983**, The origin of the iron-formation-rich Hamersley Group of Western Australia-deposition on a platform: *Prec. Res.*, v. 21, p. 273-297.
- Morris, R.C., and Trendall, A.F., 1988**, Discussion: a model for the deposition of the microbanded Precambrian iron-formations: *Am. J. Sci.*, v. 288, p. 664-668.
- Mucci, A., 1988**, Manganese uptake during calcite precipitation from seawater: Conditions leading to the formation of a pseudokutnahorite: *Geoch. Cosm. Acta*, v. 52, p. 1859-1868.
- Myers, C.R., and Nealson, K.H., 1988a**, Bacterial manganese reduction and growth with manganese oxide as the sole electron acceptor: *Science*, v. 240, p. 1319-1321.
- Myers, C.R., and Nealson, K.H., 1988b**, Microbial reduction of manganese oxides: interactions with iron and sulfur: *Geoch. Cosm. Acta*, v. 52, p. 2727-2732.
- Nealson, K.H., and Myers, C.R., 1990**, Iron reduction by bacteria: a potential role in the genesis of banded iron-formations: *Am. J. Sci.*, v. 290-A, p. 35-45.
- Nel, C.J., 1984**, Die mineralogie en geochemie van die Mamatwan-ertsligaam, Kalahari mangaanveld, Transvaal-Supergroep: *Unpublished MSc thesis, Rand Afrikaans Univ., Johannesburg, S. Africa*, 119 p.
- Nel, C.J., Beukes, N.J., and De Villiers, J.P.R., 1986**, The Mamatwan manganese mine of the Kalahari manganese field, in: Mineral deposits of Southern Africa, eds., C.R. Anhaeuser, and S. Maske: *Geol. Soc. S. Afr.*, v. I, p. 963-978.
- Norrish, K., and Chapell, B.W., 1967**, X-ray fluorescence spectrography, in: Physical methods in determinative mineralogy, ed., Zussman, J.: *Academic Press, London*, p. 161-214.
- Norrish, K., and Hutton, J.T., 1969**, An accurate x-ray spectrographic method for the analysis of a wide range of geological samples: *Geoch. Cosm. Acta*, v. 33, p. 431-453.
- Ohmoto, H., 1996**, Evidence in pre-2.2 Ga paleosols for the early evolution of atmospheric oxygen and terrestrial biota: *Geol.*, v. 24, p. 1135-1138.
- Ohmoto, H., 1997**, When did the earth's atmosphere become oxic?: *Geoch. News*, v. 93, p. 12-13 & 26-27.
- Okita, P.M., 1992**, Manganese carbonate mineralisation in the Molango District, Mexico: *Econ. Geol.*, v. 87, p. 1345-1366.
- Okita, P.M., and Shanks, W.C., 1992**, Origin of stratiform sediment-hosted manganese carbonate ore deposits: Examples from Molango, Mexico, and Taojiang, China: *Chem. Geol.*,

v. 99, p. 139-164.

**Okita, P.M., Maynard J.B., Spiker, E.C., and Force, E.R., 1988**, Isotopic evidence for organic matter oxidation by manganese reduction in the formation of stratiform manganese carbonate ore: *Geoch. Cosm. Acta*, v. 52, p. 2679-2685.

**Oliver, N.H.S., Dickens, G.R., Powell, C.McA., Bons, P.D., and Stewart, L.K., 1998**, Hamersley hematite ore genesis by syntectonic infiltration of heated meteoric fluid: *Abstracts, 14th Aust. Geol. Conv., Townsville, Australia*, p. 340.

**O'Neil, J.R., Clayton, R.N., and Mayeda, T.K., 1969**, Oxygen isotope fractionation in divalent metal carbonates: *J. Chem. Phys.*, v. 51, p. 5547-5558.

**Öztürk, H., and Hein, J.R., 1997**, Mineralogy and stable isotopes of black shale-hosted manganese ores, southwestern Taurides, Turkey: *Econ. Geol.*, v. 92, p. 733-744.

**Perry, E.C.Jr., 1983**, Oxygen isotope geochemistry of iron-formation, in: Iron-formations: facts and problems, eds., Trendall, A.F., and Morris, R.C.: *Developments in Precambrian Geology 6*, Elsevier Sci. Pbl., p. 359-371.

**Perry, E.C., and Ahmad, S.N., 1980**, Oxygen isotope study of Transvaal system iron-formation from the vicinity of Kuruman, Cape Province, South Africa: *Geol. Soc. Am. Abstr. Progr.*, v. 12, 497 p.

**Perry, E.C., and Ahmad, S.N., 1981**, Oxygen and carbon isotope geochemistry of the Krivoy Rog iron-formation, USSR: *Lithos*, v. 14, p. 83-92.

**Perry, E.C.Jr., and Bonnicksen, B., 1966**, Quartz and magnetite: Oxygen-18<sup>2</sup>-Oxygen-16 fractionation in metamorphosed Biwabik Iron formation: *Science*, v. 153, p. 528-529.

**Perry, E.C.Jr, and Tan, F.C., 1973**, Significance of carbon isotope variations in carbonates from the Biwabik iron-formation, Minnesota, in: Genesis of Precambrian iron and manganese deposits: *Proc. Kiev Symposium 1970, UNESCO Paris*, p. 299-305.

**Perry, E.C., Tan, F.C., and Morey, G.B., 1973**, Geology and stable isotope geochemistry of the Biwabik iron-formation, Northern Minnesota: *Econ. Geol.*, v. 68, p. 1110-1125.

**Perry, E.C., Ahmad, S.N., and Swulius, T.M., 1978**, The oxygen isotope composition of 3800 million old metamorphosed chert and iron-formation from IsuKasia, West Greenland: *J. Geol.*, v. 86, p. 223-239.

**Peters, T., 1988**, Geochemistry of manganese-bearing cherts associated with Alpine ophiolites and the Hawasina formations in Oman: *Mar. Geol.*, v. 84, p. 229-238.

- Plehwé-Leisen, E. Von, and Klemm, D.D., 1995**, Geology and ore genesis of the manganese ore deposits of the Postmasburg manganese-field, South Africa: *Mineral. Dep.*, v. 30, p. 257-267.
- Polgari, M., Okita, P.M., and Hein, J.R., 1991**, Stable isotope evidence for the origin of the Úrkút manganese deposit, Hungary: *J. Sed. Petr.*, v. 61, p. 384-393.
- Powell, C.McA., Oliver, N.H.S., Li, Z.X., Martin, D.McB., and Ronaszeki, J., 1999**, Synorogenic hydrothermal origin for giant Hamersley iron oxide ore bodies: *Geology*, v. 27, p. 175-178.
- Pratt, L.M., Force, E.R., and Pomerol, B., 1991**, Coupled manganese and carbon-isotopic events in marine carbonates at the Cenomanian-Turonian boundary: *J. Sed. Petr.*, v. 61, p. 370-383.
- Pride, D.E., and Hagner, A.F., 1972**, Geochemistry and origin of the Precambrian iron-formation near Atlantic City, Fremont Count, Wyoming: *Econ. Geol.*, v. 67, p. 329-338.
- Rabouille, C., and Gaillard, J.F., 1991**, Towards the EDGE: Early diagenetic global explanation. A model depicting the early diagenesis of organic matter, O<sub>2</sub>, NO<sub>3</sub>, Mn, and PO<sub>4</sub>: *Geoch. Cosm. Acta*, v. 55, p. 2511-2525.
- Redwood, S.D., 1993**, Crocidolite and magnesite associated with Lake Superior-type banded iron-formation in the Chapare Group of Eastern Andes, Bolivia: *Trans. Inst. Min. Metall. (Sect. B: Applied Earth Science)*, v. 102, p. B114-121.
- Rollinson, H.R.**, Using geochemical data: evaluation, presentation, interpretation: *Longman Group Ltd.*, 352 p.
- Rosenbaum, J., and Sheppard, S.M.F., 1986**, An isotopic study of siderites, dolomites and ankerites at high temperatures: *Geoch. Cosm. Acta*, v. 50, p. 1147-1150
- Roy, S., 1981**, Manganese deposits: *London Academic Press*, 458 p.
- Roy, S., 1992**, Environments and processes of manganese deposition: *Econ. Geol.*, v. 87, p. 1218-1236.
- SACS - South African Committee for Stratigraphy, 1980**, Stratigraphy of South Africa (part 1, comp. L.E., Kent): Lithostratigraphy of the Republic of South Africa, South West Africa/Namibia and the Republics of Bophuthatswana, Transkei and Venda: *Handbook, Geol. Sur. S. Afr.*, v. 8, 690 p.
- Sakamoto, T., 1950**, The origin of Precambrian banded iron-ores: *Am. J. Sci.*, v. 248, p. 449-474.

- Schissel, D., and Aro, P., 1992**, The major Early Proterozoic sedimentary iron and manganese deposits and their tectonic setting: *Econ. Geol.*, v. 87, p. 1367-1374.
- Schütte, S.S., 1992**, Ongeluk volcanism in relation to the Kalahari manganese deposits: *Unpublished PhD thesis, Univ. of Natal, Durban, South Africa*, 266 p.
- Sharpe, M.R., Brits, R., and Engelbrecht, J.P., 1983**, Rare-earth and trace element evidence pertaining to the petrogenesis of 2.3 GA old continental andesites and other volcanic rocks from the Transvaal Sequence, South Africa: *Inst. Geol. Res. Bushveld Complex, Univ. of Pretoria*, Res. Rep. 40, 63 p.
- Simonson, B.M., 1985**, Sedimentological constraints on the origins of Precambrian iron-formations: *Geol. Soc. Am. Bull.*, v. 96, p. 244-252.
- Suess, E., 1979**, Mineral phases formed in anoxic sediments by microbial decomposition of organic matter: *Geoch. Cosm. Acta*, 43, p. 339-352.
- Sumner, D.Y., and Grotzinger, J.P., 1996**, Were kinetics of Archaean calcium carbonate precipitation related to oxygen concentration?: *Geol.*, v. 24, p. 119-122.
- Sutherland, D.S., 1969**, Sodic amphiboles and pyroxenes from fenites in East Africa: *Cont. Min. Petr.*, v. 24, p. 114-135.
- Thomas, R.J., Agenbacht, A.L.D., Cornell, D.H., Moore, J.M., 1994a**, The Kibaran of southern Africa: Tectonic evolution and metallogeny: *Ore Geol. Rev.*, v. 9, p. 131-160.
- Thomas, R.J., Cornell, D.H., Moore, J.M., and Jacobs, J., 1994b**, Crustal evolution of the Namaqua-Natal metamorphic province, Southern Africa: *S. Afr. J. Geol.*, v. 97, p. 8-14.
- Towe, K.M., 1983**, Precambrian atmospheric oxygen and banded iron-formations: a delayed ocean model: *Prec. Res.*, v. 20, p. 161-170.
- Trendall, A.F., 1973a**, Time-distribution and type-distribution of Precambrian iron-formations in Australia, in: Genesis of Precambrian iron and manganese deposits: *Proc. Kiev Symposium 1970, UNESCO Paris*, p. 49-57.
- Trendall, A.F., 1973b**, Iron-formations of the Hamersley Group of Western Australia: type examples of varved Precambrian evaporites, in: Genesis of Precambrian iron and manganese deposits: *Proc. Kiev Symposium 1970, UNESCO Paris*, p. 257-270.
- Trendall, A.F., 1973c**, Precambrian iron-formation of Australia: *Econ. Geol.*, v. 68, p. 1023-1034.
- Trendall, A.F., 1973d**, Varve cycles in the Weeli Wolli Formation of the Precambrian

Hamersley Group, Western Australia: *Econ. Geol.*, V. 68, p. 1089-1097.

**Trendall, A.F., 1983**, The Hamersley Basin, in: Iron-formations: facts and problems, eds., Trendall, A.F., and Morris, R.C.: *Developments in Precambrian Geology 6*, Elsevier Sci. Pbl., p. 69-129.

**Trendall, A.F., and Blockley, J.G., 1970**, The iron-formations of the Precambrian Hamersley Group, Western Australia, with special reference to the associated crocidolite: *West. Aust. Geol. Sur. Bull. 119*, 366 p.

**Tsikos, H., 1994**, The mineralogy and geochemistry of the Voëlwater banded iron-formation, Northern Cape Province: *Unpublished MSc thesis, Rhodes Univ., South Africa*, 190 p.

**Tsikos, H., and Moore, J.M., 1997**, Petrography and geochemistry of the Paleoproterozoic Hotazel iron-formation Kalahari Manganese Field, South Africa: Implications for Precambrian manganese metallogenesis: *Econ. Geol.*, v. 92, p.87-97.

**Tsikos, H., and Moore, J.M., 1998**, The Kalahari manganese field: an enigmatic association of iron and manganese. *S. Afr. J. Geol.*, v.101, p. 287-290.

**Urban, H., Stribrny, B., and Lippolt, H.J., 1992**, Iron and manganese deposits of the Urucum District, Matto Grosso do Sul, Brazil: *Econ. Geol.*, v. 87, p. 1375-1392.

**Van Hise, C.R., and Leith, C.K., 1911**, Geology of the Lake Superior Region: *U.S. Geol. Survey, Mon. 52*, 641 p.

**Van Schalkwyk, and Beukes, N.J., 1986**, The Sishen iron-ore deposit, Griqualand West, in: Mineral deposits of Southern Africa, eds., Anhaeusser, C.R., and Maske, S.: *Geol. Soc. S. Afr.*, v. I, p. 931-956.

**Veizer, J., Clayton, R.N., and Hinton, R.W., 1992**, Geochemistry of Precambrian carbonates: IV. Early Paleoproterozoic (2.25±0.25 Ga) seawater: *Geoch. Cosm. Acta*, v. 56, p. 875-885.

**Vennemann, T.W., and Smith, H.S., 1990**, The rate and temperature of reaction of ClF<sub>3</sub> with silicate minerals, and their relevance to oxygen isotope analysis: *Chem. Geol. (Isotope Geosci.)* v. 86, p. 83-88.

**Walker, J.C.G., 1977**, Evolution of the atmosphere: *MacMillan, New York*, 318 p.

**Walker, J.C.G., 1984**, Suboxic diagenesis in banded iron-formations: *Nature*, v. 309, p. 340-342.

**Wheatley, C.J.V., Whitfield, G.G., Kenny, K.J., and Birch, A., 1986**, The Pering carbonate-hosted zinc-lead deposit, Griqualand West, in: Mineral deposits of Southern Africa, eds.,

Anhaeusser, C.R., and Maske, S.: *Geol. Soc. S. Afr.*, v. I, p. 867-874.

**Winter, B.L., and Knauth, P.L., 1992**, Stable isotope geochemistry of cherts and carbonates from the 2.0 Ga Gunflint iron formation: implications for the depositional setting, and the effects of diagenesis and metamorphism: *Prec. Res.*, v. 59, p. 283-313.

**Williams, D.M., Kasting, J.F., and Frakes, L.A., 1998**, Low-latitude glaciation and rapid changes in the Earth's obliquity explained by obliquity-oblateness feedback: *Nature*, v. 396, p. 453-455.

**Yapp, C.J., 1990a**, Oxygen isotope effects associated with the solid state  $\alpha$ -FeOOH to  $\alpha$ -Fe<sub>2</sub>O<sub>3</sub> phase transformation: *Geoch. Cosm. Acta*, v. 54, p. 229-236.

**Yapp, C.J., 1990b**, Oxygen isotopes in iron (III) oxides: 1. Mineral-water fractionation factors: *Chem. Geol.*, v. 85, p. 329-335.

**Yapp, C.J., 1990c**, Oxygen isotopes in iron (III) oxides: 2. Possible constraints on the depositional environment of a precambrian quartz-hematite banded iron-formation: *Chem. Geol.*, v. 85, p. 337-344.

**Yapp, C.J., 1993**, Paleoenvironment and the oxygen isotope geochemistry of ironstone of the Upper Ordovician Neda Formation, Wisconsin, USA: *Geoch. Cosm. Acta*, v. 57, p. 2319-2327.

**Zajac, I.S., 1974**, The stratigraphy and mineralogy of the Sokoman iron-formation in the Knob Lake area, Quebec and Newfoundland: *Geol. Surv. Can. Bull.*, v. 220, 159 p.

**Zheng, Y., 1992**, Calculation of oxygen isotope fractionation in anhydrous silicate minerals: *Geoch. Cosm. Acta*, v. 57, p. 1079-1091.

## **PART 7: APPENDICES**

### **Appendix I: Borehole localities and sample selection**

Samples from six borehole intersections of the Hotazel Formation were obtained from the South African Manganese Corporation (SAMANCOR) in Hotazel, South Africa, in 1993. Four of these (R59, R63, R65 and R70) were drilled on the farm RISSIK to the north-northeast of the open-cast, low-grade Mamatwan Mn mine (Fig. A1). Sixty-six iron-formation and forty Mn ore samples were collected from these boreholes, fifty-three of which were used for a preliminary whole-rock geochemical investigation as part of an MSc project by the author between 1993 and 1994 at Rhodes University (Tsikos, 1994). Shortly after the commencement of this PhD study, an additional 15 samples were collected for further analyses from borehole SM31 drilled to the west of the currently defunct SMARTT open-cast mine (Fig. A1), and 9 of these have been included in this study. Borehole SM31 and the four above-mentioned borehole intersections constitute all representative material of the Hotazel Formation as it develops in the southernmost parts of the KMF (Fig. A2). In addition to this material, a portion of the Mooidraai Carbonate Formation immediately overlying the Hotazel Formation as developed in borehole OLP7 drilled in farm OLIVEPAN (Fig. A1), was made available to the author during a short second visit to the SAMANCOR premises in Hotazel, in mid-1995. Ten out of the eleven samples collected from the Mooidraai intersection were also included in this investigation (Fig. A3),

The remaining eight boreholes were kindly made accessible to the author by the Associated Manganese Mines of South Africa Limited (ASSMANG LTD), for detailed sampling of the iron-formation units. The boreholes were drilled in the northernmost parts of the KMF, where extensive underground mining of high grade Mn ore is carried out at present (Fig. A1). Seven of these boreholes were drilled in farms N'CHWANING (N12D, N91B), BELGRAVIA (BEL4C, BEL7A) and MUKULU (MK2G, MK2H, MK3I; see Fig. A.1), in close proximity to the presently operating, underground N'chwaning mine. An eighth borehole (GL26) comes from the farm GLORIA, located to the south-southeast of the N'chwaning mine, where the only underground operation of low-grade manganese ore in the KMF (Gloria Mine) is currently in progress (Fig. A1). A total of 162 samples were collected from these boreholes for the purposes of this study (Figs. A3, A4), providing a thorough representation of the iron-formation stratigraphy in the area.

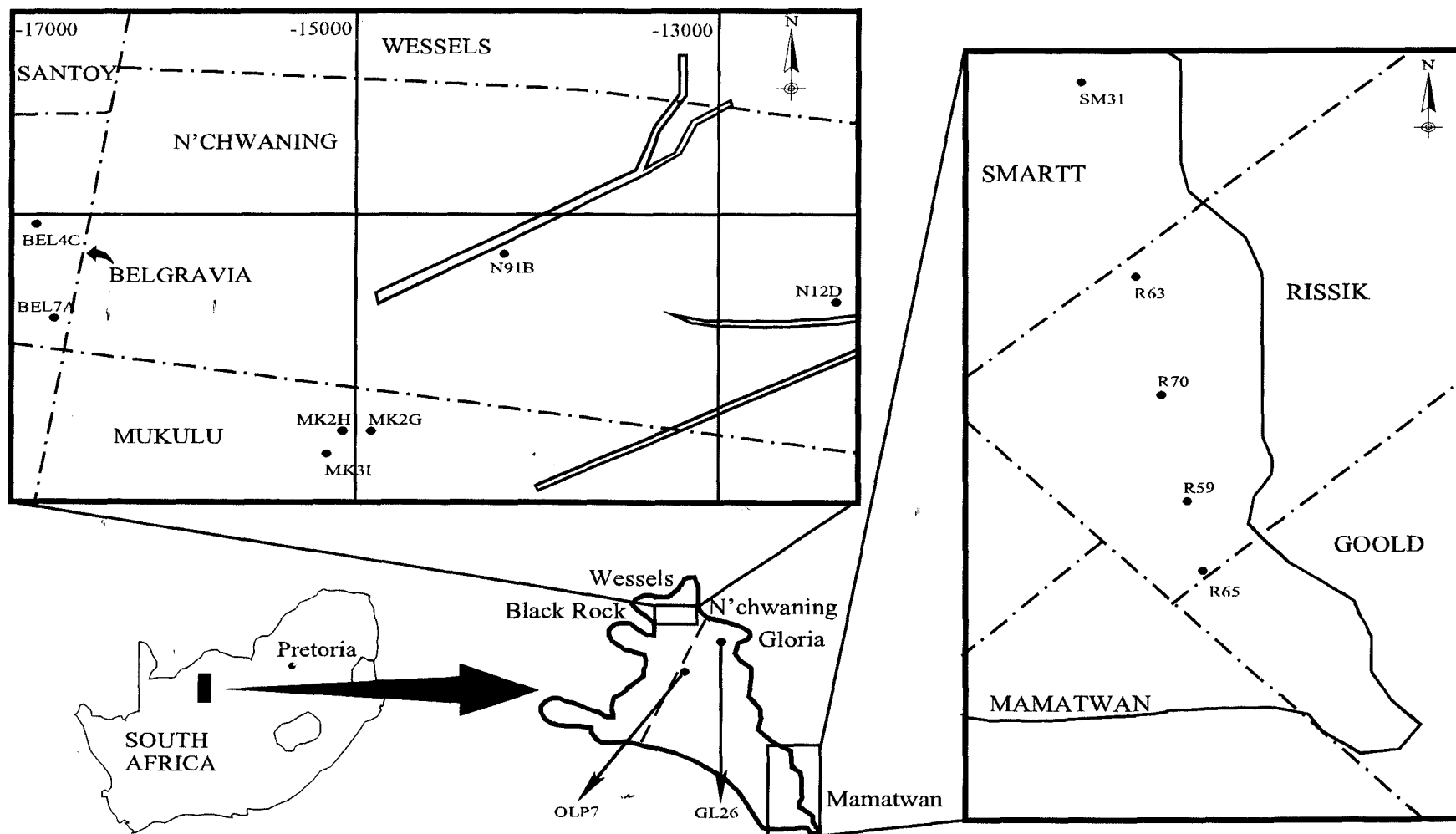


**Figure A1:** Simplified sketch map of the Kalahari Manganese Field (KMF) showing details on major geographical areas and localities of all boreholes used in this thesis



## KEY



Mooirdraai Formation and other limestone units



Carbonate-rich iron-formation



Carbonate-poor iron-formation



Carbonate-poor, hematitic iron-formation



Manganese ore-units



Oxidised iron-formation



Altered iron-formation/locally massive hematite



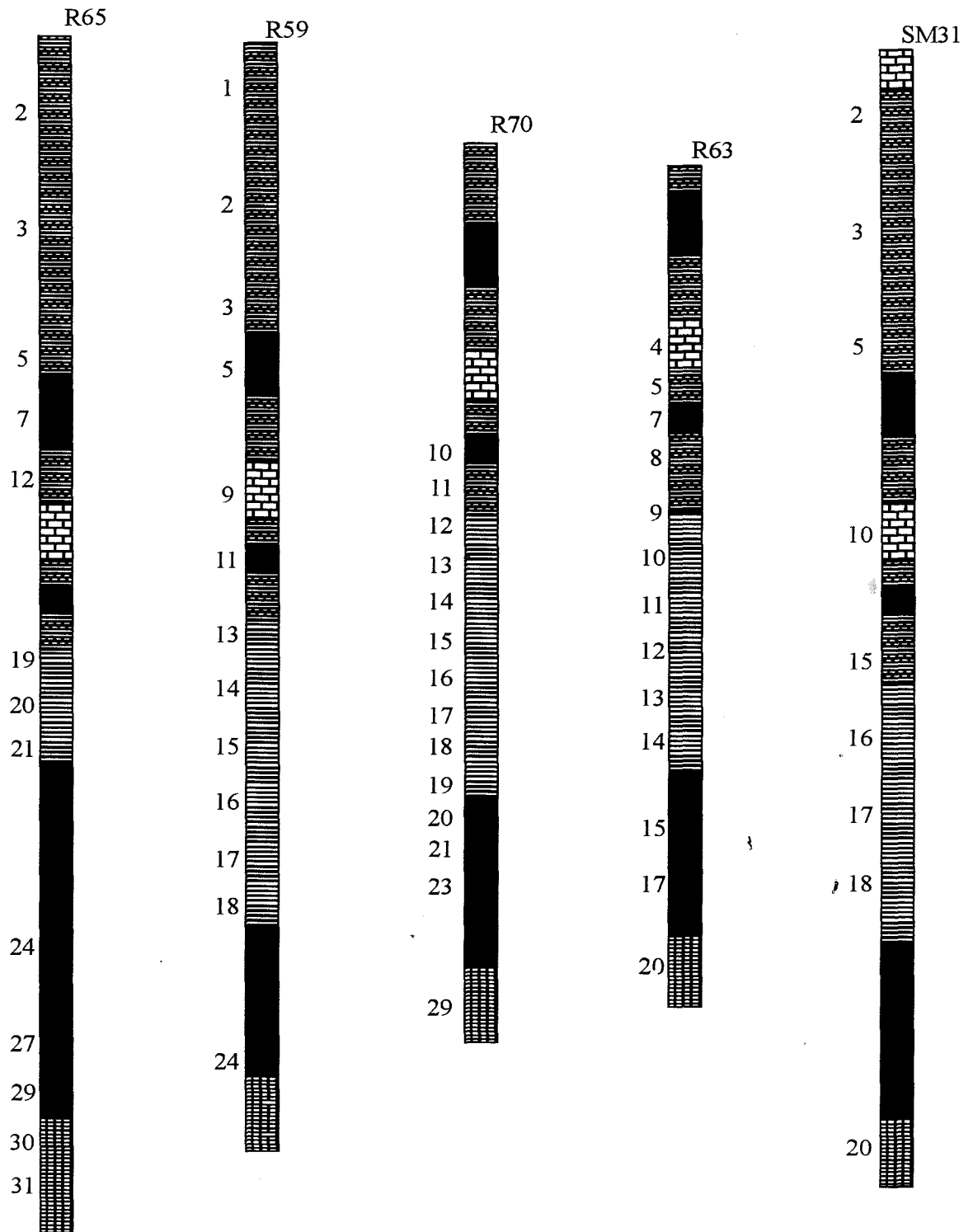
Dwyka diamictite



Transitional, hematite/carbonate-rich units



Acmite-rich units



-Figure A2: Approximate stratigraphic locations for samples of the Hotazel Formation selected for the purposes of this thesis from boreholes drilled in the southernmost portion of the KMF. Not to scale.

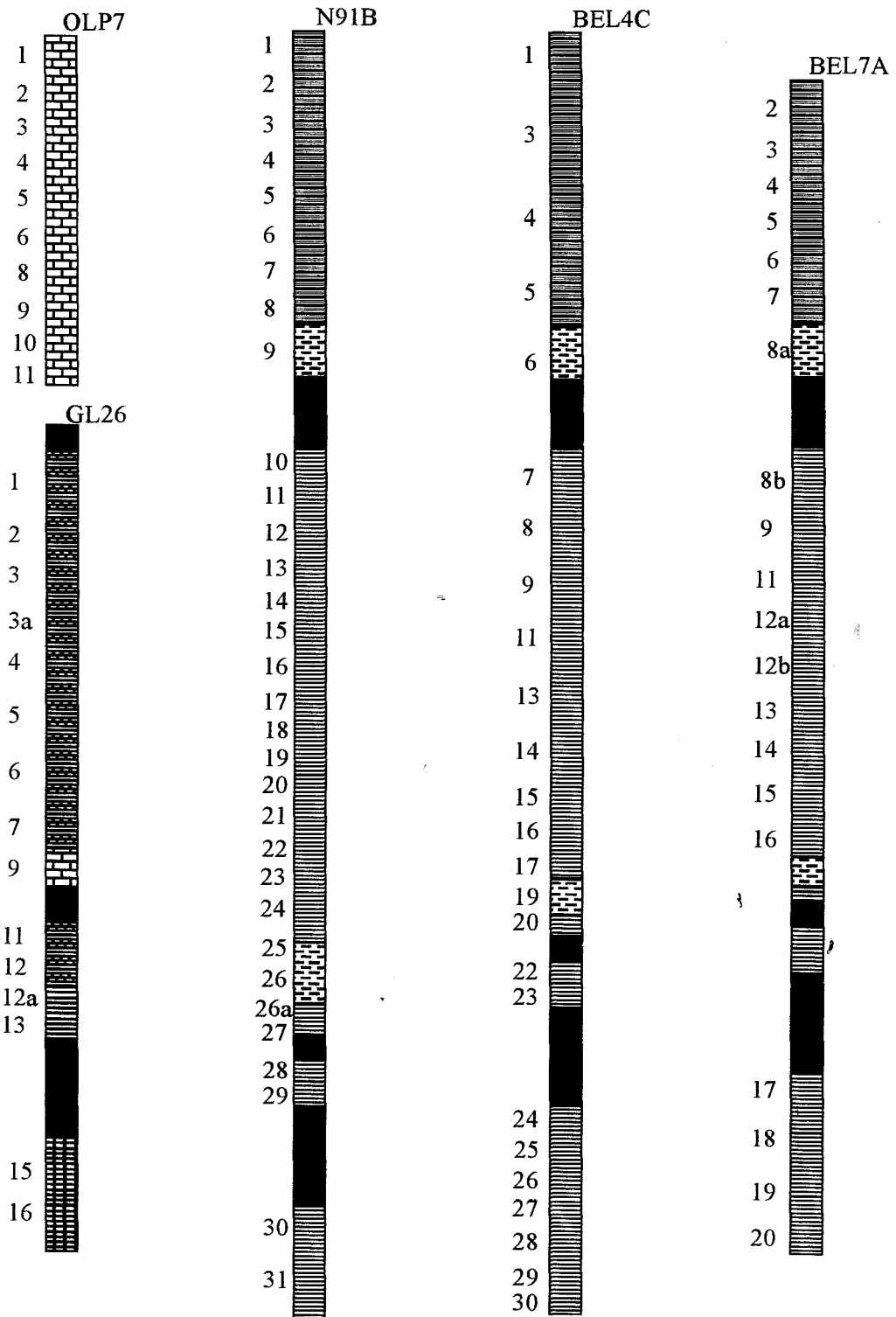


**Figure A3:** Approximate stratigraphic locations for samples of the Hotazel and Moidraai Formation selected for the purposes of this thesis from boreholes drilled in the northernmost portion of the KMF. Not to scale.

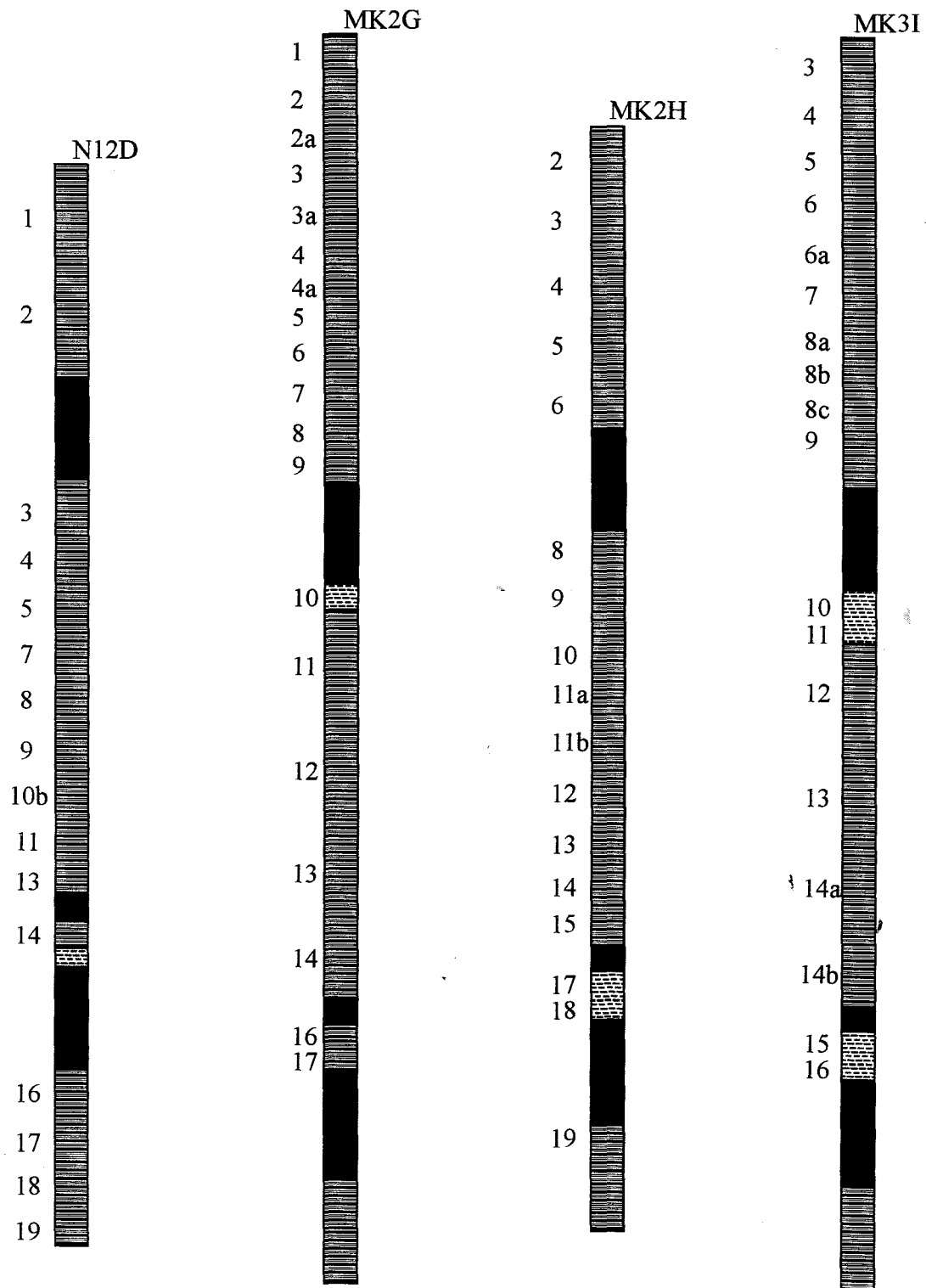


**Figure A4:** Approximate stratigraphic locations for samples of the Hotazel Formation selected for the purposes of this thesis from boreholes drilled in the northernmost portion of the KMF. Not to scale.

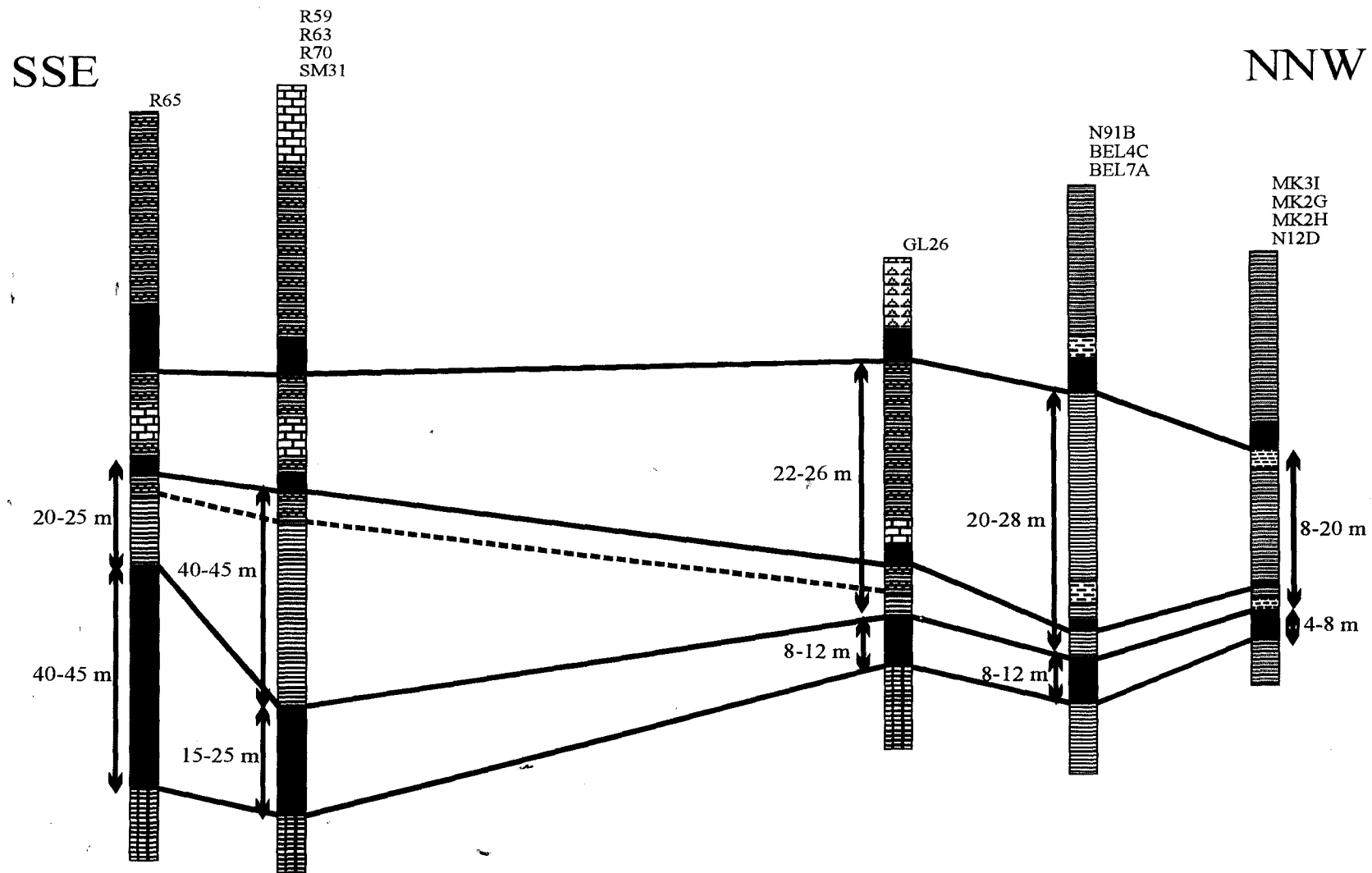


**Figure A5:** Schematic profile along a SSE-NNW direction in the KMF, showing the distribution of major lithotypes and relative lateral thickness variations for a large portion of the Hotazel stratigraphy. The profile is drawn using information from boreholes selected in this thesis and additional borehole-log information supplied by ASSMANG and SAMANCOR. Not to scale.



## **Appendix II: Analytical techniques**

### **i. Sample preparation**

Preparation of sample material was done at the Department of Geology, Rhodes University. Quartered borehole-core samples of iron-formation of a minimum length of 10cm were selected in order to ensure compositional homogeneity. The samples were fragmented with a hammer into cm-size chips. Chips devoid of weathering crusts, secondary veins or other contaminating material were handpicked. Approximately 300-500g of those chips were cleaned in an air stream and subsequently crushed for approximately 2-3 minutes in a swing mill, using a hardened steel set and rings. The set and rings were thoroughly cleaned after each sample with distilled water and dried with an air stream. Pure quartz chips were milled in between each sample, in order to minimise cross-contamination of the samples. The finely crushed samples were then stored in glass vials.

### **ii. X-ray diffraction (XRD)**

The majority of samples used in this study were analysed by standard x-ray diffraction (XRD) techniques at the Department of Chemistry, Rhodes University. Approximately 1.5-2 g of finely milled powder was used from each sample. These were loosely packed<sup>1</sup> in side-loaded sample holders, in order to minimize any effects of preferred orientation and allow recovery of the samples. XRD patterns were obtained on a Phillips water-cooled diffractometer, using a CuK $\alpha_1$  radiation generated at 40kv and 20-30 mA. Patterns were acquired on a routine basis in the range of 5-60°2 $\theta$ , using a scan speed of 30sec/1° at a step width of 0.05°. Phase identification was done based on published reference patterns of the Joint Committee on Powder Diffraction Standards (JCPDS, 1974, 1980). Few selected samples characterised by particularly fine-grained and complex assemblages, were also analysed at the Department of Geology at Rand Afrikaans University by Dr J. Gutzmer, using CoK $\alpha$  radiation at 40kv and 40mA. Patterns were obtained in the range 3-140°2 $\theta$ , using a scan speed of 50sec/1° at a step width of 0.02°. Identification of phases was conducted semi-automatically, using available CD-ROM packages containing up-to-date powder diffraction data.

### iii. Determination of $H_2O^-$ and loss on ignition (LOI)

Determination of LOI and  $H_2O^-$  values were performed at the Department of Geology, Rhodes University. Results are reported in Appendix III.

Approximately 2 g of powder for each sample were weighed into china clay crucibles. The crucibles had been previously cleaned in 1:1 HCl/HNO<sub>3</sub> acid solution, rinsed with distilled water, and ignited to weight constancy at 1000°C for 6 hours. The total weights of crucible and sample mass were recorded to the fourth decimal. Samples were dried overnight in an oven in the open crucibles at 110°C. The dried samples were allowed to cool in a desiccator and then weighed, again to the fourth decimal. The weight differences before and after the above procedure is called the  $H_2O^-$  content of the samples and is assumed to be a measure for the amount of water that is adsorbed bound to the sample material.

Subsequently, the open crucibles with the sample powders were ignited for a minimum of 6 h at 1000°C in a blast furnace. Crucibles and samples were allowed to cool down in a desiccator and then weighed to the fourth decimal. The differences in weight corresponds to the total of adsorbed and structurally bound volatiles in the samples (e.g.  $H_2O^+$ , CO<sub>2</sub>, SO<sub>3</sub>, etc.), reduced by a factor corresponding quantitatively to the oxidation of Fe<sup>+2</sup> and/or Mn<sup>+2</sup>-bearing compounds during ignition.

### iv. X-ray fluorescence (XRF)

Major rock-forming oxides were analysed by XRF techniques using the procedure of Norrish and Hutton (1969). Subsequent to the procedure presented earlier for determination of LOI values, the ashed sample powders were fused with a lithium tetraborate + lithium carbonate + lanthanum oxide flux and formed into glass disks. These disks were then analysed using the K-alpha line for each of the major elements. Corrections for background were made by counting disks made from "blank" materials in the same fusion mixture at the analyte peak positions. Na<sub>2</sub>O was analysed on a pressed powder briquette of each sample (prepared with -300# powder) with background corrections derived from two measurements made on either side of the Na K-alpha line position.



Inter-element absorption and enhancement effects (“matrix effects”) were corrected by iterative calculations using the factors given in Norrish and Hutton (1969), and corrections for Ca interference on P (when a PET crystal was used) and for crystal fluorescence interferences on Mg (due to Fe, Mn, Ti, Ca and K) were also made.

Trace element analyses were carried out on pressed powder pellets. The elements determined were Zn, Cu, Ni, Co, Cr, V, Ba, Sc, Th, Pb, Y, Nb, Zr, Rb, and Sr. The K-alpha spectral line was used for analysis of most of those elements except for Pb, Th and Ba, where an L spectral line was used. Data reduction procedures included the correction of dead-time losses, instrumental drift, count-rate differences due to different positions in the sample-holder carousel, determination of background and its removal, and correction for interferences from other spectral lines and from impurities in the X-ray tube anode. Matrix effects were corrected using the appropriate mass absorption coefficients which for those elements whose wavelengths are shorter than the Fe K-absorption edge were determined by direct measurement (Norrish and Chappell, 1967). For those elements whose wavelengths fall on the long wavelength side of the Fe absorption edge, the primary and secondary mass absorption coefficients were calculated from major element analyses using Heinrich’s (1966) values for elemental mass absorption coefficients.

Background corrections were made by counting at spectral positions chosen as “interference free” and by calculating background correction factors from measurements on high purity SiO<sub>2</sub> “blank” samples. Interferences from tube anode impurities were determined using the same blank samples and correction factors calculated by ratioing the net tube impurity peak either to the mass absorption coefficient of the sample or to the measured intensity of a primary tube peak. Spectral line interferences were corrected for by determining interference correction factors from specially prepared “interference standards” which are blank samples to which 2000 ppm of a single element was added in the form of a suitable spec-pure chemical. Iterative correction procedures were applied in all cases where two or more elements produce spectral line interference with each other. The following elements were corrected for spectral line interferences (the interfering elements are given in parentheses): Nb (Y, Th); Zr (Sr, Th); Y (Rb, Th); Sr (Th); Th (Pb); Pb (Th); Ba (Ti, Sc); Co (Fe); Cr (V); V (Ti).

International and in-house-rock standards rock standards were used for calibration for both major and trace elements. The XRF spectrometer used was a Philips PW1410 instrument in the Geology Department, Rhodes University.

#### **v. Whole-rock FeO determination**

Determinations of whole-rock ferrous iron contents were performed on 12 selected iron-formation samples at the Council for Geoscience, Pretoria, South Africa.

1 g of each sample was decomposed in a mixture of diluted  $\text{H}_2\text{SO}_4$  (1:1) and 48% HF. Decomposition was performed in a thick-wall PTFE vessel with screw-type lid heated in a microwave. After completion of decomposition and rapid cooling of the vessel, the latter with its entire content is plunged into 300 ml of 5% freshly prepared boric acid in a 600 ml plastic beaker. The contents of the beaker are stirred gently, and the vessel and its lid are removed. 15 ml of a mixture of sulphuric/phosphoric acid and 10 drops of 1% barium diphenylamine sulphonate solution indicator are then added and titrated with standard potassium di-chromate solution (0.1N), until a constant purple colour is achieved.

A blank and certified reference material of similar chemical and mineralogical composition to the sample, was run with each sample through the entire procedure to ensure reproducibility of results. The difference (in ml) between the volume of the titrant used and the volume of the titrant for the blank is then calculated to wt% FeO in the sample using the following formula:

$$1\text{ml } 0.1\text{N K}_2\text{Cr}_2\text{O}_7 = 0.00718 \text{ g FeO}$$

#### **vi. Stable isotope determinations**

Carbon and oxygen isotopē ratios of calcite, ankerite and kutnahorite were obtained by reacting 10-30 mg of each of 43 whole-rock powdered samples from the Hotazel and Mooidraai Formations with 100% phosphoric acid, according to the method of McCrea (1950). Carbon dioxide from coexisting carbonate phases was separated by means of sequential acid treatment

at different temperatures depending on the mineralogical nature of the carbonate assemblage, as described by Al-Aasm et al. (1990; see also PART 4, section 4.1.2). A fractionation factor of 1.01025 was used to correct the  $\delta^{18}\text{O}$  value of the acid liberated  $\text{CO}_2$  at  $25^\circ\text{C}$  to that of calcite, while factors of 1.009, 1.01057 and 1.01065 were used to correct the  $\delta^{18}\text{O}$  values of the  $\text{CO}_2$  liberated at  $50^\circ\text{C}$  to those of calcite, ankerite and kutnahorite respectively. The oxygen and carbon isotope values are reported with respect to the SMOW and PDB reference standards respectively, to which they were calibrated using an internal carbonate standard which has been calibrated to the SMOW and PDB scales using NBS-19 carbonate standard ( $\delta^{18}\text{O} = 28.64$ ;  $\delta^{13}\text{C} = 1.95\text{‰}$ ). Repeated analyses of the internal standard suggest that  $\delta^{18}\text{O}$  and  $\delta^{13}\text{C}$  determinations are precise to better than 0.2 and 0.1‰ respectively.

Oxygen isotope data for silicate and oxide minerals were obtained by standard methods using  $\text{ClF}_3$  as a reagent (Borthwick and Harmon, 1982). Thirty-one samples were analysed in total, corresponding to ten chemically separated samples of microcrystalline quartz and two handpicked acmite separates, as well as binary mixtures of seven quartz-magnetite, ten quartz-hematite and two hematite-acmite samples (see also PART 4, section 4.2.2.1). Reaction times varied from 4 hours for quartz/acmite to overnight for magnetite and hematite-rich samples, and the extraction procedures are described in detail in Venemann and Smith (1990). The quartz standard NBS-28 was analysed in duplicate along with eight samples in each run, and data were normalised to the SMOW scale using the value of 9.64‰ recommended by Coplen et al. (1983). The average mean deviation of 8 duplicate NBS-28 quartz standard analyses was 0.15‰.

### **vii. Ion chromatography**

High-performance ion chromatography was applied for the analysis of rare earth elements in 12 iron-formation samples of the Hotazel iron-formation. The analyses were performed at the Department of Geological Sciences, University of Cape Town, using a Dionex® 4000i Gradient ion chromatograph in which eluent composition and flow rate are microprocessor controlled. Separation of the REE was effected using a Dionex® CS5 column, while the eluted REE were reacted with a colour complexing agent and detected photometrically using a UV/visible light detector at a wavelength of 520nm. Sample dissolution and removal of matrix elements that

would otherwise interfere with the chromatogram, were achieved using standard cation-exchange procedures routinely applied in the preparation of samples for ICP analysis. Details on the technique can be found in the paper by le Roex and Watkins (1990).

#### **viii. Inductively coupled plasma - mass spectrometry (ICP-MS)**

The technique was implemented at the Department of Geological Sciences, University of Cape Town on 5 selected samples of the Mooidraai Formation. For each sample, 50 mg of sample powder were dissolved using a standard, multi-stage HF/HNO<sub>3</sub> digestion procedure, and were finally taken up in 50 ml of ~2 % HNO<sub>3</sub> containing 10 ppb each of In and Re (used as internal standards), resulting in a 1000-fold dilution. Only high-purity bottle-distilled acids and milli-pore water were used. Standard solutions were made using an artificial multi-element REE standard solution and the same internal standard ~2% HNO<sub>3</sub> solution used to dissolve the samples.

The samples and standards were analysed on a Perkin Elmer/Sciex Elan 6000 ICP-MS in peak-hopping mode and using the autolens option, with dwell times of 50 ms per AMU and total integration times of 3 sec per analyte peak. Calibration was achieved by external standardisation using a blank and two standard solutions of 20 ppb and 50 ppb; linear calibration was forced through the origin. Blank subtraction was carried out after internal standardisation to In and Re for both samples and standards. All samples were run in duplicate and the data represent average values of these two analyses. The instrument was set up to minimise potential interferences by oxide and doubly charged species (CeO/Ce < 3 %; Ba<sup>++</sup>/Ba<sup>+</sup> < 3 %). Furthermore, the data were corrected for interferences by REE oxides and BaO. The ICP-MS instrument parameters used were as follows:

- nebuliser gas flow: 0.92 L/min
- main gas flow: 15 L/min
- auxiliary gas flow: 0.75 L/min ICP
- RF forward power: 1100 watts
- vacuum in quadrupole chamber:  $1.89 \cdot 10^{-5}$  torr.

### **Appendix III: Whole-rock geochemical data**

This Appendix contains tabulated bulk-rock geochemical data obtained for all samples analysed in this thesis. Data are separated in two major groups, namely those obtained from samples from borehole intersections drilled in the southernmost KMF, and those obtained from boreholes drilled in the northernmost portions. Major element data are expressed in weight percent (wt%) whereas trace element concentrations are presented in parts per million (ppm). Analytical totals have been calculated by adding up major element concentrations only.

Total Fe-oxide concentrations are shown as  $\text{Fe}_2\text{O}_3$ ; total Mn-oxide concentrations as MnO.

#### Abbreviations used:

LOI: Loss on ignition

lId: lower than the limit of detection

nd: not determined

Sample wt%	SiO <sub>2</sub>	TiO <sub>2</sub>	Al <sub>2</sub> O <sub>3</sub>	Fe <sub>2</sub> O <sub>3</sub>	MnO	MgO	CaO	Na <sub>2</sub> O	K <sub>2</sub> O	P <sub>2</sub> O <sub>5</sub>	LOI	H <sub>2</sub> O	Total
<b>Southern KMF</b>													
R65-2	37.66	0.03	0.19	34.79	0.15	2.22	12.95	0.01	0.01	0.05	12.40	0.23	100.69
R65-3	35.97	0.04	0.18	43.97	0.37	2.49	7.58	0.01	0.01	0.11	8.92	0.30	99.95
R65-5	6.23	0.07	0.39	12.66	11.16	3.32	35.23	0.08	0.01	0.04	31.16	0.4	100.75
R65-12	30.16	0.04	0.20	42.28	1.12	3.04	12.29	0.02	0.03	0.11	11.20	0.46	100.95
R65-19	42.89	0.04	0.18	45.90	0.39	2.66	4.07	0.01	0.04	0.18	4.40	0.22	100.98
R65-20	39.60	0.05	0.04	49.18	0.52	2.64	2.58	0.01	0.02	0.18	5.02	0.29	100.13
R65-21	26.27	0.05	0.44	51.12	1.96	2.51	8.55	0.01	0.05	0.19	9.16	0.46	100.77
R65-30	28.63	0.05	0.32	48.14	5.24	2.81	4.44	0.02	0.04	0.07	9.60	0.37	99.73
R65-31	17.08	0.06	0.23	45.90	17.65	5.32	0.96	0.02	0.02	0.07	11.39	0.32	99.02
R59-1	36.00	0.04	0.18	39.56	0.13	2.45	11.12	0.02	0.04	0.05	11.11	0.28	100.98
R59-2	39.35	0.04	0.18	44.33	0.32	2.75	6.23	0.02	0.02	0.10	7.31	0.24	100.89
R59-3	30.38	0.05	0.46	32.81	2.21	2.18	15.77	0.05	0.07	0.05	15.65	0.37	100.05
R59-9	12.96	0.05	0.31	10.87	7.17	1.39	35.69	0.03	0.04	0.04	30.93	0.36	99.84
R59-13	41.83	0.04	0.30	45.76	0.29	2.48	4.21	0.02	0.05	0.14	5.54	0.22	100.88
R59-14	40.89	0.05	0.36	46.39	0.24	2.42	3.55	0.01	0.04	0.15	6.29	0.42	100.81
R59-15	41.87	0.04	0.36	45.67	0.20	2.19	2.06	0.02	0.02	0.13	7.34	0.40	100.30
R59-16	45.38	0.07	0.86	36.70	0.04	2.77	7.67	0.02	0.02	0.11	6.29	0.42	100.35
R59-17	40.31	0.05	0.45	42.70	0.64	2.72	3.85	0.01	0.02	0.19	9.21	0.68	100.83
R59-18	38.67	0.05	0.28	52.43	0.60	2.09	2.37	0.01	0.01	0.28	3.43	0.36	100.58
R63-4	8.05	0.05	0.17	9.12	8.40	1.58	38.11	0.10	0.02	0.04	33.39	0.27	99.30
R63-5	33.50	0.04	0.16	39.60	1.38	3.04	10.74	0.02	0.01	0.08	10.45	0.38	99.40
R63-8	30.30	0.03	0.15	35.32	0.55	2.40	15.62	0.01	0.01	0.07	14.49	0.35	99.30
R63-9	39.15	0.04	1.33	39.36	0.13	3.12	8.27	0.11	0.48	0.13	7.56	0.70	100.98
R63-10	36.10	0.04	0.02	51.24	0.14	1.98	5.05	0.01	0.01	0.18	5.96	0.23	100.96
R63-11	36.60	0.04	0.13	52.21	0.09	1.95	3.80	0.01	0.02	0.13	5.64	0.27	100.89
R63-12	39.82	0.04	0.16	50.99	0.09	2.01	3.12	0.01	0.01	0.17	4.21	0.34	100.97
R63-13	45.77	0.06	0.62	39.77	0.33	3.24	2.42	0.02	0.05	0.09	7.86	0.72	100.95

Sample wt%	SiO <sub>2</sub>	TiO <sub>2</sub>	Al <sub>2</sub> O <sub>3</sub>	Fe <sub>2</sub> O <sub>3</sub>	MnO	MgO	CaO	Na <sub>2</sub> O	K <sub>2</sub> O	P <sub>2</sub> O <sub>5</sub>	LOI	H <sub>2</sub> O	Total
R63-14	46.24	0.05	0.28	50.00	0.35	1.01	1.35	0.02	0.01	0.01	1.44	0.16	100.92
R63-20	23.07	0.06	0.40	47.59	10.51	2.96	3.61	0.02	0.01	0.08	10.25	0.52	99.08
R70-11	24.51	0.05	0.28	36.40	0.75	0.90	20.63	0.03	0.06	0.07	16.92	0.27	100.87
R70-12	52.64	0.05	3.85	31.46	0.07	5.64	0.22	0.26	1.76	0.01	3.28	1.17	100.41
R70-13	43.15	0.04	0.15	45.58	0.12	1.90	4.60	0.01	0.04	0.10	4.85	0.20	100.74
R70-14	40.49	0.03	0.16	46.09	0.14	1.86	5.60	0.01	0.04	0.14	6.00	0.30	100.86
R70-15	38.06	0.04	0.12	50.02	0.14	2.24	4.69	0.01	0.03	0.20	5.10	0.25	100.90
R70-16	37.84	0.04	0.12	52.96	0.16	2.24	2.75	0.01	0.02	0.14	4.20	0.20	100.68
R70-17	40.15	0.04	0.16	50.70	0.16	2.13	2.33	0.01	0.03	0.22	4.24	0.32	100.49
R70-18	43.86	0.05	0.49	41.39	0.40	2.83	2.54	0.01	0.02	0.09	8.42	0.53	100.63
R70-19	42.99	0.04	0.32	44.00	0.48	0.94	6.27	0.02	0.02	0.14	5.25	0.40	100.87
R70-29	20.82	0.06	0.37	34.99	16.25	9.22	2.50	0.03	0.03	0.04	14.91	0.36	99.58
SM31-2	30.86	0.02	0.28	42.80	0.29	2.32	11.46	0.01	0.03	0.08	11.89	0.18	100.22
SM31-3	37.20	0.03	0.26	45.90	0.31	2.20	6.61	lld	0.03	0.09	7.37	0.15	100.15
SM31-5	35.40	0.03	0.14	46.55	0.58	2.33	7.23	0.01	0.04	0.09	7.78	0.14	100.32
SM31-10	7.73	0.04	0.19	10.39	9.75	1.63	36.66	0.01	lld	0.07	32.81	0.30	99.58
SM31-15	29.52	0.04	0.40	43.23	0.50	1.79	13.04	0.06	0.10	0.11	11.29	0.20	100.28
SM31-16	45.29	0.05	2.85	42.21	0.13	3.79	0.56	0.31	1.34	0.15	3.61	0.02	100.31
SM31-17	34.47	0.03	0.10	51.38	0.15	2.02	5.06	lld	lld	0.23	6.42	0.21	100.07
SM31-18	42.59	0.04	0.35	45.08	0.49	2.13	3.74	0.03	0.05	0.16	5.88	0.21	100.75
SM31-20	25.16	0.04	0.30	50.38	11.21	4.90	5.07	0.11	0.11	0.10	1.79	0.23	99.40
Mn ore													
R59-5	7.60	0.06	0.27	15.35	42.21	3.80	12.85	lld	lld	0.05	17.64	0.22	100.05
R59-11	7.93	0.04	0.34	17.56	28.84	5.66	15.24	0.02	0.01	0.06	28.58	0.18	99.46
R59-24	11.34	0.05	0.44	20.82	39.93	3.98	6.94	lld	lld	0.07	15.59	0.11	99.27
R63-7	10.50	0.05	0.42	14.69	23.18	2.89	18.98	0.02	0.09	0.10	27.68	0.46	99.06
R63-15	5.50	0.05	0.70	7.17	45.02	5.24	16.78	lld	lld	0.08	18.68	0.09	99.31
R63-17	5.19	0.05	0.27	5.61	45.55	5.23	17.49	lld	lld	0.08	19.42	0.17	99.06

Sample wt%	SiO <sub>2</sub>	TiO <sub>2</sub>	Al <sub>2</sub> O <sub>3</sub>	Fe <sub>2</sub> O <sub>3</sub>	MnO	MgO	CaO	Na <sub>2</sub> O	K <sub>2</sub> O	P <sub>2</sub> O <sub>5</sub>	LOI	H <sub>2</sub> O	Total
R65-7	7.44	0.05	0.33	9.21	49.98	3.41	13.12	lld	lld	0.06	15.37	0.10	99.07
R65-24	4.33	0.07	0.37	5.94	38.67	3.63	22.49	lld	lld	0.08	23.55	0.09	99.22
R65-27	3.90	0.06	0.26	4.93	53.63	2.16	18.68	lld	lld	0.08	15.96	0.19	99.85
R65-29	8.29	0.06	0.35	18.83	41.42	5.37	10.52	lld	lld	0.08	14.49	0.13	99.54
R70-10	6.76	0.04	0.36	22.13	25.41	3.20	16.27	lld	0.03	0.07	25.42	0.26	99.95
R70-20	4.85	0.05	0.38	9.62	20.50	3.77	28.29	lld	0.01	0.09	31.61	0.32	99.49
R70-21	5.05	0.05	0.49	16.62	33.16	4.09	19.05	lld	lld	0.08	20.23	0.22	99.04
R70-23	5.14	0.07	0.46	6.37	38.41	3.62	22.19	lld	lld	0.08	23.28	0.25	99.87
<b>Northern KMF</b>													
GL26-1	35.03	0.03	0.23	44.80	0.79	0.95	9.97	0.05	0.05	0.11	8.15	0.10	100.26
GL26-2	38.59	0.02	0.12	42.63	0.69	0.85	9.50	0.03	0.03	0.11	7.67	0.06	100.30
GL26-3	35.67	0.03	0.15	48.70	0.57	1.03	7.80	0.01	0.02	0.11	6.16	0.07	100.32
GL26-3a	37.89	0.03	0.10	45.74	0.56	1.13	8.01	lld	lld	0.13	6.46	0.10	100.15
GL26-4	34.13	0.03	0.39	49.63	0.45	1.21	7.75	lld	0.02	0.11	6.48	0.13	100.33
GL26-5	35.76	0.02	0.17	44.70	0.44	1.21	9.91	lld	0.01	0.12	8.01	0.13	100.48
GL26-6	28.82	0.03	0.16	44.74	0.39	0.78	14.05	lld	0.01	0.15	10.75	0.08	99.96
GL26-7	26.17	0.03	0.19	32.36	0.55	0.85	21.69	0.01	0.03	0.15	17.76	0.13	99.92
GL26-9	7.22	0.05	0.21	16.75	11.18	1.30	33.20	lld	0.01	0.08	30.06	0.23	100.28
GL26-11	27.72	0.03	0.17	31.43	1.67	0.79	20.46	lld	lld	0.12	17.25	0.06	99.70
GL26-12	33.86	0.03	0.18	31.64	1.98	0.98	16.65	lld	lld	0.18	14.46	0.07	100.03
GL26-12a	47.25	0.03	0.11	47.34	0.92	0.66	2.44	lld	lld	0.20	1.62	0.01	100.58
GL26-13	41.50	0.03	0.80	47.70	1.19	1.33	3.88	lld	lld	0.26	3.58	0.07	100.34
GL26-15	25.82	0.04	0.55	61.50	1.88	1.04	3.93	lld	lld	0.08	4.59	0.05	99.48
GL26-16	45.55	0.04	0.30	48.49	0.37	2.31	1.45	lld	lld	0.22	0.77	0.11	99.61
MK2H-2	12.00	0.25	5.33	50.49	25.30	0.48	0.92	0.11	1.52	0.09	3.22	0.26	99.97
MK2H-3	0.44	0.05	0.41	98.05	0.46	0.05	0.40	0.01	0.01	0.19	0.55	0.08	100.70
MK2H-4	1.18	0.04	0.40	95.52	0.62	0.09	0.69	0.14	0.01	0.28	0.83	0.05	99.85
MK2H-5	0.69	0.03	0.25	95.57	1.34	0.10	0.86	0.08	0.02	0.36	0.90	0.04	100.24



Sample wt%	SiO <sub>2</sub>	TiO <sub>2</sub>	Al <sub>2</sub> O <sub>3</sub>	Fe <sub>2</sub> O <sub>3</sub>	MnO	MgO	CaO	Na <sub>2</sub> O	K <sub>2</sub> O	P <sub>2</sub> O <sub>5</sub>	LOI	H <sub>2</sub> O	Total
MK2H-6	4.33	0.07	0.24	58.40	32.39	0.18	2.48	lld	lld	0.06	1.15	0.12	99.42
MK2H-8	45.69	0.03	0.12	53.76	0.09	lld	0.17	0.22	0.01	0.11	0.11	0.04	100.35
MK2H-9	42.24	0.03	0.38	57.22	0.08	lld	0.14	0.06	0.02	0.10	0.12	0.01	100.40
MK2H-10	45.18	0.02	0.14	54.63	0.07	lld	0.10	0.04	0.02	0.08	0.17	0.01	100.46
MK2H-11a	40.89	0.03	0.11	58.66	0.08	lld	0.12	0.08	0.01	0.09	0.13	0.01	100.21
MK2H-11b	42.28	0.03	0.15	56.55	0.11	0.03	0.20	0.33	0.01	0.11	0.15	0.02	99.97
MK2H-12	39.75	0.02	0.18	58.77	0.13	0.03	0.25	0.50	0.01	0.12	0.14	0.07	99.97
MK2H-13	40.51	0.03	0.18	58.53	0.09	lld	0.29	0.12	0.01	0.19	0.13	0.07	100.15
MK2H-14	41.76	0.03	0.22	56.23	0.26	0.06	0.46	0.69	0.01	0.19	0.15	0.05	100.11
MK2H-15	50.04	0.02	0.12	49.48	0.28	0.04	0.11	0.13	0.01	0.05	0.09	0.05	100.42
MK2H-17	35.68	0.03	0.34	49.03	1.63	1.80	4.80	5.35	0.01	0.05	0.42	0.16	99.30
MK2H-18	3.52	0.05	0.42	68.55	7.02	1.18	10.37	0.01	0.01	0.06	7.90	0.15	99.24
MK2H-19	12.28	0.04	0.33	74.21	0.91	5.13	5.09	0.01	0.01	0.18	1.65	0.19	100.03
MK3I-3	47.25	0.02	0.08	51.09	0.68	lld	0.50	lld	lld	0.25	0.16	0.05	100.08
MK3I-4	47.62	0.02	0.08	50.87	0.68	0.01	0.60	lld	0.01	0.03	0.52	0.06	100.50
MK3I-5	35.62	0.03	0.23	63.50	0.75	0.01	0.08	lld	0.01	0.04	0.09	0.06	100.42
MK3I-6	45.46	0.02	0.67	54.05	0.27	lld	0.13	lld	0.01	0.07	0.07	0.04	100.79
MK3I-6a	47.27	0.03	0.21	52.55	0.15	lld	0.13	lld	lld	0.12	0.02	0.04	100.52
MK3I-7	45.53	0.03	0.09	53.56	0.33	lld	0.01	lld	lld	0.01	0.08	0.04	99.68
MK3I-8a	46.96	0.02	0.15	53.11	0.39	0.02	0.07	lld	0.01	0.04	0.01	0.08	100.86
MK3I-8b	45.92	0.02	0.11	53.82	0.25	0.01	0.07	lld	lld	0.05	0.01	0.11	100.37
MK3I-8c	45.04	0.02	0.06	54.46	0.24	lld	0.06	lld	lld	0.05	0.04	0.07	100.04
MK3I-9	42.39	0.02	0.12	56.66	0.46	lld	0.11	lld	lld	0.04	0.18	0.05	100.03
MK3I-10	31.80	0.03	0.20	58.16	1.13	0.09	0.29	6.88	lld	0.02	0.34	0.11	99.05
MK3I-11	33.49	0.03	0.21	56.59	0.67	0.02	0.19	6.74	lld	0.04	0.64	0.40	99.02
MK3I-12	40.57	0.02	0.17	58.52	0.08	lld	0.23	0.19	0.01	0.16	0.15	0.07	100.16
MK3I-13	39.17	0.03	0.15	60.25	0.09	lld	0.09	0.09	0.01	0.07	0.13	0.06	100.14
MK3I-14a	38.41	0.03	0.21	60.71	0.08	lld	0.22	0.15	0.01	0.14	0.15	0.05	100.16
MK3I-14b	40.37	0.03	0.13	58.28	0.07	lld	0.56	0.07	0.01	0.41	0.12	0.06	100.11

Sample wt%	SiO <sub>2</sub>	TiO <sub>2</sub>	Al <sub>2</sub> O <sub>3</sub>	Fe <sub>2</sub> O <sub>3</sub>	MnO	MgO	CaO	Na <sub>2</sub> O	K <sub>2</sub> O	P <sub>2</sub> O <sub>5</sub>	LOI	H <sub>2</sub> O	Total
MK3I-15	41.59	0.03	0.16	49.97	3.45	0.35	0.91	3.13	0.05	0.03	0.19	0.10	99.96
MK3I-16	50.02	0.03	0.10	40.73	1.16	0.45	2.66	4.59	0.09	0.05	0.45	0.09	100.42
N12D-1	4.17	0.03	0.71	88.45	2.18	0.41	1.38	0.09	0.21	0.33	1.31	0.17	99.44
N12D-2	0.72	0.04	0.25	90.58	2.78	0.21	2.49	lld	0.08	0.16	1.77	0.09	99.17
N12D-3	43.02	0.02	0.03	54.23	0.34	0.38	1.00	0.19	lld	0.13	0.32	0.14	99.80
N12D-4	38.65	0.02	0.15	60.6	0.07	lld	0.24	0.04	0.01	0.16	0.12	0.06	100.12
N12D-5	36.87	0.03	0.37	62.38	0.06	0.01	0.37	lld	0.01	0.20	0.20	0.06	100.56
N12D-7	43.88	0.02	0.14	55.74	0.06	lld	0.13	lld	lld	0.10	0.06	0.07	100.20
N12D-8	42.26	0.02	0.14	57.23	0.05	lld	0.13	lld	lld	0.11	0.07	0.05	100.06
N12D-9	43.77	0.02	0.10	55.64	0.05	lld	0.15	lld	lld	0.12	0.07	0.05	99.97
N12D-10b	43.61	0.02	0.05	56.3	0.06	0.01	0.11	lld	lld	0.09	0.05	0.05	100.35
N12D-11	46.26	0.02	0.13	53.35	0.05	lld	0.38	lld	lld	0.27	0.09	0.05	100.60
N12D-13	48.72	0.02	0.27	50.95	0.13	0.04	0.28	lld	0.01	0.19	0.02	0.07	100.70
N12D-14	40.65	0.02	0.25	56.42	0.27	1.28	0.39	0.93	0.03	0.03	0.14	0.09	100.50
N12D-16	1.56	0.04	0.24	53.24	1.09	1.30	23.74	lld	0.01	0.15	17.54	0.28	99.19
N12D-17	2.06	0.05	0.13	61.89	0.88	1.25	17.97	lld	lld	0.10	14.83	0.33	99.49
N12D-18	36.14	0.03	0.23	62.21	0.15	0.36	0.23	lld	lld	0.12	0.16	0.12	99.75
N12D-19	46.93	0.03	0.26	52.51	0.07	0.08	0.28	lld	0.03	0.09	0.09	0.06	100.43
MK2G-1	9.17	0.58	2.83	83.17	1.58	0.04	0.32	0.94	0.02	0.20	0.17	0.10	99.12
MK2G-2	40.71	0.02	0.11	58.62	0.68	0.01	0.09	0.01	lld	0.06	-0.02	0.03	100.32
MK2G-2a	39.53	0.02	0.13	59.82	0.66	lld	0.05	lld	lld	0.03	-0.01	0.06	100.29
MK2G-3	46.16	0.02	0.13	53.75	0.42	lld	0.03	lld	lld	0.03	-0.01	0.03	100.56
MK2G-3a	49.74	0.03	0.15	50.22	0.31	lld	0.05	lld	lld	0.05	-0.05	0.05	100.55
MK2G-4	45.04	0.03	0.06	54.80	0.36	lld	0.02	lld	lld	0.03	-0.01	0.04	100.37
MK2G-4a	42.97	0.03	0.06	56.49	0.44	lld	0.03	lld	lld	0.04	-0.03	0.04	100.07
MK2G-5	47.89	0.02	0.10	51.26	0.79	lld	0.15	lld	lld	0.03	0.16	0.06	100.46
MK2G-6	47.77	0.03	0.12	50.91	0.97	0.01	0.20	lld	lld	0.04	0.23	0.08	100.36
MK2G-7	48.76	0.02	0.19	51.38	0.41	lld	0.05	lld	lld	0.04	-0.08	0.06	100.83
MK2G-8	49.75	0.02	0.07	50.18	0.39	lld	0.04	lld	lld	0.03	-0.05	0.06	100.49

Sample wt%	SiO <sub>2</sub>	TiO <sub>2</sub>	Al <sub>2</sub> O <sub>3</sub>	Fe <sub>2</sub> O <sub>3</sub>	MnO	MgO	CaO	Na <sub>2</sub> O	K <sub>2</sub> O	P <sub>2</sub> O <sub>5</sub>	LOI	H <sub>2</sub> O	Total
MK2G-9	46.89	0.02	0.12	52.67	0.44	lld	0.08	0.01	lld	0.07	-0.07	0.06	100.29
MK2G-10	34.85	0.03	0.41	52.82	0.83	0.15	1.97	6.98	lld	0.09	1.03	0.09	99.25
MK2G-11	40.30	0.03	0.19	59.36	0.07	lld	0.12	0.02	0.01	0.09	-0.03	0.06	100.22
MK2G-12	38.89	0.03	0.17	60.94	0.07	lld	0.18	lld	0.01	0.14	0.00	0.06	100.49
MK2G-13	36.96	0.03	0.50	62.47	0.06	0.02	0.17	0.01	0.01	0.12	-0.03	0.07	100.39
MK2G-14	45.17	0.02	0.13	55.16	0.05	lld	0.14	lld	lld	0.12	-0.06	0.05	100.78
MK2G-16	43.44	0.02	0.13	40.94	2.60	1.51	4.88	lld	lld	0.18	6.53	0.09	100.32
MK2G-17	43.95	0.03	0.24	41.81	2.72	1.20	4.20	lld	lld	0.20	5.52	0.07	99.94
N91B-1	46.73	0.03	0.15	53.58	0.16	lld	0.14	lld	0.01	0.12	-0.14	0.12	100.90
N91B-2	53.80	0.02	lld	45.99	0.08	lld	0.19	lld	lld	0.14	-0.10	0.56	100.68
N91B-3	46.42	0.03	0.74	53.06	0.17	0.03	0.19	lld	0.02	0.13	-0.06	0.08	100.81
N91B-4	41.66	0.02	0.07	57.98	0.16	lld	0.08	lld	lld	0.07	-0.04	0.06	100.06
N91B-5	43.49	0.02	0.08	56.30	0.14	lld	0.11	lld	lld	0.09	-0.03	0.07	100.27
N91B-6	42.36	0.02	0.01	57.23	0.06	lld	0.11	lld	lld	0.09	-0.06	0.07	99.89
N91B-7	46.92	0.02	0.04	52.93	0.07	lld	0.09	lld	lld	0.08	-0.08	0.09	100.16
N91B-8	44.29	0.03	0.19	55.19	0.08	0.13	0.10	lld	0.01	0.08	0.01	0.06	100.17
N91B-9	21.03	0.03	0.20	38.85	16.37	5.37	4.05	0.70	0.18	0.08	11.96	0.26	99.08
N91B-10	21.36	0.03	0.19	38.83	16.52	5.75	3.90	0.73	0.19	0.08	11.18	0.30	99.06
N91B-11	31.05	0.03	0.16	49.69	1.02	1.12	8.86	lld	0.01	0.10	7.47	0.13	99.64
N91B-12	31.63	0.03	0.18	43.81	1.20	1.35	11.19	lld	lld	0.13	10.12	0.12	99.76
N91B-13	33.23	0.03	0.16	51.97	0.79	0.88	7.02	lld	lld	0.10	5.71	0.13	100.02
N91B-14	36.64	0.03	0.24	50.50	1.22	1.59	4.70	lld	lld	0.10	5.08	0.12	100.22
N91B-15	31.69	0.03	0.30	51.97	1.18	2.28	6.05	lld	lld	0.11	6.85	0.11	100.57
N91B-16	37.31	0.03	0.16	45.69	1.04	2.11	6.58	lld	lld	0.09	7.00	0.09	100.10
N91B-17	36.12	0.02	0.19	49.15	0.72	2.89	5.14	lld	lld	0.11	6.21	0.08	100.63
N91B-18	37.95	0.02	0.46	52.60	0.57	1.84	3.49	lld	0.01	0.11	3.77	0.07	100.89
N91B-19	38.89	0.02	0.24	46.13	0.77	2.77	5.11	lld	lld	0.11	6.19	0.09	100.32
N91B-20	33.77	0.03	0.24	55.75	0.55	1.97	3.67	lld	0.01	0.12	3.89	0.11	100.11
N91B-21	31.22	0.02	0.12	43.21	0.96	4.72	8.30	lld	lld	0.12	11.23	0.08	99.98

Sample wt%	SiO <sub>2</sub>	TiO <sub>2</sub>	Al <sub>2</sub> O <sub>3</sub>	Fe <sub>2</sub> O <sub>3</sub>	MnO	MgO	CaO	Na <sub>2</sub> O	K <sub>2</sub> O	P <sub>2</sub> O <sub>5</sub>	LOI	H <sub>2</sub> O	Total
N91B-22	38.87	0.02	0.14	48.94	0.75	2.10	4.15	lld	lld	0.15	4.86	0.10	100.08
N91B-23	33.25	0.03	0.20	45.46	1.32	2.27	8.42	lld	lld	0.17	8.94	0.05	100.11
N91B-24	30.94	0.03	0.21	51.90	2.13	2.20	5.71	lld	lld	0.08	6.17	0.04	99.41
N91B-25	13.09	0.03	0.22	26.36	10.98	1.70	23.31	lld	lld	0.09	23.29	0.22	99.29
N91B-26	18.32	0.03	0.16	30.64	5.61	1.96	21.68	lld	lld	0.09	20.72	0.14	99.35
N91B-26a	25.87	0.02	0.19	53.54	1.80	1.40	6.06	lld	lld	0.10	10.90	0.18	100.06
N91B-27	31.17	0.03	0.28	45.17	2.87	2.22	11.00	lld	lld	0.11	6.35	0.07	99.27
N91B-28	36.82	0.03	0.32	32.86	2.11	2.05	14.11	lld	lld	0.16	10.87	0.08	99.41
N91B-29	43.11	0.03	lld	37.21	1.56	0.52	3.41	lld	lld	0.14	13.96	0.12	100.06
N91B-30	19.40	0.02	0.20	50.07	11.86	9.66	3.66	lld	lld	0.09	4.08	0.08	99.12
N91B-31	42.52	0.05	0.68	49.42	1.25	1.17	2.32	lld	lld	0.11	2.57	0.10	100.19
BEL7A-2	4.04	0.39	3.87	70.36	7.83	4.28	2.44	lld	0.01	0.21	6.67	0.28	100.38
BEL7A-3	47.13	0.02	0.16	50.60	0.24	0.17	0.45	lld	0.02	0.07	0.86	0.04	99.76
BEL7A-4	37.81	0.03	0.23	45.54	1.59	2.38	4.94	lld	0.01	0.22	7.22	0.05	100.02
BEL7A-5	46.10	0.02	0.13	53.48	0.04	0.02	0.19	lld	lld	0.14	0.01	0.03	100.16
BEL7A-6	53.13	0.02	0.07	46.13	0.32	0.03	0.22	lld	lld	0.14	0.20	0.06	100.32
BEL7A-7	43.96	0.03	0.12	55.32	0.11	0.07	0.24	lld	lld	0.09	0.21	0.04	100.19
BEL7A-8a	32.73	0.02	0.15	45.07	1.71	3.57	5.42	lld	lld	0.14	10.91	0.10	99.82
BEL7A-8b	20.16	0.04	0.29	40.51	14.79	3.79	5.36	lld	0.01	0.08	13.85	0.23	99.11
BEL7A-9	34.78	0.03	0.22	45.26	1.51	3.50	4.41	lld	lld	0.09	10.50	0.06	100.36
BEL7A-11	35.57	0.03	0.18	42.63	1.46	3.67	5.06	lld	lld	0.12	11.47	0.10	100.29
BEL7A-12a	29.37	0.03	0.24	51.10	1.35	3.41	4.54	lld	lld	0.09	9.94	0.08	100.15
BEL7A-12b	31.29	0.03	0.21	48.06	1.46	3.58	4.68	lld	lld	0.09	10.86	0.05	100.31
BEL7A-13	32.71	0.03	0.12	38.32	1.50	4.77	8.10	lld	0.01	0.10	14.54	0.03	100.22
BEL7A-14	33.52	0.03	0.14	53.55	0.84	2.27	3.30	lld	lld	0.12	6.22	0.06	100.05
BEL7A-15	33.14	0.03	0.18	37.78	1.31	4.68	8.54	lld	lld	0.12	14.51	0.07	100.36
BEL7A-16	28.34	0.03	0.26	33.66	1.80	6.36	10.76	lld	lld	0.13	18.64	0.18	100.16
BEL7A-17	17.55	0.03	0.14	49.14	9.75	9.14	3.44	lld	lld	0.08	9.67	0.17	99.11
BEL7A-18	32.65	0.04	0.23	55.34	1.70	1.59	3.95	lld	lld	0.17	4.33	0.08	100.08

Sample wt%	SiO <sub>2</sub>	TiO <sub>2</sub>	Al <sub>2</sub> O <sub>3</sub>	Fe <sub>2</sub> O <sub>3</sub>	MnO	MgO	CaO	Na <sub>2</sub> O	K <sub>2</sub> O	P <sub>2</sub> O <sub>5</sub>	LOI	H <sub>2</sub> O	Total
BEL7A-19	32.21	0.04	0.23	60.34	0.70	1.30	2.56	lld	lld	0.15	2.31	0.05	99.89
BEL7A-20	45.24	0.04	0.49	51.21	0.24	0.82	1.61	lld	0.01	0.15	0.45	0.04	100.30
BEL4C-1	3.43	0.06	1.83	52.78	39.59	0.81	0.46	lld	lld	0.10	-0.12	0.14	99.08
BEL4C-3	47.34	0.02	0.04	52.01	0.04	0.02	0.21	lld	lld	0.14	0.09	0.07	99.98
BEL4C-4	49.91	0.02	0.15	49.52	0.10	0.07	0.51	lld	0.01	0.25	0.25	0.04	100.83
BEL4C-5	37.42	0.03	0.28	56.73	0.74	0.70	1.76	lld	0.04	0.11	2.26	0.06	100.13
BEL4C-6	25.43	0.03	0.21	40.63	10.16	4.17	5.73	lld	lld	0.07	12.62	0.13	99.18
BEL4C-7	30.56	0.03	0.16	49.35	1.09	3.49	6.84	lld	lld	0.14	8.77	0.08	100.51
BEL4C-8	36.98	0.03	0.13	43.95	1.13	3.11	6.30	lld	lld	0.10	8.43	0.09	100.25
BEL4C-9	36.50	0.02	0.24	49.12	0.93	2.34	4.99	lld	lld	0.11	6.17	0.09	100.51
BEL4C-11	33.72	0.03	0.26	51.61	0.85	2.38	5.05	lld	lld	0.09	6.37	0.07	100.43
BEL4C-13	31.31	0.03	0.23	44.35	1.15	3.87	8.09	lld	lld	0.12	11.03	0.07	100.25
BEL4C-14	29.49	0.03	0.17	46.16	1.03	3.97	8.20	lld	lld	0.12	10.81	0.05	100.03
BEL4C-15	34.52	0.02	0.23	48.20	0.86	2.77	6.03	lld	lld	0.13	7.60	0.09	100.45
BEL4C-16	34.03	0.02	0.11	35.53	1.32	4.81	9.90	lld	lld	0.15	14.19	0.08	100.14
BEL4C-17	40.42	0.02	0.19	45.28	0.81	2.51	5.11	lld	lld	0.22	5.86	0.02	100.44
BEL4C-19	21.34	0.03	0.20	39.78	4.26	4.94	12.00	lld	lld	0.10	16.61	0.10	99.36
BEL4C-20	32.07	0.02	0.14	52.50	1.42	2.43	5.33	lld	lld	0.10	6.29	0.04	100.34
BEL4C-22	39.20	0.02	0.05	47.59	1.92	4.02	2.86	lld	lld	0.15	4.50	0.11	100.42
BEL4C-23	52.07	0.02	0.01	34.38	2.16	4.74	2.51	lld	lld	0.16	4.42	0.24	100.71
BEL4C-24	14.00	0.03	0.26	52.88	10.01	7.28	3.81	lld	lld	0.08	10.71	0.17	99.23
BEL4C-25	33.58	0.03	0.28	54.35	2.33	2.52	2.87	lld	lld	0.10	4.15	0.16	100.37
BEL4C-26	28.58	0.03	0.13	59.93	1.40	1.34	3.94	lld	lld	0.13	4.10	0.04	99.62
BEL4C-27	29.44	0.04	0.24	58.23	1.23	1.58	4.49	lld	0.02	0.16	4.46	0.05	99.94
BEL4C-28	30.16	0.03	0.29	61.82	0.61	2.01	2.62	0.04	0.05	0.17	2.27	0.10	100.17
BEL4C-29	38.18	0.04	0.27	51.70	0.77	2.57	3.08	lld	0.03	0.06	3.56	0.07	100.33
BEL4C-30	35.94	0.04	0.41	59.46	0.42	1.47	1.28	0.04	0.06	0.12	0.64	0.14	100.02

Sample wt%	SiO <sub>2</sub>	TiO <sub>2</sub>	Al <sub>2</sub> O <sub>3</sub>	Fe <sub>2</sub> O <sub>3</sub>	MnO	MgO	CaO	Na <sub>2</sub> O	K <sub>2</sub> O	P <sub>2</sub> O <sub>5</sub>	LOI	H <sub>2</sub> O	Total
Moodraai Fm													
OLP-1	4.63	0.05	0.21	9.50	1.18	0.88	46.18	lld	lld	0.90	36.48	0.20	100.21
OLP-2	8.35	0.05	0.47	13.14	1.30	1.23	42.40	lld	0.02	0.09	32.30	0.31	99.66
OLP-3	8.88	0.04	0.13	10.97	0.14	1.51	44.55	0.01	lld	0.09	33.17	0.20	99.69
OLP-4	9.15	0.05	0.20	13.89	0.38	1.31	43.17	0.02	0.01	0.09	31.47	0.26	100.00
OLP-5	13.50	0.05	0.27	23.92	0.62	1.94	34.07	0.01	0.03	0.09	25.21	0.33	100.04
OLP-6	1.76	0.04	0.09	2.89	0.84	0.95	51.64	lld	lld	0.08	41.08	0.17	99.54
OLP-8	2.02	0.04	0.13	3.74	0.58	0.72	51.43	lld	lld	0.08	40.67	0.14	99.55
OLP-9	1.39	0.04	0.53	2.42	0.66	0.60	52.56	lld	0.01	0.08	41.59	0.16	100.04
OLP-10	2.15	0.04	0.10	3.83	0.59	0.70	51.78	lld	lld	0.08	40.25	0.22	99.74
OLP-11	5.57	0.04	0.12	12.29	0.61	1.03	45.18	lld	0.01	0.09	34.79	0.30	100.03

Sample <i>ppm</i>	Zn	Cu	Ni	Co	Cr	V	Ba	Sc	Pb	Th	Zr	Nb	Y	Rb	Sr
Moidraai Fm															
OLP-1	33	15	16	6	5	nd	74	nd	lld	nd	nd	lld	7	nd	940
OLP-2	34	18	18	5	7	nd	64	nd	nd	nd	lld	2	7	nd	1145
OLP-3	28	16	16	nd	5	lld	9	nd	nd	nd	nd	nd	5	lld	815
OLP-4	35	18	20	lld	6	nd	36	nd	nd	nd	nd	lld	5	nd	1117
OLP-5	38	22	22	5	8	lld	63	nd	lld	lld	nd	2	8	lld	1080
OLP-6	25	16	13	5	5	nd	58	nd	nd	nd	2	nd	2	nd	789
OLP-8	27	16	13	lld	6	nd	nd	nd	nd	nd	nd	lld	2	lld	1465
OLP-9	29	13	15	lld	5	nd	59	nd	nd	nd	nd	lld	2	nd	1269
OLP-10	29	16	14	<4	5	nd	17	nd	nd	nd	lld	lld	3	nd	1019
OLP-11	33	18	17	3	7	nd	105	nd	nd	nd	nd	lld	5	nd	1524

Sample <i>ppm</i>	Zn	Cu	Ni	Co	Cr	V	Ba	Sc	Pb	Th	Y	Nb	Zr	Rb	Sr
<b>Southern KMF</b>															
R65-2	11	19	39	lld	24	lld	6	lld	4	7	7	3	3	lld	231
R65-3	17	25	43	nd	31	lld	lld	3	8	12	9	lld	4	lld	93
R65-5	18	21	40	18	25	nd	6860	nd	nd	nd	nd	nd	nd	nd	385
R65-12	16	26	48	5	30	lld	73	2	7	9	11	lld	6	3	156
R65-19	15	26	44	lld	31	lld	lld	3	8	11	14	lld	5	5	79
R65-20	16	27	54	lld	54	9	lld	3	9	16	17	4	6	lld	24
R65-21	11	28	59	lld	49	6	17	4	11	14	18	5	8	lld	125
R65-30	37	25	52	35	42	6	72	3	10	15	10	lld	7	4	14
R65-31	40	30	58	31	47	nd	3537	2	7	15	nd	nd	nd	nd	14
R59-1	23	20	41	lld	26	lld	36	2	7	8	7	lld	4	4	145
R59-2	15	25	40	lld	28	lld	20	2	8	10	9	lld	4	lld	82
R59-3	17	20	42	6	33	5	147	lld	3	4	7	lld	5	9	305
R59-9	9	17	35	9	19	nd	106	nd	nd	nd	7	nd	nd	4	905
R59-13	17	21	43	nd	31	5	15	3	8	12	10	4	5	4	68
R59-14	13	22	42	nd	36	7	3	4	9	15	16	lld	9	2	58
R59-15	17	23	43	nd	37	9	8	4	10	11	15	4	9	2	45
R59-16	16	18	42	lld	41	17	4	6	9	8	12	4	11	5	140
R59-17	19	19	42	lld	40	11	3	4	10	13	17	lld	9	3	54
R59-18	14	24	53	nd	43	8	7	3	10	15	21	5	8	lld	52
R63-4	16	18	37	22	17	nd	1818	nd	nd	nd	nd	nd	nd	lld	870
R63-5	31	24	43	6	27	lld	38	2	6	9	10	4	6	nd	169
R63-8	13	22	41	lld	23	lld	40	nd	6	4	5	lld	lld	lld	299
R63-9	17	21	38	lld	29	lld	111	2	8	11	11	3	11	47	214
R63-10	14	25	51	lld	35	lld	7	3	8	14	10	lld	lld	lld	95
R63-11	24	24	46	lld	35	lld	14	2	9	14	10	5	4	lld	140
R63-12	18	26	50	lld	33	lld	13	2	11	15	10	lld	3	lld	117
R63-13	19	21	40	lld	37	10	18	4	9	10	10	3	12	5	55



Sample <i>ppm</i>	Zn	Cu	Ni	Co	Cr	V	Ba	Sc	Pb	Th	Y	Nb	Zr	Rb	Sr
R63-14	lld	26	54	lld	53	9	21	3	8	15	5	4	9	lld	22
R63-20	15	30	59	70	48	lld	2003	3	11	18	lld	nd	nd	nd	39
R70-11	12	26	49	lld	29	lld	117	nd	5	4	7	lld	lld	8	602
R70-12	15	15	26	lld	25	lld	535	2	10	16	3	nd	26	189	30
R70-13	12	23	45	lld	32	lld	12	3	9	11	7	lld	3	4	95
R70-14	16	23	46	nd	31	lld	6	2	8	11	7	nd	lld	3	112
R70-15	13	25	47	lld	32	lld	13	2	9	14	9	nd	lld	5	119
R70-16	20	26	53	nd	34	lld	14	2	9	17	11	nd	lld	lld	79
R70-17	15	21	44	nd	33	lld	6	2	9	15	13	nd	lld	4	64
R70-18	15	21	38	lld	35	9	7	4	9	11	8	nd	6	4	53
R70-19	13	25	46	lld	38	9	56	4	8	10	11	nd	4	4	252
R70-29	38	24	48	53	44	lld	179	3	nd	nd	4	nd	4	lld	18
SM31-2	20	22	35	nd	14	lld	20	nd	4	8	9	lld	4	lld	230
SM31-3	23	26	36	lld	16	lld	17	2	7	13	10	lld	6	lld	107
SM31-5	22	24	37	lld	16	lld	63	2	9	12	9	lld	5	3	88
SM31-10	33	19	21	21	9	nd	463	nd	<3	nd	8	lld	2	6	1058
SM31-15	26	25	32	nd	13	lld	50	nd	6	10	9	nd	4	10	280
SM31-16	16	18	65	nd	14	lld	232	nd	10	17	11	3	22	158	33
SM31-17	20	27	42	nd	15	lld	38	2	nd	nd	16	lld	4	lld	104
SM31-18	14	23	36	lld	23	9	13	3	9	12	15	lld	10	5	42
SM31-20	47	32	51	48	26	7	133	4	13	16	13	nd	8	14	28
Mn ore															
R59-5	37	27	40	13	14	nd	406	nd	3	6	nd	5	9	533	lld
R59-11	32	18	28	17	9	nd	328	nd	lld	3	lld	4	8	359	6
R59-24	64	24	46	38	20	lld	537	5	7	10	nd	6	7	57	nd
R63-7	31	23	30	27	15	lld	969	nd	lld	2	nd	4	8	600	11
R63-15	34	27	40	32	22	nd	522	nd	lld	5	2	4	10	389	lld
R63-17	37	25	35	23	18	nd	538	nd	3	4	nd	5	8	387	nd

Sample <i>ppm</i>	Zn	Cu	Ni	Co	Cr	V	Ba	Sc	Pb	Th	Y	Nb	Zr	Rb	Sr
R65-7	32	27	39	19	17	nd	335	nd	lld	7	3	4	9	436	nd
R65-24	38	24	35	30	15	nd	324	nd	lld	4	lld	6	10	374	nd
R65-27	60	32	43	24	14	nd	265	nd	3	6	lld	4	7	324	lld
R65-29	33	27	43	35	19	lld	2535	3	14	10	lld	4	7	168	lld
R70-10	30	21	39	27	14	nd	331	nd	4	7	nd	3	8	519	15
R70-20	28	21	31	38	12	nd	435	nd	nd	lld	lld	5	10	888	2
R70-21	30	25	37	25	13	nd	503	nd	3	7	lld	4	9	488	nd
R70-23	37	27	39	39	18	nd	422	nd	3	4	lld	6	10	576	nd

#### Northern KMF

GL26-1	20	33	42	lld	19	lld	82	2	6	9	12	lld	5	4	293
GL26-2	12	24	32	nd	14	5	54	2	7	10	10	nd	4	4	306
GL26-3	24	27	39	lld	15	lld	39	2 <sup>a</sup>	5	10	14	lld	5	lld	236
GL26-3a	21	24	36	lld	14	lld	46	2	6	10	14	lld	5	lld	282
GL26-4	20	29	40	nd	15	lld	38	2	8	15	13	lld	5	lld	173
GL26-5	29	27	35	lld	12	lld	32	1	7	11	14	lld	5	lld	197
GL26-6	30	30	38	lld	17	lld	36	nd	4	10	13	lld	5	lld	293
GL26-7	29	26	31	lld	9	6	51	nd	3	5	13	lld	5	lld	489
GL26-9	29	26	26	6	11	lld	140	nd	<3	lld	13	lld	4	lld	481
GL26-11	20	38	25	lld	9	lld	4	nd	3	4	11	lld	5	lld	143
GL26-12	20	28	25	lld	11	lld	nd	nd	4	8	16	lld	5	lld	76
GL26-12a	12	24	35	lld	20	9	9	2	8	13	13	lld	5	lld	7
GL26-13	13	29	36	lld	22	7	8	4	7	13	19	lld	7	lld	9
GL26-15	23	28	52	nd	27	6	36	3	9	19	13	lld	6	nd	10
GL26-16	23	27	36	nd	20	8	15	2	7	11	16	lld	5	lld	5
MK2H-2	41	134	155	31	106	141	4317	22	50	26	26	5	97	44	312
MK2H-3	34	30	106	nd	62	24	122	5	31	44	13	lld	12	nd	15
MK2H-4	16	41	109	lld	70	16	48	9	32	45	21	nd	11	lld	23
MK2H-5	16	45	113	lld	69	21	54	5	28	42	25	nd	10	nd	23

Sample <i>ppm</i>	Zn	Cu	Ni	Co	Cr	V	Ba	Sc	Pb	Th	Y	Nb	Zr	Rb	Sr
MK2H-6	49	116	77	16	31	34	3064	5	135	17	38	nd	6	lld	447
MK2H-8	12	30	48	lld	33	11	16	2	22	15	13	lld	4	lld	12
MK2H-9	11	34	56	7	35	9	16	2	26	18	12	nd	5	lld	14
MK2H-10	14	33	50	6	29	9	16	1	22	20	11	lld	5	nd	11
MK2H-11a	11	28	49	nd	25	9	19	1	20	20	8	3	5	nd	11
MK2H-11b	12	29	52	nd	29	12	32	1	17	18	10	lld	4	lld	13
MK2H-12	13	30	48	lld	29	11	17	2	22	20	13	nd	5	nd	11
MK2H-13	13	28	48	5	42	9	24	2	20	19	13	lld	6	nd	11
MK2H-14	12	26	54	6	24	19	562	2	21	19	16	lld	4	nd	19
MK2H-15	11	30	47	6	29	12	18	2	16	16	15	lld	8	nd	15
MK2H-17	33	30	42	lld	22	20	343	2	17	15	13	lld	5	nd	153
MK2H-18	64	40	112	14	21	7	56	2	23	28	22	lld	9	lld	124
MK2H-19	59	39	84	21	29	11	145	3	26	31	13	nd	10	lld	14
MK3I-3	15	33	48	lld	45	21	101	2	17	15	11	lld	7	lld	10
MK3I-4	13	29	48	lld	52	21	103	2	19	18	8	lld	5	lld	11
MK3I-5	13	33	56	lld	33	20	31	2	25	19	8	lld	8	nd	7
MK3I-6	12	32	47	lld	36	14	23	2	15	18	4	3	6	nd	5
MK3I-6a	10	30	47	lld	31	13	21	1	15	16	7	4	7	lld	7
MK3I-7	8	32	42	lld	30	11	24	2	15	18	6	3	5	lld	7
MK3I-8a	12	33	43	lld	33	12	23	1	15	17	4	lld	6	lld	7
MK3I-8b	5	31	47	nd	46	15	22	1	15	16	4	lld	8	lld	5
MK3I-8c	11	33	47	lld	39	10	23	1	16	16	5	lld	7	lld	3
MK3I-9	8	30	45	nd	34	11	28	1	17	18	<3	lld	6	lld	7
MK3I-10	21	107	50	6	38	9	26	2	19	20	12	nd	6	nd	91
MK3I-11	9	152	57	lld	32	12	27	2	34	17	14	lld	8	nd	69
MK3I-12	21	35	51	lld	32	9	18	2	19	20	13	lld	8	nd	14
MK3I-13	16	39	56	lld	32	9	19	1	22	20	9	nd	7	lld	13
MK3I-14a	13	35	57	lld	31	7	18	2	23	20	13	lld	6	lld	17
MK3I-14b	12	32	51	lld	31	10	18	2	22	19	20	lld	7	lld	19

Sample ppm	Zn	Cu	Ni	Co	Cr	V	Ba	Sc	Pb	Th	Y	Nb	Zr	Rb	Sr
MK3I-15	26	34	40	lld	31	11	36	2	11	15	10	lld	5	lld	104
MK3I-16	17	25	37	6	21	8	30	2	6	9	9	lld	5	3	40
N12D-1	21	35	97	15	39	16	95	5	26	37	23	nd	11	lld	18
N12D-2	38	42	101	9	63	12	218	4	140	42	28	lld	8	10	279
N12D-3	22	28	50	lld	51	7	725	2	24	17	7	lld	5	nd	25
N12D-4	15	27	58	lld	69	6	24	3	21	20	12	lld	8	lld	6
N12D-5	10	27	59	lld	63	7	25	2	25	25	8	nd	9	nd	5
N12D-7	10	27	49	lld	96	8	20	2	21	17	9	lld	6	nd	7
N12D-8	14	25	50	lld	80	lld	19	1	22	19	8	lld	5	nd	5
N12D-9	13	25	46	lld	62	lld	20	2	25	19	11	lld	8	lld	8
N12D-10b	13	26	44	lld	108	lld	21	2	20	16	10	lld	5	lld	7
N12D-11	17	22	69	lld	86	lld	19	2	17	18	9	lld	4	nd	5
N12D-13	9	26	55	lld	72	7	23	2	19	14	12	nd	6	lld	8
N12D-14	34	27	47	lld	36	9	24	2	16	17	5	nd	5	nd	24
N12D-16	44	31	54	lld	32	lld	98	nd	84	13	18	nd	8	lld	221
N12D-17	52	32	61	8	19	lld	861	nd	28	19	20	lld	7	nd	85
N12D-18	17	35	51	lld	40	13	37	2	17	20	16	lld	8	lld	7
N12D-19	10	76	40	lld	31	12	22	1	10	15	8	lld	6	lld	6
MK2G-1	20	40	125	32	102	60	75	9	60	35	36	lld	38	nd	19
MK2G-2	7	32	53	lld	31	30	29	2	14	15	4	lld	6	nd	6
MK2G-2a	lld	35	54	lld	33	33	28	2	15	17	4	nd	6	nd	7
MK2G-3	7	31	49	lld	29	23	26	2	14	16	3	nd	7	nd	5
MK2G-3a	10	26	47	lld	35	22	22	1	13	16	9	nd	5	nd	4
MK2G-4	9	27	53	lld	32	13	23	2	13	16	4	lld	6	nd	4
MK2G-4a	8	31	48	lld	32	11	27	2	15	16	5	lld	5	nd	6
MK2G-5	9	27	50	lld	37	10	31	2	11	16	5	lld	8	nd	7
MK2G-6	11	28	54	lld	38	11	37	2	13	16	5	lld	5	lld	7
MK2G-7	9	30	45	lld	36	15	26	2	17	15	10	lld	7	nd	5
MK2G-8	8	28	44	lld	36	12	24	2	11	15	5	nd	6	nd	6

Sample <i>ppm</i>	Zn	Cu	Ni	Co	Cr	V	Ba	Sc	Pb	Th	Y	Nb	Zr	Rb	Sr
MK2G-9	10	31	46	lld	44	12	30	1	24	15	9	nd	4	nd	6
MK2G-10	46	45	44	7	26	10	350	3	26	16	12	lld	6	nd	48
MK2G-11	10	34	56	lld	40	10	20	2	25	19	10	nd	6	nd	6
MK2G-12	16	31	56	nd	40	7	22	2	23	20	12	nd	7	lld	12
MK2G-13	8	38	61	lld	45	8	29	1	23	21	11	lld	6	nd	9
MK2G-14	9	30	46	lld	31	8	87	2	17	16	34	lld	6	lld	9
MK2G-16	15	23	33	lld	26	5	8	3	9	11	11	lld	3	lld	10
MK2G-17	11	23	37	lld	23	lld	10	3	6	12	12	lld	4	nd	8
N91B-1	11	29	48	nd	53	21	33	2	11	17	7	lld	5	nd	6
N91B-2	8	19	33	lld	34	8	24	2	10	13	6	lld	5	nd	4
N91B-3	12	26	47	lld	40	15	31	3	11	18	4	nd	6	lld	5
N91B-4	6	28	50	lld	31	18	29	2	14	19	6	lld	7	nd	3
N91B-5	6	27	55	8	34	15	451	2	14	17	6	lld	6	nd	8
N91B-6	11	26	50	lld	33	28	36	2	10	16	5	lld	7	nd	5
N91B-7	9	26	46	lld	40	19	27	2	11	14	7	lld	6	nd	4
N91B-8	17	28	54	11	50	18	36	2	13	19	8	lld	8	nd	4
N91B-9	43	24	41	65	11	9	375	4	5	8	11	nd	7	11	36
N91B-10	43	23	40	74	15	nd	499	4	9	14	10	lld	7	10	38
N91B-11	25	29	37	lld	18	lld	22	2	7	12	13	lld	5	nd	213
N91B-12	24	24	35	lld	16	lld	23	1	8	10	13	lld	4	nd	301
N91B-13	21	29	43	lld	23	lld	22	3	6	15	13	lld	7	lld	185
N91B-14	23	26	42	nd	23	lld	13	3	9	15	13	lld	7	nd	37
N91B-15	19	25	41	nd	23	lld	15	3	11	15	14	nd	8	nd	42
N91B-16	13	38	32	lld	21	lld	8	3	6	12	12	lld	6	lld	35
N91B-17	18	27	40	nd	20	lld	9	2	9	14	13	nd	5	nd	11
N91B-18	19	25	42	nd	23	lld	14	3	10	15	13	lld	3	lld	11
N91B-19	12	27	36	lld	23	lld	9	3	10	14	14	lld	6	nd	12
N91B-20	13	30	47	nd	26	lld	16	3	10	17	15	lld	5	lld	11
N91B-21	17	21	31	nd	17	lld	6	2	5	10	14	lld	4	nd	15

Sample <i>ppm</i>	Zn	Cu	Ni	Co	Cr	V	Ba	Sc	Pb	Th	Y	Nb	Zr	Rb	Sr
N91B-22	32	28	37	nd	26	6	11	3	9	16	26	lld	5	lld	13
N91B-23	15	34	33	nd	19	5	8	3	6	10	17	lld	6	nd	32
N91B-24	41	31	41	26	25	lld	14	3	14	16	18	lld	6	nd	25
N91B-25	37	25	32	lld	12	nd	70	nd	3	6	15	lld	4	nd	299
N91B-26	44	24	29	23	11	nd	26	nd	4	7	16	lld	3	nd	310
N91B-26a	16	34	45	6	22	lld	15	3	9	17	12	lld	6	nd	71
N91B-27	18	28	34	6	16	lld	3	1	5	10	11	lld	7	nd	75
N91B-28	17	20	24	nd	13	lld	nd	lld	3	8	12	lld	4	nd	63
N91B-29	9	30	33	nd	23	lld	9	2	7	11	13	nd	2	nd	9
N91B-30	46	23	49	24	12	nd	22	3	8	13	16	nd	6	lld	11
N91B-31	14	26	44	nd	47	12	15	5	8	15	11	lld	11	nd	4
BEL7A-2	140	37	164	165	149	62	4073	16	41	32	45	lld	76	nd	118
BEL7A-3	11	29	51	lld	31	nd	7419	3	10	15	11	nd	6	nd	138
BEL7A-4	12	26	40	14	24	11	23	4	10	12	16	lld	7	nd	14
BEL7A-5	8	32	43	nd	31	11	29	2	10	17	8	lld	5	lld	9
BEL7A-6	9	27	36	lld	30	12	24	2	8	12	12	lld	5	lld	6
BEL7A-7	17	26	49	lld	29	11	31	1	11	18	15	lld	6	nd	8
BEL7A-8a	12	24	36	6	20	5	7	2	7	12	13	lld	4	lld	13
BEL7A-8b	27	27	43	78	17	lld	391	3	9	15	11	3	7	nd	38
BEL7A-9	19	21	40	7	18	7	9	3	8	13	13	lld	5	lld	8
BEL7A-11	14	21	28	lld	18	6	8	3	8	14	13	lld	6	lld	8
BEL7A-12a	18	25	42	lld	21	5	8	3	8	16	12	lld	6	lld	8
BEL7A-12b	16	25	42	6	22	8	7	2	7	14	12	lld	7	lld	6
BEL7A-13	12	24	32	lld	21	5	nd	1	5	10	14	lld	7	nd	6
BEL7A-14	15	28	41	5	22	7	10	2	8	15	14	lld	5	nd	8
BEL7A-15	18	22	26	lld	14	5	2	2	5	9	14	lld	5	lld	8
BEL7A-16	19	19	25	lld	15	8	nd	2	5	8	14	lld	6	nd	8

Sample <i>ppm</i>	Zn	Cu	Ni	Co	Cr	V	Ba	Sc	Pb	Th	Y	Nb	Zr	Rb	Sr
BEL7A-17	40	24	47	50	16	lld	16	3	9	15	10	lld	8	nd	5
BEL7A-18	19	38	49	29	29	12	10	3	13	17	18	lld	8	nd	4
BEL4C-1	616	53	95	9	58	588	6421	14	91	27	8	nd	13	nd	112
BEL4C-3	12	26	44	lld	28	6	28	2	9	14	7	nd	6	nd	8
BEL4C-4	10	23	38	lld	29	11	21	3	8	12	11	lld	6	nd	7
BEL4C-5	18	27	46	7	31	5	37	3	10	16	15	nd	4	lld	11
BEL4C-6	16	30	42	68	16	lld	190	3	7	14	10	nd	5	nd	16
BEL4C-7	14	23	38	8	18	lld	7	3	8	13	13	lld	5	nd	18
BEL4C-8	16	25	36	7	16	lld	6	3	5	10	14	lld	5	lld	10
BEL4C-9	11	27	41	7	22	lld	8	3	8	14	12	nd	6	lld	10
BEL4C-11	13	25	41	lld	22	lld	18	2	6	13	11	lld	5	nd	11
BEL4C-13	22	26	33	5	15	lld	lld	1	7	11	12	nd	5	nd	13
BEL4C-14	21	24	33	5	16	lld	6	2	7	12	12	lld	5	lld	12
BEL4C-15	16	22	38	lld	19	lld	18	3	6	13	13	lld	5	nd	12
BEL4C-16	17	18	25	lld	14	lld	22	2	4	7	16	lld	4	nd	12
BEL4C-17	20	24	34	6	19	9	9	4	7	11	19	lld	7	nd	16
BEL4C-19	25	27	32	28	13	lld	nd	1	7	10	12	lld	6	lld	30
BEL4C-20	15	28	39	lld	21	lld	6	3	10	15	11	lld	5	nd	14
BEL4C-22	21	24	36	lld	19	nd	33	2	8	13	13	nd	4	nd	8
BEL4C-23	17	18	26	14	14	lld	46	1	7	8	9	lld	4	lld	13
BEL4C-24	47	27	54	22	15	nd	51	3	10	21	11	lld	4	lld	15
BEL4C-25	28	26	45	nd	25	lld	29	3	11	19	13	nd	7	nd	9
BEL4C-26	18	33	52	nd	23	lld	21	3	9	18	11	lld	5	nd	22
BEL4C-27	22	29	45	nd	23	lld	28	3	10	15	12	nd	6	lld	18
BEL4C-28	18	27	52	nd	25	lld	37	3	10	16	15	lld	9	lld	6
BEL4C-29	19	24	36	lld	22	5	16	3	10	15	11	nd	5	lld	4
BEL4C-30	15	37	48	nd	30	7	27	3	11	19	13	lld	9	6	3

**Appendix IV: Additional bibliography**

**Acharya, S., Amstutz, G.C., and Sarangi, S.K., 1982**, Diagenetic crystallisation and migration in the banded iron-formations of Orissa, India, in: Ore genesis: the state of the art, eds., Amstutz, G.C., Goresy, A.El., Frenzel, G., Kluth, C., Moh, G., Wauschkuhn, A., and Zimmermann, R.A.: Spec. Publ., Soc. Geol. Ap. Min. Dep., #2, p. 442-451.

**Adegbuyi, O., and Olade, M.A., 1990**, The Precambrian Itakpe iron ore deposit in central Nigeria, in: Ancient banded iron-formations (regional presentations): Theophrastus publ., Athens, p.105-118.

**Alexandrov, E.A., 1973**, The Precambrian banded iron-formations of the Soviet Union: Econ. Geol., v. 68, p. 1035-1062.

**Altermann, W., and Hälbich, I.W., 1990**, The Tectogenesis of Proterozoic banded iron-formations on the south-western Kaapvaal Craton: Abstracts, Geocongress '90, Geol. Soc. S. Afr., p. 192-195.

**Anderson, G.J., 1970**, The Marquette District, Michigan, in: Ore deposits of the United States, ed., Ridge, J.D.: Am. Inst. Min. Metall. & Petr. Eng., Graton-Sales vol., v. I, p. 508-517.

**Anhaeusser, C.R., and Button, A., 1976**, A review of Southern African stratiform deposits-their position in time and space, in: Handbook of stratabound and stratiform ore-deposits, ed., Wolf, K.H.: Els. Sci. Pbl., v. 5, 319p.

**Appel, P.W.U., 1974**, On an unmetamorphosed iron-formation in the Early Precambrian of south-west Greenland: Min. Dep., v. 9, p. 75-82.

**Appel, P.W.U., 1979**, Cosmic grains in an iron-formation from the Early Precambrian Isua supracrustal belt, West Greenland: J. Geol., v. 87, p. 573-578.

**Appel, P.W.U., 1980**, On the Early Archaean Isua iron-formation, West Greenland: Prec. Res., v. 11, p. 73-87.

**Appel, P.W.U., 1987**, Geochemistry of the Early Archaean Isua iron-formation, West Greenland, in: Precambrian iron-formations, eds., Appel, P.W.U., and LaBerge, G.L.: Theophrastus publ., Athens, p. 31-68.

**Ayres, D.E., 1972**, Genesis of iron-bearing minerals in banded iron-formation mesobands in the Dales Gorge Member, Hamersley Group, Western Australia: Econ. Geol., v. 67, p. 1214-1233.



**Astrup, J., and Tsikos, H., 1998**, Manganese, in: Mineral resources of southern Africa, eds, Wilson, M.J., and Anhaeusser, C.R: Handbook 16, Council for Geoscience, Pretoria, South Africa, p. 450-460.

**Babinski, M., Chemale, F. Jr., and Van Schmus, W.R., 1995**, The Pb/Pb age of the Minas Supergroup carbonate rocks, Quadrilátero Ferrífero, Brazil: *Prec. Res.*, v. 72, p. 235-245.

**Bao, H., and Koch, P.L., 1999**, Oxygen isotope fractionation in ferric oxide-water systems: low temperature synthesis: *Geoch. Cosm. Acta*, v. 63, p. 599-613.

**Barbosa, A.L.M., and Grossi Sad, J.H., 1973**, Tectonic control of sedimentation and trace-element distribution in iron-ores of central Minas Gerais (Brazil), in: *Genesis of Precambrian iron and manganese deposits: Proc. Kiev Symposium 1970, UNESCO Paris*, p. 125-131.

**Barley, M.E., Pickard, A.L., and Sylvester, P.J., 1997**, Emplacement of a large igneous province as a possible cause of banded iron formation 2.45 billion years ago: *Nature*, v. 385, p. 55-58.

**Barley, M.E., Pickard, A.L., Hageman, S., and Folkert, S., 1998**, A hydrothermal origin for the giant Paleoproterozoic Mount Tom Price iron ore deposit: *Abstracts, 14th Aust. Geol. Conv., Townsville, Australia*, p. 162.

**Bau, M., 1993**, Effects of syn- and post-depositional processes on the rare-earth element distribution in Precambrian iron-formations: *Eur. Jour. Mineral.*, v. 5, p. 257-267.

**Bau, M., and Dulski, P., 1992**, Small-scale variations of the rare-earth element distribution in Precambrian iron-formations: *Eur. J. Min.*, v. 4, p. 1429-1433.

**Bau, M., and Dulski, P., 1993**, Distribution of rare-earth elements in Precambrian sedimentary Fe-, Mn-, and P-deposits: *Extended abstracts, 16th Colloquium of African Geology, Swaziland*, v. I, p. 27-28.

**Bau, M., Höhndorf, A., Dulski, P., and Beukes, N.J., 1997**, Sources of rare-earth elements and iron in Paleoproterozoic iron-formations from the Transvaal Supergroup, South Africa: Evidence from Neodymium Isotopes. *J. Geol.*, v. 105, p. 121-129.

**Bayley, R.W., and James, H.L., 1973**, Precambrian iron-formations of the United States: *Econ. Geol.*, v. 68, p. 934-959.

**Belevtsev, Ya.N., 1973**, Genesis of high grade iron-ores of Krivoyrog type, in: *Genesis of Precambrian iron and manganese deposits: Proceedings Kiev Symposium 1970, UNESCO Paris*, p. 167-180.

- Belevtsev, Ya.N., Belevtsev, R.Ya., and Siroshstan, R.I., 1983**, The Krivoy Rog basin, in: Iron-formations: facts and problems, eds., Trendall, A.F., and Morris, R.C.: *Developments in Precambrian Geology* 6, Els. Sci. Pbl., p. 211-251.
- Belkova, L.N., 1990**, Banded ferruginous Precambrian formations of the folded areas of the Soviet Union, in: *Ancient banded iron-formations (regional presentations)*: Theophrastus publ., Athens, p. 225-232.
- Beukes, N.J., 1977**, Transition from siliciclastic to carbonate sedimentation near the base of the Transvaal Supergroup at Bothithong in the northern Cape Province, South Africa: *Sed. Geol.*, v. 18, p. 201-222.
- Beukes, N.J., 1979**, Litostratigrafiese onderverdeling van die Schmidtsdrif-Subgroep van die Ghaap-Groep in Noord-Kaapland: *Trans. Geol. Soc. S. Afr.*, v. 82, p. 313-327.
- Beukes, N.J., 1980**, Stratigrafie en litofasies van die Campbellrand-Subgroep van die Proterofitiese Ghaap-Groep, Noord-Kaapland: *Trans. Geol. Soc. S. Afr.*, v. 83, p. 141-170.
- Beukes, N.J., 1986**, Sedimentology, structure and mineral deposits of Transvaal-aged basins: Excursion guidebook, Geocongress '86, *Geol. Soc. S. Afr.*, 48 p.
- Beukes, N.J., 1987**, Facies relations, depositional environments and diagenesis in a major Early Proterozoic stromatolitic carbonate platform to basinal sequence, Campbellrand Subgroup, Transvaal Supergroup, Southern Africa: *Sed. Geol.*, v. 54, p. 1-46.
- Beukes, N.J., and Kleyenstüber, A.S.E., 1986**, Sedimentology, diagenesis and hydrothermal alteration of the Kalahari manganese deposit, Transvaal Sequence, Griqualand West: Extended abstracts, Geocongress '86, *Geol. Soc. S. Afr.*; p. 497-500.
- Beukes, N.J., and Klein, C., 1990**, Sedimentology and geochemistry of Early Proterozoic storm-dominated deposits in a transition zone from microbanded Kuruman to granular Griquatown iron-formation, Griqualand West: Abstracts, Geocongress '90, *Geol. Soc. S. Afr.*, p. 50-52.
- Beukes, N.J., Klein, C., Kaufman, A.J., and Hayes, J.M., 1990**, The palaeoenvironmental implications of carbonate petrography, kerogen distribution and carbon and oxygen isotope variations in the Early Proterozoic transition from Campbellrand limestone to Kuruman iron-formation deposition in Griqualand West: Abst., Geocongress '90, *Geol. Soc. S. Afr.*, p. 53-55.
- Birnbaum, S.J., and Wireman, J.W., 1985**, Sulfate-reducing bacteria and silica solubility: a possible mechanism for evaporite diagenesis and silica precipitation in banded iron-formations: *Can. J. Earth Sci.*, v. 22, p. 1904-1909.

- Blockley, J.G., Trendall, A.F., and Thorne, A.M., 1989**, Early Precambrian crustal evolution and mineral deposits, Pilbara craton and adjacent Ashburton trough, in: *Origin and Evolution of sedimentary basins and their energy and mineral resources*, ed., R.A., Price: Geophysical monograph 48, IUGG v. 3, p. 159-167.
- Blockley, J.G., and Myers, J.S., 1990**, Proterozoic rocks of the Western Australian shield-geology and mineralisation, in: *Geology of the mineral deposits of Australia and Papua New Guinea*, ed. Hughes, F.E.: Austr. Inst. Min. Metall., v. 2, Monograph #14, p. 607-616.
- Bonnichsen, B., 1975**, Geology of the Biwabik iron-formation, Dunka River Area, Minnesota: *Econ. Geol.*, v. 70, p. 319-340.
- Borchert, H., 1960**, Genesis of marine sedimentary iron ores: *Trans. Inst. Min. Met.*, v. 69, p. 261-279.
- Brandt, R.T., 1973**, The origins of the jaspilitic ores of Australia, in: *Genesis of Precambrian iron and manganese deposits: Proc. Kiev Symposium 1970*, UNESCO Paris, p. 59-68.
- Braterman, P.S., and Cairns-Smith, A.G., 1987**, Iron photoprecipitation and the genesis of the banded iron-formations, in: *Precambrian iron-formations*, eds., Appel, P.W.U., and LaBerge, G.L.: Theophrastus publ., Athens, p. 215-250.
- Bronner, G., Chauvel, J.J., and Triboulet, C., 1990**, Geochemistry and knowledge of banded iron-formations: the West African Shield, an example, in: *Ancient banded iron-formations (regional presentations)*: Theophrastus publ., Athens, p. 135-156;
- Brown, D.A., Gross, G.A., and Sawicki, J.A.,** A review of the microbial geochemistry of banded iron-formations: *Can. Min.*, v. 33, p. 1321-1334.
- Burdett, J.W., Grotzinger, J.P., and Arthur, M.A., 1990**, Did major changes in the stable-isotope composition of Proterozoic seawater occur? *Geol.*, v. 18, p. 227-230.
- Butler, P.Jr., 1969**, Mineral compositions and equilibria in the metamorphosed iron-formation of the Cagnon region, Quebec, Canada: *J. Petr.*, v. 10, p. 56-101.
- Button, A., 1976a**, Iron-formation as an end-member in carbonate sedimentary cycles in the Transvaal Supergroup, South Africa: *Econ. Geol.*, v. 71, p. 193-201.
- Button, A., 1976b**, Transvaal and Hamersley basins-review of basin development and mineral deposits: *Min. Sci. Eng.*, v. 8, p. 262-293.
- Button, A., 1981**, The cratonic environment: the Transvaal Supergroup, in: *Precambrian of the southern hemisphere*, ed., Hunter, D.R.: *Developments in Precambrian geology 2*, Els. Sci. Pbl.,

882 p.

**Calvert, S.E., and Pedersen, T.F., 1996**, Sedimentary geochemistry of manganese: implications for the environment of formation of manganese black shales: *Econ. Geol.*, v. 91, p. 36-47.

**Cameron, E.M., 1982**, Sulphate and sulphate reduction in early Precambrian oceans: *Nature*, v. 296, p. 145-148.

**Cameron, E.M., 1983**, Genesis of Proterozoic iron-formation: Sulphur isotope evidence: *Geoch. Cosm. Acta*, v. 47, p. 1069-1074.

**Canfield, D.E., 1998**, A new model for Proterozoic ocean chemistry: *Nature*, v. 396, p. 450-453.

**Castro, L.O., 1995**, Genesis of banded iron-formations: *Econ. Geol.*, v. 89, p. 1384-1397.

**Castro, L.O., 1996**, Genesis of banded iron-formations-a reply: *Econ. Geol.*, v. 91, p. 468-469.

**Chakraborty, K.L., 1963**, Relationship of anthophyllite, cummingtonite and mangano-cummingtonite in the metamorphosed Wabush iron-formation, Labrador: *Can. Min.*, v. 7(5), p. 738-750.

**Chakraborty, K.L., and Taron, P.B., 1968**, Thermal metamorphism of the banded iron-formation of Orissa, India: *Geol. Soc. Am. Bull.*, v. 79, p. 365-374.

**Cheney, E.S., 1996**, Sequence stratigraphy and plate tectonic significance of the Transvaal succession of southern Africa and its equivalent in Western Australia. *Prec. Res.*, vol. 79, p. 3-24.

**Cheng, Y., and Wu, J., 1990**, On the occurrences of banded iron-ore beds and magnetite-rich hornblende rocks in an Archaean metamorphic iron formation near Tungguan, Shaanxi, China, in: *Ancient banded iron-formations (regional presentations): Theophrastus publ.*, Athens, p. 389-418.

**Chernov, V.M., 1973**, The ferruginous siliceous formations of the eastern part of the Baltic Shield, in: *Genesis of Precambrian iron and manganese deposits: Proc. Kiev Symposium 1970*, p. 85-87.

**Choubert, G., 1973**, Occurrences of manganese in the Guianas (South America) and the relation with fundamental structures, in: *Genesis of Precambrian iron and manganese deposits: Proc. Kiev Symposium 1970, UNESCO Paris*, p. 143-151.

**Choubert, G., and Faure-Muret, A., 1973**, The Precambrian iron and manganese deposits of the Anti-Atlas, in: *Genesis of Precambrian iron and manganese deposits: Proc. Kiev Symposium 1970, UNESCO Paris*, p. 115-124.

**Cisne, J.L., 1984**, A basin model for massive banded iron-formations and its geophysical

applications: *J. Geol.*, v. 92, #5, p. 471-488.

**Clayton, R.N., and Epstein, S., 1958**, The relationship between  $O^{18}/O^{16}$  ratios in coexisting quartz, carbonate and iron oxides from various geological deposits: *J. Geol.*, 66, 352-373.

**Clemmey, H., and Badham, N., 1982**, Oxygen in the Precambrian atmosphere: an evaluation of the geological evidence: *Geology*, v. 10, p. 141-146.

**Cloud, P., 1965**, Significance of the Gunflint (Precambrian) microflora: *Science*, v. 148, p. 27-45.

**Cloud, P., 1983**, Banded iron-formation-a gradualist's dilemma, in: *Iron-formations: facts and problems* eds., Trendall, A.F., and Morris, R.C.: *Developments in Precambrian Geology* 6, *Els. Sci. Pbl.*, p. 401-416.

**Cloud, P., Curtis, C.D., Folinsbee, R.E., Holland, H.D., Jenkyns, H.C., Langridge, J., Lerman, A., Miller, S.L., Nissenbaum, A., and Veizer, J., (Awramik, S.M., Rapporteur), 1982**, Biogeochemical evolution of the ocean-atmosphere system: state of the art report, in: *Mineral deposits and the evolution of the biosphere*, eds., Holland, H.D., and Schidlowski, M.: Springer-Verlag, p. 309-320.

**Danielson, A., 1990**, REE in the Griqualand-West carbonates-evidence for seawater/ freshwater mixing?: *Abstracts, Geocongress '90, Geol. Soc. S. Afr.*, p. 116-118.

**Dasgupta, S., Roy, S., and Fukuoka, M., 1992**, Depositional models for the manganese oxide and carbonate deposits of the Precambrian Sausan Group, India: *Econ. Geol.*, v. 87, p. 1412-1418.

**Dasgupta, S., Banerjee, H., and Bandyopadhyay, G., 1992**, Manganese deposition in the Proterozoic-global perspective and Indian scenario, in: *Metallogeny related to the tectonics of the Proterozoic mobile belts*, ed., Sarkar S.C.: A.A. Balkema/Rotterdam, p. 163-176.

**Des Marais, D.J., Strauss, H., Summons, R.E., and Hayes, J.M., 1992**, Carbon isotope evidence for the stepwise oxidation of the Proterozoic environment: *Nature*, v. 359, p. 605-609.

**Derry, L.A., Kaufman, A.J., and Jacobsen, S.B., 1992**, Sedimentary cycling and environmental change in the late Proterozoic: evidence from stable and radiogenic isotopes: *Geoch. Cosm. Acta*, v. 56, p. 1317-1329.

**De Villiers, P.R., and Visser, J.N.J., 1977**, The glacial beds of the Griqualand West Supergroupas revealed by four deep boreholes between Postmansburg and Sishen: *Trans. Geol. Soc. S. Afr.*, v. 80, p. 1-8.

**Dimroth, E., 1977**, Facies models-5: Models of physical sedimentation of iron-formations:

Geosc. Can., v. 4(1), p. 23-30.

**Dixon, R., 1986**, Metamorphism in the Kalahari manganese field: Ext. Abstr. Geocongress '86, Geol. Soc. S. Afr., p. 505-508.

**Dorr, J.V.N., 1964**, Supergene iron-ores of Minas Gerais, Brazil: *Econ. Geol.*, v. 59, p. 1203-1240.

**Dutton, C.E., and Zimmer, P.W., 1970**, Iron-ore deposits of the Menominee District, Michigan, in: *Ore deposits of the United States*, ed., Ridge, J.D.: Am. Inst. Min. Metall. & Petr. Eng., Graton-sales vol., v. I, p. 538-550.

**Egorov, E.V., and Timofeieva, M.W., 1973**, Effusive iron-silica formations and iron-ore deposits of the Maly Khingan, in: *Genesis of iron and manganese deposits: Proc. Kiev Symposium 1970*, UNESCO Paris, p. 181-185.

**Eichler, J., 1976**, Origin of the Precambrian banded iron-formations, in: *Handbook of stratabound and stratiform ore-deposits*, ed., Wolf, K.H.: *Els. Sci. Pbl.*, v. 7, 656 p.

**Elueze, A.A., and Okolo, E.C., 1990**, Metallographic and chemical appraisal of the iron-ore body associated with Precambrian basement units in Kakun district, southwestern Nigeria, in: *Ancient banded iron-formations (regional presentations): Theophrastus publ.*, Athens, p. 119-134.

**Erriksson, P.G., and Cheney, E.S., 1992**, Evidence for the transition to an oxygen-rich atmosphere during the evolution of red beds in the Lower Proterozoic sequences of southern Africa: *Prec. Res.*, v. 54, p. 257-269.

**Eriksson, P.G., Schweitzer, J.K., Bosch, P.J.A., Schreiber, U.M., Van Deventer, J.L., and Hatton, C.J., 1993**, The Transvaal Sequence: an overview: *J. Afr. Earth Sci.*, v. 16, p. 25-51.

**Ewers, W.E., 1980**, Chemical conditions for the precipitation of banded iron-formations, in: *Biogeochemistry of ancient and modern environments*, eds., Trundiger, P.A., Walter, M.R., and Ralph, M.J.: New York, Springer-Verlag, p. 83-92.

**Ewers, W.E., 1983**, Chemical factors in the deposition and diagenesis of banded iron-formation, in: *Iron-formations: facts and problems*, eds., Trendall, A.F., and Morris, R.C.: *Developments in Precambrian geology* 6, *Els. Sci. Pbl.*, p. 491-512.

**Fan Delian, Liu Tiebing, and Ye Jie, 1992**, The process of formation of manganese carbonate deposits hosted in black shale series: *Econ. Geol.*, v. 87, p. 1419-1429.

**Fan Delian, Dasgupta, S., Bolton, B.R., Hariya, Y., Momoi, H., Miura, H., Li Jiaju, and**

- Roy, S., 1992**, Mineralogy and geochemistry of the Proterozoic Wafangzi ferromanganese deposit, China: *Econ. Geol.*, v. 87, p. 1430-1440.
- Foster, R.P., and Gilligan, J.M., 1987**, Archaean iron-formation and gold mineralisation in Zimbabwe, in: *Precambrian iron-formations*, eds., Appel, P.W.U., and LaBerge, G.L.: Theophrastus publ., Athens, p. 635-674.
- Fralick, P., 1987**, Depositional environment of Archaean iron-formation: inferences from layering in sediments and volcanic hosted end members, in: *Precambrian iron-formations*, eds., Appel, P.W.U., and LaBerge, G.L.: Theophrastus publ., Athens, p. 251-266.
- Frick, C., 1986**, The mineralogy and geochemistry of the banded ironstones in the Griqualand West and Olifantshoek Sequences: *Ext. Abstr. Geocongress '86*, Johannesburg, p. 513-517.
- Frietch, R., 1973**, Precambrian iron-ores of sedimentary origin in Sweden, in: *Genesis of Precambrian iron and manganese deposits: Proc. Kiev Symposium 1970*, UNESCO Paris, p. 77-83.
- Frost, B.R., 1979**, Metamorphism of iron-formation: parageneses in the system Fe-Si-C-O-H: *Econ. Geol.*, v. 74, p. 775-785.
- Fryer, B.J., 1972**, Age determinations in the Circum-Ungava geosyncline and the evolution of Precambrian banded iron-formations: *Can. J. Earth Sci.*, v. 9, p. 652-663.
- Fryer, B.J., 1977a**, Trace-element geochemistry of the Sokoman iron-formation: *Can. J. Earth Sci.*, v. 14, p. 1598-1610.
- Fryer, B.J., 1977b**, Rare-earth evidence in iron-formations for changing Precambrian oxidation states: *Geoch. Cosm. Acta*, V. 41, p. 361-367.
- Fryer, B.J., 1983**, Rare-earth elements in iron-formation, in: *Iron-formations: facts and problems*, eds., Trendall, A.F., and Morris, R.C.: *Developments in Precambrian Geology* 6, *Els. Sci. Pbl.*, p. 345-358.
- Fryer, B.J., Fyfe, W.S., and Kerrich, R., 1979**, Archaean volcanogenic oceans: *Chem. Geol.*, v.24, p. 25-33.
- Gaal, G., 1992**, Global Proterozoic tectonic cycles and Early Proterozoic metallogeny: *S. Afr. J. Geol.*, v. 95, p. 80-87.
- Gair, J.E., 1973**, Iron deposits of Michigan (United States of America), in: *Genesis of Precambrian iron and manganese deposits: Proc. Kiev Symposium 1970*, UNESCO Paris, p. 365-

375.

**Gapara, C.S., 1993**, A review of the deposition of iron-formation and genesis of the related iron-ore deposits as a guide to exploration for Precambrian iron-ore deposits in Southern Africa: Unpubl. MSc Diss., Rhodes Univ., 114 p.

**Garrels, R.M., 1988**, Reply: A model for the deposition of the microbanded Precambrian iron-formations: *Am. J. Sci.*, v. 288, p. 669-673.

**Gauthier, M., Brown, A.C., and Morin, G., 1987**, Small iron-formations as a guide to base- and precious-metal deposits in the Grenville Province of southern Quebec, in: *Precambrian iron-formations*, eds., Appel, P.W.U., and LaBerge, G.L.: Theophrastus publ., Athens, p. 297-328.

**Gehor, S., and Laajoki, K., 1987**, The mineralogy and regional metamorphism of the Precambrian iron-formations in Finland, in: *Precambrian iron-formations*, eds., Appel, P.W.U., and LaBerge, G.L.: Theophrastus publ., Athens, p. 393-422.

**Gibbs, A.K., and Wirth, K.R., 1990**, Geologic setting of the Serra dos Carajas iron deposits, Brazil, in: *Ancient banded iron-formations (regional presentations)*: Theophrastus publ., Athens, p. 83-104.

**Goldich, S.S., 1973**, Ages of Precambrian banded iron-formations: *Econ. Geol.*, v. 68, p. 1126-1134.

**Goode, A.D.T., Hall, W.D.M., and Bunting, J.A., 1983**, The Nabberu Basin of Western Australia, in: *Iron-formations: facts and problems*, eds., Trendall, A.F., and Morris, R.C.: *Developments in Precambrian Geology* 6, Els. Sci. Pbl., p. 295-323.

**Goodwin, A.M., 1973a**, Archaean volcanogenic iron-formation of the Canadian Shield, in: *Genesis of Precambrian iron and manganese deposits: Proc. Kiev Symposium 1970*, UNESCO Paris, p. 23-34.

**Goodwin, A.M., 1973b**, Archaean iron-formations and tectonic basins of the Canadian Shield: *Econ. Geol.*, v. 68, p. 915-933.

**Goodwin, A.M., Monster, J., and Thode, H.G., 1976**, Carbon and sulfur isotope abundances in Archaean iron-formations and early Precambrian life: *Econ. Geol.*, v. 71, p. 870-891.

**Goodwin, A.M., Thode, H.G., Chou, C.L., and Karkhansis, S.N., 1985**, Chemostratigraphy and origin of the Late Archaean siderite-pyrite-rich Helen iron-formation, Michipicoten Belt, Canada: *Can. J. Earth Sci.*, v. 22, p. 72-84.

**Goryainov, P.M., 1973**, Structural-tectonic environments of iron-ore process in the Baltic Shield



Precambrian, in: Genesis of Precambrian iron and manganese deposits: Proc. Kiev Symposium 1970, UNESCO Paris, p. 95-99.

**Goryainov, P.M., 1990**, Precambrian iron ore formations of the Baltic Shield and their role in structural-substantial arrangement of the continental crust, in: Ancient banded iron-formations (regional presentations): Theophrastus publ., Athens, p. 251-280.

**Grobbelaar, W.S., 1988**, The N'chwaning manganese mine of the Kalahari manganese field: Geobulletin, v. 31, #2, p. 34-35.

**Grobbelaar, W.S., and Beukes, N.J., 1986**, The Bishop and Glosam manganese mines and the Beeshoek iron-ore mine of the Postmasburg area, in: Mineral deposits of Southern Africa, eds., Anhaeusser, C.R., and Maske, S.: Geol. Soc. S. Afr., v. I, p. 957-961.

**Grobler, N.J., and Botha, B.J.V., 1976**, Pillow-lavas and hyaloclastite in the Ongeluk Andesite formation in a road-cutting west of Griquatown, South Africa: Trans. Geol. Soc. S. Afr., v. 79, p. 53-57.

**Gross, G.A., 1990**, Manganese and iron facies in hydrolithic systems, in: Sediment-hosted mineral deposits, eds., Parnell, J., Lianjun, Ye, and Changming Chen: Intern. Assoc. Sedim., Spec. Publ. #11, Blackwell Scientific Publications, 227 p.

**Gross, G.A., 1991**, Genetic concepts for iron-formation and associated metalliferous sediments, in: Historical perspectives of genetic concepts and case histories of famous discoveries, eds., Hutchinson, R.W., and Grauch, R.I.: Econ. Geol., Monograph 8, p. 51-81.

**Grout, F.F., 1919**, The nature and origin of the Biwabik iron-bearing formation of the Mesabi range, Minnesota: Econ. Geol., v. 14, p. 452-464.

**Grubb, P.L.C., 1971**, Silicates and their paragenesis in the Brockman iron-formation of Wittenoom Gorge, Western Australia: Econ. Geol., v. 66, p. 281-292.

**Gruner, J.W., 1926**, The Soudan formation and a new suggestion as to the origin of the Vermillion ores: Econ. Geol., v. 21, p. 629-644.

**Gruss, H., 1973**, Itabirite iron-ores of the Liberia and Guyana shields, in: Genesis of Precambrian iron and manganese deposits: Proc. Kiev Symposium 1970, UNESCO Paris, p. 335-359.

**Haase, C.S., 1982a**, Metamorphic petrology of the Negaunee iron-formation, Marquette District, Northern Michigan: mineralogy, metamorphic reactions and phase equilibria: Econ. Geol., v. 77, p. 60-81.

**Haase, C.S., 1982b**, Phase equilibria in metamorphosed iron-formations: qualitative T-X(CO<sub>2</sub>)

petrogenetic grids: *Am. J. Sci.*, v. 282, p. 1623-1654.

**Haese, R.R., Petermann, H., Dittert, L., and Schulz, H.D., 1998**, The early diagenesis of iron in pelagic sediments: a multidisciplinary approach: *Earth Plan. Sci. Let.*, v. 157, p. 233-248.

**Hälbich, I.W., and Altermann, W., 1992**, The genesis of BIF in the Transvaal Supergroup, South Africa, in: *Source, transport and deposition of metals*, eds., Pagel, M., and Leroy, J.L.: A.A. Balkema, Rotterdam, 841 p.

**Hälbich, I.W., Lamprecht, D., Altermann, W., and Horstmann, U.E., 1992**, A carbonate-banded iron-formation transition in the Early Proterozoic of South Africa: *Jour. Afr. Earth Sci.*, v. 15, No 2, p. 217-236.

**Hall, W.D.M., and Goode, A.D.T., 1978**, The Early Proterozoic Nabberu basin and associated iron formations of Western Australia. *Prec. Res.*, v. 7, p. 129-184.

**Han, Tsu-Ming, 1988**, Origin of magnetite in Precambrian iron-formations of low metamorphic grade, in: *Proceedings Seventh IAGOD Symposium*, ed., Zachrisson, E.: The Intern. Assoc. on the Genesis of Ore Deposits., p. 641-656.

**Harmsworth, R.A., Kneeshaw, M., Morris, R.C., Robinson, C.J., and Shirastava, P.K., 1990**, BIF-derived iron-ores of the Hamersley Province, in: *Geology of mineral deposits of Australia and Papua New Guinea*, ed., Hughes, F.E.: *Austr. Inst. Min. Metall.*, v. 2, Monogr. #14, p. 617-643.

**Hasshimoto, T., and Beland, R., 1968**, Low- to medium-grade metamorphism in silicate iron-formations of the Cape Smith Belt, New Quebec: *Can. J. Earth Sci.*, v. 5, p. 881-893.

**Hayashi, K., Fujisawa, H., Holland, H., and Ohmoto, H., 1997**, Geochemistry of ~1.9 Ga sedimentary rocks from northeastern Labrador, Canada: *Geoch. Cosm. Acta*, v. 61, p. 4115-4137.

**Hem J.D., 1972**, Chemical factors that influence the availability of iron and manganese in aqueous systems: *Geol. Soc. Am. Bull.*, v. 83, p. 443-450.

**Holm, N.G., 1988**, Carbon isotope distribution in organic matter and siderite of a modern metalliferous hydrothermal sediment and possible implications for gold associated with banded iron formation: *Mar. Geol.*, v. 84, p. 201-207.

**Hoppe, A., Schobbenhaus, C., and Walde, D.H.G., 1987**, Precambrian iron formation in Brazil, in: *Precambrian iron-formations*, eds., Appel, P.W.U., and LaBerge, G.L.: Theophrastus publ., Athens, p. 347-392.

**Huber, N.K., 1958**, The environmental control of sedimentary iron minerals: *Econ. Geol.*, v. 53,

p. 82-118.

**Huber, N.K., 1959**, Some aspects of the origin of the Ironwood iron-formation of Michigan and Wisconsin: *Econ. Geol.*, v. 54, p. 82-118.

**Huckriede, H., and Meischner, D., 1996**, Origin and environment of manganese-rich sediments within black-shale basins. *Geoch. Cosm. Acta*, v. 60, p. 1399-1414.

**Hunter, D.R., 1974**, Crustal development in the Kaapvaal Craton, II. The Proterozoic. *Prec. Res.*, v. 1, p. 295-326.

**Jahn, B.-m, and Simonson, B.M., 1995**, Carbonate Pb-Pb ages of the Wittenoom Formation and Carawine Dolomite, Hamersley Basin, Western Australia (with implications for their correlation with the Transvaal Dolomite of South Africa): *Prec. Res.*, v. 72, p. 247-261.

**Jahn, B.-m, Bertrand-Sarfati, J., Morin, N., and Macé, J., 1990**, Direct dating of stromatolitic carbonates from the Schmidtsdrif Formation (Transvaal dolomite), South Africa, with implications on the age of the Ventersdorp Supergroup: *Geology*, v. 18, p. 1211-1214.

**James, H.L., 1951**, Iron formation and associated rocks in the Iron River district, Michigan: *Geol. Soc. Am. Bull.*, v. 62, p. 251-266.

**James, H.L., 1966**, Chemistry of the iron-rich sedimentary rocks: U.S. Geol. Surv., Prof. Pap. 440-W, 61 p.

**James, H.L., 1969**, Comparison between Red Sea deposits and older ironstone and iron-formation, in: *Hot Brines and recent heavy metal deposits in the Red Sea*, eds., Degens, E. T., and Ross, D.A.: Springer-Verlag, Berlin, p. 525-532.

**James, H.L., 1983**, Distribution of banded iron-formation in space and time, in: *Iron-formations: facts and problems*, eds., Trendall, A.F., and Morris, R.C.,: *Developments in Precambrian Geology* 6, *Els. Sci. Pbl.*, p. 471-490.

**James, H.L., and Sims, P.K., 1973**, Precambrian iron-formations of the world: *Econ. Geol.*, v. 68, p. 913-914.

**Jennings, M., 1986**, The Middelplaats manganese ore deposit, Griqualand West, in: *Mineral deposits of Southern Africa*, eds., C.R. Anhaeuser, and S. Maske, *Geol. Soc. S. Afr.* v. I. p. 979-983.

**Jin, B., and Hui, L., 1987**, Tectonic control of BIF in the Wutaishan Region, Shanxi Province, China, in: *Precambrian iron-formations*, eds., Appel, P.W.U., and LaBerge, G.L.: Theophrastus publ., Athens, p. 467-486.

**Kalayev, G.I., Novikova, A.S., and Schichipansky, A.A., 1990**, Early Proterozoic iron-ore sedimentary basins of Krivoy Rog (USSR) and Hamersley-Naberu (Australia): comparative tectonics and geodynamic settings, in: *Ancient banded iron-formations (regional presentations)*: Theophrastus publ., Athens, p. 233-250.

**Kalugin, A.S., 1973**, Geology and genesis of the Devonian banded iron-formation in Altai, western Siberia and eastern Kazakhstan, in: *Genesis of Precambrian iron and manganese deposits*: Proc. Kiev Symposium 1970, UNESCO Paris, p. 159-165.

**Karlin, R., Lyle, M., and Heath, G.R., 1987**, Authigenic magnetite formation in suboxic marine sediments: *Nature*, v. 326, p. 490-493.

**Kasting, J.F., Liu, S.C., and Donahue, T.M., 1979**, Oxygen levels in the prebiological atmosphere: *Jour. Geoph. Res.*, v. 84, p. 1147-1158.

**Kaufman, A.J., 1996**, Geochemical and mineralogic effects of contact metamorphism on banded iron-formation: an example from the Transvaal Basin, South Africa. *Prec. Res.*, v. 79, p. 171-194.

**Kimberley, M.M., 1983**, Constraints on genetic modelling of Proterozoic iron-formations, in: *Proterozoic geology: selected papers from an international symposium*, eds., L.G. Medaris, Jr., D.M. Mickelson, C.W. Byers, and W.C. Shanks: *Geol. Soc. Am., Mem.* 161, p. 227-235.

**Klein, C., 1997**, Igneous ferromagnetite at Hamersley: *Nature*, v. 385, p. 25-26.

**Klein, C., Beukes, N.J., and Schopf, J.W., 1987**, Filamentous microfossils in the Early Proterozoic Transvaal Supergroup: their morphology, significance, and palaeoenvironmental setting: *Prec. Res.*, v. 36, p. 81-94.

**Klemm, D.D., 1979**, A biogenetic model of the formation of the banded iron-formation in the Transvaal Supergroup, South Africa: *Min. Dep.*, v. 14, p. 381-385.

**Klemm, D.D., 1991**, The formation of highly concentrated iron-ore bodies within the BIF: The Sishen case, in: *Source, transport and deposition of metals*, eds., Pagel, M., and Leroy, J.L.: A.A. Balkema, Rotterdam, 841 p.

**Kleyenstüber, A.S.E., 1991**, ICAM'91 Excursion Guide, Kalahari manganese field: *International Congress on Applied Mineralogy*, 23 p.

**Klinger, F.R., 1975**, Iron-ore, in: *Mineral facts and problems (bicentennial edition)*: U.S. Bureau of Mines, Bull. 667, 1259 p.

**Konhauser, K.O., and Ferris, F.G., 1996**, Diversity of iron and silica precipitation by microbial mats in hydrothermal waters, Iceland: *Implications for Precambrian iron formations*: *Geology*, v.

24, p. 323-326.

**Kranck, S.H., 1961**, A study of phase equilibria in a metamorphic iron-formation: *J. Petr.*, v. 2, p. 137-184.

**Krauskopf, K.B., 1957**, Separation of manganese from iron in sedimentary processes: *Geoch. Cosm. Acta*, v. 9, p. 1-32b.

**Krishnan, M.S., 1973**, Occurrence and origin of the iron-ores of India, in: *Genesis of Precambrian iron and manganese deposits: Proc. Kiev Symposium 1970, UNESCO Paris*, p. 69-76.

**Krumbein, W.C., and Garrels, R.M., 1952**, Origin and classification of chemical sediments in terms of pH and oxidation-reduction potential: *J. Geol.*, v. 60, p. 1-33.

**Laajoki, K., and Gehor, S., 1990**, The Precambrian iron-formations of Finland and their tectono-sedimentary settings, in: *Ancient banded iron-formations (regional presentations): Theophrastus publ., Athens*, p. 445-462.

**LaBerge, G.L., 1964**, Development of magnetite in iron-formations of the Lake Superior Region: *Econ. Geol.*, v. 59, p. 1313-1342.

**LaBerge, G.L., 1967**, Microfossils and Precambrian iron-formations: *Geol. Soc. Am. Bull.*, v. 78, p. 331-342.

**LaBerge, G.L., 1973**, Possible biological origin of Precambrian iron-formations: *Econ. Geol.*, v. 68, p. 1098-1109.

**LaBerge, G.L., Robbins, E.I., and Han, T.M., 1987**, A model for the biological precipitation of Precambrian iron-formations - A: Geological evidence, in: *Precambrian iron-formations*, eds., Appel, P.W.U., and LaBerge, G.L.: *Theophrastus publ., Athens*, p. 31-69.

**Lagoeiro, L.E., 1998**, Transformation of magnetite to hematite and its influence on the dissolution of iron oxide minerals: *J. Met. Geol.*, v. 16, p. 415-423.

**Lamprecht, D.F., and Hälbich, I.W., 1988**, A vertical transition from carbonates to banded iron-formation in the Griqualand West Sequence of the Transvaal Supergroup, at Finsch diamond mine, Northern Cape Province: *Abstracts, Geocongress '88, Geol. Soc. S. Afr.*, p. 783-786.

**Lepp, H., 1963**, The relation of iron and manganese in sedimentary iron formations: *Econ. Geol.*, v. 58, p. 515-526.

**Lepp, H., 1966**, Chemical composition of the Biwabik iron-formation, Minnesota: *Econ. Geol.*, v. 61, p. 243-250.

**Lepp, H., 1968**, The distribution of manganese in the Animikian iron-formation of Minnesota:

Econ. Geol., v. 63, p. 61-75.

**Lepp, H., 1972**, Normative mineral composition of the Biwabik Formation: a first approach, in: Studies in mineralogy and Precambrian geology, eds., Doe, B.R., and Smith, D.K.: Geol. Soc. Am. Mem. 135, p. 265-278.

**Lepp, H., 1987**, Chemistry and origin of Precambrian iron-formations, in: Precambrian iron-formations, eds., Appel, P.W.U., and LaBerge, G.L.: Theophrastus publ., Athens, p. 3-30.

**MacDonald, A.J., 1990**, Banded oxide facies iron-formation as a host for gold mineralization, in: Ancient banded iron-formation (regional presentations): Theophrastus publ., Athens, p. 63-82.

**MacLeod, W.N., 1973**, Iron-ores of the Hamersley Iron Province, Western Australia, in: Genesis of Precambrian iron and manganese deposits: Proc. Kiev Symposium 1970, UNESCO Paris, p. 291-298.

**Mahabaleswar, B., Basavanna, M., and Maaskant, P., 1987**, Iron formations of Archaean high grade region, Karnataka, India, in: Precambrian iron-formations, eds., Appel, P.W.U., and LaBerge, G.L.: Theophrastus publ., Athens, p. 487-512.

**Majumder, T., 1990**, Precambrian banded iron formation of Eastern India: an overview, in: Ancient banded iron-formations (regional presentations): Theophrastus publ., Athens, p. 351-388.

**Majumder, T., and Chakraborty, K.L., 1977**, Primary sedimentary structures in the banded iron formation of Orissa: Sed. Geol., v. 19, p. 287-300.

**Majumder, T., Chakraborty, K.L., and Bhattacharyya, A., 1982**, Geochemistry of banded iron-formation of Orissa, India: Min. Dep., v. 17, p. 107-118.

**Mancuso, J.J., Lougheed, M.S., and Wygant, T., 1971**, Possible biogenic structures from the Precambrian Negaunee iron-formation, Marquette range, Michigan: Am. J. Sci., v. 271, p. 181-186.

**Mancuso, J.J., Lougheed, M.S., and Shaw, R., 1975**, Carbonate-apatite in Precambrian cherty iron-formation, Baraga County, Michigan: Econ. Geol., v. 70, p. 583-586.

**Marchig, V., Gundlach, H., Moller, P. and Schley, F., 1982**, Some geochemical indicators for discrimination between diagenetic and hydrothermal metalliferous sediments: Mar. Geol., v. 50, p. 241-256.

**Markov, M.S., Schichipansky, A.A., Shukolyukov, Yu.A., and Verkhovsky, A.B., 1990**, Distribution and origin of noble gases in magnetites from Precambrian iron ores, in: Ancient banded iron-formations (regional presentations): Theophrastus publ., Athens, p. 281-294.

- Markun, C.D., and Randazzo, A.F., 1980**, Sedimentary structures in the Gunflint iron-formation, Schreiber Beach, Ontario: *Prec. Res.*, v. 12, p. 287-310.
- Marsden, R.W., 1970**, Geology of the iron-ores of the Lake Superior Region in the United States, in: *Ore deposits of the United States*, ed., Ridge, J.D.: Amer. Inst. Min. Metall. & Petr. Eng., Graton-Sales vol., v. I, p. 489-507.
- Marsden, R.W., Emanuelson, J.W., Owens, J.S., Walker, N.E., and Werner, R.F., 1970**, The Mesabi iron-range, Minnesota, in: *Ore deposits of the United States*, ed., Ridge, J.D.: Amer. Inst. Min. Metall. & Petr. Eng., Graton-Sales vol., v. I, p. 518-537.
- Marsh, J., 1984**, Geochemical characterization of lavas of the Ongeluk Formation, Northern Cape: SAMANCOR, unpubl. rep., 5 p., 2 tbl., 2 fig.
- Martin, D.McB., Clendenin, C.W., Krapez, B., and McNaughton, N.J., 1998**, Tectonic and geochronological constraints on late Archaean and Palaeoproterozoic stratigraphic correlation within and between the Kaapvaal and Pilbara Cratons: *J. Geol. Soc.*, v. 155, p. 311-322.
- Martin, D.McB., Li, Z.X., Nemchin, A.A., and Powell, C.McA., 1998**, A pre-2.2 GA age for giant hematite ores of the Hamersley Province, Australia: *Econ. Geol.*, v. 98, p. 000-000.
- Maynard, B.J., 1983**, *Geochemistry of sedimentary ore deposits*: Springer-Verlag, New York Inc., 305 p.
- McConchie, D., 1987**, The geology and geochemistry of the Joffre and Whale-back shale members of the Brockman iron-formation, Western Australia, in: *Precambrian iron-formations*, eds., Appel, P.W.U., and LaBerge, G.L.: Theophrastus publ., Athens, p. 541-600.
- Mel'nik, Y.P., and Siroshtan, R.I., 1973**, Physico-chemical conditions of the metamorphism of cherty-iron rocks, in: *Genesis of Precambrian iron and manganese deposits*: Proc. Kiev Symposium 1970, UNESCO Paris, p. 209-216.
- Miller, R.G., and O'Nions, R.K., 1985**, Sources of Precambrian chemical and clastic sediments: *Nature*, v. 314, p. 325-330.
- Min-Zhi, Y., 1990**, Some data on the sedimentation and metamorphism of the iron-ore deposits of Mid-Lower Proterozoic to Archaean and their classification, in: *Ancient banded iron-formations (regional presentations)*: Theophrastus publ., Athens, p. 419-444.
- Miyano, T., and Klein, C., 1986**, Fluid behavior and phase relations in the system Fe-Mg-Si-C-O-H: application to high grade metamorphism of iron-formations: *Am. J. Sci.*, v. 286, p. 540-575.
- Monster, J., Appel, P.W.U., Thode, H.G., Schidlowski, M., Carmichael, C.M., and**

- Bridgwater, D., 1979**, Sulfur isotope studies in Early Archaean sediments from Isua, West Greenland: implications for the antiquity of bacterial sulfate reduction: *Geoch. Cosm. Acta.* v. 43, p. 405-413.
- Morey, G.B., 1973**, Mesabi, Gunflint and Cuyuna Ranges, Minnesota (United States of America), in: *Genesis of Precambrian iron and manganese deposits: Proc. Kiev Symposium 1970, UNESCO Paris*, p. 193-208.
- Morey, G.B., and Southwick, D.L., 1995**, Allostratigraphic relationships of early Proterozoic iron-formations in the Lake Superior Region: *Econ. Geol.*, v. 90, p. 1983-1993.
- Morey, G.B., Papike, J.J., Smith, R.W., and Weiblen, P.W., 1972**, Observations on the contact metamorphism of the Biwabik iron-formation, East Mesabi District, Minnesota, in: *Studies in mineralogy and Precambrian geology*, eds. Doe, B.R., and Smith, D.K., *Geol. Soc. Am., Mem.* 135, p. 225-264.
- Morris, R.C., 1983**, Supergene alteration of banded iron-formations, in: *Iron-formations: facts and problems*, eds., Trendall, A.F., and Morris, R.C.,: *Developments in Precambrian Geology* 6, *Els. Sci. Pbl.*, p. 513-534.
- Morris R.C., Thornber, M.R., and Ewers, W.E., 1980**, Deep-seated iron-ores from banded iron-formation: *Nature*, 288, p. 250-252.
- Mueller, R.F., 1960**, Compositional characteristics and equilibrium relations in mineral assemblages of a metamorphosed iron-formation. *Am. J. Sci.*, v. 258, p. 449-497.
- Mücke, A., and Annor, A., 1993**, Examples and genetic significance of the formation of iron oxides in the Nigerian banded iron-formations: *Min. Dep.*, v. 28, p. 136-145.
- Mücke, A., Annor, A., and Neumann, U., 1996**, The Algoma-type iron-formations of the Nigerian metavolcano-sedimentary schist belts. *Min. Dep.*, v. 31, p. 113-122.
- Murthy, P.S.N., 1990**, Origin of the cyclothem patterns in the Precambrian banded iron formation of Donimalai area in Sandur schist belt, Karnataka State, India, in: *Ancient banded iron-formations (regional presentations): Theophrastus publ., Athens*, p. 327-350.
- Novokhatsky, I.P., 1973**, Precambrian ferruginous-siliceous formations of Kazakhstan, in: *Genesis of Precambrian iron and manganese deposits: Proc. Kiev Symposium 1970, UNESCO Paris*, p. 153-157.
- Ohmoto, H., 1997**, Evidence in pre-2.2 Ga paleosols for the early evolution of atmospheric oxygen and terrestrial biota: Reply: *Geology*, v. 25, p. 858-859.



- O'Rourke, J.E., 1961**, Palaeozoic banded iron-formation: *Econ. Geol.*, v. 56, p. 331-361.
- Owens, J.S., 1965**, Discussion of origin of Precambrian iron-formations by Lepp and Goldich: *Econ. Geol.*, v. 60, p. 1731-1734.
- Percival, F.G., 1973**, Enrichment of banded iron-ore, Kedia d' Idjil, in: *Genesis of Precambrian iron and manganese deposits: Proc. Kiev Symposium 1970, UNESCO Paris*, p. 281-289.
- Patwardhan, A.M., Patil, D.N., and Sukhtankar, R.K., 1987**, On magnetite quartzites occurring around Narnaul, Haryana, India, in: *Precambrian iron-formations*, eds., Appel, P.W.U., and LaBerge, G.L.: Theophrastus publ., Athens, p. 513-540.
- Perry, E.C.Jr, and Tan, F.C., 1972**, Significance of oxygen and carbon isotope variations in early Precambrian cherts and carbonate rocks of southern Africa: *Bull. Geol. Soc Am.*, v. 83, p. 647-664.
- Plaksenko, N.A., Koval, I.K., and Shchogolev, I.N., 1973**, Precambrian ferruginous-siliceous formations associated with the Kursk Magnetic Anomaly, in: *Genesis of Precambrian iron and manganese deposits: Proc. Kiev Symposium 1970, UNESCO Paris*, p. 89-94.
- Powell, C.McA., Li, Z.X., Martin, D.McB., and Oliver, N.H.S., 1998**, Giant Hamersley iron ore bodies formed by orogenic fluids in an early Proterozoic fold-and thrust belt: Abstracts, 14th Aust. Geol. Conv., Townsville, Australia, p. 362.
- Qiusheng, Z., 1987**, Banded iron-formations in China, in: *Precambrian iron-formations*, eds., Appel, P.W.U., and LaBerge, G.L.: Theophrastus publ., Athens, p. 423-448.
- Quirk, T.T., 1961**, Geology of the Temiscamie iron-formation, Lake Albanel iron range, Mistassini Territory, Quebec: *Econ. Geol.*, v.55, p. 311-326.
- Quirk, T.T., Goldich, S.S., and Krueger, H.W., 1960**, Composition and age of the Temiscamie iron formation, Mistassini Territory, Quebec: *Econ. Geol.*, v. 55, p. 311-326.
- Rai, K.L., Sarkar, S.N., and Paul, P.R., 1980**, Primary depositional and diagenetic features in the banded iron-formation and associated iron-ore deposits of Noamundi, Singhbhum District, Bihar, India: *Min. Dep.*, v. 15, p. 189-200.
- Rai, K.L., and Paul, P.R., 1990**, Geochemistry of banded iron-formation, iron ores and associated lithologies from Jamda-Koira valley of Bihar, India, in: *Ancient banded iron-formations (regional presentations): Theophrastus publ., Athens*, p. 311-327.
- Reimer, T.O., 1987**, Weathering as a source of iron in iron-formations: the significance of alumina- enriched palaeosols from the Proterozoic of Southern Africa, in: *Precambrian iron-*

- formations, eds., Appel, P.W.U., and LaBerge, G.L.: Theophrastus publ., Athens, p. 601-620.
- Reczko, B.F.F., 1994**, The geochemistry of the sedimentary rocks of the Pretoria Group, Transvaal Sequence: Unpubl. PhD thesis, Univ. of Pretoria, South Africa, 385 p.
- Robbins, E.I., 1987**, *Appellella Ferrifera*, a possible new iron-coated microfossil in the Isua iron-formation, southwestern Greenland, in: Precambrian iron-formations, eds., Appel, P.W.U., and LaBerge, G.L.: Theophrastus publ., Athens, p. 141-154.
- Robbins, E.I., LaBerge, G.L., and Schmidt, R.G., 1987**, A model for the biological precipitation of Precambrian iron-formations - B: Morphological evidence and modern analogues, in: Precambrian iron-formations, eds., Appel, P.W.U., and LaBerge, G.L.: Theophrastus publ., Athens, p. 97-140.
- Robertson, D.J., 1984**, Silicate facies iron-formation and stratabound alteration: tuffaceous exhalites derived by mixing - evidence from Mn garnet-stilpnomelane rocks at Redstone, Ontario: Econ. Geol., v. 79, p. 1796-1817.
- Rosière, C.A., and Chemale F.Jr., 1996**, Genesis of banded-iron-formations-a discussion: Econ. Geol., p. 466-467.
- Roy, S., 1973**, Genetic studies of the Precambrian manganese formations of India with particular reference to the effects of metamorphism, in: Genesis of Precambrian iron and manganese deposits: Proc. Kiev Symposium 1970, UNESCO Paris, p. 229-242.
- Roy, S., 1976**, Ancient manganese deposits, in: Handbook of stratabound and stratiform ore deposits, ed., Wolf, K.H.: Els. Sci. Pbl., v. 7, 656 p.
- Ruhlin, D.E., and Owen, R.M., 1986**, The rare earth element geochemistry of hydrothermal sediments from the East Pacific Rise: examination of a seawater scavenging mechanism: Geoch. Cosm. Acta, v. 50, p. 393-400.
- Rye, R., Kuo, P.H., and Holland, H.D., 1995**, Atmospheric carbon dioxide concentrations before 2.2 billion years ago: Nature, v. 378, p. 603-605.
- Schidlowski, M., 1988**, A 3800-million-year isotopic record of life from carbon in sedimentary rocks: Nature, v. 333, p. 313-318.
- Schidlowski, M., Eichmann, R., and Junge, C., 1975**, Precambrian sedimentary carbonates: Carbon and oxygen isotope geochemistry and implications for the terrestrial oxygen budget: Prec. Res., v. 2, p. 1-69.
- Schieber, J., 1987**, Small scale sedimentary iron deposits in a Mid-Proterozoic basin: viability of

- iron supply by rivers, in: Precambrian iron-formations, eds., Appel, P.W.U., and LaBerge, G.L.: Theophrastus publ., Athens, p. 267-296.
- Schütte, S.S., and Cornell, D.H., 1990**, Spilitization processes in the Proterozoic Ongeluk andesite Formation in Griqualand West, South Africa: Abstracts, Geocongress '90, Geol. Soc. S. Afr., p. 505-508.
- Semenenko, N.P., 1973**, The iron-chert formations of the Ukrainian shield, in: Genesis of Precambrian iron and manganese deposits: Proc. Kiev Symposium 1970, UNESCO Paris, p. 135-142.
- Shegelski, R.J., 1987**, The depositional environment of Archaean iron-formations, Sturgeon-Savant Greenstone belt, Ontario, Canada, in: Precambrian iron-formations, eds, Appel, P.W.U., and LaBerge, G.L.: Theophrastus publ., Athens, p. 329-346.
- Shimizu, H., Unemoto, N., Masuda, A., and Appel, P.W.U., 1987**, Sources of iron-formations in the Archaean Isua and Malene supracrustals, West Greenland: evidence from La-Ce and Sm-Nd isotopic data and REE abundances: *Geoch. Cosm. Acta*, v. 54, p. 1147-1154.
- Shkolnik, E.L., 1973**, Effusive jasper iron-formation and iron-ores of the Uda area, in: Genesis of Precambrian iron and manganese deposits: Proc. Kiev Symposium 1970, UNESCO Paris, p. 187-189.
- Shtsherbak, V.M., Kryukov, A.S., and Tilepov, Z.T., 1973**, On the issue of genesis and metamorphism of ferromanganese formations in Kazakhstan, in: Genesis of Precambrian iron and manganese deposits: Proc. Kiev Symposium 1970, UNESCO Paris, p. 249-254.
- Siever, R., 1992**, The silica cycle in the Precambrian: *Geoch. Cosm. Acta*, v. 56, p. 3265-3272.
- Sills, J.D., Wang, K., Windley, B.F., Yan, Y., and Zhai, M., 1987**, Banded iron-formations in the Early Precambrian of NE China, in: Precambrian iron-formations, eds., Appel, P.W.U., and LaBerge, G.L.: Theophrastus publ., Athens, p. 449-466.
- Simonson, B.M., 1987**, Early silica cementation and subsequent diagenesis in arenites from four Early Proterozoic iron-formations of North America: *J. Sed. Petr.*, v. 57, #3, p. 494-511.
- Simonson, B.M., 1992**, Geological evidence for a strewn field of impact spherules in the early Precambrian Hamersley Basin of Western Australia: *Geol. Soc. Am. Bull.*, v. 104, p. 829-839.
- Simonson, B.M., 1997**, Discovery of a Neoproterozoic impact spherule horizon in the Transvaal Supergroup of South Africa and possible correlations to the Hamersley basin of Western Australia: Lunar and Planetary Science Conf., Houston, Texas, p. 1323-1324.

- Simonson, B.M., and Hassler, S.W., 1996**, Was the deposition of large Precambrian Iron Formations linked to major marine transgressions? *J. Geol.*, v. 104, p. 665-676.
- Simonson, B.M., and Hassler, S.W., 1997**, Revised correlations in the early Precambrian Hamersley Basin based on a horizon of resedimented impact spherules: *Aust. J. E. Sci.*, v. 44, p. 37-48.
- Simonson, B.M., and Lanier, W.P., 1987**, Early silica cementation and microfossil preservation in cavities in iron-formation stromatolites, Early Proterozoic of Canada, in: *Precambrian iron-formations*, eds., Appel, P.W.U., and LaBerge, G.L.: Theophrastus publ., Athens, p. 187-214.
- Sims, S.J., 1973**, The Belinga iron-ore deposit (Gabon), in: *Genesis of Precambrian iron and manganese deposits: Proc. Kiev Symposium 1970, UNESCO Paris*, p. 323-334.
- Smith, R.E., Perdrix, J.L., and Parks, T.C., 1982**, Burial metamorphism in the Hamersley Basin, Western Australia: *J. Pet.*, v. 23, p. 75-102.
- Söhnge, P.G., 1977**, Timing aspects of the manganese deposits of the Northern Cape Province (South Africa), in: *Time and stratabound ore deposits*, eds., D.D. Klemm, and Schneider, H.J.: Springer-Verlag, p. 115-122.
- Sokolov, G.A., and Grigor'ev, V.M., 1977**, Deposits of iron, in: *Ore deposits of the USSR*, ed., Smirnov, V.I.: Pitman Publ., v. I, 352 p.
- Strauss, H., and Beukes, N.J., 1996**, Carbon and sulfur isotopic compositions of organic carbon and pyrite in sediments from the Transvaal Supergroup, South Africa. *Prec. Res.*, v. 79, p. 57-72.
- Strauss, H., Des Marais, D.J., Hayes, J.M., and Summons, R.E., 1992**, The carbon-isotopic record, in: *The Proterozoic biosphere: A multidisciplinary study*, eds., Schopf, J.W., and Klein, C. New York, Cambridge University Press, p. 117-127.
- Strydom, D., van der Westhuisen, W.A., and Schoch, A.E., 1987**, The iron-formations of Bushmanland in the north-western Cape Province, South Africa, in: *Precambrian iron-formations*, eds., Appel, P.W.U., and LaBerge, G.L.: Theophrastus publ., Athens, p. 621-634.
- Stulchikov, V.A., 1990**, Geochemistry of iron-banded formations of the Verkhovtsevo syncline (central part of the Ukrainian Shield), in: *Ancient banded iron-formations (regional presentations): Theophrastus publ.*, Athens, p. 295-310.
- Sumner, D.Y., 1997**, Carbonate precipitation and oxygen stratification in late Archaean seawater as deduced from facies and stratigraphy of the Gamohaam and Frisco Formations, Transvaal Supergroup, South Africa: *Am. J. Sci.*, v. 297, p. 455-487.

**Sumner, D.Y., and Bowring, S.A., 1996**, U-Pb geochronologic constraints on deposition of the Campbellrand Subgroup, Transvaal Supergroup, South Africa: *Prec. Res.*, v. 79, p. 25-36.

**Tankard, A.J., Jackson, M.P.A., Eriksson, K.A., Hobday, D.K., Hunter, D.R., and Minter, W.E.L., 1982**, Crustal evolution of Southern Africa: 3.8 Billion years of earth history: Springer-Verlag, 523 p.

**Taylor, J.H., 1974**, Sedimentary ores of iron and manganese and their origin, in: *Sedimentary ores (Ancient & Modern rev.)*, ed., James, C.H.: Special Publication #1, Dep. of Geology. Univ. of Leicester, p. 171-186.

**Thode, H.G., and Goodwin, A.M., 1983**, Further sulfur and carbon isotope studies of late Archaean iron-formations of the Canadian Shield and the rise of sulfate-reducing bacteria: *Prec. Res.*, v. 20, p. 337-356.

**Tokhtuev, G.V., 1973**, Structural control of the localisation of rich iron-ores of Krivoyrog, in: *Genesis of Precambrian iron and manganese deposits: Proc. Kiev Symposium 1970*, UNESCO Paris, p. 361-364.

**Tolbert, G.E., Tremaine, J.W., Melcher, G.C., and Gomes, C.B., 1973**, Geology and iron-ore deposits of Serra dos Carajas, Para (Brazil), in: *Genesis of Precambrian iron and manganese deposits: Proc. Kiev Symposium 1970*, UNESCO Paris, p. 271-280.

**Trendall, 1965**, Discussion of origin of Precambrian iron-formations: *Econ. Geol.*, v. 60, p. 1065-1070.

**Trendall, A.F., 1968**, Three great basins of Precambrian banded iron-formation deposition: a systematic comparison: *Geol. Soc. Am. Bull.*, v. 79, p. 1527-1544.

**Trendall, A.F., 1975**, Geology of Western Australian iron-ore, in: *Economic Geology of Australia and Papua New Guinea*, ed., Knight, C.L.: The Austr. Inst. Min. Metal., Monogr. Ser. #5, p. 883-892.

**Trendall, A.F., 1979**, *Iron: Mining in Western Australia*, ed., Prider, R.T.: Un. W. Aus. 304 p.

**Trendall, A.F., 1983**, Introduction, in: *Iron-formations: facts and problems*, eds., Trendall, A.F., and Morris, R.C.: *Developments in Precambrian Geology* 6, *Els. Sci. Pbl.*, p. 1-12.

**Truswell, J.F., 1990a**, The Transvaal and Griqualand West Sequences-some current issues: *Econ. Geol. Res. Unit, Univ. of the Witwatersrand, Johannesburg, Inf. Circ. #232*, 69 p.

**Truswell, J.F., 1990b**, Early Proterozoic red beds on the Kapvaal Craton: *Econ. Geol. Res. Unit, University of the Witwatersrand, Johannesburg, Inf/tion Circ. #223*, 96 p.

**Tsikos, H., and Moore, J.M., 1998**, Processes of primary manganese concentration in the Kalahari Manganese Field, South Africa: Abstracts, AGC•AMC•APGGQ Conference, Quebec, Canada, p. A-187.

**Tsikos, H., and Moore, J.M., 1998**, Iron formation-hosted manganese deposits in the Paleoproterozoic Transvaal Supergroup, South Africa: The Kalahari Manganese Field revisited. Extended Abstracts, Geocongress '98, Pretoria, South Africa, p. 98-100.

**Tsikos, H., Moore, J.M., and Harris, C. 1999**, Stable isotope evidence on the origin, diagenesis and alteration of the Palaeoproterozoic Hotazel Fe-Mn Formation, Kalahari Manganese Field: Special abstracts issue, GSA 11 - Earth Resources for Africa Conference, Cape Town, South Africa, *J. Afr. E. Sci.*, v. 28, #4A, p. 80-81.

**Tugarinov, A.I., Bergman, I.A., and Gavrilova, L.K., 1973**, The facial nature of the Krivoyrog iron-formation, in: Genesis of Precambrian iron and manganese deposits: Proc. Kiev Symposium 1970, UNESCO Paris, p. 35-40.

**Tyler, S.A., 1949**, Development of Lake Superior soft iron ores from metamorphosed iron-formation: *Geol. Soc. Am. Bull.*, v. 60, p. 1101-1024.

**Tyler, S.A., and Bailey, S.W., 1961**, Secondary glauconite in the Biwabic iron-formation of Minnesota: *Econ. Geol.*, v. 56, p. 1033-1044.

**Van Wyk, C.J., 1987**, Die mineralogie en geochemie van sedimentere siklusse in die Kuruman-en Griquatown-ysterformasies van die Transvaal-Supergroep in Griekwaland-Wes: Unpubl. MSc thesis, Rand Africaans Univ., Johannesburg, 265 p.

**Veizer, J., Clayton, R.N., Hinton, R.W., von Brunn, V., Mason, T.R., Buck, S.G., and Hoefs, J., 1990**, Geochemistry of Precambrian carbonates: 3-shelf seas and non-marine environments of the Archaean: *Geoch. Cosm. Acta*, v. 54, p. 2717-2729.

**Visser, J.N.J., 1971**, The deposition of the Griquatown glacial member in the Transvaal Supergroup: *Trans. Geol. Soc. S. Afr.*, v. 74, p. 187-199.

**Vorona, I.D., Kravchenko, V.M., Pervago, V.A., and Frumkin, I.M., 1973**, Precambrian ferruginous formations of the Aldan shield, in: Genesis of Precambrian iron and manganese deposits: Proc. Kiev Symposium 1970, UNESCO Paris, p. 246-254.

**Walker, J.C.G., 1983**, Possible limits on the composition of the Archaean ocean: *Nature*, v. 302, p. 518-520.

**Walker, J.C.G., 1984**, Suboxic diagenesis in banded iron-formations: *Nature*, v. 309, p. 340-342.

- Walker, J.C.G., and Brimblecombe, P., 1985**, Iron and sulfur in the prebiological ocean: *Prec. Res.*, v. 28, p. 205-222.
- Walter, M.R., and Hofmann H.J., 1983**, The palaeontology and palaeoecology of Precambrian iron-formations, in: *Iron-formations: facts and problems*, eds., Trendall, A.F., and Morris, R.C.: *Developments in Precambrian Geology* 6, Els. Sci. Pbl., p. 373-400.
- Weber, F., 1973**, Genesis and supergene evolution of the Precambrian sedimentary manganese deposit at Moanda (Gabon), in: *Genesis of Precambrian iron and manganese deposits: Proc. Kiev Symposium 1970*, UNESCO Paris, p. 307-322.
- Widdel, F., Schnell, S., Heising, S., Ehrenreich, A., Assmus, B., and Shink, B., 1993**, Ferrous iron oxidation by anoxygenic phototrophic bacteria: *Nature*, v. 362, p. 834-837.
- Wiggering, H., and Beukes, N.J., 1990**, Petrography and geochemistry of a 2000-2200-ma-old hematitic palaeo-alteration profile on Ongeluk basalt of the Transvaal Supergroup, Griqualand West, South Africa: *Prec. Res.*, v. 46, p. 241-258.
- Wildeman, T.R., and Haskin, L.A., 1973**, Rare-earths in Precambrian sediments: *Geoch. Cosm. Acta*, v. 37, p. 419-438.
- Williams, D.M., Kasting, J.F., and Frakes, L.A., 1998**, Low-latitude glaciation and rapid changes in the Earth's obliquity explained by obliquity-oblateness feedback: *Nature*, v. 396, p. 453-455.
- Wilson, M.L., and Hyndman, D.W., 1990**, Tectonic interpretation of an Archaean lithologic package enclosing iron-formation in the southern Tobacco Root and northern ruby Ranges of southwestern Montana, USA, in: *Ancient banded iron-formations (regional presentations): Theophrastus publ.*, Athens, p. 27-62.
- Windley, B.F., 1983**, Banded iron-formations in Proterozoic greenstone belts: call for future studies: *Prec. Res.*, v. 20, p. 585-588.
- Young, G.M., 1988**, Proterozoic plate tectonics, glaciation and iron-formations: *Sed. Geol.*, v. 58, p. 127-144.
- Young, T.P., 1989**, Phanerozoic ironstones: an introduction and review, in: *Phanerozoic ironstones*, eds., Young, T.P., and Taylor, W.E.G.: *Geol. Soc. London, Sp. Publ. No 46*, 251 p.
- Zaitsev, Yu.S., 1973**, Geology of the Precambrian cherty iron-formations of the Belgorod iron-ore region, in: *Genesis of Precambrian iron and manganese deposits: Proc. Kiev Symposium 1970*, UNESCO Paris, p. 101-103.

**Zhai, M., and Windley, B.F., 1990,** The Archaean and Early Proterozoic banded iron-formations of North China: their characteristics, geotectonic relations, chemistry and implications for crustal growth: *Prec. Res.*, v. 48, p. 267-286.

**Zhang, C., Liu, S., Phelps, T.J., Cole, D.R., Horita, J., Fortier, S.M., Elless, M., and Valley, J.W., 1997,** Physiochemical, mineralogical, and isotopic characterization of magnetite-rich iron oxides formed by thermophilic iron-reducing bacteria: *Geoch. Cosm. Acta*, v. 61, p. 4621-4632.